Deployment System for the RABSII Antenna

Design Analysis of a Deployment System for a 5-meter long Dipole Antenna onboard the Delfi-Twin

Master Aerospace Engineering

Aboubakr el Jouhri

Delft University of Technology

TU Delft

Deployment System for the RABSII Antenna

Design Analysis of a Deployment System for a 5-meter long Dipole Antenna onboard the Delfi-Twin

by

Aboubakr el Jouhri

to obtain the degree of Master of Science
at the Delft University of Technology
to be defended publicly on **TBD**

Thesis committee:	Dr.Ir. J. Bouwmeester	Chair
	Dr. J.A.M. Vanhamel	Supervisor
	I. Uriol Balbin	External examiner
Place:	Faculty of Aerospace Engineering, Delft	
Project Duration:	February, 2024 - May, 2025	

An electronic version of this thesis is available at `http://repository.tudelft.nl/`.

Faculty of Aerospace Engineering Delft University of Technology

TU Delft

Preface

This is it.
After almost 7 years at TU Delft, I am concluding my university career with this thesis. I vividly remember my first day at TU Delft, where I entered the Faculty of Mechanical Engineering alone. I felt out of touch, and did not think that I would succeed. It was a period in my life, which consisted of a lot of ups and downs. But with the guidance and support from a lot of people, I was able to persevere and succeed.

First, I would like to express my sincere gratitude to everyone who contributed to the completion of this thesis. I am especially thankful to my supervisor, Dr. Jurgen Vanhamel, for his continuous guidance, support, and willingness to meet and address any questions throughout the project. I would also like to thank Şevket Uludağ and Stefano Sperretta for their invaluable input during the Delfi-Twin meetings. Their detailed answers to my questions and the insights they provided greatly contributed to the development of the final design. A special thanks goes to Ines Uriol Balbín for her valuable feedback and dedicated time. Her prompt responses, critical perspective, and thoughtful guidance enabled me to take a more analytical approach and significantly improved the quality of this work.

I would also like to thank all my friends. Some of them I have known since high school, while others I met during my time at university. The many dinners, shared activities, and unforgettable trips we took together brought me happiness and helped me clear my mind. Without their support, encouragement, and guidance, I honestly do not know where I would have ended up. I am deeply grateful to know them and to have them in my life.

Finally, I would like to thank my family and especially my parents. Their unwavering support, while not always understanding what I am doing, was a great motivation for me. Throughout my university career, my goal was always to say one thing to them:

I did it, Alhamdulillah

Aboubakr el Jouhri
Delft, May 2025

Abstract

The miniaturization of satellite platforms, driven by the introduction of standardized architectures such as the CubeSat and PocketQube, has revolutionized access to space. However, this reduction in form factor has introduced significant engineering challenges, particularly for subsystem integration. While the CubeSat standard has led to a surge in compatible commercial solutions, the smaller PocketQube standard still lacks equivalent support infrastructure. Delfi-Twin, a 3P PocketQube satellite developed at TU Delft under the Delfi Program, embodies these constraints. The satellite hosts the RABSII (Radio Amateur Beacons aboard a nanoSatellite for the Investigation of the Ionosphere) payload, which incorporates a 5-meter dipole antenna composed of two 2.5-meter elements. The deployment system must achieve a deployment angle between 90° and 130°. Existing CubeSat-class and commercially available off-the-shelf solutions are not compatible with the stringent constraints of the Delfi-Twin mission, thereby necessitating the development of a novel and reliable deployment mechanism specifically tailored to PocketQube-class satellites.

The RABSII antenna elements must adhere to specific mass, stowed volume and power constraints. These constraints, which are provided by the Delfi-Twin stakeholders, include the deployment system developed in this research. Each antenna element and its respective deployment system has an allocated stowed volume of 17.8x5x0.2 cm^3 on an external side panel of the satellite. Additionally, the full top panel, measuring 5x5x0.2 cm^3, was made available to support integration. To further accommodate the deployment system, localized milling of the satellite's external plate was permitted, thereby increasing the allowable thickness from 0.2 cm to 0.357 cm. The combined mass budget for both antenna elements and their deployment systems was limited to 40 g, with a power budget of 10 W for 10 s during deployment.

The methodology of the development process followed a systematic systems engineering approach. Based on a literature review, a categorization of the critical components required for a nanosatellite deployment system was established. Following an extensive concept development phase, a final deployment system architecture was selected and refined. The resulting design adopts a modular configuration, consisting of three hinge mechanisms per antenna element. Each hinge mechanism integrates a commercially available torsion spring (Lesjöfors 8318) and consists of hard-anodized Al7075-T6 hinge leaves and an anodized Ti6-Al4-V hinge rod. To mitigate the risk of cold welding in the space environment, the design incorporates the use of dissimilar materials, hard-coating treatments, and an additional solid lubricant layer of MoS_2.

The deployment systems performance was evaluated across three criteria: deployment performance, structural integrity, and compliance with mass, volume, and power constraints. The expected deployment angle is 92.57°, assuming a resistive torque of 10.547 Nmm, consistent with European Cooperation for Space Standardization (ECSS) recommendations. Structural integrity was assessed under worst-case quasi-static acceleration loads and in-orbit thermal extreme loads. Material selections ensured minimal deformation and adequate safety margins to prevent mechanical failure. The complete deployment system for each RABSII antenna element has a mass of 4.978g and occupies a volume of 4.75x5x2.8 cm^3. To comply with volume constraints, panel milling is necessary to accommodate the extruded thickness, which must remain below 0.2 cm. The longitudinal length of 4.75 cm includes the minimum adhesive bond length of 33 mm between the antenna and hinge mechanism.

Several recommendations are proposed for future work. In the early stages of development, it is advised to adopt a more accurate approach to estimating resistive torque, to refine the supporting structural analyses and to improve the assessment and integration of the RABSII payload. In the later stages, the focus should shift toward the development of a proto-flight model and the execution of a functional test campaign to validate the system's performance under mission-representative conditions.

Contents

List of Figures

List of Tables

Nomenclature

Abbreviations

Abbreviation	Definition
ADCS	Attitude Determination and Control Systems
AIALC	Actuator Integrated Angular Limit Control
AWS	Autonomous Wireless Sensor
CAD	Computer Aided Design
Cal Poly	California Polytechnic State University
CFRP	Carbon Fiber Reinforced Plastic
CHSC	Closed Hinge Stowed Configuration
CNC	Computer Numerical Control
COTS	Commercially-off-the-Shelf
DOT	Design Option Tree
DSSP	Delfi Space Satellite Project
ECSS	European Cooperation for Space Standardization
E_s	Sporadic E
FHL	Fixated Hinge Leaf
FMEA	Failure Mode and Effects Analysis
FOS	Factor of Safety
FOSU	Ultimate design Factor of Safety
FOSY	Yield design Factor of Safety
FR-4	Flame Retardant 4
FTL	Fixated Turntable Leaf
HDRM	Hold-down and Release Mechanism
ISARA	The Integrated Solar Array and ReflectArray Antenna
JPL	NASA's Jet Propulsion Laboratory
KaPDA	Ka-band Parabolic Deployable Antenna for CubeSats
KPP	Key Performance Parameter
LEO	Low Earth Orbit
MIALC	Mechanism Integrated Angular Limit Control
ND	Not Disclosed
OHSC	Open Hinge Stowed Configuration
PCB	Printed Circuit Board
RABSII	Radio Amateur Beacons aboard a nanoSatellite for the Investigation of the Ionosphere
RAHSC	Right-Angle Hinge Stowed Configuration
Ref.	Reference
RHL	Rotating Hinge Leaf
RTL	Rotational Turntable Leaf
RTM	Requirement Traceability Matrix

Abbreviation	Definition
Sc	Score
SMA	Shape Memory Alloy
SME	Shape Memory Effect
SOA	State Of the Art
SSDL	Stanford University's Space Systems Development Laboratory
STEM	Storable Tubular Extendible Member
TFSC	Thin Film Solar Cell
TRL	Technology Readiness Level
TU Delft	Delft University of Technology
VMS	von Mises Stress
W	Criteria Weight

Symbols

Symbol	Definition	SI Unit
A	Area	[m^2]
A_{bond}	Area of the Adhesive bond	[m^2]
A_f	Austenite Finish Temperature	[°C]
A_s	Austenite Start Temperature	[°C]
A_{RABSII}	Area of RABSII Antenna	[m^2]
$A_{RABSII-Folded}$	Area of Folded RABSII antenna	[m^2]
$A_{RABSII-Unfolded}$	Area of Unfolded RABSII antenna	[m^2]
$A_{satellite}$	Area of satellite	[m^2]
$[A]$	Non-Zero Quadrants of the Laminate Compliance Matrix	[-]
$[B]$	Non-Zero Quadrants of the Laminate Compliance Matrix	[-]
C_d	Drag Coefficient	[-]
c_p	Specific Heat Capacity	[$J.kg^1.K^{-1}$]
$[D]$	Non-Zero Quadrants of the Laminate Compliance Matrix	[-]
D_o	Outer Diameter	[m]
$D_{Retention}$	Diameter of Retention Wire	[m]
f	Frequency	[Hz]
F_d	Drag Force	[N]
$F_{d-Deployed}$	Drag Force of the Satellite with deployed RABSII antenna	[N]
$F_{d-RABSII}$	Drag Force of the RABSII antenna	[N]
$F_{d-Stowed}$	Drag Force of the Satellite with stowed RABSII antenna	[N]
F_g	Gravity Force	[N]
F_{peel}	Peel Strength	[$N.mm^{-1}$]
F_r	Resistive Torque due to Friction Forces	[Nm]
h	Altitude of the Orbit	[m]
H	Height	[m]
H_a	Resistive Torque due to the Wire Harness and Aerodynamic Drag	[Nm]
H_d	Resistive Torque due to Adhesion	[Nm]
H_m	Resistive Torque due to Magnetic Effects	[Nm]
H_t	Thickness of the Deployment System	[m]
H_{Leaf}	Thickness of the Hinge or Turntable Leaf	[m]
H_y	Resistive Torque due to Hysteresis	[Nm]
I	Resistive Torque due to Accelerations in the Inertial Frame of Reference	[Nm]
I_{Fold}	Inertia of the folded RABSII Antenna Element	[$kg.m^3$]
I_{RABSII}	Inertia of the unfolded RABSII Antenna Element	[$kg.m^3$]
k_{spring}	Spring Constant of a Torsion Spring	[°.N^1]
K	Uncertainty Factor	[-]
L	Length	[m]
L_{bond}	Length of the Adhesive bond	[m]
$L_{FR4-Req}$	Overlap of the FR-4 Plate on the Deployment System	[m]
L_{FTL}	Fixated Turntable Leaf Length	[m]
L_{Leaf}	Leaf length	[m]

Symbol	Definition	SI Unit
M_d	Martensite permanently deformed Temperature	[°C]
M_f	Martensite Finish Temperature	[°C]
M_s	Martensite Start Temperature	[°C]
$M_{Deployed}$	Deployment Torque	[Nm]
M_{RABSII}	Mass of RABSII Antenna	[Kg]
$M_{satellite}$	Mass of Satellite	[Kg]
$n_{springs}$	Amount of Springs	[-]
P	PocketQube Standardized Unit	[-]
R	Curvature of Tape Spring	[m]
r	Bending Radius of Tape Spring	[m]
r_{TFL}	Radius of Fixated Turntable Leaf	[m]
S	Resistive Torque due to Spring Load	[Nm]
$T_{actuation}$	Actuation Torque	[Nm]
T_{avg}	Average Supplied Actuation Torque	[Nm]
T_d	Inertial Resistance caused by the acceleration function	[Nm]
T_L	Deliverable Output Torque	[Nm]
T_m	Melting Point	[°C]
T_{min}	Minimum Required Actuation Torque	[Nm]
T_{mst}	Maximum Service Temperature	[°C]
t	Thickness	[m]
U	CubeSat Standardized Unit	[-]
v_s	Speed of Satellite w.r.t. the atmosphere	[m.s^{-1}]
α_{dep}	Deployment Angle	[°]
λ	Wavelength	[m]
Λ	Thermal conductivity	[W.m^{-1}.K^{-1}]
ω	Angular Velocity	[rad.s^{-1}]
ρ	Density	[kg.m^{-3}]
$\rho(h)$	Atmospheric Density Function	[kg.m^{-3}]
σ_{shear}	Shear strength	[Pa]
σ_{yield}	Tensile yield strength	[Pa]
θ_{TS}	Spanned angle of a Tape Spring	[°]
μ_d	Dynamic Coefficient of Friction	[-]
μ_s	Static Coefficient of Friction	[-]

Constants

Symbol	Definition	Value
c	Speed of Light in Vacuum	2.99792458x10^8 [m.s^{-1}]
G	Gravitational Constant	6.6743x10^{-11} [m^3.kg^{-1}.s^{-2}]
H_{FR4}	FR-4 Plate thickness	1.57 [mm]
M_{earth}	Mass of Earth	5.97219x10^{24} [kg]

Symbol	Definition	Value
R_{earth}	Radius of Earth	6378 [km]

1

Introduction

The introduction of the CubeSat standard in 1999 by Prof. Jordi Puig-Suari at California Polytechnic State University (Cal Poly) and Prof. Bob Twiggs at Stanford University's Space Systems Development Laboratory (SSDL) marked a significant shift in satellite design and accessibility in the space industry [1]. Interest in satellite miniaturization grew due to its inexpensive nature and quick development timeline. These smaller-sized satellites, defined by strict form factors and a weight limit of less than 10 kg, became known as nanosatellites [2, 3]. While the Vanguard 1, launched in 1958, was the first satellite to meet these criteria [2], the establishment of the CubeSat standard [1] was the turning point that made nanosatellites more accessible and widespread. Figure 1.1 illustrates the yearly launch rate of nanosatellites from 1998 to 2024.

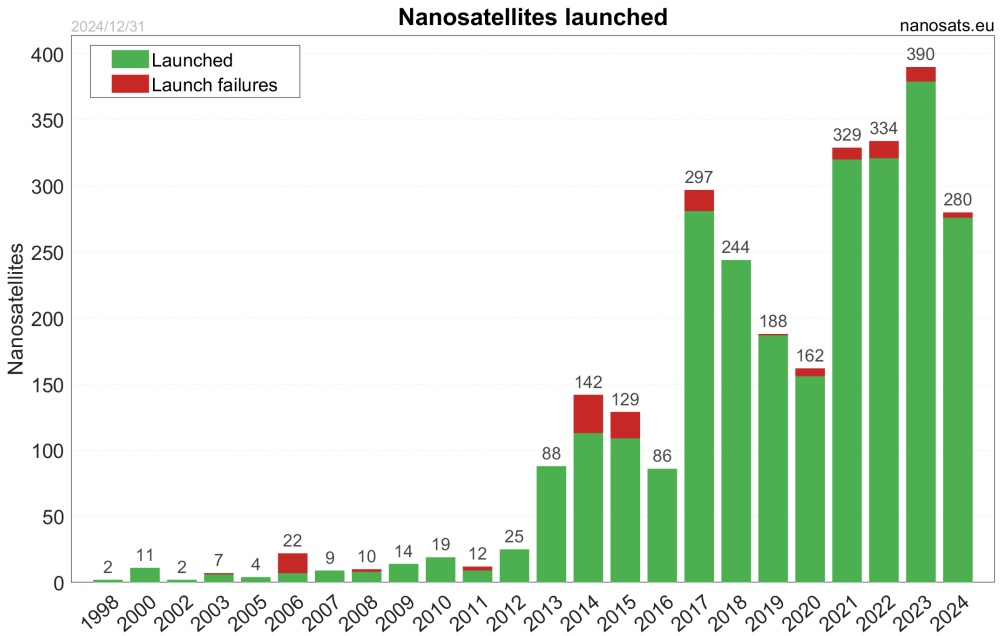

Figure 1.1: Yearly launch rate of nanosatellites from 1998 to 2024 [4].

The CubeSat standard defines a class of satellites with a standardized size and form factor with "U" as the unit of measurement. Each unit is defined as 10×10×10 cm^3 (with minor variations for larger CubeSats) and has a maximum weight of 2 kg. This standard enabled smaller companies and research institutes to enter the space industry, leveraging its cost-effective nature and quick development timelines. Examples include the Delfi-C^3 and Delfi-n3Xt satellites, developed under the Delfi

Space Satellite Project (DSSP). These nanosatellites adhered to the CubeSat standard, meeting the volume (10×10×34 cm^3) and mass constraints (less than 6 kg) of a 3U CubeSat [1].

Following the introduction of the CubeSat standard in 1999, the PocketQube standard was proposed in 2009 [5]. This standard defines a smaller class of satellites with units designated as "P". Each unit is defined as 5×5×5 cm^3 (with minor variations for larger PocketQubes) and has a maximum weight of 250 g per unit. Similar to the CubeSat, the PocketQube standard enabled even smaller companies and research institutes to enter the space industry. An example is the Delfi-PQ, developed under the DSSP. The Delfi-PQ adheres to the volume (5×5×17.8 cm^3) and mass constraint (less than 750 g) of a 3P PocketQube [5].

1.1. Research Framework

The Delfi-Twin, the latest addition of the DSSP, consists of a pair of nanosatellites adhering to the 3P PocketQube Standard. These satellites, which are identical in payload, dimensions and mass, operate in a constellation. Onboard each satellite is the RABSII (Radio Amateur Beacons aboard a nanoSatellite for the Investigation of the Ionosphere) instrument, an antenna system designed for ionospheric research [6]. One satellite is equipped with a 28 MHz ($\lambda \approx 10.7$ m) RABSII antenna, while the other carries the 50 MHz ($\lambda \approx 6$ m) variant. A key component of the RABSII instrument is a self-actuating deployment mechanism, designed to ensure reliable antenna deployment at a fixed angle of 130°.

1.2. Need & Mission Statement

A need statement establishes the rationale behind a project, outlining its specific need and highlighting the reasons for its importance. For the deployment system, the need statement is defined as follows:

The Delfi-Twin satellite, part of the PocketQube class, requires a reliable, cost-effective self-actuating deployment mechanism for the deployment of a 5-meter dipole RABSII antenna. Due to the lower mass and volume budgets of PocketQube satellites, existing CubeSat-class deployment systems and COTS (commercially-of-the-shelf) solutions are inadequate. Alternative deployment systems need to be designed, developed and tested, to meet the specific needs of Delfi-Twin while ensuring the integration of the RABSII antenna system. This deployment system must optimize reliability while minimizing mass, volume and cost.

The mission statement provides a concise summary that complements the need statement. While the need statement explains the rationale, the mission statement summarizes the core objectives and scope of the project. For the deployment system, the mission statement is as follows:

For Delfi-Twin, a 3P PocketQube satellite, a reliable deployment system for the RABSII antenna will be designed and developed, ensuring optimal performance during all stages of the mission of Delfi-Twin.

1.3. Research Goal and Objectives

The objective of this research is to develop a deployment system for a 5-meter long dipole antenna compatible with nanosatellites.
Based on this, the research question is:

"What is a reliable deployment system design for a 5-meter long dipole antenna onboard a 3P PocketQube that optimizes deployment success while minimizing the risk of mechanical or operational failure?"

In order to answer the research question, several relevant sub-questions have been formulated, which are as follows:

- *What is an actuation method, hold-down-and-release-mechanism and deployment mechanism suitable for integration into a 3P PocketQube?*
- *What are the critical factors that influence the successful deployment of a dipole antenna onboard a 3P PocketQube?*
- *How effectively can an actuation method achieve the full deployment of an unfolded 5m dipole antenna?*
- *How can the deployment system be assessed to ensure validation with systems requirements and determine its reliability?*

1.4. Thesis Outline

This master's thesis is structured as follows. Chapter 2 provides essential background information, including an overview of TU Delft's *Delfi Space Satellite Project* and the design framework guiding this research. Chapter 3 presents a comprehensive literature review, identifying the main components of an antenna deployment system. For each component, both commercially-off-the-shelf and state-of-the-art solutions are discussed, with attention to their flight heritage. In Chapter 4, the system requirements and key performance parameters are defined. A design option tree is developed to evaluate feasible design options. Chapter 5 details the concept development phase, where multiple design concepts are created based on the option tree and systematically evaluated. A trade-off study is conducted to select the final design. Chapter 6 introduces a Failure Mode and Effects Analysis to initiate an iterative design process, addressing potential risks and refining the system's performance. Chapter 7 presents the final design, evaluates its performance, constructs a risk map and verifies compliance with the defined requirements. Finally, Chapter 8 summarizes the main conclusions of the study and Chapter 9 offers recommendations for future work.

2

Background

Developing a deployment system necessitates a comprehensive understanding of the history of nanosatellites and the specific contributions of TU Delft on this field. Furthermore, it is essential to establish a systematic framework to guide the design of the deployment system. To that end, section 2.1 presents an overview of TU Delft's DSSP, highlighting previous satellite missions and notable achievements. Last, Section 2.2 outlines the design framework of the deployment system, identifying key factors that influence its development.

2.1. Delfi Space Satellite Project

In 2004, TU Delft entered the space industry to capitalize on the growing prominence of nanosatellites. Through the DSSP, TU Delft aimed to achieve three primary objectives:

- **Education:** To provide students with optimal preparation for careers in the space industry, including the improvement of engineering skills, teamwork, scientific writing, communication and a general understanding of all aspects of a real space project.
- **Technology Demonstration:** To demonstrate small and innovative space technologies emerging from TU Delft and its external partners in the space sector.
- **Small Satellite Bus Development:** To enable novel applications (with distributed networks) of nanosatellites that are not yet feasible in terms of technology or cost-effectiveness with the state-of-the-art (SOA) technology.

To date, DSSP has launched three satellites: the Delfi-C^3, the Delfi-n3Xt and the Delfi-PQ. These satellites conform to either the CubeSat standard (Delfi-C^3 and Delfi-n3Xt) or PocketQube standard (Delfi-PQ). Figure 2.1 provides a timeline of the Delfi Space satellites that have been launched.

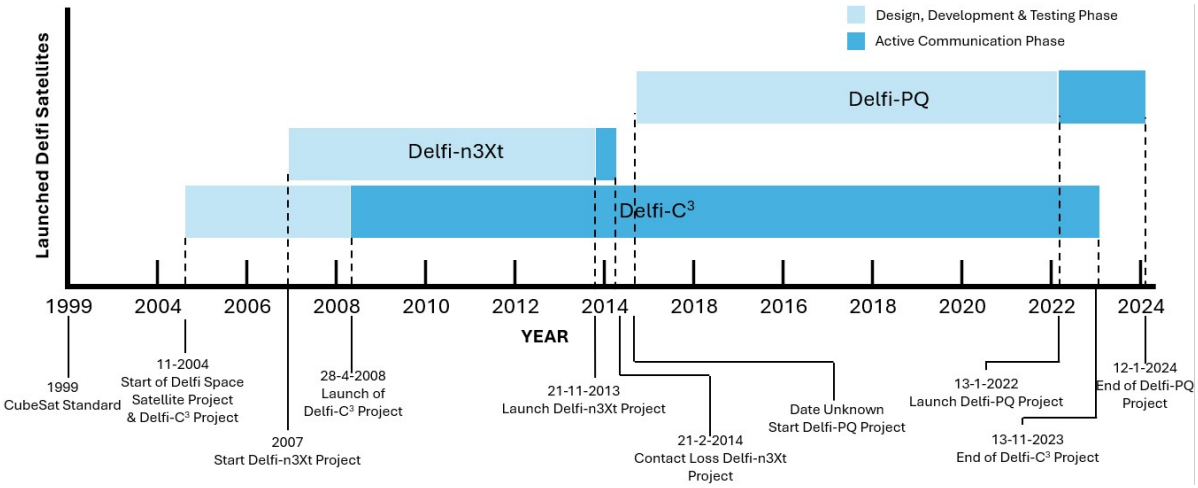

Figure 2.1: Timeline of launched Delfi Space Satellites since the introduction of the CubeSat standard until 05-2024.

2.1.1. Delfi-C^3

The Delfi-C^3, shown in Figure 2.2, was the first satellite developed and launched under the DSSP. Four years after the project's inception (28-04-2008), the Delfi-C^3 was successfully deployed from the Satish Dhawan Space Centre in India. Notably, the satellite remained operational for nearly 15 years, significantly exceeding its originally projected mission duration of three months [7].

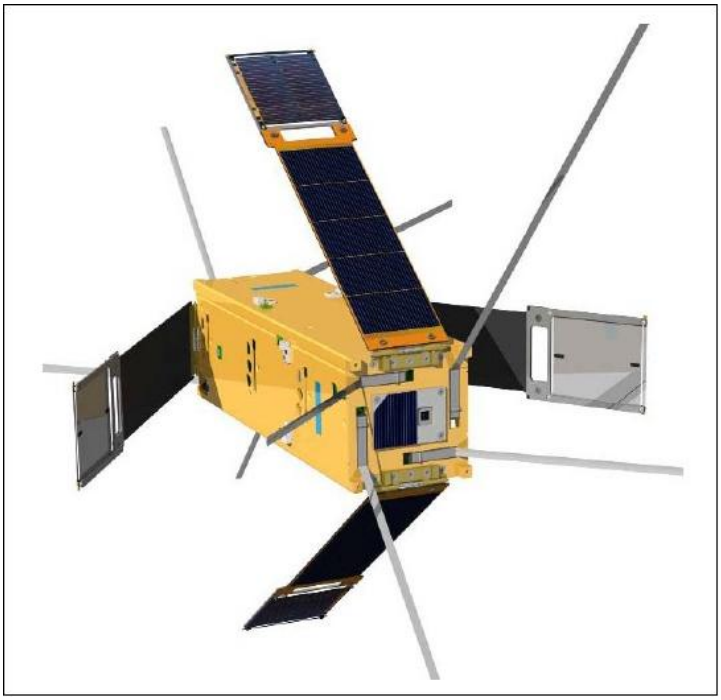

Figure 2.2: Deployed configuration of the Delfi-C^3 [8].

The DSSP was established to provide educational opportunities for students, demonstrate innovative small satellite technologies and enable novel applications of small satellites. The Delfi-C^3 mission aimed to fulfill these goals while conforming to the CubeSat standard for a 3U satellite. This corresponds to a volume of 10x10x34 cm^3 and a mass of less than 6 kg [1]. Ultimately, the Delfi-C^3 was realized as a 3U satellite with a total mass of 2.2 kg. Its mission objectives included demonstrating advanced technologies, such as a novel Thin Film Solar Cell (TFSC) technique, an Autonomous Wireless Sun Sensor (AWS) and a high-efficiency radio transceiver [9].

The Delfi-C antenna system[3], shown in Figure 2.2, comprises two separate subsystems for up- and downlink communications, each consisting of four antennas (Figure 2.3b). While the two subsystems are similar in design, the primary difference between them lies in their respective antenna lengths, which are either 18 cm or 50 cm. Each antenna is housed within a modular antenna box (Figure 2.3a), utilizing a tape spring actuation method combined with a burn wire-based Hold-down and Release Mechanism (HDRM). A total of eight modular antenna boxes were integrated into the Delfi-C^3, divided equally between the up- and downlink communication systems [10].

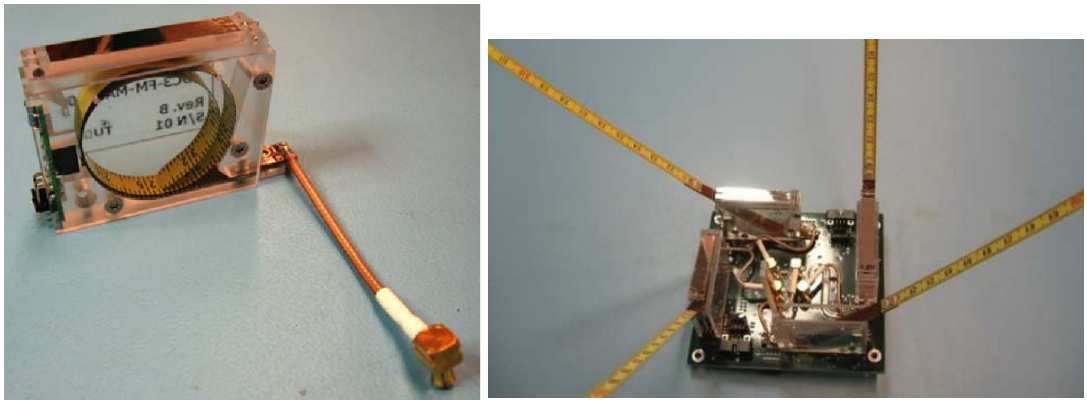

(a) Modular antenna box with stowed antenna used for the Delfi-C^3 [10].

(b) One of two antenna systems onboard the Delfi-C^3, each consisting of four modular antenna boxes [10].

Figure 2.3: Delfi-C^3 Antenna system and its main component, the modular antenna box

Extensive testing during the development phase led to multiple refinements of the antenna system's design. While all antenna deployments were successfully confirmed during operations [10], certain issues arose. Prolonged storage of the antennas resulted in plastic deformation, causing slight warping upon deployment [11]. Subsequent iterations of the antenna system addressed this challenge and the refined design eventually became the foundation for commercially off-the-shelf (COTS) applications, such as the dipole antenna developed by ISISpace [12].

2.1.2. Delfi-n3Xt

The Delfi-n3Xt, depicted in Figure 2.4, succeeded the Delfi-C^3. It was initiated in 2007 and launched in 2013 from Russia. The satellite maintained continuous communication with the ground station for three months, although sporadic signals were detected afterwards [13]. Attempts to re-establish continuous communication were unsuccessful and the source and nature of the sporadic signals remain undetermined.

Similar to its predecessor, the Delfi-n3Xt adhered to the 3U CubeSat standard, but had an increased mass of 3.5 kg [13]. Its primary mission was to demonstrating innovative small satellite technologies and it included multiple payloads [15]:

- T3μPS micro propulsion system from TNO
- Multi-functional Particle Spectrometer from Cosine
- Si Solar Cells from DIMES
- High-efficiency modular communications platform from ISISpace
- Commercial SSD storage devices from NLR

Significant changes between the Delfi-C^3 and Delfi-n3Xt included an increased payload capacity, the addition of an onboard battery and a reduction in the number of antennas compared to the Delfi-C^3 [11].

The antenna system and its deployment mechanism for the Delfi-n3Xt inherited design elements from the Delfi-C^3. Given the successful deployment of all Delfi-C^3 antennas, only minor adjustments were

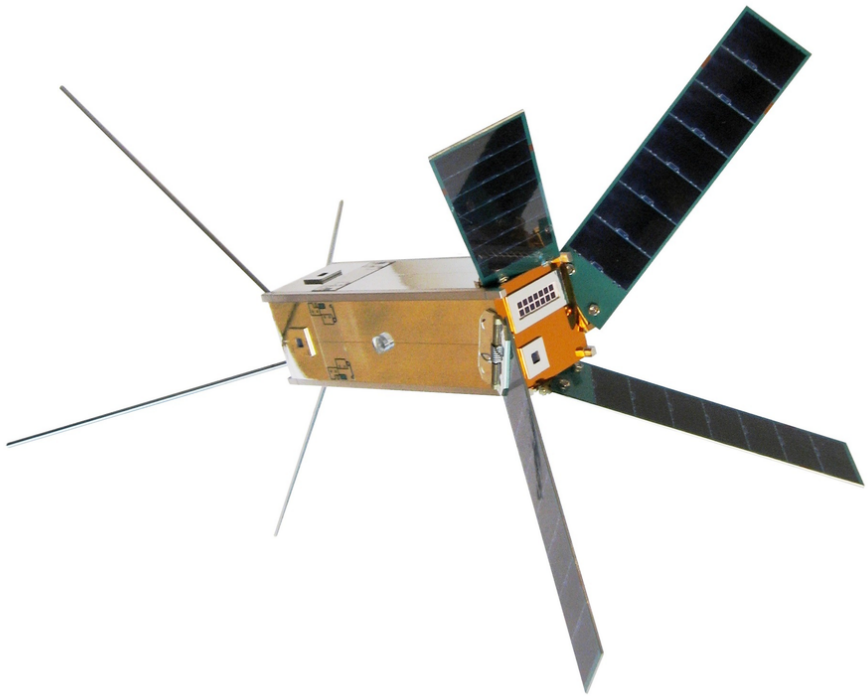

Figure 2.4: Deployed configuration of the Delfi-n3Xt [14]

necessary. A notable modification was the use of a single modular antenna box for both up- and downlink frequencies, thereby reducing the number of antenna systems required. This optimization was achieved using an advanced phasing circuit, enabling the same antenna to support both up- and downlink communications effectively. The uplink frequency, with a wavelength one-third that of the downlink frequency, made this dual-purpose design possible [15, 16].

2.1.3. Delfi-PQ

The Delfi-PQ, shown in Figure 2.5, succeeded the Delfi-n3Xt and was launched in 2022 from Cape Canaveral, USA [17]. Unlike its predecessors, which adhered to the CubeSat standard, the Delfi-PQ was developed following the PocketQube standard. The operational lifetime of the Delfi-PQ was nearly two years, concluding with re-entry into the Earth's atmosphere.

The Delfi-PQ adhered to the PocketQube standard for a 3P satellite, characterized by strict volume (5x5x17.8 cm^3) and mass (<750 grams) constraints [5]. Ultimately, Delfi-PQ was developed as a 3P satellite with a mass of 600 grams. Its mission included an Attitude Determination and Control System (ADCS) and a dual-thruster micro-propulsion resistojet [18, 19].

The antenna system and deployment mechanism of the Delfi-PQ, shown in Figure 2.6, differed significantly from those of its predecessors. The modular antenna boxes of the Delfi-C^3 (Figure 2.3) were replaced by a simplified design: a rigid rod with spring-loaded actuation. The complete antenna system consisted of six components. A rigid, fixed-size antenna element was stowed using a burn wire mechanism combined with a rotating elbow. Upon activation of the burn wire mechanism, deployment was performed by two springs in conjunction with the rotating elbow [18, 20].

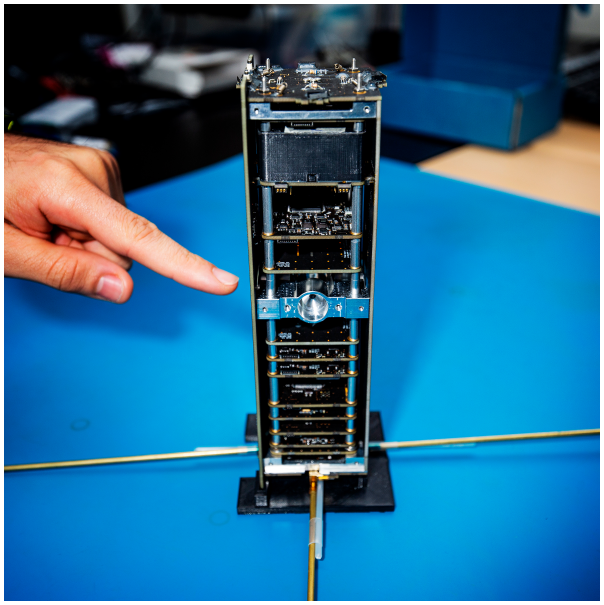

Figure 2.5: Deployed configuration of the Delfi-PQ [17].

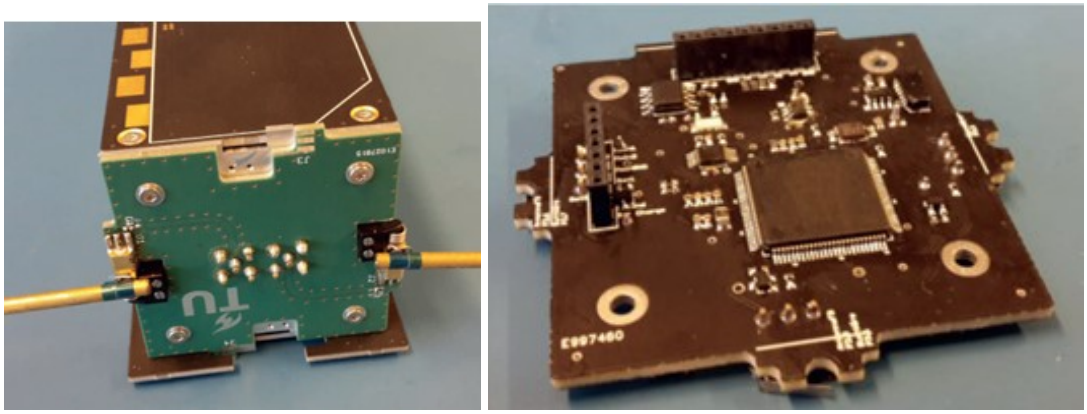

(a) Delfi-PQ deployment system of its dipole antenna [20]. **(b)** Deployment board with the burn wire mechanism [20].

Figure 2.6: Delfi-PQ antenna system and its respective deployment board.

2.2. Peripherals

This section outlines the research framework related to the deployment system. Section 2.2.1 provides an overview of the mission objectives and details of the selected spacecraft platform, Delfi-Twin. Subsequently, Section 2.2.2 elaborates on the RABSII antenna, for which the deployment system is specifically designed.

2.2.1. Delfi-Twin

The Delfi-Twin is the next project under the DSSP. As the successor to Delfi-PQ, the Delfi-Twin project consists of a pair of satellites with similar payloads and dimensions. Both satellites will adhere to the PocketQube standard for 3P PocketQubes, as did Delfi-PQ. The primary objective of the Delfi-Twin project is to demonstrate formation flying with a separation distance of less than 100 km. This separation will be adjusted by using ”high” and ”low” drag configurations of the satellites’ solar panels to respectively increase or decrease drag forces. The target orbit is a sun-synchronous orbit at an altitude of 550 km [6].

The payload of both Delfi-Twin satellites will include the RABSII instrument, which consists of two antenna elements (see Section 2.2.2) [6]. The developed deployment system is specifically designed for

this instrument to be placed onboard each Delfi-Twin. Within the mass and volume budget of the Delfi-Twin mission, 40 grams and 17.8x5x0.2 cm^3 on two external satellite side panels have been allocated for this instrument. Additionally, the use of the top panel (5x5x0.2 cm^3) has also been permitted.

2.2.2. RABSII Project

The RABSII (Radio Amateur Beacons aboard a nanoSatellite for the Investigation of the Ionosphere) instrument is an antenna onboard each Delfi-Twin satellite to advance the understanding of E_s (Sporadic E). E_s is a phenomenon occurring in the Earth's E-region of the ionosphere (altitude: 95–150 km), where frequencies in the HF band (3–30 MHz) and VHF band (30–300 MHz) are significantly affected [21]. This phenomenon can disrupt communication and navigation systems by interfering with radio wave propagation, directly impacting the accuracy and reliability of satellite-based communication and navigation [22]. Although the effects of E_s are well-documented, the underlying mechanisms remain poorly understood [21]. While extensive Earth-based research has been conducted on this topic, the RABSII instrument will be the first instrument using a dedicated beacon system to measure frequencies as low as 28 MHz and 50 MHz from a space-based platform [6].

The RABSII instrument is part of the Delfi-Twin project (Section 2.2.1), where one satellite carries the 28 MHz RABSII instrument and dedicated antenna and the other satellite the 50 MHz RABSII instrument and accompanying antenna. The instrument consists of a deployment system and a dipole antenna, both mounted on the exterior of a Delfi-Twin satellite. Two longitudinal sides of the satellite accommodate a stowed volume of 17.8x5x0.6 cm^3. Since the dipole antenna comprises two elements on opposite sides of the satellite, this volume is mirrored on the other side. The expected final configuration of the deployment is shown in Figure 2.7 where the deployment angle is illustrated.

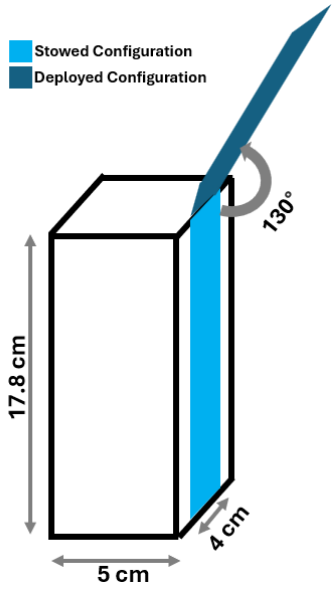

Figure 2.7: Required stowed and deployed position of the RABSII antenna element aboard the Delfi-Twin.

Dipole Antenna

The current design iteration of the RABSII instrument is a dipole antenna. A dipole antenna is a commonly used type of antenna on nanosatellites due to its simplicity and effectiveness in achieving reliable communications [23]. Structurally, a dipole antenna consists of two conductive elements with a ground plane created between them. These elements can be made from various conductive materials, such as metal wires, PCB traces, or even advanced materials like Nitinol [24]. The latter is often used for its flexibility and shape memory alloy properties. Each element of the dipole antenna must have a specific length relative to the desired operating frequency [24]. This requirement arises from the need for resonance, a phenomenon that occurs when the antenna elements are equal in length to a quarter of the wavelength (λ) or a multiple thereof. This phenomenon optimizes the antenna for efficient signal

transmission and reception of the dipole antenna [25].

Dipole antennas operate in the VHF and UHF bands, which covers a frequency range of 30 to 1000 MHz. This frequency range includes amateur radio frequencies commonly used in small satellite communication [26]. To achieve resonance in this frequency range, each antenna element must be at least $\frac{1}{4}\lambda$ in length. This results in a total dipole antenna length of approximately $\frac{1}{2}\lambda$. This ensures optimal performance within the specified frequency range, maximizing signal strength and transmission efficiency. This is particularly critical for low-power nanosatellite systems where energy resources are limited.

The RABSII instrument on the Delfi-Twin uses a dipole antenna with two separate elements positioned on opposite sides of the satellite structure. An example of one element's position is depicted in Figure 2.7. These elements are designed for frequencies of 28 and 50 MHz. The corresponding wavelengths can be calculated using the formula:

$$\lambda = \frac{c}{f} \tag{2.1}$$

where λ is the wavelength, c is the speed of light in a vacuum (299,792,458 m/s) and f is the frequency.

For a frequency of 28 MHz, the dipole antenna length would be approximately 5 m, whereas for 50 MHz, it would be around 3 m. Antennas of this length present significant challenges for integration and deployment on nanosatellites due to their compact size. Consequently, designing these antennas requires meticulous planning to optimize both space and functionality.

Due to their simple design, low cost, low weight and reliable performance across a broad frequency range, dipole antennas are widely used in nanosatellites. However, when designed for lower frequency ranges, the length of their elements must increase to achieve resonance. In nanosatellites, this results in larger antenna elements, complicating deployment. Deviating from the optimal resonance dimensions on the other hand, leads to power losses and reduces communication effectiveness. While power losses can be partially mitigated using power converters or impedance-matching circuits, these solutions increase the satellite system's volume and mass. Consequently, when operating in lower frequency ranges, antenna design often involves a trade-off between incorporating complex power-conversion systems and deploying larger, more intricate antenna structures.

Table 2.1 provides examples of SOA dipole antennas, both with and without flight heritage, illustrating current best practices and trade-offs in the design and deployment of dipole antennas for nanosatellite applications.

Table 2.1: Overview of SOA Dipole antennas, with or without known Flight Heritage.

Reference	***Type***	***Element Length (cm)***	***Frequency (MHz)***	***Application***	***Flight Heritage***
[12]	Dipole	55	30-300	Telemetry & Telecommand Tracking and Control	Delfi-C3
[27]	Dipole	35	430	Telemetry & Telecommand Beacon	XI
[28]	Dipole	20.6	2500 and 4700	Technology Demonstration	-
[29] [30]	Dipole	16	430	Down link Communications	HIT-SAT

3

Background for the Deployment System

Before generating any design concepts, it is essential to review the current SOA as a reference point. Based on Delfi-PQ, a distinction has been made between the main components of a deployment system. Subsequently, an in-depth literature study on each of these main components has been conducted, focusing on potential COTS and SOA options, along with their relevant flight heritage.

3.1. General Components of a Deployment System

Figure 3.1 illustrates the antenna system of the Delfi-PQ with its main components highlighted. These include the HDRMs, the actuation method and the stowage method.

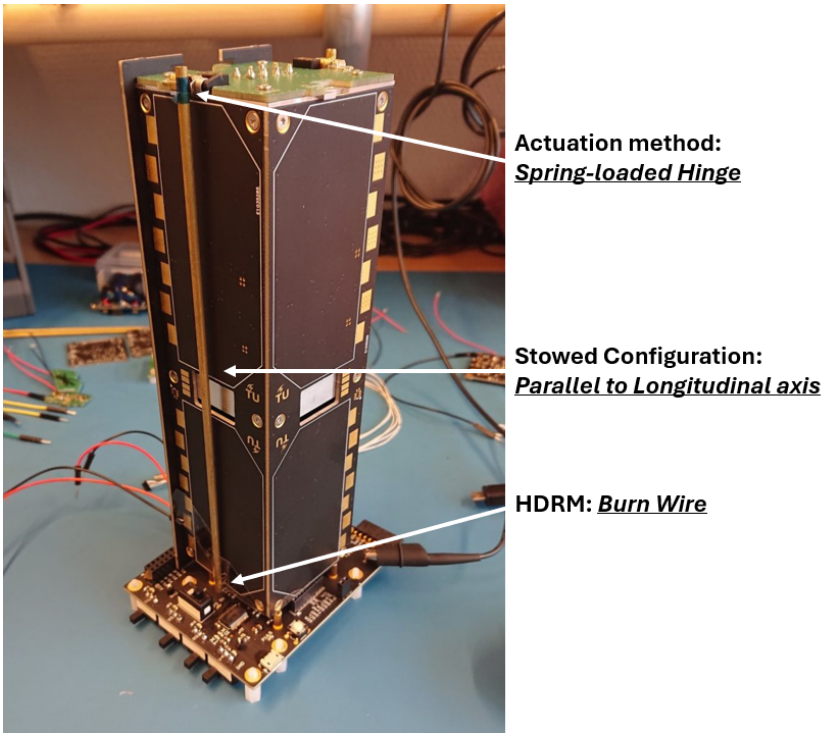

Figure 3.1: Complete Delfi-PQ antenna system with relevant the components of its deployment system

Actuation methods initiate the deployment of appendages by providing the necessary displacement through the use of force, energy or a combination of both. In Figure 3.1, the utilized actuation method is a spring-loaded hinge. Section 3.2 will offer further insights into applicable actuation methods for the deployment system, along with relevant SOA and COTS applications.

HDRMs secure appendages in a stowed configuration until the satellite reaches orbit. Once in orbit, environmental parameters or an external command release the HDRM, allowing the deployment process to begin. In Figure 3.1, the HDRM is a burn wire mechanism. Section 3.3 will provide additional details on applicable HDRMs and include examples of SOA and COTS applications.

Stowage methods focus on storing large appendages in a compact manner by folding and optimizing their placement. For the design of the deployment system, the placement of the antenna is predetermined and therefore, folding methods falls outside the scope of this research. However, gaining insights into SOA stowage methods remains valuable for understanding applicable deployment systems. The stowed configuration of the RABSII antenna is similar to that of the Delfi-PQ antenna. As shown in Figure 3.1, the antenna is stored parallel to the longitudinal axis of the Delfi-PQ in its stowed configuration. Its final deployed state is illustrated in Figure 2.6a. Section 3.4 will delve deeper into potential folding methods and provide examples of SOA and COTS appendages.

3.2. Actuation Methods

An actuation method is an overarching term to group any methods which are capable of initiating the deployment of appendages. This is done by providing the required displacement through the application of force, energy or a combination of both. In this section, the following methods are discussed:

- **SMA-based (Shape Memory Alloy) deployment**: This method uses the unique properties of SMAs to actuate deployment. The flight heritage of the ALBus CubeSat [31] will be used to show the potential implementation of a SMA as an actuation method.
- **Tape spring-based deployment**: This includes STEMs (Storable Tubular Extendible Members) and booms, which rely on the restoring forces of tape springs for deployment.
- **Spring-based deployment**: As one of the simplest methods, spring-based deployment offers significant flight heritage and has demonstrated flexibility and adaptability in various use cases. Relevant examples from flight heritage will be discussed.

Although other actuation methods can be applied in nanosatellite, they are not considered in this study due to their limited relevance, applicability, or increased complexity which do not align with the objectives of this study. Examples of methods which are explicitly excluded:

- **Self-induced centrifugal-based deployment**: This method uses the satellite's rotational acceleration to actuate deployment. A comparable approach was used on the IKAROS satellite [32], albeit on a much larger scale. This method could potentially achieve the required deployment angle of 130° relative to the longitudinal axis of Delfi-Twin. However, it would negate the ability of the RABSII instrument to remain compatible with a wide array of host satellites. Requiring PocketQubes to meet specific angular acceleration constraints complicates the potential integration of the system.
- **Electrical motor-based deployment**: This method uses a small motor to control deployment through precise rotations. However, its dimensions, power consumption and mass are expected to exceed the allocations for the Delfi-Twin mission. Therefore, it is not considered a suitable option.

3.2.1. Shape Memory Alloy (Deployment Method)

SMAs are a class of materials capable of returning to their original shape after being exposed to a thermal load. This behavior is based on their ability to exist in two distinct phases: the austenite and martensite phase. Within the martensite phase, the crystal structure can take two forms: twinned and detwinned martensite [33]. The transformation process that enables shape changes during phase transitions is known as the Shape Memory Effect (SME) and is temperature-dependent.

At higher temperatures, the SMA is stable in its austenite phase, while at lower temperatures it remains in its martensite phase. The phase transition, assuming constant pressure, occurs as a function of temperature. During heating, the SMA begins to transform from martensite to austenite at A_s, completing the transformation at A_f. Conversely, during cooling, the SMA transitions back to martensite starting at M_s and completes this transformation at M_f. Additionally, M_d represents the highest temperature at which martensite can still be stress-induced; above M_d, permanent deformation of the SMA occurs. The critical transformation temperatures are A_s, A_f, M_s, M_f and M_d. The hierarchy of these transformation temperatures, from lowest to highest, is as follows: $M_f < M_s < A_s < A_f < M_d$ [33, 34].

In summary, within the specific temperature range from M_s to M_f, a stress or load can deform the SMA. Upon heating to A_s or higher, the SMA will return to its original shape. Figure 3.2 shows relationships between the various phases and crystal structures, while Table 3.1 lists commonly used SMA alloys and their material properties. Additionally, Table 3.2 provides the transition temperatures of these commercially available SMAs [35].

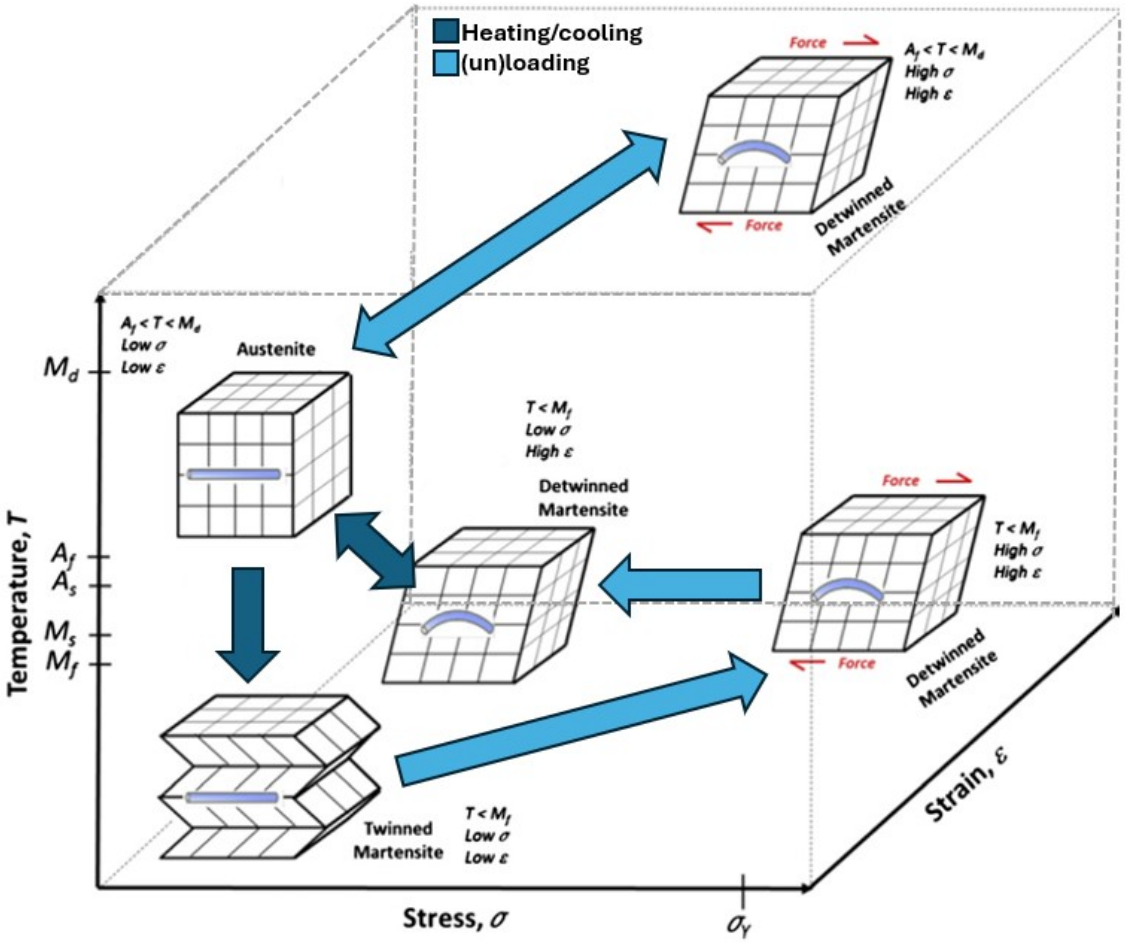

Figure 3.2: Simplified depiction of the relations between shape memory alloy phases and crystal structures [34]

Table 3.1: Material properties of NiTi, CuZnAl and CuAlNi shape memory alloys [35].

Property	**NiTi**	**CuZnAl**	**CuAlNi**
Specific heat (J/Kg°C)	450–620	390–400	373–574
Thermal conductivity (20°C) (W/mK)	8.6–18	84–120	30–75
Density (Kg/m^3)	6400–6500	7540–8000	7100–7200
Electrical resistivity ($\mu\Omega$m)	0.5–1.1	0.07–0.12	0.1–0.14
Thermal expansion coefficient (10^{-6}/K)	6.6–11	17	17
Normal number of thermal cycles	> 10^5	> 10^4	> 5 × 10^3
Young's Modulus (GPa)	28–83	70–100	80–100
Shape memory transformation temperature (°C)	-200–200	-200–150	-200–200
Hysteresis (°C)	2–50	5–20	20–50
Maximum overheating temperature (°C)	400	150	300
Damping capacity (SDC%)	15–20	30–85	10–20
Grain size (μm)	1–100	50–150	25–100
Melting, casting and composition control	Difficult	Fair	Fair
Forming (rolling, extrusion)	Difficult	Easy	Difficult
Cold-working	Fair	Restricted	Very difficult
Machinability	Difficult	Very good	Good
Cost ratio	10–100	1–10	1.5–20

Table 3.2: Transition temperatures of NiTi (where M$_f$ is < 100°C), CuZnAl and CuAlNi compositions.

SMA	***Composition***	M_f °C	M_s °C	A_s °C	A_f °C	*Ref.*
NiTi						
	$Ti_{44}Ni_{47}Nb_9$	-175	-90	-85	-35	[36]
	$Ti_{49}Ni_{51}$	-153	-114	-89	-40	[36]
	$Ti_{49.5}Ni_{50.5}$	-78	-19	9	54	[36]
	$Ti_{50}Ni_{40}Pt_{10}$	-8	18	27	36	[36]
	$Ti_{49}Ni_{41}Cu_{10}$	8	30	35	50	[36]
	$Ti_{50}Ni_{45}Pt_5$	10	29	36	49	[36]
	$Ti_{50}Ni_{50}$	15	55	80	89	[36]
	$Ti_{48}Ni_{47}Zr_5$	20	65	75	138	[36]
	$Ti_{50}Ni_{40}Cu_{10}$	21	41	53	67	[36]
	$Ti_{43}Ni_{47}Zr_{10}$	45	100	113	165	[36]
	$Ti_{42.2}Ni_{49.8}Hf_8$	50	69	111	142	[36]
	$Ti_{40.7}Ni_{49.8}Hf_{9.5}$	61	90	118	159	[36]
	$Ti_{35.2}Ni_{49.8}Hf_{15}$	95	136	140	210	[36]
CuZnAl						
	69.8 wt%Cu-26.3wt%Zn-3.9wt%Al	-37	-17	-12	-5	[37]
CuAlNi						
	Cu-Al-Ni	224.4	230.2	231.8	242	[38]
	Cu-Al-Ni-0.99 wt% Mn	225.1	231.6	232.2	242.7	[38]
	Cu-Al-Ni-0.97 wt% Mn	230.85	238.4	239.9	248.9	[38]
	Cu-Al-Ni-1 wt% Co	241.3	248.1	249.7	258.9	[38]

Flight Heritage

Flight heritage of SMA-based actuation methods is present on the ALBus CubeSat [31, 39], as depicted in Figure 3.3. In this mission, the deployment of solar arrays was achieved using a mechanism actuated by SMAs. The deployment system utilized super-elastic SMAs composed of Ni-rich Nitinol ($Ni_{50.7}Ti_{49.3}$ (atomic%)). These SMAs were incorporated into a deployment mechanism consisting of an aluminum hinge system with steel and polyimide plastic components. One of these components was a spring steel latch hook, included to account for environmental factors such as temperature variations that could potentially influence the deployment angle of the solar arrays. The M_s of the super-elastic SMA was below 0°C [39] and the peak torque provided was 0.190 Nm within a temperature range of -20°C to 61°C. In addition to actuation, the SMA components facilitated power transfer between the solar panels and the satellite.

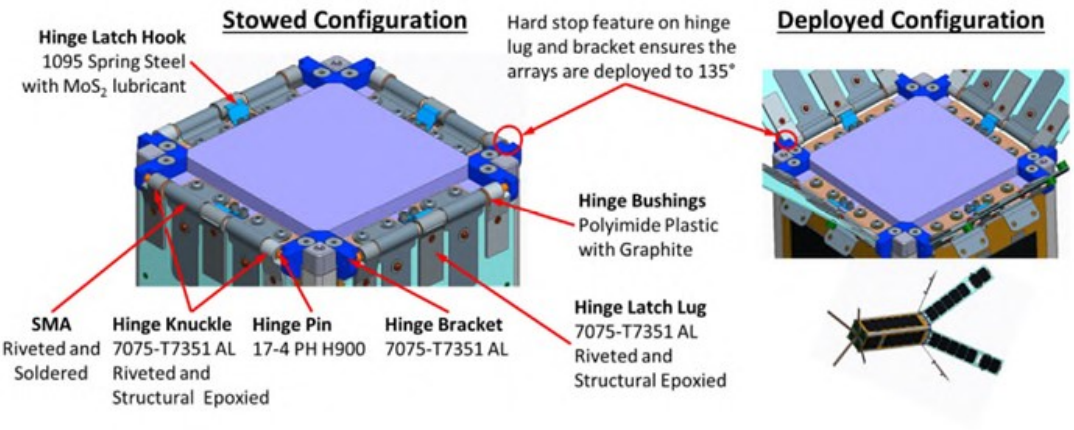

Figure 3.3: Detailed depiction of the deployment system of the solar panels onboard ALBus [39].

3.2.2. Tape Springs

Tape springs are thin metallic strips with a curved cross-section, also known as carpenter tape. Their curved cross-section is achieved by deforming a flat strip followed by a heat treatment. This process allows the tape spring to store strain energy when wound up and become stress-free when extended [40]. Figure 3.4 shows the cross-section of various types of thin metallic strips with a curved cross-section.

In this study, a distinction will be made between tape springs, STEMs (storable Tubular Extendible Mast) and lenticulars. As shown in Figure 3.4, three parameters are depicted: thickness t, curvature radius r and spanned angle θ_{TS}. Tape springs are thin metallic strips with a curved cross-section and a spanned angle that allows for an open section. Lenticulars are multiple tape springs intertwined into a configuration with a closed section. STEMs are metallic strips with a curved cross-section where the spanned angle is close to or exceeds $360°$, resulting in a (almost) closed section. These definitions of tape springs and STEMs are consistent with those mentioned in [41].

Although tape springs, lenticulars and STEMs have distinct structural characteristics, this study will focus primarily on tape springs as they are most relevant to the deployment system for the RABSII antenna. Applications for STEMs and lenticulars are typically restricted to deployment systems that require long boom structures [32], which is not the case for the RABSII antenna deployment system.

Tape springs can be classified as bi-stable and neutrally stable. A bi-stable tape spring has two different stable configurations: coiled and fully deployed. In the coiled configuration, strain energy is stored and released in its transition from the coiled to deployed configuration [42]. A neutrally stable tape spring is static in a continuum of positions without requiring external forces to remain stationary [43]. A small force can roll and unroll the neutrally stable tape spring. However, in the absence of this force, the tape

spring will remain static for prolonged periods of weeks or months [44].

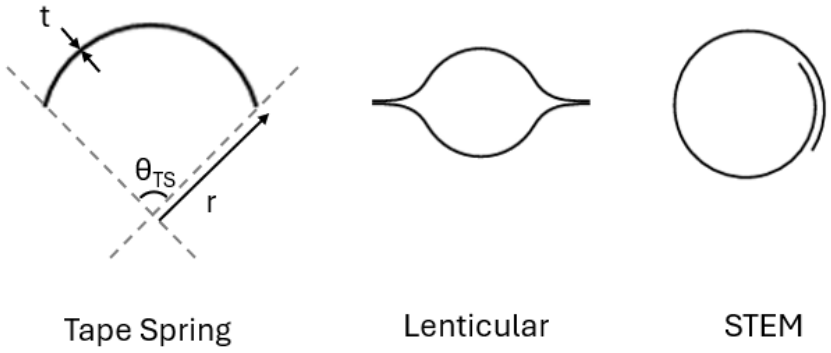

Figure 3.4: Cross-sections of a traditional tape-spring, a lenticular and STEM.

Applicable materials for tape springs include metals (e.g., beryllium copper and high-strength steel) or a wide array of dry fibers and prepregs with fabric-woven fibers (e.g., glass, carbon and aramid) [45]. For aerospace applications, single-ply plain woven fabrics made of CFRP (Carbon Fiber Reinforced Platsic) is widely used [46].

Tape springs are an attractive solution within the miniaturization process due to their unique properties. They are self-locking, relatively simple and do not require lubrication. Additionally, they can be folded elastically and possess structural characteristics that eliminate the need for bulky mechanical components or folding devices [47]. Their self-locking ability negates the need for complex and heavy-duty HDRMs and the lack of lubrication simplifies integration with other satellite systems as there is no risk of contamination or outgassing in space [48]. For neutrally stable tape springs, a controlled deployment (and retraction) can be achieved while remaining mass-efficient for their stiffness and strength [43].

Limitations of tape springs are primarily associated with their uncontrollable deployment. The inability to regulate the deployment speed of bi-stable tape springs, along with the resulting shock, results in a significant disadvantage. This is particularly critical for nanosatellites, which often lack an ADCS. The induced shock can generate unwanted angular accelerations and potentially cause tumbling. In the case of a neutrally stable tape spring, the need for an additional actuator to initiate deployment reclassifies it as a structural component rather than an actuation method. For both bi-stable and neutrally stable tape springs, the stiffness in the folded configuration is low, introducing uncertainties during deployment and forcing gravity compensation during ground testing.

Flight Heritage and Proposals

Deployable systems utilizing tape springs have been implemented on various nanosatellites [10, 12, 27, 49] and proposals for such systems have also been made [42].

The Delfi-C^3 utilized a tape spring in its modular antenna boxes to enable deployment (see Figure 2.3b). Similar systems were used on Delfi-n3Xt and served as the basis for a COTS dipole antenna [12]. Figure 3.5 depicts the dipole antenna developed by ISISpace, which has stowed dimensions of 9.8x9.8x0.7 cm^3. Elements of up to 50 cm in length can be deployed while maintaining a mass of less than 100 grams [12].

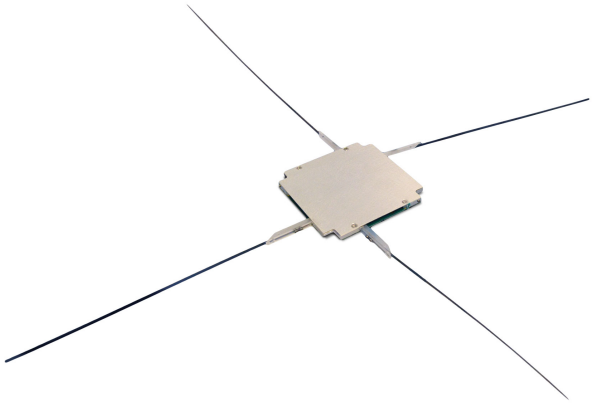

Figure 3.5: ISISpace dipole antenna system [12].

Figure 3.6 depicts a proposed 1-meter boom that can be stowed within a 1U CubeSat. By using bi-stable tape springs, the system achieves both structural integrity and actuation. In its stowed configuration, the system has dimensions of 5x3.8x3.8 cm^3 and a mass of 86 grams. Simulations indicate that an actuation force ranging from 2.7 N to 3.47 N, provided by the bi-stable tape springs, is sufficient for deployment [42].

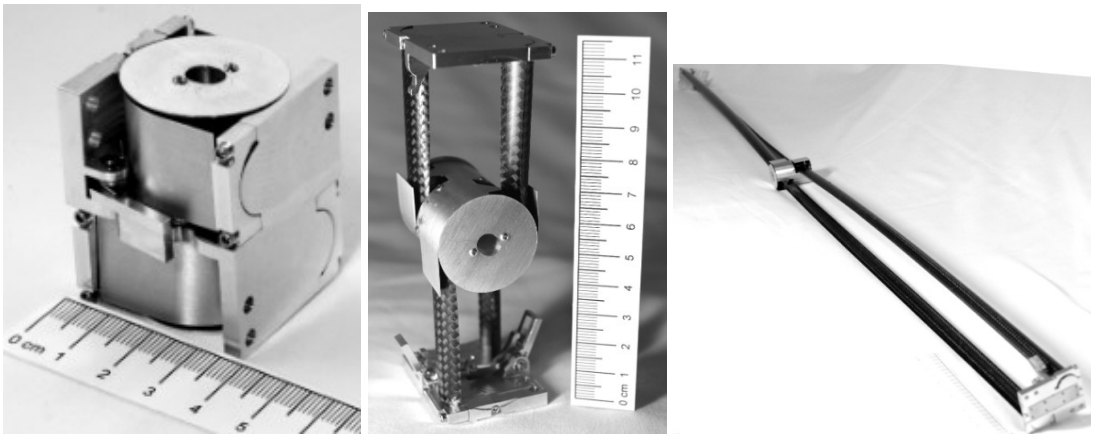

(a) Stowed configuration of the 1m boom **(b)** Initial deployment of the 1m boom **(c)** Fully deployed configuration of the 1m boom

Figure 3.6: Deployment stages of a 1m boom [42].

Figure 3.7 depicts the tape spring integration in a deployment system for ULMAAS (Ultra Light Mechanism for Advanced Antenna Systems) [49]. The system features a hinge-like mechanism that functions as a deployment system with embedded motorization, guidance, latching and pointing stability functionalities. It has a mass of 0.6 kg and fits within an envelope of 14x20x8 cm^3. For ULMAAS, four pairs of CFRP tape springs are used to ensure high pointing stability across a wide temperature range. The selection of CFRP tape springs was primarily driven by the favorable ratio between thermal conductivity and thermal expansion coefficient which was critical for achieving the desired performance [49].

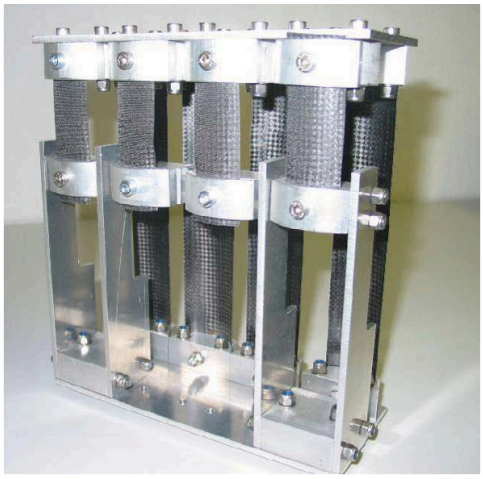

Figure 3.7: ULMAAS, a SOA tape-spring hinge [49].

3.2.3. (Torsion) Springs

Spring-based actuation methods are an overarching term for actuation methods that use extension, coil, constant force or torsion springs. Compared to Section 3.2.2 and Section 3.2.1, where more complex actuation methods with relatively complex working principles are described, spring-based actuation methods are simple and well understood. Their predictable behavior and ease of simulation significantly simplify the risk mitigation process. Additionally, spring-based deployment methods offer advantages such as cost-effectiveness, lightweight construction and compactness.

Limitations of spring-based actuation methods are primarily driven by their inherent behavior. The force exerted by a spring varies with its displacement, which can complicate the deployment process. Although constant-force springs are available to mitigate this issue, they do not eliminate variations in force output. Furthermore, springs are prone to fatigue from repeated cycling, which can alter their mechanical properties and increase the likelihood of failure over time.

Flight Heritage

Spring-based actuation methods have been implemented on various nanosatellites, including MARCo [50, 51] and RainCube [52]. On these satellites, torsion and constant-force springs were used to actuate the deployment of various appendages.

Figure 3.8 and Figure 3.21 depict the reflect-array antenna onboard MARCo, a 6U CubeSat. The spring-based actuation method included spring-loaded winglet panel hinges and 90° spring-loaded root hinges [50]. These were used to deploy the reflect-array antenna and solar arrays. It is assumed that torsion springs were used based on their function within the deployment system.

Figure 3.9 shows the deployment sequence of the KaPDA (Ka-band Deployable Antenna for CubeSats), a reflector-based antenna used in RainCube [52, 53]. The deployment system utilized a constant-force spring-based actuation method to ensure the full deployment of the antenna ribs. In addition to the constant-force springs, design iterations demonstrated the need to attach kick-off springs to enhance deployment reliability [54].

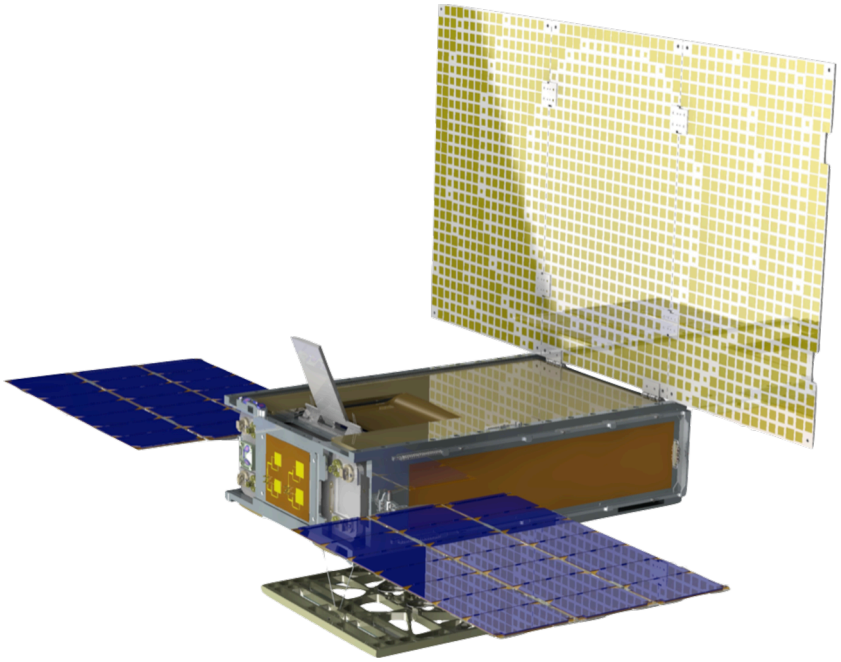

Figure 3.8: Reflect-array antenna onboard the MarCO CubeSat [50], used for planetary exploration.

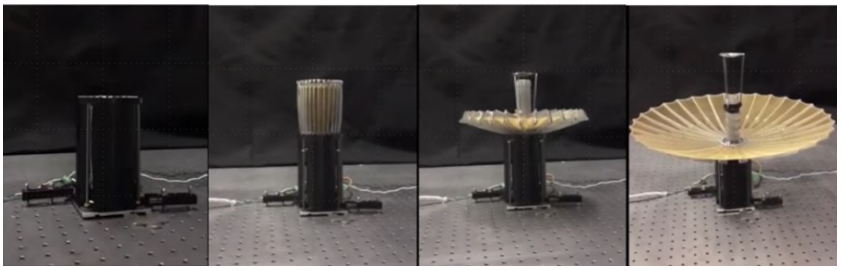

Figure 3.9: Spring-based deployment of the reflector-based antenna onboard the RainCube CubeSat[52].

3.3. Hold-down and Release Mechanism

Hold-down and Release Mechanisms (HDRMs) are mechanisms designed to hold appendages in their stowed configuration until the satellite is in orbit. HDRMs prevent premature deployment of appendages under unfavorable conditions. The release of an HDRM requires an external command or certain environmental parameters to be met. This section will discuss various types of HDRMs, providing relevant flight heritage, proposals and COTS examples. The types of HDRMs covered include burn wire, SMA-based, frangibolts, paraffin and piezoelectric. Each mechanism will be evaluated for its functionality, advantages and application scenarios.

3.3.1. Burn Wire

A burn wire mechanism is an HDRM that uses a thermal knife (an electrically heated wire) to cut through a restraining material. The wire, made from a high-resistance material, generates heat when an electrical current passes through it, enabling it to act as a thermal knife. In aerospace applications, commonly used high-resistance materials include Nichrome (Nickel-Chromium) and Kanthal A1 [55, 56]. Important material properties of Nichrome and Kanthal A1 are presented in Table 3.3. Based on these material properties, it can be concluded that achieving high temperatures quickly is more efficient when using Nichrome, while higher operating temperatures can be achieved with Kanthal A1. Kanthal A1 has better oxidation resistance, which translates to a longer lifespan [57]. These characteristics allow for the selection of the most suitable material for the specific requirements of a mission, balancing factors such as response time, durability and environmental conditions.

	Kanthal A1	***Nichrome 60-15***
Density, ρ, $kg.m^{-3}$	7100	8200
Tensile yield strength, σ_{yield}, GPa	220	220
Melting point, T_m, $^{\circ}C$	1500	1390
Max. service temperature, T_{mst}, $^{\circ}C$	1400	1150
Specific heat capacity, c_p, $J.kg^{-1}.K^{-1}$	460-800	480
Thermal Conductivity, Λ, $W.m^{-1}.K^{-1}$	11-35	13

Table 3.3: Properties of Kanthal A1 (T_{range}: 20–1400°C) [57] and Nichrome (Nichrome 60-15) [58].

For the restraining material in a burn wire mechanism, the melting point must be below the T_{mst} of the heated wire but higher than the environmental operating conditions. High yield and tensile strength combined with low creep over time are desirable properties for the restraining material. SOA burn wire mechanisms often use restraining materials such as Dyneema [59], nylon [56], or Vectran [60].

Figure 3.10 provides an example of a burn wire mechanism, depicting both the Nichrome wire (thermal knife) and the Vectran tie (restraining material). In addition to the depicted thermal knife and restraining material, a simple burn wire mechanism only requires a burner circuit and power supply. This makes it an inexpensive (20–160 euros [60]), lightweight (<20 grams [61]) and quick (<15 s [55, 56, 61]) HDRM.

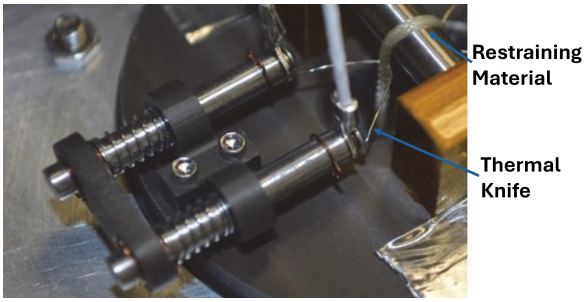

Figure 3.10: Assembly of a burn wire mechanism, consisting of a Nichrome wire (thermal knife) and a Vectran cable (retention wire) [60].

Integrating a burn wire mechanism on satellites requires careful consideration of both outgassing, as well as thermal and power requirements. Both the PocketQube and CubeSat standards impose strict limits on the emission of fumes during all deployment stages, to prevent contamination of the satellite environment [1, 5]. Even when (low) outgassing is allowed, such as in orbit, the potential release of fumes can pose a risk to sensitive payloads. Thermal management is equally critical, as the burn wire mechanism can reach temperatures exceeding 200°C during operation. This necessitates careful design to prevent heat from damaging nearby components or compromising the satellite's thermal stability. Power requirements must also be considered, as the mechanism requires sufficient energy to quickly heat the wire to its operational temperature. Lastly, the manual assembly process for the burn wire mechanism introduces the risk of over- or under-tightening the restraining material. Over-tightening may lead to material or deployment failure, while under-tightening could result in unreliable deployment or damage during transportation.

Flight Heritage and Proposals

Burn wire mechanisms have been used on various satellites [20, 55] and proposed for others [56, 61].

Figure 3.11 depicts both the deployed and stowed configurations of an antenna on the BIRDS-2, a 1U CubeSat. Two monopole antennas were secured using a burn wire mechanism, with polyethylene wire serving as the restraining material and Nichrome wire as the thermal knife. The polyethylene and Nichrome wires were positioned on the exterior of the satellite, while the burner circuit and power source

were housed inside. Pre-launch experiments demonstrated that deployment could be initiated within 5 seconds using the burn wire mechanism. However, to reduce the risk of incomplete deployment, the activation time was doubled while maintaining the same current of 2.75 A [55]. This approach ensured reliable deployment while minimizing potential operational risks.

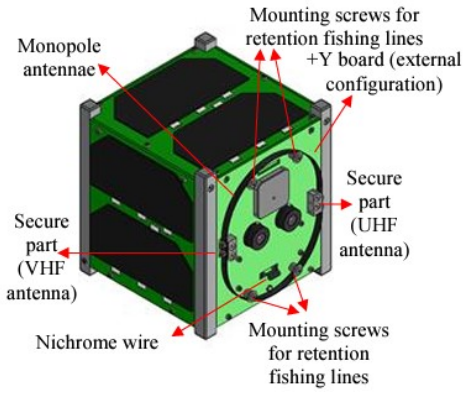

(a) Stowed configuration of BIRDS-2 deployment system [55]

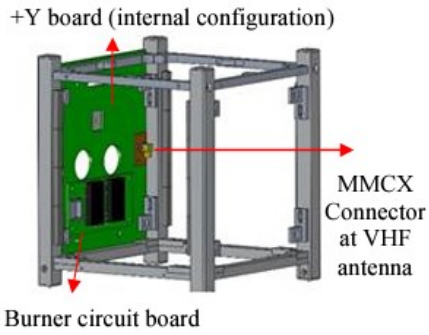

(b) Internal view of the deployment board of BIRDS-2 [55]

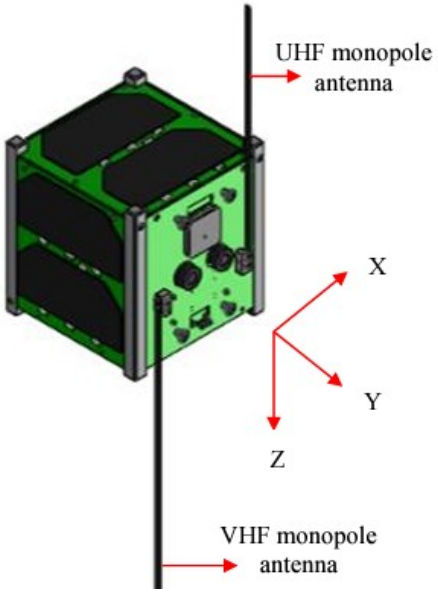

(c) Deployed configuration of BIRDS-2 deployment system [55]

Figure 3.11: Antenna System of BIRDS-2 in both stowed and deployed configuration [55].

The Delfi-PQ, shown in Figure 2.5, also used a burn wire mechanism to prevent premature deployment. For its antenna, which used a spring-based actuation method, the burn wire mechanism consisted of a Dyneema wire as the restraining material and a resistor (of which the material is not specified) as the thermal knife. A temperature of 140°C for the thermal knife was sufficient to ensure successful deployment [20].

Proposals for deployment systems utilizing burn wire mechanisms are also prevalent. One such system involved the deployment of an optical baffle on a nanosatellite, where a burn wire mechanism was used as the HDRM. This mechanism used Kanthal A1 as the thermal knife and a 0.5 mm thick nylon wire as the restraining material. Extensive testing demonstrated that the HDRM failed after 29 cycles when it was power cycled between a temperature range of 35°C to 245°C while holding a lateral load of 20 N [56].

Figure 3.12 shows a proposed system which combines a spring-based actuation method with a burn wire mechanism. In this design, a 0.2 mm nylon wire was used as the restraining material and a 4.7 Ω resistor as the thermal knife. The restraining material had a yield force of 57.88 N. Under ambient conditions of 20°C, deployment was achieved after 6.1 seconds, with the resistor reaching a temperature of 104°C [61, 62]. These proposals demonstrate the versatility and reliability of burn wire mechanisms when integrated with various deployment systems.

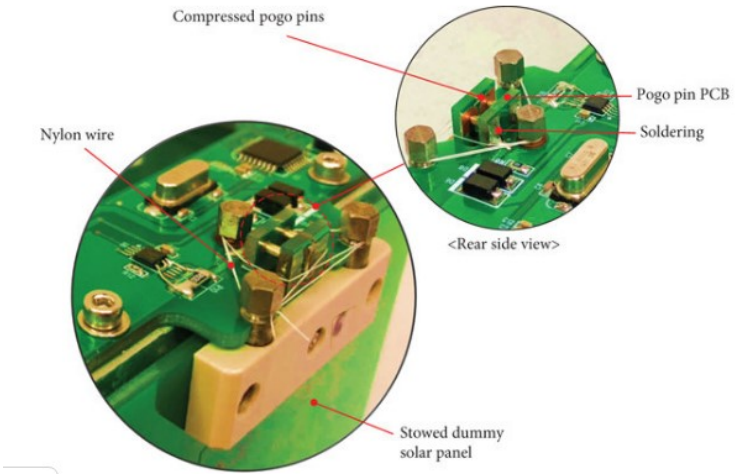

Figure 3.12: Burn wire mechanism for the deployment of a solar panel (design proposal) [62].

3.3.2. Shape Memory Alloy (HDRM)

In Section 3.2.1, the properties of SMAs, along with their applications and flight heritage as actuation methods, are discussed. SMAs have also been implemented as HDRMs in nanosatellites [31, 39] and proposed for future missions [63]. Even COTS SMA-based HDRMs have been developed [64, 65].
This section introduces various implementations of SMAs in HDRMs, with the exception of frangibolts, which are discussed in Section 3.3.3. The implementations discussed include pin-pushers (Figure 3.15a), pin-pullers (Figure 3.15b) and a patented SMA wire actuator (Figure 3.13).

SMA-based HDRMs offer several advantages, making them suitable for nanosatellite applications. They can generate large forces while adhering to the strict power, mass and volume constraints of nanosatellites [63]. Additionally, SMAs operate effectively across a wide temperature range, from -140 to 500°C [39]. Unlike burn wire or frangibolt mechanisms, SMA-based HDRMs discussed in this section do not produce any space debris [31].

Implementation of SMA-based HDRMs is complicated. Their integration into specific use cases is often complex and requires a high level of understanding of the mechanism's design and operation. While they can generate significant forces, the displacement length is relatively limited, typically achieving only a 4–8% increase in length [66, 63]. Furthermore, although SMA-based HDRMs are resettable, they are susceptible to cycling fatigue, which must be carefully considered during the design and testing phases to ensure long-term reliability.

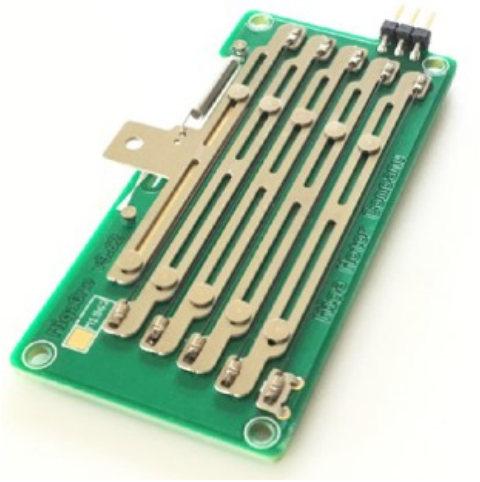

Figure 3.13: Patented SMA wire actuator used on the ALBus CubeSat [31, 66].

Flight Heritage, Proposals and COTS Examples

Figure 3.13 shows the two-stage SMA-based pin-puller mechanism used on the ALBus, a 3U CubeSat. This HDRM, which was used for solar array deployment, uses an SMA wire actuator to achieve a displacement of 7.11 mm. The SMA material, weighing 8 grams, consisted of a Nickel, Titanium, Lead and Platinum alloy ($Ni_{19.5}Ti_{50.5}Pd_{25}Pt_5$), allowing for a release within 10 seconds while consuming 18 W of power. The relevant components of the SMA-based HDRM—namely the SMA wire, guides and base plate—had a combined mass of 30 grams [31, 39].

Figure 3.14 shows a proposed design for a deployment system for solar panels on a CubeSat. A combination of a mechanical and SMA-based spring enables the hook to move when the temperature rises. With the contraction force of the mechanical spring at 6 N, the SMA-based springs can enable displacement of the hook while consuming only 1.9 A at 3.3 V for 10 seconds [63].

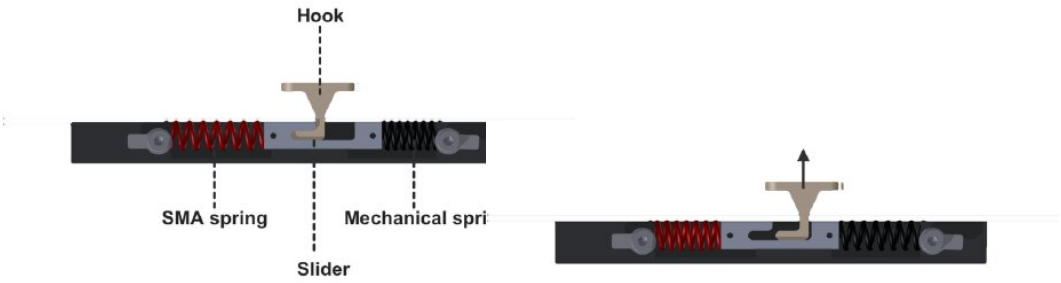

(a) Closed configuration of a SMA-based HDRM [63] **(b)** Open configuration of a SMA-based HDRM [63]

Figure 3.14: HDRM designed for solar panel deployment onboard CubeSat which utilizes an SMA to move a hook [63].

Besides the provided SMA-based flight heritage [31] and proposed designs [63], COTS examples of SMA-based HDRMs are also available:

- DCUBED Nano Release Nut (Figure 3.15a): 12 g and 17x17x17 mm^3. The HDRM can operate at temperatures from -65°C to 75°C, is resettable and has a TRL of 9 [64].
- EBAD Nano P5 Pin Puller (Figure 3.15b): 18 g, ⌀23.5x25.4 mm^3. The HDRM can operate at temperatures from -65°C to 70°C, is resettable and has a pull force of 22 N [65].

(a) DCUBED Nano Release Nut, SMA-based HDRM designed for space applications [64]

(b) EBAD Nano P5 Pin Puller, SMA-based HDRM designed for space applications [65]

Figure 3.15: Examples of COTS SMA-based HDRMs which are applicable for space applications.

3.3.3. Frangibolt

A frangibolt is an HDRM capable of precisely fracturing a notched bolt without the use of pyrotechnics. Figure 3.16a depicts the components of a frangibolt: a heater, a notched bolt and an SMA cylinder. The heater element, powered by an electrical current, heats the SMA cylinder, causing it to return to its pre-deformed shape. The SMA cylinder, typically made of Nitinol (see Table 3.2), is pre-compressed at a lower temperature and elongates when heated. During this elongation, the SMA cylinder can exert forces of several kilonewtons [67]. The notched bolt, made of a material with a low elongation-to-failure rate, fractures under the force generated by the SMA cylinder. As the cylinder elongates, it strains the bolt beyond its ultimate tensile limit, causing it to fail. Materials such as stainless steel are commonly used for the bolt due to their low elongation-to-failure properties [68, 69]. Figure 3.16b illustrates this process.

Frangibolts provide a reliable and non-pyrotechnic solution for severing high-strength bonds. Previously, severance of high-strength bonds was often achieved using pyrotechnic alternatives, which posed risks and introduced shocks to the system [69].Unlike their pyrotechnic counterparts, they are resettable and reusable [70]. Current COTS and SOA frangibolts can fit within a 2.2x2.2x3.5 cm^3 volume and weigh less than 30 g [67]. Furthermore, frangibolts are more reliable and precise, allowing for smoother integration into satellite applications and testing plans.

Despite their advantages, frangibolts have some limitations. A specialized hydraulic tool is required to reset the frangibolt, increasing the initial cost. While the ability of a frangibolt to output large forces can be beneficial in certain applications, this capability is often unnecessary for nanosatellite missions. Lastly, their precise control is accompanied by slow release speeds, with a release time of approximately two minutes [59].

Flight Heritage and COTS Examples

Since large output forces are rarely required in nanosatellite applications, relevant flight heritage is limited. However, examples of frangibolt usage have been documented on the OSIRIS-REx [71] and DICE [72] missions. Additionally, COTS examples have been developed by LEAT [67] and EBAD [70, 73].

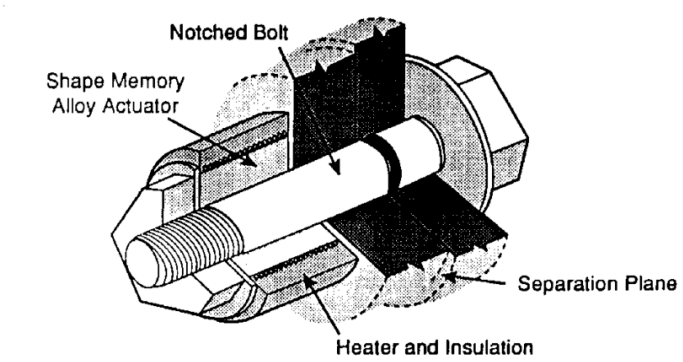

(a) Basic design of a frangibolt HDRM[69]

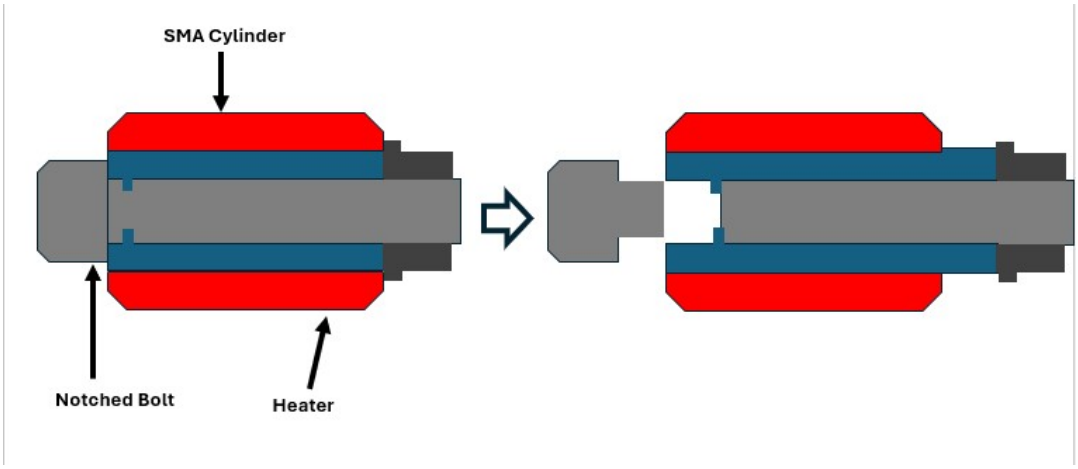

(b) Basic principle of a frangibolt, exaggerations are made on dimensional changes of the SMA. Inspiration drawn from [67]

Figure 3.16: Basics of the Frangibolts HDRM.

OSIRIS-REx, a large-scale satellite, uses frangibolts as the HDRM for the radiation cover of a payload instrument. Since the bond between the satellite and the radiation cover needed to be severed after several years, reliability and a low chance of degradation were the driving factors for selecting a frangibolt as the HDRM. The chosen frangibolt can output 2450 N with a stroke of 1 mm, extending from 12.7 mm to 13.7 mm. The testing process demonstrated that while deployment times varied under constant pre-load, voltage (9–10 V) and ambient temperature conditions, the variations were not significant enough to raise concerns. At an ambient temperature of 25°C, deployment was completed within one minute, while at temperatures below -30°C, deployment times ranged from 30 to 180 seconds [71].

Figure 3.17a shows the COTS EBAD TiNi mini frangibolt, which was utilized in the DICE mission, a CubeSat project consisting of two identical 1.5U CubeSats. The frangibolts were used to secure the scissor booms and antennas, ensuring they remained stowed during launch. The deployment system successfully released these components 50 minutes after ejection from the launch pod [72].

Figures 3.17a and 3.17b show examples of COTS frangibolts [67, 70, 73]. These frangibolts can output forces between 1650 N and 6277 N within an envelope of $\varnothing$22x30.5 mm^3. While deployment times vary slightly among these frangibolts, the variation is minimal, typically ranging between 20 and 50 seconds. Additionally, these frangibolts are designed to operate reliably within a temperature range of -50 to 80°C.

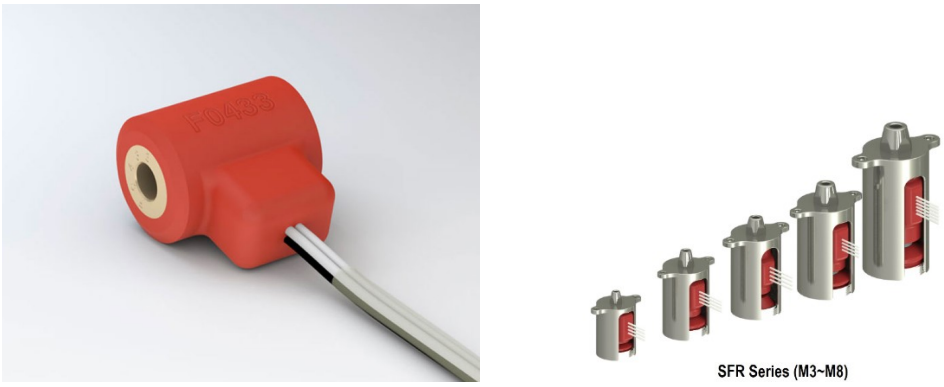

(a) EBAD TiNi mini Frangibolt [73] used on several CubeSats, such as the DICE [72]

(b) LEAT SMA-based SFR-series Frangibolts, designed for Space applications [67]

Figure 3.17: Examples of COTS Frangibolt HDRM which are applicable for space applications and/or have been used in space applications.

3.3.4. Paraffin HDRM

Paraffin HDRMs are a type of phase-changing HDRM that uses the thermal expansion of paraffin during a phase-transition between the solid and liquid state. Figure 3.18 illustrate the basic principle where the thermal expansion within an enclosed chamber forces out a rod. While six elements are depicted in Figure 3.18, the mechanism can be simplified to three primary components: the encasing with the paraffin, a rod and a heater element.

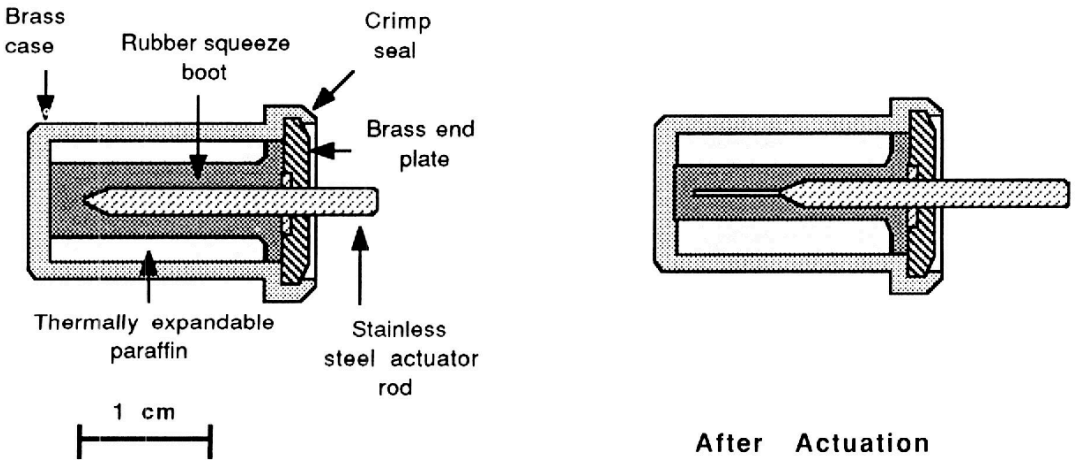

Figure 3.18: Basic principle behind a paraffin HDRM [74]

The process in a paraffin HDRM relies on the thermal expansion of paraffin during its phase transition, allowing it to be resettable and providing a high output force-to-weight ratio (e.g., 156 N at 35 grams [75]). Additionally, the limited number of moving components in this HDRM contributes to its high reliability while maintaining its reset capability.

Paraffin HDRMs have several disadvantages. The deployment speed is constrained by the performance of the heaters, making the process time-consuming (e.g., 200 seconds under advantageous conditions [75]). The stroke length is limited by mechanical factors, such as deployment system design and available volume. Within smaller envelopes, the stroke length of the HDRM is reduced. In addition to challenges related to thermal management and power requirements, the reliance on temperature changes for the phase transition makes the paraffin actuator susceptible to environmental temperature fluctuations. These fluctuations can impact performance and must be accounted for during the design phase.

Flight Heritage and COTS Examples

Figure 3.19 shows the Sierra Space EH-3525 High Output Paraffin actuator, an HDRM used on several space missions, e.g., Cassini-Huygens, SOHO (Solar and Heliospheric Observatory) and MUSES (Multi-User System for Earth Sensing) [75]. With a mass of 35 g and dimensions of ⌀14.2x42.42 mm^3, this paraffin actuator can output 156 N with a full stroke length of 63.5 mm. Its operating temperature range of -60 to 80°C and an actuation time of 200 seconds at 24°C when provided 5 W at 28 V, make it suitable for a wide variety of space missions [75].

Figure 3.19: Sierra Space EH-3525 High-Output Paraffin actuator, an HDRM which has been used for several space applications [75].

Paraffin HDRM implementation on nanosatellites has been limited. MiniCOR, a 6U CubeSat, briefly mentions the usage of a pin-pulling paraffin HDRM embedded within its boom deployment system [76]. However, specific details regarding the design, performance, or operational characteristics of the HDRM have not been provided.

3.3.5. Piezoelectric HDRM

Piezoelectric HDRMs operate by utilizing the piezoelectric effect: a phenomenon where certain crystalline materials can convert mechanical stress into electrical current, and vice versa [77]. These mechanisms are capable of achieving small, ultra-precise and rapid displacements (<10 seconds [78]) while delivering high output forces within a compact form factor [79]. Their use in nanosatellite applications remains limited due to the high voltage required to produce sufficient displacements. These voltage demands can reach several hundred volts, often rendering piezoelectric HDRMs infeasible for nanosatellites [80].

Flight Heritage

Although piezoelectric HDRMs are not widely used and detailed specifications of their performance are scarce, the following two examples of their use in space applications have been identified [78, 81].
PEASS, a 3U CubeSat, utilizes piezoelectric elements for various roles, such as the deployment of side panels and the pointing of instruments [81].
Another example is a proposal for a Ka-band deployable antenna that uses various piezoelectric HDRMs to enable the initial stages of deployment [78]. Unfortunately, neither example provides comprehensive data on performance, design, or operational characteristics.

3.4. Stowage Methods

To enable the deployment of complex appendages, it is essential to research suitable stowage methods. These methods allow the components of the deployable appendage to be stowed within a small volume, optimizing packaging efficiency without hindering or unnecessarily complicating the deployment process. For the RABSII instrument, the primary components affected by the stowage method will be the antenna elements.

As outlined in Section 2.2.1, the RABSII instrument consists of a dipole antenna with elements up to 2.5 m in length, based on a frequency band of 28 MHz. The latest design iteration of the RABSII antenna expects each element to consist of a short FR-4 plate combined with a Nitinol (SMA) wire of ⌀0.3 mm. The majority of the deployed length, which would benefit the most from a stowage method, will be the SMA wire component of the RABSII antenna. Implementing an efficient stowage method for this component is crucial to ensure successful deployment. However, as stakeholders have already defined the stowed configuration, this section will focus on exploring applicable stowage methods and researching their integration with the corresponding actuation method and HDRM. The objective is to gain insight into how these components can be effectively combined to achieve a functional and efficient deployment system.

3.4.1. Parallel Stowage Method

The parallel stowage method refers to a configuration where the sub-elements of an appendage are stowed parallel to each other. These sub-elements can include rods, wires, or even sheets. Often positioned on the external surfaces of the satellite, these elements are arranged either parallel (Figure 3.20a) or perpendicular (Figure 3.20b) to the satellite's longitudinal axis. This method is frequently used to optimize the available space while maintaining simplicity in deployment.

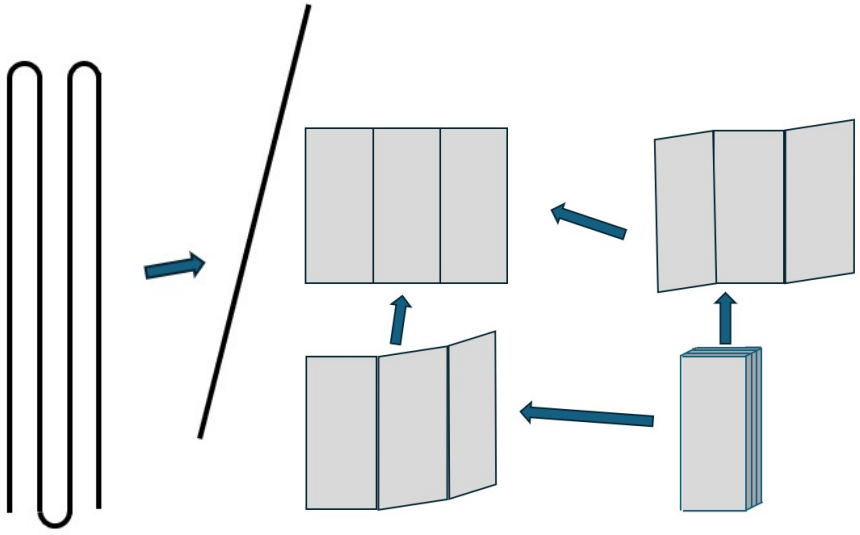

(a) Abstract depiction of parallel sideways configuration of a wire

(b) Abstract depiction of parallel stacked configuration with two different folding styles eventually deploying in the same solar panel

Figure 3.20: Depiction of parallel stowage methods applicable for panels, wires or rods.

When applying the parallel stowage method, expanding the deployed dimension is relatively straightforward. This can be achieved by increasing the number of sub-elements, with deployment relying on repeated unfolding techniques. However, increasing the number of elements can occupy large sections of the satellite's external area. This is accompanied by an increased risk of failure during folding and unfolding sequences, particularly for large structural appendages which are inherently more prone to deployment issues. To mitigate these risks, in-depth analysis is required to assess potential failures and prevent system malfunctions due to incomplete deployment. Incorporating redundancy into the design might be necessary to enhance reliability, although this will increase the mass, volume and complexity of the system.

Flight Heritage

Figure 3.8 and Figure 3.21 depict the stowed and deployed configurations of the onboard solar array and high-gain antennas of MarCo, a 6U CubeSat. The parallel stowage method was used due to the large surface area of the high-gain antenna (59.7x33.3 cm^2). The folding technique employed is similar

to that shown in Figure 3.20b, with deployment performed using distinct hinges [50, 51].

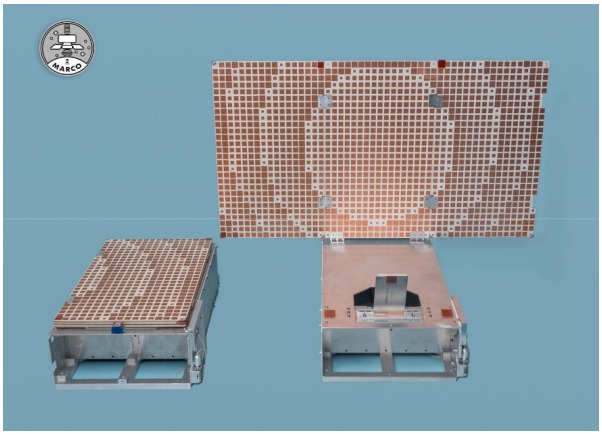

Figure 3.21: Flight model of the MarCO Antenna, which uses a parallel stowage method [50].

Figure 3.22 depicts the deployment sequence of the solar array and reflectarray antenna of ISARA (Integrated Solar Array and Reflectarray Antenna), a 3U CubeSat. This dual-use appendage serves as both a solar array on one side and a reflectarray antenna on the other. A total of seven panels, each measuring 8.3x34 cm^2, were stowed on three of the satellite's four external side panels. When fully deployed, the system achieved a combined surface area of 60.76x34 cm^2, with a hinge gap of 1.13 cm [82, 83].

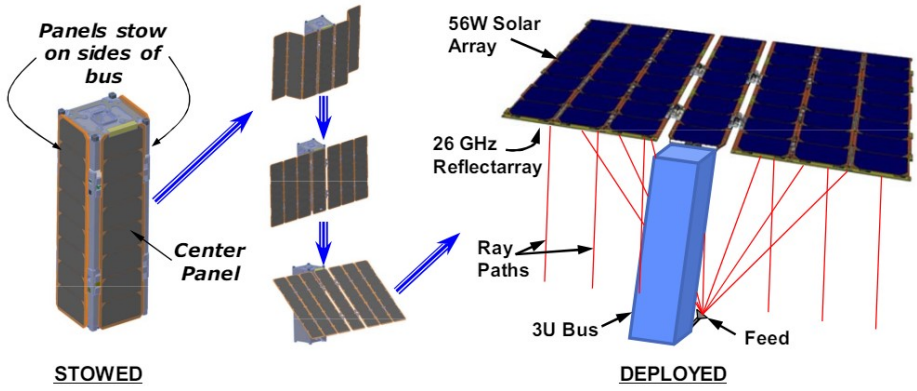

Figure 3.22: Stowed and deployed configuration of the reflect-array antenna and solar-array onboard ISARA [82].

3.4.2. Rotational Stowage Method

Rotational stowage methods involve stowing elements around an axis of rotation, a method commonly used for wire or tape spring systems due to its ability to achieve a compact stowed configuration.

The main distinction in rotational stowage methods lies in the external forces required to maintain the stowed configuration. In the **spooled configuration**, the element is rotated around a circular structural mechanism without an encasing, as the outward forces are negligible. Conversely, the **coiled configuration** forces the elements into a rotational shape, where they exert outward pressure. Without an encasing, the coiled system deploys aggressively, requiring a stronger HDRM to keep it stowed.

Rotational stowage methods have the advantage of storing long elements in compact volumes. For spooled configurations, the lack of a requirement for a strong HDRM reduces the weight of the deployment system, as lightweight HDRMs are sufficient. Coiled configurations benefit from their inherent

outward forces, which reduce or eliminate the need for actuation methods. This is especially advantageous for larger systems, as smaller actuation methods can suffice. Furthermore, since the coiled configuration exerts outward pressure, it naturally releases the maximum amount of tension and pressure within its encasing. This enhances resistance to failures caused by prolonged storage periods by minimizing stress buildup and potential degradation of the stowed elements.

However, rotational stowage methods also have disadvantages. Both configurations require additional components, increasing the system's power, mass and volume requirements. Spooled configurations require a rotational structure to wrap the wire, while coiled configurations require an encasing to counteract the outward force. Coiled configurations, due to their aggressive deployment nature, necessitate stronger HDRMs and mechanisms to control deployment speed. Additionally, forcing elements into a rotational shape can introduce unwanted stresses, increasing the risk of failure in both tape springs and wires. Pre-tensioning in spooled configurations can lead to plastic deformation, such as kinks, when stowed for extended periods. Finally, due to the inherent design of rotational stowage methods and their often preferred placement on satellites, particularly on external side panels, additional mechanisms are required to ensure proper functionality.

Flight Heritage

Figure 3.23 shows a crossed dipole antenna stowed within an envelope of 10x10x2.2 cm^3 with a mass of 450 grams. A spooled configuration was used to stow the antenna elements, each measuring 3 meters in length. Deployment was achieved using a tape spring-based actuation method [84].

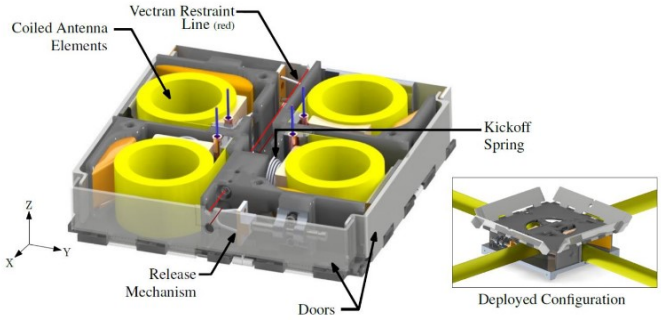

Figure 3.23: Stowed and deployed configurations of the coiled stowage of a 6 m cross-dipole antenna [84]

Figure 2.3a shows the modular antenna boxes of the Delfi-C^3, where a coiled configuration was used to stow antenna elements measuring 18 cm and 50 cm. As discussed in Section 2.1.1, prolonged stowage and the stresses induced by encasing the elements led to warping, demonstrating a potential drawback of the coiled configuration when used over extended periods within small volumes.

4

Design Exploration for the Deployment System

The design development process follows a systematic and structured approach. First, general terminology is introduced, which will be consistently applied throughout this research. This is followed by the definition of the deployment system requirements and key performance parameters. Once these have been established, a comprehensive design option tree is constructed, in which each option is evaluated based on its feasibility within the constraints of the Delfi-Twin mission.

4.1. Terminology and Definitions

Throughout this research, several terms appear frequently and have specific definitions. These are outlined below:

RABSII Antenna: The RABSII antenna is a scientific instrument developed by Dr. Vanhamel. References to the ”RABSII antenna” specifically refer to the antenna instrument itself, excluding the deployment system.

RABSII Antenna Element: The current design of the RABSII antenna follows a dipole configuration, which consists of two poles of equal length. The term ”RABSII antenna element” refers to a single pole of the dipole antenna.

Deployment System: The deployment system consists of the deployment mechanism, actuation method and HDRM. It enables the deployment of the RABSII antenna and is analyzed per individual RABSII antenna element.

Antenna System: The antenna system refers to the complete antenna assembly onboard the satellite. In this research, it typically encompasses both RABSII antenna elements and their corresponding deployment systems.

Folded and Unfolded These terms refer to the configuration states of the RABSII antenna elements. In the folded state, the elements remain in their stowed configuration (see Section 3.4.1). In the unfolded state, the elements are fully deployed, extending to a total length of 2.5 m.

Longitudinal and Lateral axis: Figure 4.1 depicts the longitudinal and lateral axes of the Delfi-PQ. These definitions also apply to the Delfi-Twin and any other host satellite conforming to the CubeSat or PocketQube standards.

External Top Panel: The term 'Top Panel' refers to any external surface of the satellite that lies parallel to the lateral axis. Contrary, the term 'Side Panel' refers to any external surface that lies parallel to the longitudinal axis.

External Side Panel: The term 'Side Panel' refers to any external surface of the satellite that lies parallel to the longitudinal axis.

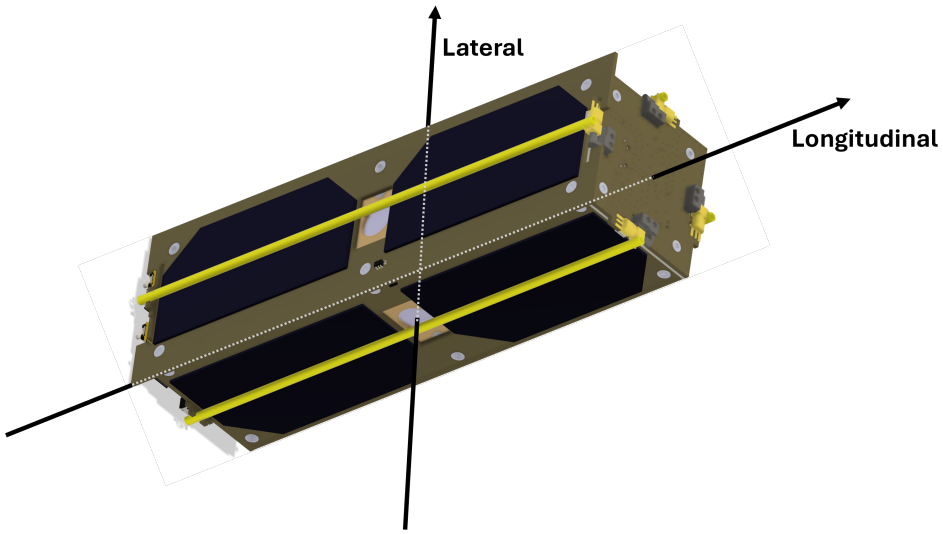

Figure 4.1: Longitudinal and lateral axis of the Delfi-PQ

4.2. Deployment System Requirements

Before identifying potential design concepts, it is essential to define a comprehensive list of design requirements. These requirements are primarily derived from various stakeholder expectations. Each requirement is assigned a unique identifier and a rationale to ensure both clarity and justification.

4.2.1. Identifiers

To ensure traceability and maintain consistency throughout this study, distinct identifiers are assigned to each requirement. While these identifiers primarily aid in organizing the requirements by category, they also allow for prioritization based on their significance.

The identifier format follows the structure XXX-YY-NUM, where the first three characters represent the type or subsystem to which the requirement relates. The prefixes of the main types/subsystems currently used in the requirement list are summarized in Table 4.1.

Prefix	Type/Subsystem
GEN	General Requirements
MIS	Mission Requirements
BDG	Budget Constraints
SFT	Safety Requirements
MAT	Material Requirements
STR	Structural Requirements

Table 4.1: Definition of type/subsystem prefixes used in requirement identifiers.

Next, the two characters in the YY-prefix indicate the priority of the requirement based on the MoSCoW prioritization method, as detailed in Table 4.2.

Prefix	MoSCoW Method	Rationale
MH	Mo	Must-Have, a non-negotiable requirement
SH	S	Should-Have, important but not vital
CH	Co	Could-Have, desirable but non-essential
WH	W	Want-to-Have, no priority, often cosmetic

Table 4.2: Definition of prioritization prefixes used in requirement identifiers based on the MoSCoW method.

The final prefix, NUM, indicates a sequential numerical identifier to ensure the uniqueness of each requirement. This prefix ranges from 001 to 999, allowing for the identification of up to one thousand distinct requirements.

4.2.2. General Requirements

The general design requirements outlined in Table 4.3 aim to ensure that the deployment system meets its primary objectives. Requirements **GEN-MH-001** and **GEN-MH-002** specify the basic integration of the deployment system with the Delfi-Twin and the RABSII antenna, both of which are integral to the mission's success. More detailed integration requirements are elaborated in **GEN-CH-005**, **GEN-MH-006**, **GEN-CH-007** and **GEN-CH-008**.

GEN-CH-006, **GEN-CH-007** and **GEN-CH-008** have a distinct level of importance compared to **GEN-MH-001**, **GEN-MH-003** and **GEN-MH-006**. The ability of the deployment system to accommodate varying stowed configurations of the RABSII antenna (**GEN-CH-005**) is important, but not critical for mission success. Meanwhile, the integration of communication and electrical interfaces (**GEN-CH-006** and **GEN-CH-007**) is desirable, but non-essential, offering flexibility in the design process.

Besides requirements defining the integration of the deployment system with the Delfi-Twin and the RABSII antenna, the deployment environment is specified in **GEN-MH-006**. Notably, **GEN-MH-005** includes integration with the launch deployer, as the deployment system must be self-constrained and not dependent on the launch deployer. This is derived from the PocketQube Standard's PQ-Mech-10 [5]. **GEN-MH-002** and **GEN-MH-003** specify the role of the actuation method of the deployment system, where deployment system must be capable of deploying the stowed RABSII antenna. Deploying an unfolded RABSII Antenna requires a significantly larger torque (specified in Appendix A), with further insights provided in the risk analysis. Lastly, **GEN-MH-009** addresses structural integrity, ensuring that the deployment system stays within safe operational limits throughout every mission phase. This is derived from PQ-Mat-01 of the PocketQube Standard, which outlines the need for materials to withstand environmental testing to ensure mission viability [5].

ID	*Requirement*	*Rationale*
GEN-MH-001	The Deployment System shall be compatible with the Delfi-Twin.	Self-derived, based on the objective of the deployment system.
GEN-MH-002	The Deployment System shall be compatible with the RABSII Antenna.	Self-derived, based on the objective of the deployment system.
GEN-MH-003	The Deployment System shall be capable of deploying the stowed RABSII Antenna in orbit	Self-derived, based on the objective of the deployment system.
GEN-SH-004	The Deployment System shall be capable of deploying the unfolded RABSII Antenna in orbit	Self-derived, based on the objective of the deployment system.
GEN-CH-005	The Deployment System shall accommodate varying stowed configurations of the RABSII antenna.	Self-derived, based on the uncertainties in the design of the RABSII antenna.
GEN-MH-006	The Deployment System shall include an HDRM.	Based on PQ-Mech-10 [5].
GEN-CH-007	The Deployment System shall accommodate communication interfaces required for the operation of the RABSII antenna.	Self-derived, based on ensuring functionality of the RABSII antenna.
GEN-CH-008	The Deployment System shall accommodate electrical interfaces required for the operation of the RABSII antenna.	Self-derived, based on ensuring functionality of the RABSII antenna.
GEN-MH-009	The Deployment System shall remain within safe structural limits during each stage of operation.	Based on PQ-Mat-01 [5]
GEN-MH-010	The Deployment System shall adhere to the ECSS Standard	Self-Derived

Table 4.3: General Design Requirements of the deployment system with their Identifiers (ID) and Rationale.

4.2.3. Mission Requirements

The mission requirements outlined in Table 4.4 provide detailed insights into the functionality of the deployment system and its integration within the Delfi-Twin mission. These requirements are based on extensive discussions with stakeholders from both the Delfi-Twin team and the RABSII antenna team, ensuring that all specific mission needs are addressed.

Requirements **MIS-MH-011** and **MIS-MH-012** establish the operational lifetime of the deployment system and align it with the expected lifetime of the Delfi-Twin satellite. Specifically, **MIS-MH-011** is derived from operational constraints experienced during the launch of a previous DSSP satellite, the Delfi-PQ [18]. During the Delfi-PQ launch, no touch-ups were permitted for six months. To ensure that the deployment system remains functional under similar conditions, a stowage period for the Delfi-Twin has been accounted for and implemented in the deployment system design.

Next, **MIS-MH-013** defines the operational temperature range of the deployment system, based on the trajectory and operational orbit of the Delfi-Twin. Followed, **MIS-MH-014** focuses on the deployment angle to optimize the performance of the RABSII antenna throughout its mission lifetime.

Finally, **MIS-SH-015**, a requirement that is not critical but desired, addresses the need for confirmation of successful deployment. Given the potential for the RABSII antenna to interfere with other satellite components, confirming deployment would enable mission control to assess its performance and potentially rule it out as a cause in the event of any operational issues.

ID	*Requirement*	*Rationale*
MIS-MH-011	The Deployment System shall remain stowed for 1 year without any significant decrease in its deployment performance.	Self-derived, based on previous instances [17] where the launch deployer did not allow for touch-ups during storage.
MIS-MH-012	The Deployment System shall have a lifetime of 5 years after its deployment in orbit.	Self-derived, based on the mission lifetime of the Delfi-Twin.
MIS-MH-013	The Deployment System shall withstand temperatures in the range of -40°C to +80°C.	Self-derived, numerical values provided by Delfi-Twin stakeholders based on the targeted trajectory and orbit of the Delfi-Twin.
MIS-MH-014	The Deployment System ensures a deployment angle between 90° and 130° in-orbit	Self-derived
MIS-SH-015	The Deployment System shall confirm a successful deployment.	Self-derived, based on requirements stated by Delfi-Twin stakeholders.

Table 4.4: Mission Design Requirements of the deployment system with their Identifiers (ID) and Rationale.

4.2.4. Budget Constraints

The budget constraints, which are a critical aspect of the deployment system design, are detailed in Table 4.5. **BDG-MH-016** and **BDG-MH-017** define the mass and power limitations for the overall deployment system system, including the RABSII antenna. **BDG-MH-020** and **BDG-SH-021** specify the volume constraints per element, as the RABSII antenna (a dipole antenna) consists of two elements, each requiring its own deployment system. Furthermore, a distinction has been made volume restriction of the mechanical structure (**BDG-MH-020**) and the complete deployment system (**BDG-SH-021**). The latter slightly differs due to potential ability of milling in the external plate of the Delfi-Twin to enable integration of COTS components.

Based on the power allocations for the deployment system (**BDG-MH-018**), it is assumed that the deployment system shall not consume significant power outside the deployment process. Lastly, **BDG-SH-019** represents the only non-essential budget constraint, as the Delfi-Twin project allows for some flexibility regarding costs.

ID	*Requirement*	*Rationale*
BDG-MH-016	The Deployment System shall weigh less than 40 grams.	Self-derived, numerical value provided by Delfi-Twin stakeholders.
BDG-MH-017	The Deployment System shall not consume more than 8 watts for 15 seconds during its deployment phase.	Self-derived, numerical value provided by Delfi-Twin stakeholders.
BDG-MH-018	The Deployment System shall not consume any power during phases other than its deployment phase.	Self-derived, based on the phrasing of BDG-MH-015.
BDG-SH-019	The Deployment System shall have a cost of less than 500 euros.	Self-derived, based on the MSc thesis budget.
BDG-MH-020	The Deployment System's mechanical structure shall have dimensions of less than 17x6x0.2 cm per element.	Self-derived, numerical value provided by Delfi-Twin stakeholders.
BDG-SH-021	The complete Deployment System shall (including fasteners and actuation) have dimensions of less than 17x6x0.2 cm per element.	Self-derived, numerical value provided by Delfi-Twin stakeholders.

Table 4.5: Budget Constraints of the deployment system with their Identifiers (ID) and rationale.

4.2.5. Safety Requirements

The safety design requirements outlined in Table 4.6 provide additional constraints derived from the PocketQube and CubeSat Standards [1, 5]. Meeting these requirements is critical to ensure that component failures within the deployment system do not compromise the Delfi-Twin and minimize the risk of interference or damage to other satellites sharing the same launch deployer. This is partly addressed in **SFT-MH-022**, which prohibits the deliberate detachment of components during any phase of operation. Besides this constraint, other requirements from the PocketQube and CubeSat Standards prohibit specific technologies, such as pyrotechnic devices (**SFT-MH-23**) or passive magnets exceeding specified magnetic field limits (**SFT-MH-25**). Compliance with environmental and operational standards during launch and deployment is described in **SFT-MH-24**, ensuring the continued functionality of onboard components. Finally, **SFT-MH-026** specifies that the deployment system must be designed to accommodate ascent venting. This requirement is essential for managing the pressure differential during ascent, reducing the risk of structural damage to the deployment system.

These safety requirements ensure that the deployment system not only meets mission objectives, but also adheres to safety protocols, minimizing risks to the Delfi-Twin and other satellites, while optimizing performance during the launch and deployment phases.

4.2.6. Material Requirements

The material design requirements outlined in Table 4.7 introduce additional constraints derived from the PocketQube and CubeSat Standards [1, 5]. These requirements (**MAT-MH-027** and **MAT-MH-028**) must only be enforced to the components of the deployment system that act as a structural component. Furthermore, **MAT-MH-029** specifies the adherence to expected loads which could occur during deployment. Lastly, **MAT-MH-030** and **MAT-MH-031** state the ultimate design factor of safety (FOSU) and yield design factor of safety (FOSY).

ID	*Requirement*	*Rationale*
SFT-MH-022	The Deployment System shall ensure no deliberate detachment of any components throughout the lifetime of the entire mission: launch, ejection and in-orbit operation.	Based on PQ-Gen-01 [5]
SFT-MH-023	The Deployment System shall not consist of any pyrotechnics.	Based on PQ-Gen-02 [5]
SFT-MH-024	The Deployment System shall meet outgassing requirements.	Based on PQ-Gen-04 [5]
SFT-MH-025	The Deployment System shall not have any passive magnets which have a magnetic field above 0.5 Gauss above Earth's magnetic field, outside the CubeSat static envelope.	Based on CubeSat Standard (2.1.8) [1]
SFT-MH-026	The Deployment System shall be designed to accommodate ascent venting per ventable volume/area of less than 50.8 meters.	Based on CubeSat Standard (2.1.9) [1]

Table 4.6: Safety Design Requirements of the deployment system with their added Identifier (ID) and Rationale.

ID	*Requirement*	*Rationale*
MAT-MH-027	The Deployment System shall only use metallic materials that are hard anodized if they are in contact with the deployer and/or standoffs if it acts as structural component	Based on PQ-Mat-03 [5].
MAT-MH-028	The Deployment System shall either be made of FR4, Aluminum (7075, 6061, 6065, 6082), or other materials requiring stakeholder approval if they are in contact with the deployer and/or standoffs if it acts as structural component .	Based on PQ-Mat-04 [5].
MAT-MH-029	The Deployment System shall conform to the specified stiffness, strength and safety requirements derived from the launcher and the spacecraft structural requirements	Derived from the ECSS Standard [85]
MAT-MH-030	The Deployment System shall conform to a FOSU of 2	Derived from the ECSS Standard [86]
MAT-MH-031	The Deployment System shall conform to a FOSY of 1.25	Derived from the ECSS Standard [86]

Table 4.7: Material Design Requirements of the deployment system with their added Identifier (ID) and rationale.

4.3. Key Performance Parameters

Key Performance Parameters (KPPs) are functional criteria the deployment system aims to achieve to ensure optimal performance and alignment with stakeholder expectations. While some overlap with Section 4.2, KPPs specifically define the target performance levels, rather than the minimum 'must-have' requirements. Adherence to these parameters ensures that the system delivers maximum performance and satisfies mission objectives to the fullest extent. The identified KPPs, presented in no particular order, are as follows:

1. The deployment system shall deploy the RABSII antenna in-orbit at an angle of 130° with respect to the longitudinal axis of the host-satellite.
2. The deployment system shall maintain a constant deployment angle of 130° throughout the mission lifetime.
3. The deployment system shall comply with all requirements for systems onboard a PocketQube, including but not limited to structural, operational and environmental constraints.
4. The deployment system shall not interfere with the general mission objectives or operational functionalities of the host-satellite.
5. The deployment system shall be adaptable to varying final configurations of the RABSII antenna, with emphasis on accommodating different stowage methods of a dipole antenna.
6. The deployment system shall support and integrate all necessary electrical and communication interfaces from the RABSII antenna and its onboard systems, ensuring seamless connectivity and functionality.
7. The deployment system shall adhere to the following cost, volume, mass and power constraints:
    - Total material and component cost (deployment system): < 500 euros
    - Volume (antenna System): <$17.8 \times 5 \times 0.2$ cm^3
    - Mass (antenna system): < 40 grams
    - Power usage (antenna system): < 4 watts for 10 seconds

These KPPs establish a clear set of measurable and enforceable design constraints for the deployment system. Adhering to these parameters ensures that the system is optimized for reliable performance, fulfilling both the technical requirements and stakeholder expectations. Appendix B presents a Requirement Traceability Matrix (RTM), in which the KPPs are mapped to the corresponding design requirements.

4.4. Design Option Tree and Rationale

A Design Option Tree (DOT) is a systematic approach to organize and present the subsystems and their possible design options for a system. For the deployment system, the DOT is shown in Figure 4.2. A rationale follows the DOT, justifying the color-coded feasibility scale assigned to each option based on technical considerations.

Mitigating Angular Overshoot During Deployment

One of the primary objectives of the deployment system is to achieve a deployment angle of 130°, ensuring reliable performance of the RABSII antenna. Over- or undershooting this angle may result in sub-optimal antenna performance, system failure, or even mission failure of Delfi-Twin (or any other host-satellite). Undershooting must primarily be prevented through the selection of an appropriate actuation method, whereas overshooting necessitates additional mitigation strategies. Various design options are depicted in Figure 4.2.

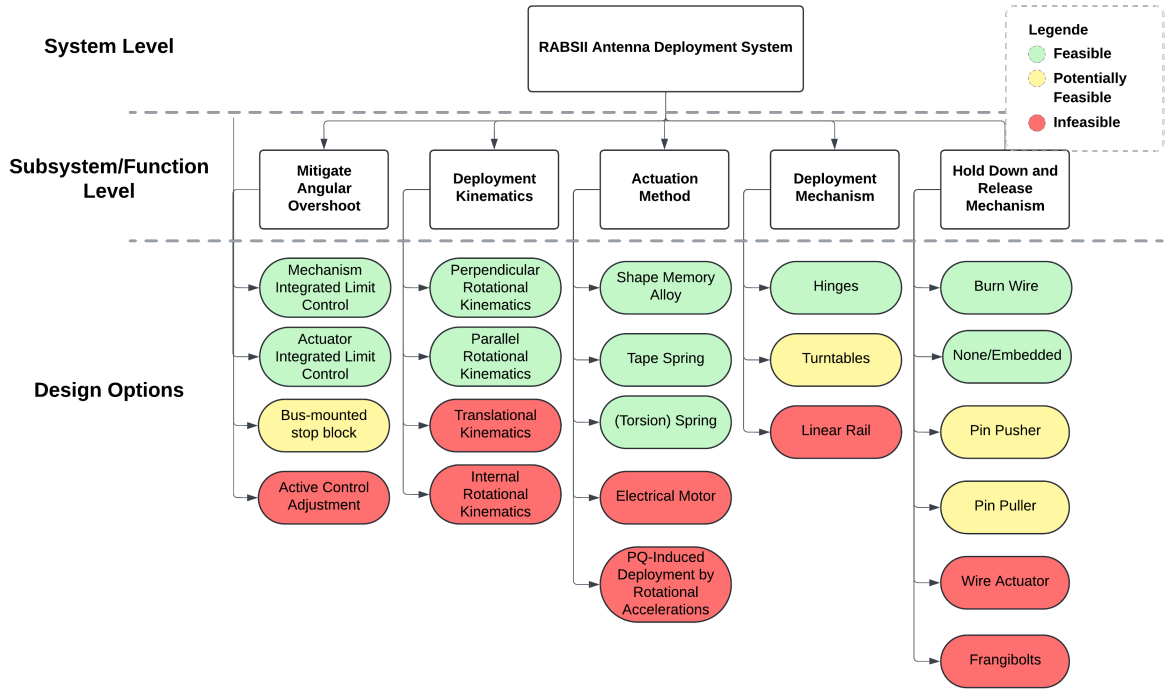

Figure 4.2: Design Option Tree for the deployment system, incorporating COTS and SOA options from literature.

Active Control Adjustment mitigates angular overshooting by integrating a feedback loop within the actuation method. For example, actuation methods powered by heaters, such as SMAs, could adjust the deployment angle based on real-time feedback between the measured angle and the power supplied to the heater. Although this approach is promising, the complexity of the required control system, combined with the limited allowable power budget (BDG-MH-017), renders it infeasible within the scope of this research. A more feasible alternative is an**Actuator- or Mechanism-Integrated Limit Control**, which embeds the mitigation of angular overshooting within the actuation method or the deployment mechanism itself. Compared to active control adjustment, this approach is less complex and does not necessarily require additional components or power. Another potential solution is the implementation of a **Physical Stop-Block**. This involves integrating a mechanical stop within the bus structure of Delfi-Twin or another host-satellite. This provides a reliable physical constraint, preventing overshooting and ensuring the system deploys within the desired range. This solution does necessitate additional components, complicating integration with other host-satellite due to additional requirements (assembly and modifications of the bus structure).

Deployment Kinematics

Deployment kinematics refers to the movement path the deployment system will follow to transition between its stowed and deployed configurations. Based on the literature study performed in Section 3, various methods have been used in previous nanosatellite applications, as depicted in Figure 4.2.

Internal Rotational Kinematics describe a movement path in which an appendage is wrapped around a fixed point, resulting in a rotation exceeding 360°. This method has previously been used within the DSSP (as depicted in Figure 2.3), where antenna elements were deployed by rotating them around such a point. However, for the RABSII antenna, its elements are designed to be folded (see Section 3.4.1). Consequently, internal rotational kinematics are deemed infeasible for this application. **Translational Kinematics** describe a linear path that the entire appendage follows during deployment. For the RABSII antenna system, the final deployment angle must fall within the range of 90 to 130°. To achieve this with a purely linear motion, the required deployment dimensions would exceed the available volume constraints of $17.8 \times 5 \times 0.2$ cm^3. As such, translational kinematics are deemed unfeasible within

the context of this research. **Perpendicular and Parallel Rotational Kinematics** describe movement paths in which the entire appendage rotates around an axis. In contrast to internal rotational kinematics, the rotation angle in these configurations is significantly lower than 360°. Section 4.1 depicts the longitudinal and lateral axes of the host satellite, which are referenced in defining these kinematics. In parallel rotational kinematics, the appendage remains parallel to the longitudinal axis throughout its deployment path. In contrast, perpendicular rotational kinematics involve the appendage moving in a plane perpendicular to the longitudinal axis. To achieve a deployment angle of 130° using perpendicular rotational kinematics, a slight offset in the rotation axis is required. Otherwise, the appendage would deploy to an angle of 180°. This offset is not necessary for parallel rotational kinematics, which can achieve the desired deployment angle without modification.

Actuation Methods

Actuation methods refer to the methods used to initiate and control the deployment of the appendage, considering the volume, mass and power constraints provided for the system.

Electrical motors are a potential actuation method for PocketQubes and have been used for the deployment of solar panels onboard Delfi-PQ. However, for the deployment of the RABSII antenna, their use is deemed unfeasible. Given the allocated volume, mass and power budgets, electrical motors are considered large, heavy and power-intensive. Additionally, their complex design relative to other actuation methods makes them impractical for this application. **PocketQube-Induced Deployment via Rotational Accelerations** is an approach in which the angular velocity and acceleration of Delfi-Twin (or another host satellite) are used to enable deployment. This method was implemented in the IKAROS mission for the deployment of a solar sail [32]. Adopting this approach would require specific angular motion capabilities from the host satellite, which contradicts the goal of developing a compatible deployment system. Imposing such requirements could interfere with other payloads and mission operations. Furthermore, PocketQubes and nanosatellites in general, typically lack an advanced ADCS, which is essential for executing the required tumbling and detumbling maneuvers. Therefore, this actuation method is also deemed infeasible. More feasible approaches include the use of **SMAs, tape springs and (torsion) springs**. SMAs are already applied to the RABSII antenna elements and have relevant flight heritage on nanosatellites in similar use cases [31]. Tape springs have been successfully used in previous DSSP missions, including Delfi-C^3 and Delfi-n3Xt and represent a reliable and commercially available solution. (Torsion) springs are a well-established, low-cost actuation method with a high level of reliability and simplicity, making them an attractive option for this application.

Deployment Mechanism

The deployment mechanism refers to the structural system responsible for enabling the deployment kinematics of the RABSII antenna. They serve as the structural interface between the host-satellite and the RABSII antenna. Their role also includes accommodating the selected actuation method and integrating the HDRM.

Hinge mechanisms represent a straightforward approach to deployment mechanisms. Their simplicity and compatibility make them a suitable and feasible option, particularly when paired with parallel rotational kinematics. **Turntables**, while suitable for perpendicular rotational kinematics, are a more complex solution. Integrating such a mechanism within the allocated volume could introduce various risks and challenges, including increased friction, cold welding and unworkable deployment angles. **Linear rail mechanisms** are inherently linked to translational kinematics. Their linear motion is not well-suited for the required deployment configuration. It would necessitate an additional mechanism to achieve the correct deployment angle, thereby making them inefficient and impractical for this application.

Hold Down and Release Mechanism

The various HDRMs discussed in Section 3.3 are depicted in Figure 4.2.
Frangibolts and wire actuators are both HDRMs with relevant flight heritage. However, for the deployment system of the RABSII antenna, their use is considered incompatible. Frangibolts are typically

used to sever high-strength structural bonds and are excessive for this application. Wire actuators, while functional, are relatively bulky and heavy and their mechanical complexity makes them unsuitable for the constrained design envelope. Therefore, both methods are deemed infeasible. **Pin pushers and pullers** offer a slightly more compatible solution for the RABSII antenna. They provide precise control, but occupy a large volume and necessitate continuous power, reducing their practicality. **Burn wire mechanisms** represent a simple and widely used solution within DSSP missions. Their integration into the deployment system could be achieved by leveraging existing hardware and expertise developed for the deployment of the solar panels. Additionally, burn wire mechanisms are straightforward to implement and highly space-efficient. **No HDRM or an embedded HDRM** is another viable approach. Although the ECSS standards typically require a distinct HDRM [85], the placement of the complete antenna system, stowed beneath the solar panels, may render this requirement unnecessary. Furthermore, some actuation methods, such as SMAs, inherently include delay or control mechanisms (e.g., reliance on heaters or environmental conditions) that could serve as embedded HDRMs.

5

Concept Design

With the mission parameters defined, expected performance outlined and design options identified, the next phase of the design process is initiated. Feasible design options are used to develop preliminary concepts for the deployment system. First, general terminology and the assessment methodology used to evaluate the concepts are introduced. Following that, a brief explanation of the three preliminary concepts and an identification of required revisions is provided. Subsequently, the revised concepts are examined in detail, resulting in the development of a trade-off matrix and the selection of the final concept.

5.1. Terminology and Assessment Method

5.1.1. Terminology

The requirements outlined in Section 4.2 specify that three locations are reserved for the deployment system of the RABSII antenna. Opposing side panels and the top panel can be utilized, with a maximum allowable thickness of 2 mm for the Delfi-Twin mission. Other nanosatellites conforming to the PocketQube Standard allow a thickness of up to 6 mm [5].

Assuming that the majority of the RABSII Antenna is stowed on an external side-panel, three distinct configurations are identified:

- **Closed Hinge Stowed Configuration (CHSC)**: In this configuration, the hinge leaves are stacked on top of each other when stowed and rotate away from each other during deployment, as depicted in Figure 5.1a. The key advantage of this configuration is that the hinge is positioned on only one external surface of the satellite (the external side-panel). Additionally, when stowed, the CHSC occupies less surface area compared to the other configurations.
- **Open Hinge Stowed Configuration (OHSC)**: In this configuration, the hinge leaves are positioned parallel to each other when stowed and rotate toward each other during deployment, as shown in Figure 5.1b. Similar to the CHSC, this configuration positions the hinge on only one external surface of the satellite (the external side-panel). However, while the OHSC allows for thicker hinge leaves, it occupies more surface area than the CHSC.
- **Right-Angle Hinge Stowed Configuration (RAHSC)**: In this configuration, the hinge leaves are positioned at a 90° angle relative to each other when stowed and rotate toward each other during deployment, as depicted in Figure 5.1c. Unlike the CHSC and OHSC, the hinge in the RAHSC configuration is mounted on two external surfaces of the satellite (the external top- and side-panels).

These configurations only apply to hinge mechanisms as the turntable mechanism does not account for varying stowed configurations.

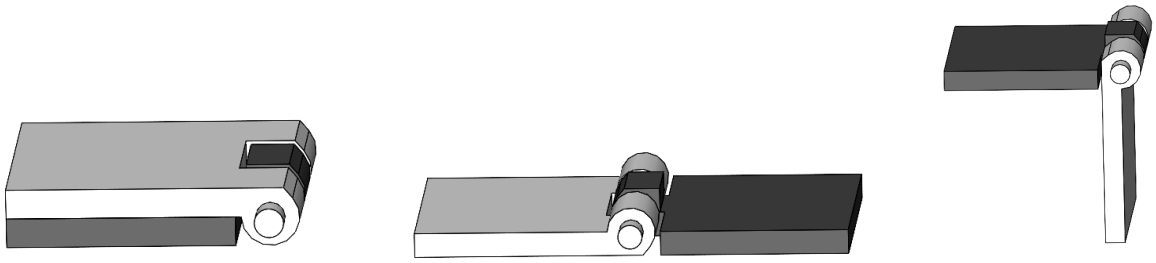

(a) Closed Hinge Stowed Configuration (CHSC)

(b) Open Hinge Stowed Configuration (OHSC)

(c) Right-Angle Hinge Stowed Configuration (RAHSC)

Figure 5.1: Considered stowed configurations for a hinge mechanism.

In addition to the described stowed hinge configurations, the terminology for hinge components are shown in Figure 5.2. The figure shows an exploded view of a simple hinge mechanism, highlighting its main elements: the hinge leaves, knuckles and pin. The two hinge leaves are connected by the pin, which passes through the hinge knuckles.

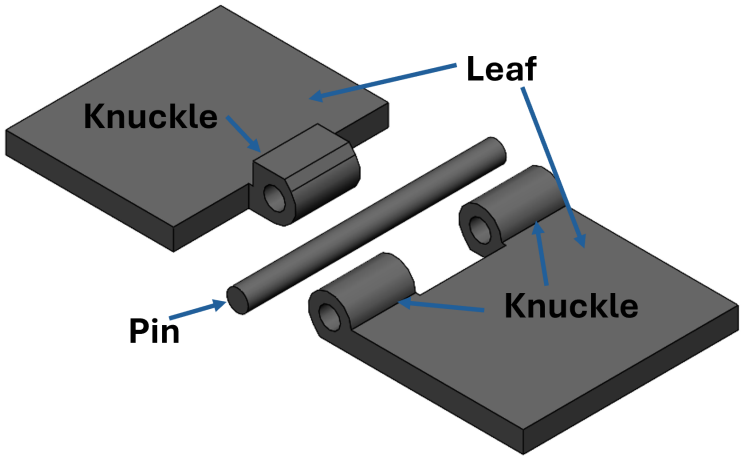

Figure 5.2: Exploded view of a hinge mechanism, illustrating the key elements of the hinge mechanism.

5.1.2. Assessment Method

As multiple design concepts have been developed, a clear and qualitative assessment method is necessary to evaluate their expected performance. The requirements outlined in Section 4.2, along with the KPPs detailed in Section 4.3, define the following criteria:

- Reliability
- Delfi-Twin Compatibility
- RABSII Antenna Compatibility
- Nanosatellite Compatibility

Appendix B includes the Requirement Traceability Matrix, which links the KPPs and requirements to their respective criteria.

The first criterion, '**Reliability**', is essential, as the deployment system must maintain a certain level of performance. The reliability of each design concept is evaluated by analyzing potential failure points, including the impact of minor design errors, vibrations and manufacturing margins on the deployment

system's performance.

The second criterion, '**Delfi-Twin Compatibility**', assesses adherence to the requirements outlined in Section 4.2. Each concept is evaluated based on factors that may complicate integration with the Delfi-Twin system. Additionally, this criterion may consider the estimated component cost for each design, where outliers thereof are highlighted.

The third criterion, '**RABSII Antenna Compatibility**', focuses on the 'low-priority' requirements such as GEN-SH-004, GEN-CH-005 and MIS-SH-015. This provides additional insights into the intricacies of deployment performance and RABSII Antenna integration.

Finally, '**Nanosatellite Compatibility**' addresses the potential for future iterations in which the deployment system could be scaled up. This evaluation builds upon the previous criteria, reassessing them within a larger design envelope and consequently, larger system budgets. Furthermore, design flexibility, including various stowed configurations, is taken into account. This assessment prioritizes adaptability to different nanosatellite platforms, emphasizing flexibility over strict constraints on volume, mass, or power.

Following the development of the initial design concepts, the RABSII and Delfi-Twin stakeholders provided their priorities, which influenced the weighting of each criterion. It was determined that the most important criterion is **Reliability**, closely followed by **Delfi-Twin Compatibility**. **RABSII Antenna Compatibility** and **Nanosatellite Compatibility** were identified as lower-priority considerations, with the latter being slightly less significant.

The final weights assigned to each criterion are summarized in the trade-off matrix depicted in Table 5.1.

5.2. Preliminary Concepts

The preliminary concepts were determined based on the DOT depicted in Figure 4.2. Only feasible design options were considered, with each preliminary concept centered around a unique actuation method. Concept Tape Spring, SMA and Torsion Spring explored various design options for each function and subsystem, allowing for comprehensive understanding of all feasible design options. All feasible design options were subdivided, except for the bus-mounted stop block and pin-pusher/puller. These were excluded due to, an unnecessary increase in component count and incompatibility with small-scale dimensions, respectively.

The design choices of the preliminary concepts are briefly explained, with further details available in Appendix E.

5.2.1. Concept Tape Spring

Concept Tape Spring, depicted in Figure 5.4, integrates the inherent behavior of a bi-stable tape spring with a hinge mechanism. The hinge mechanism, which enables parallel rotational kinematics, incorporates a MIALC (Mechanism Integrated Angular Limit Control) and allows for the integration of a burn wire mechanism as the HDRM.

The MIALC is implemented by modifying the hinge knuckles. These modifications, along with designating distinct rotational paths to each hinge leaf, enable compatibility with various stowed configurations (OHSC, CHSC and RAHSC). Figure 5.3 shows the side view of the hinge leaves, where the dimensions are shown while ensuring adherence to the Delfi-Twin mission requirements. Figure 5.4 depicts the stowed and deployed states of the OHSC, CHSC and RAHSC. The integration of the RABSII antenna (FR-4 plate) and a burn-wire mechanism are also considered.

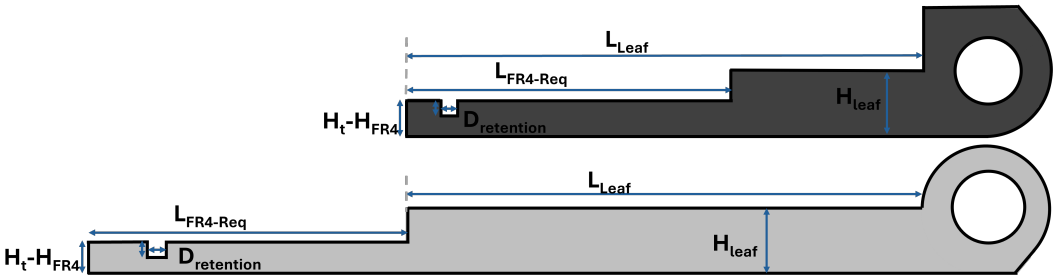

Figure 5.3: Parametrized dimensions of Concept Tape Spring's hinge leaves.

Tape spring integration varies dependent on the stowed configuration. The applied approach can be summarized as maximizing the bending radius while minimizing the number of required bends in the tape spring. For the Delfi-Twin mission, only the RAHSC configuration is considered feasible. Integration of a tape spring into the OHSC and CSHC configurations would require a bending radius of less than 2 mm over a spanned angle of 180°, which is infeasible with COTS options. The RAHSC configuration requires a larger bending radius, but is limited to a deployment angle of 90°. However, experimental validation is necessary to mitigate the risk of warping during deployment [8].

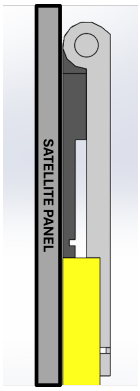

(a) Concept Tape Spring, final design in CSHC, stowed

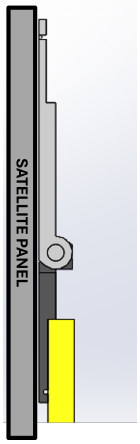

(b) Concept Tape Spring, final design in OHSC, stowed

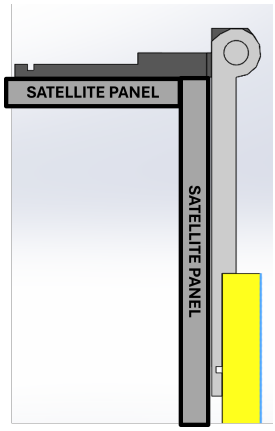

(c) Concept Tape Spring, final design in RAHSC, stowed

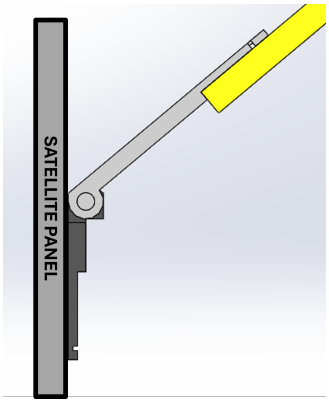

(d) Concept Tape Spring, final design in CHSC, deployed

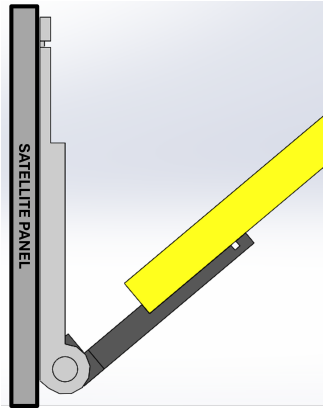

(e) Concept Tape Spring, final design in OHSC, deployed

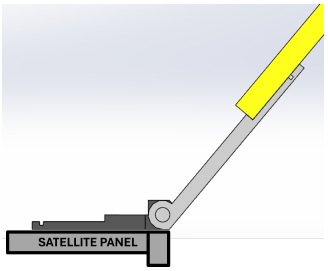

(f) Concept Tape Spring, final design in RAHSC, deployed

Figure 5.4: Deployed and stowed configuration of Concept Tape Spring in the compatible stowed configurations Concept Tape Spring, deployed and stowed states in the CSHC, OHSC and RAHSC.

Design Analysis and Trade-Off Results

Simulation and testing results revealed several issues that negatively affected the overall reliability of Concept Tape Spring. The simulations involved a structural analysis under launch conditions, while testing included the construction of a proof-of-concept prototype. The intricate hinge knuckle modifications required for integration within the Delfi-Twin envelope proved to be highly susceptible to assembly and minor design errors. Such deviations could result from improper assembly of the burn wire mechanism, where small deformations, induced by excess vibrations in the stowed configuration, could lead to significant overshooting of the deployment angle. Furthermore, vibrations and high accelerations experienced in the deployed configuration could also cause angular overshoot, potentially compromising the functionality of the RABSII antenna. As a result, Concept Tape Spring received a low reliability score in the trade-off matrix.

When fitted within the Delfi-Twin envelope, which provides a volume budget of $17.8 \times 5 \times 0.2$ cm^3, the intricate geometry of the hinge knuckles presents significant manufacturing challenges. Failure to account for manufacturing margins could easily result in substantial angular overshooting. Integration of a tape spring-based actuation method within this constrained envelope is also unfeasible when adhering to a 130° deployment angle. The minimum bending radius of COTS tape springs at a spanned angle of 180° (e.g., tape measures) is significantly larger (>0.5 cm) than the allocated thickness of 2 mm. This makes achieving a 130° deployment angle impossible and limits the potential deployment angle to 90°. Consequently, this resulted in low compatibility scores for Delfi-Twin and the RABSII antenna, as many design requirements could not be fulfilled.

For a general nanosatellite with an increased available envelope, the compatibility of the concept improves significantly. The limitations that led to the low Delfi-Twin compatibility score primarily stem from the restricted allocated volume. In a general nanosatellite application, an increased thickness allowance of 0.6 mm would reduce both manufacturing challenges and performance issues. Integration of a tape spring-based actuation method becomes more feasible, with a 90° deployment angle achievable as standard and a 130° deployment angle becomes feasible, though still complex. This results in a higher nanosatellite compatibility score.

5.2.2. Concept SMA

Concept SMA, depicted in Figure 5.6, is inspired by a deployment system used in the ALBus mission [31, 39], where a similar hinge mechanism and actuation method were used. However, Concept SMA also utilizes the actuation method to prevent both angular overshooting (AIALC (Angular Integrated Angular Limit Control)) and premature deployment (HDRM).

Concept SMA's hinge mechanism slightly differs from that of Concept Tape Spring. It features a simple design, incorporating only the necessary modifications to integrate the actuation method and RABSII antenna. The design consists of hinge brackets, a hinge leaf and a hinge rod, enabling a modular configuration. Figure 5.5 and Figure 5.6 depict the single and double hinge leaf configurations, respectively.

The selection of Concept SMA's SMA was based on various assumptions and requirements. The RABSII antenna utilizes an SMA with an activation temperature between 40°C and 80°C (at the time this design was assessed) and the Delfi-Twin mission follows a sun-synchronous orbit. This orbital configuration allowed for the assumption that any SMA with an activation temperature below 40°C would receive sufficient and relatively constant thermal flux. Additional constraints limited the allowable activation temperature range to between 29.4°C and 40°C. Based on the comparison in Table 3.1, only $Ti_{49}Ni_{41}Cu_{10}$ meets this criterion.

Figure 5.6 illustrates both the stowed and deployed configurations of Concept SMA, where its modular design is also visible.

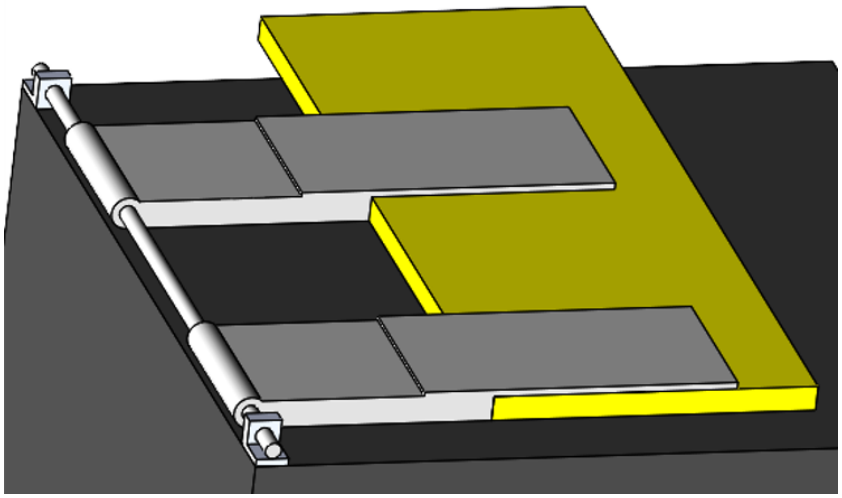

Figure 5.5: Example of the modular design of Concept SMA.

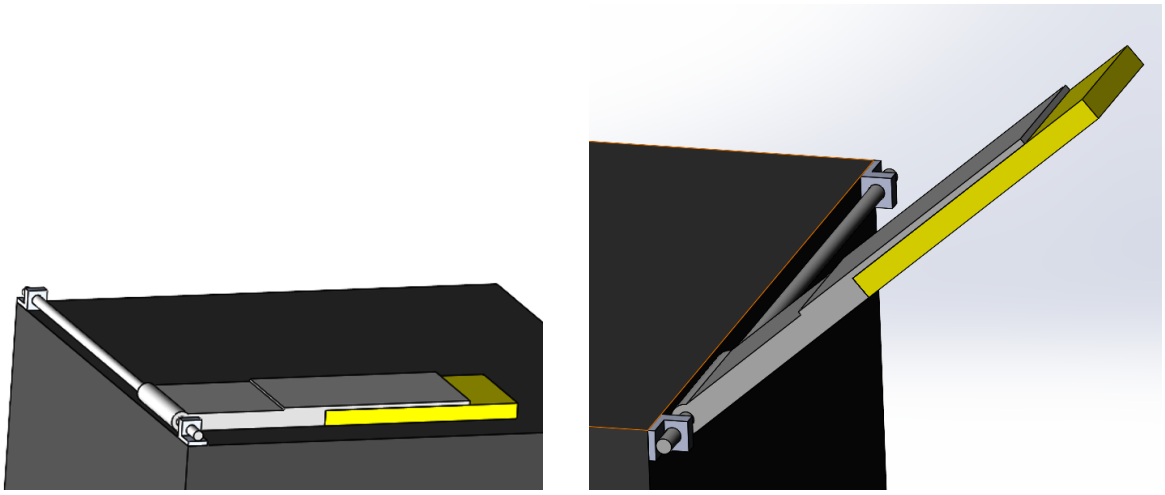

(a) Concept SMA, Isometric view of the final design, stowed

(b) Concept SMA, isometric view of the final design, deployed

Figure 5.6: Concept SMA, deployed and stowed configurations.

Design Analysis/Trade-Off Results

The reliability of Concept SMA is primarily constrained by the SMA-based actuation method and the environmental parameters it must adhere to. Theoretically, in a sun-synchronous orbit, an almost constant thermal flux can be assumed, which is sufficient to reach the activation temperature of 40°C (RABSII antenna SMA). However, the lack of a comprehensive understanding of the SME of the chosen SMA ($Ti_{49}Ni_{41}Ti_{10}$) reduces its reliability. Furthermore, COTS SMA sheets often lack a detailed and accurate data sheet, as many EU-based manufacturers bulk-order from China, primarily catering to hobbyists. As a result, extensive experimental validation and verification are required to establish the reliability of the system due to its reliance on SMA-based actuation

Delfi-Twin compatibility is primarily determined by the integration and adherence of the SMA to the mission parameters. Empirical data from the ALBus SMA indicates a deployment torque of 0.125 Nm [39], although no information is available regarding the dimensions of the applied SMA sheet. The activation temperature of Concept SMA and that of the RABSII antenna element SMAs differ by only 5°C, which may increase the risk of delayed deployment and potential interference with other external appendages on Delfi-Twin. These factors contribute to a lower Delfi-Twin compatibility score.

Nanosatellite Compatibility is similarly influenced by the feasibility of the SMA-based actuation method for various nanosatellite missions. Unlike the Delfi-Twin, nanosatellites do not necessarily operate in a sun-synchronous orbit, resulting in potentially insufficient thermal flux and large temperature deviations. Furthermore, the lower bound of the temperature range depends on the launch deployer, which also varies between nanosatellites. As a result, the nanosatellite compatibility score is lower than that of Delfi-Twin compatibility.

5.2.3. Concept Torsion Spring

Concept Torsion Spring, depicted in Figure 5.8, integrates a torsion spring with a turntable mechanism. The simplicity of a torsion spring-based actuation method allows for a focus on the turntable mechanism itself rather than on the integration and understanding of the actuation method. Additionally, a burn wire mechanism functions as the HDRM while MIALC is implemented to prevent angular overshooting.

Concept Torsion Spring's turntable mechanism consists of three main components, a Fixated Turntable Leaf (FTL), a Rotating Turntable Leaf (RTL) and a turntable rod. In this concept, the turntable rod is housed within the actuation method. Both the FTL and RTL contribute to an angular displacement of 25° each, resulting in a total deployment angle of 50° (180°-130°). Figure 5.7 shows both turntable leaves.

The geometry of the turntable knuckles primarily depends on the allocated thickness. Figure 5.7a defines r_{FTL}, which is determined by:

$$r_{FTL} = \frac{1}{2} \cdot \frac{t}{tan(25°)} \tag{5.1}$$

Substituting t = 2 mm results in r_{FTL} = 2.145 mm.

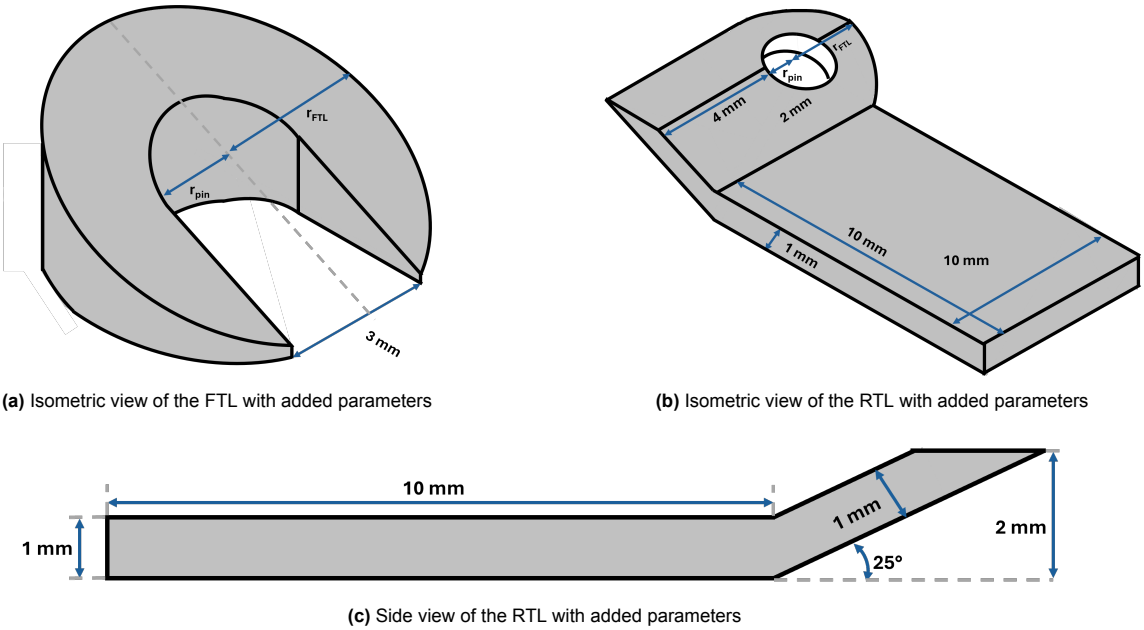

(a) Isometric view of the FTL with added parameters

(b) Isometric view of the RTL with added parameters

(c) Side view of the RTL with added parameters

Figure 5.7: Isometric views of the FTL and RTL with added parameters and side view of the RTL

Appendix C lists COTS torsion springs which could facilitate a deployment angle greater than 130°. However, the torsion spring must have a length smaller than 2 mm and a radius small than r_{FTL}, which is not commercially available. Therefore, integration of a COTS torsion spring within Concept Torsion Spring, while adhering to the Delfi-Twin mission, is not feasible.

Figure 5.8 depicts both the stowed and deployed states of Concept Torsion Spring.

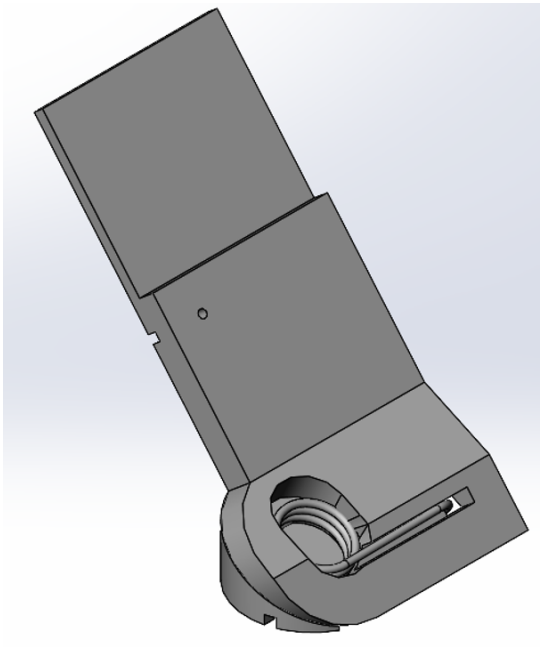

(a) Concept Torsion Spring, isometric view of the final design, deployed

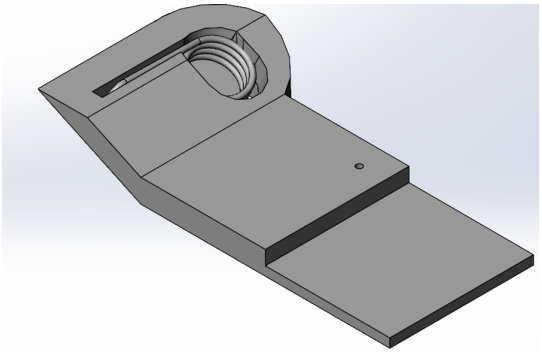

(b) Concept Torsion Spring, isometric view of the final design, stowed

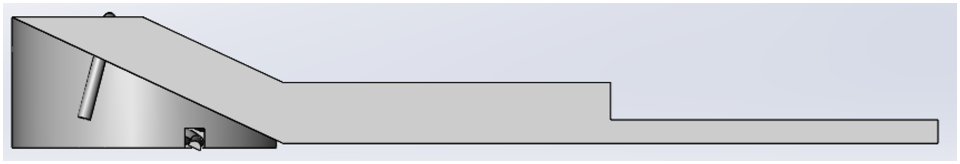

(c) Concept Torsion Spring, side view of the final design, stowed

Figure 5.8: Concept Torsion Spring, isometric views in deployed and stowed configurations and side view of the stowed configuration

Design Analysis and Trade-Off Results

The development of Concept Torsion Spring allowed to evaluate the feasibility of a turntable mechanism as part of the deployment system for the RABSII antenna. However, significant limitations arose due to the constrained Delfi-Twin envelope. The absence of space for lubricants introduced a high risk of cold welding at critical contact points. Equation 5.1 defines the allocated radius of the FTL, which consists of the hinge rod and the torsion spring. The compact design required for integration within Delfi-Twin did not allow for adequate lubrication and resulted in compromised structural integrity due to limited dimensions and constraints on torsion spring placement. These factors led to a low reliability score.

A clear distinction must be made between Delfi-Twin and nanosatellite compatibility. Due to differences in volume constraints, lubricant requirements can only be met in larger nanosatellites. For Delfi-Twin, the required rotation angle and volume specifications could not be satisfied by any COTS torsion spring. Larger nanosatellites, which provide more volume for the antenna system, allow for the use of lubricants and accommodate a more suitable torsion spring. Nevertheless, nanosatellite compatibility remains limited by the absence of multiple stowed configurations and the extensive surface area required for deployment. Overall, nanosatellite compatibility is higher than Delfi-Twin compatibility, but both scores remain lower than desired.

RABSII antenna compatibility is relatively favorable. Concept Torsion Spring enables a deployment angle of approximately 130° with minimal expected fluctuations. Integration of communication and power interfaces can be easily achieved within the current design.

5.2.4. Preliminary Concept Trade-Off

Each preliminary concept was evaluated based on its expected performance using the defined trade-off criteria (see Section 5.1.2). Table 5.1 presents the Trade-Off Matrix, with the weighted scores for all three concepts.

Concepts / ***Criterion***		***Concept Tape Spring***		***Concept SMA***		***Concept Torsion Spring***	
	Weight	**Score**	**Score x Weight**	**Score**	**Score x Weight**	**Score**	**Score x Weight**
Reliability	6	2	12	2	12	2	12
Delfi-Twin Compatibility	5	1	5	3	15	1	5
RABSII Antenna Compatibility	3	2	6	2	6	3	9
Nanosatellite Compatibility	2	5	10	2	4	2	4
Weighted Score	80	33		37		30	
Normalized Score	1	0.4125		0.4625		0.375	

Table 5.1: Trade-off matrix of Concept Tape Spring, SMA and Torsion Spring.

None of the developed concepts achieved the desired performance. All normalized scores are below 0.5, with the most critical criteria (*Reliability* and *Delfi-Twin Compatibility*), scoring a 2.0 and 1.67 on average, respectively. Given these results, further development, manufacturing and testing of any of these concepts would not be advisable in their current form.

Concept Tape Spring and Concept SMA show potential for improvement through minimal modifications in design choices and/or implementation. However, Concept Torsion Spring is fundamentally constrained by its deployment mechanism, making it unsuitable for a Delfi-Twin compatible deployment system. The next section details the improved concepts, elaborating on the proposed design modifications.

5.3. Revised Concepts

The results from the Trade-Off Matrix (Table 5.1) were unfavorable, as none of the concepts met the expected performance criteria. In particular, reliability and Delfi-Twin Compatibility were significantly compromised. These criteria state that the overall performance of the deployment system must fall within safe bounds, while also enabling integration with the Delfi-Twin project. This section presents the revised version of Concept Tape Spring and Concept SMA, incorporating modifications in design choices and/or implementation strategies to address the identified shortcomings.

5.3.1. Concept 4

Concept 4, a revision of Concept Tape Spring, improves *Reliability* and *Delfi-Twin Compatibility* by altering both the actuation method and the MIALC implementation. The actuation method is changed from a tape spring-based system to a spring-based actuation method, while the hinge knuckle modification is replaced with a hinge leaf modification to enable MIALC.

Mechanism Integrated Angular Limit Control (MIALC)

Concept 4 incorporates MIALC to prevent angular overshooting of the RABSII antenna. Unlike Concept Tape Spring, *Nanosatellite Compatibility* is not prioritized. The previous approach, which supported multiple stowed configurations, compromised both on *Reliability* and *Delfi-Twin Compatibility*. The hinge knuckle modifications in Concept Tape Spring proved complex and costly to manufacture for the Delfi-Twin mission. Furthermore, their high susceptibility to minor design errors, vibrations and manufacturing tolerances negatively affected *Reliability*, *Delfi-Twin Compatibility* and *RABSII Antenna*

Compatibility.

Concept 4 addresses these limitations by integrating a physical stop block within the Fixated Hinge Leaf (FHL) as its MIALC approach. This simplified design eliminates the drawbacks associated with Concept Tape Spring's hinge mechanism. Although this design supports only the OHSC configuration, it significantly improves Reliability and compatibility with both the RABSII antenna and Delfi-Twin by reducing susceptibility to minor design errors, vibrations and manufacturing margins.

Spring Choice

The spring-based actuation method for Concept 4 must enable parallel rotational kinematics while adhering to the volume, power and mass constraints outlined in Section 4.2. The selected spring variant is presented along with preferred parameters to achieve optimal performance. Based on available COTS springs, a final design choice is made.

Table 5.2 presents three potential spring variants capable of achieving a deployment angle of 130°: torsion springs, constant-force springs and clock springs. The listed parameters represent the smallest COTS variant of each type that can achieve the required deployment angle. Alternative spring variants, such as extension springs, were excluded due to increased design complexity and incompatibility with the specified requirements. These alternatives would require additional mechanisms to reach the desired deployment angle, rendering them unsuitable for this application.

Among the evaluated spring variants, torsion springs were identified as the only feasible option for Concept 4 due to their significantly smaller outer diameter (2.8 mm compared to 6.18 mm for constant-force springs and 26 mm for clock springs). Integration of constant-force or clock springs would necessitate additional mechanisms and increased surface area, as concentric placement relative to the hinge rod would not be possible within the allocated volume.

Type of Spring	***Torsion Spring***	***Clock Spring***	***Constant Force Spring***
Product Name	***Lesjöfors 8318***	***Lesjöfors 901***	***Lesjöfors 8036***
Outer diameter [mm]	2.8	26	6.18
Width/Length [mm]	5.2	5	3.175
Max. Rod Diameter [mm]	1.5	7	4.83
Max Rotation Angle [°]	227	354	Not specified
Torque [Nm] or Force [N]	0.01*	0.329*	0.46

Table 5.2: Relevant parameters of smallest COTS torsion, clock and constant-force spring from Dutch-based distributors (Lesjöfors, Amatec and Alcomex)
*Maximum Torque at 10.000 oscillations.

COTS torsion springs are classified based on their unloaded configuration, specifically on the angle between their pokes. Figure 5.9 depicts the four primary torsion spring configurations, each differing by 90° increments in poke angle. Additionally, the required deformation of these torsion springs to achieve a 130° deployment angle in an OHSC configuration is shown.

Selecting an appropriate spring configuration simplifies the integration of the actuation method and ensures compliance with the design requirements. Configuration C (Figure 5.9c) is preferred due to its simplified integration process. While Configuration A (Figure 5.9a) also requires a 180° rotation angle, its integration is more complex. Configuration C offers an advantage because the fixated poke is aligned with the rotating poke, whereas in Configuration A, they are misaligned. Configuration B (Figure 5.9b) and Configuration D (Figure 5.9d) both require a 270° rotation angle, which significantly increases implementation complexity and reduces the availability of suitable COTS variants.

Table 5.3 outlines the functional and performance requirements that the torsion spring preferably satisfies. Appendix C provides a list of COTS torsion springs available from Dutch-based distributors, with

an outer diameter (D_o) less than 3.57 mm and a rotation angle greater than 130°.

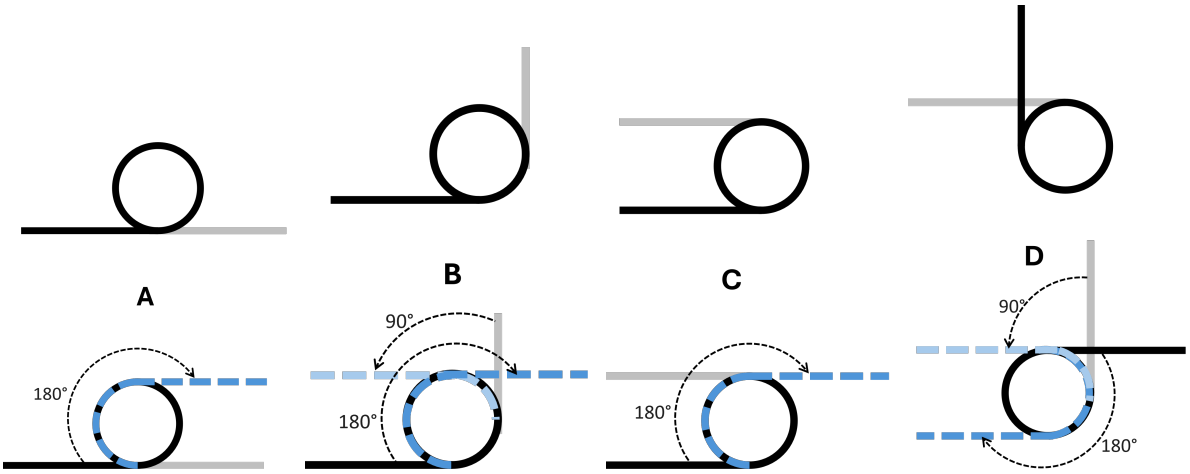

(a) Torsion Spring Configuration A **(b)** Torsion Spring Configuration B **(c)** Torsion Spring Configuration C **(d)** Torsion spring configuration D

Figure 5.9: Four primary torsion spring unloaded configurations, where their required deformation for an OHSC is depicted to ensure an eventual deployment angle of 130°.

Specification	Value	Lesjöfors 8318
Min. Rotation Angle	130	227
Max. Outer Diameter	3.57 mm	2.8 mm
Max. Width	10 mm	5.2 mm
Max. Rod Diameter	1 mm	1.5 mm
Torsion Spring Configuration	C	A
Availability in L/R Coiling	–	Yes, Lesjöfors 8428
COTS	–	Yes
Spring Constant	0.018 Nmm/°	0.0045 Nmm/°

Table 5.3: Functional/performance requirements for the torsion spring and achieved performance by torsion spring (Lesjöfors 8318).

From the list in Appendix C, the Lesjöfors 8318 variant was selected due to its optimal combination of a low D_o and a large rotation angle. Although the Amatec T012-180-067 offers comparable performance, the distributor reports a significant reduction in performance at load capacities exceeding 80%. Therefore, the Lesjöfors 8318 was preferred, as its slightly larger D_o provides increased load capacity margins and a higher maximum rotation angle, thereby enhancing overall reliability and performance.

Final Design

Concept 4 consists of two hinge leaves, the RHL (Rotating Hinge Leaf) and FHL (Fixated Hinge Leaf), which incorporate modifications to enable the integration of MIALC, the HDRM and the actuation method. The actuation system includes left- and right-coiled COTS torsion springs, while a burn wire mechanism functions as the HDRM. The fully assembled design is shown in Figure 5.10.

The FHL provides angular limit control, enables integration of the torsion spring and serves as the fixed interface between the host satellite and the RABSII antenna. Figure 5.11b shows the FHL design, which features an unconventional structure. Due to the use of a Configuration A torsion spring (see Figure 5.9a), an additional structural element was required to secure the torsion spring pokes. Given the small-scale space mission context of the deployment system, minimizing components is essential. The addition of separate components and fasteners for securing the torsion spring pokes would increase

assembly complexity and unnecessarily add mass to the system. The FHL also achieves angular limit control through the integration of a physical stop block within its design. Unlike Concept Tape Spring, this MIALC implementation is less susceptible to vibrations, minor design errors and manufacturing margins. The risk of significant deployment angle overshoot is largely mitigated and would only arise under extreme failure scenarios.

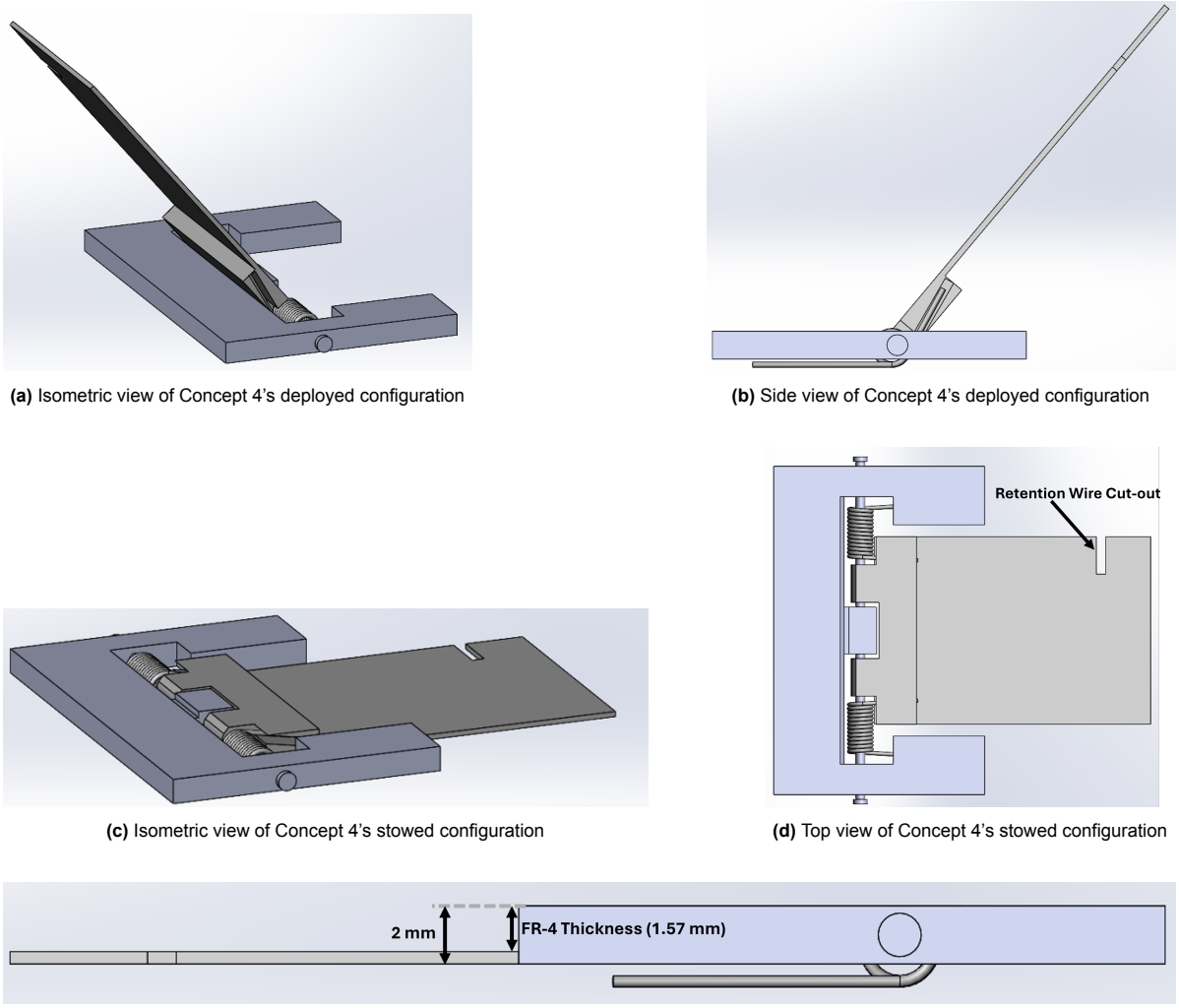

(a) Isometric view of Concept 4's deployed configuration

(b) Side view of Concept 4's deployed configuration

(c) Isometric view of Concept 4's stowed configuration

(d) Top view of Concept 4's stowed configuration

(e) Side view of Concept 4's stowed configuration

Figure 5.10: Concept 4's stowed and deployed configurations.

The RHL enables the integration of the HDRM, RABSII antenna and torsion spring. Figure 5.11a shows the RHL design. Cutouts are incorporated to ensure compliance with volume constraints while accommodating the RABSII antenna (FR-4 plate) and the burn wire mechanism (retention wire). The selected torsion springs (Lesjöfors 8318 and 8428) allow for a rotation angle of 227° and a 10° slot has been included in the RHL design to secure the torsion spring poke. The combined design of the RHL and FHL prevents any undesired rotations or movements of the torsion spring.

The actuation method of Concept 4 utilizes two torsion springs that differ only in their coiling direction. Each spring has an outer diameter of 2.8 mm, while the inner diameter ranges between 1.5 and 2 mm, depending on deformation (i.e., rotation angle). Integration of the torsion springs into the design required additional validation steps, particularly due to their offset placement relative to the system thickness. With an inner diameter of 1.5–2 mm, the hinge leaf can accommodate a centered ⌀1 mm rod hole. However, the external plate, on which the deployment system is mounted, requires minor milling modifications to comply with volume constraints. The milling profile for both springs covers an

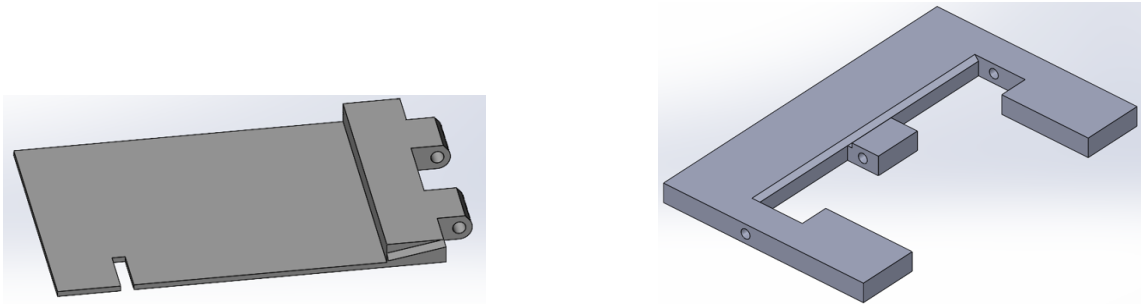

(a) Isometric view of Concept 4's Rotating Hinge Leaf (RHL)

(b) Isometric view of Concept 4's Fixated Hinge Leaf (FHL)

Figure 5.11: Isometric view of Concept 4's hinge leaves.

area of 37.12 mm^2 at a depth of 1 mm. This area is approximately equivalent to the space occupied by three M2 screws.

5.3.2. Concept 5

Concept 5, a revision of Concept SMA, reduces functional reliance on the SMA to improve *Reliability* and *Compatibility* with *Delfi-Twin, other nanosatellites and the RABSII antenna*. In this concept, the SMA serves solely as the actuation method, while a burn wire mechanism (HDRM) and MIALC have been incorporated to take over roles previously fulfilled by the SMA.

Mechanism Integrated Angular Limit Control (MIALC)

The MIALC of Concept 5 prevents angular overshooting, a role previously embedded within the actuation method of Concept SMA. The reliability of MIALC, compared to AIALC (Actuator Integrated Angular Limit Control), is significantly higher and is strongly preferred according to the ECSS standard [85] In Concept 5, the MIALC is implemented in each hinge bracket as an additional physical stop block. While more intricate hinge rod modifications were considered, these were ultimately dismissed. As with the complex modifications in Concept Tape Spring, such designs would be highly susceptible to manufacturing tolerances, with a substantial risk of negatively impacting performance.

SMA Material Choice and Integration

The SMA-based actuation method in Concept 5, similar to the RABSII antenna elements, relies on thermal flux in-orbit to enable deployment. For the RABSII antenna elements, a Nitinol ⌀0.3 mm wire currently undergoes testing, with an activation temperature (M_s) between 40°C and 60°C. The selection and integration of the SMA material for Concept 5 are based on the following assumptions:

- Thermal flux in Delfi-Twin's sun-synchronous orbit remains relatively constant throughout the mission lifetime across all external panels [87].
- Thermal flux in Delfi-Twin's orbit is sufficient to deploy any SMA with an M_s < 40°C.
- In-orbit temperatures fluctuate between -40°C and 80°C.

In Concept 5, the SMA serves solely as the actuation method, while a burn wire mechanism prevents premature deployment. The selection of the SMA material is driven by its phase transformation temperature range, wherein the M_s, A_s and A_f values must fall within defined limits to ensure a sufficient temperature differential between M_s and A_s.

The temperature boundaries for SMA activation are dictated by in-orbit conditions, pre-deployment constraints and the characteristics of the RABSII antenna elements. While the HDRM prevents premature deployment, it must also allow for timely activation. Once the RABSII antenna elements unfold, the

inertia of the elements increases significantly (Appendix A). To meet this requirement, the SMA in Concept 5 must have an M_s < 40°C. Additionally, the lower temperature boundary is determined by the in-orbit temperature range of Delfi-Twin's mission, establishing the constraint:

$$-40°\text{C} < M_s < 40°\text{C} \tag{5.2}$$

Although the HDRM prevents premature deployment, phase transformations in the SMA may still occur before release. If A_s is reached prior to HDRM release, delayed deformation may occur, which increases the risk of incomplete deployment. If A_f is reached beforehand, the SMA may not deform upon release, which further increases the risk of deployment failure. Consequently, additional temperature constraints for A_s and A_f must be defined to mitigate these risks.

During launch, ambient temperatures are expected to range between 18.3°C and 29.4°C. Therefore, for Concept 5's SMA, the following constraint must hold:

$$29.4°\text{C} \ll A_f < 80°\text{C} \tag{5.3}$$

Additionally, A_s must not be significantly below 29.4°C to prevent premature activation.

M_s and A_s directly influence the deployment angle. Prevention of unintended thermal cycling between these states is critical. This is particularly important because the antenna elements inertia increases substantially after the RABSII antenna unfolds. Consequently, A_s must remain within the expected in-orbit temperature range, while M_s must be below the lower boundary of this range.

A sun-synchronous orbit at 800 km altitude experiences temperatures between 265 K and 275 K ($-8.15°$C to 1.85°C) [87]. Although Delfi-Twin's lower orbit will experience higher in-orbit temperatures, the variation in temperature range is expected to be of a similar magnitude (approximately 10°C). Therefore, the following constraint must be satisfied:

$$A_s - M_s < 10°\text{C} \tag{5.4}$$

Table 3.2 lists various SMA compositions along with their respective M_s and A_f values. Among them, *$Ti_{49.5}Ni_{50.5}$, $Ti_{50}Ni_{40}Pt_{10}$, $Ti_{49}Ni_{41}Cu_{10}$ and $Ti_{50}Ni_{45}Pt_5$* satisfy the constraint $-40°$C < M_s < 40°C. However, only $Ti_{49.5}Ni_{50.5}$ allows for a temperature fluctuation of less than 10°C between M_s and A_s. Therefore, $Ti_{49.5}Ni_{50.5}$ is the preferred SMA composition for use in Concept 5.

The integration of the SMA must ensure quick and reliable actuation for deployment while having the capability to conduct current to and from the RABSII antenna for power and communication purposes. Figure 5.1 illustrates the considered stowed configurations. However, since the hinge mechanism in Concept SMA consists of only a single hinge leaf, the definitions of CHSC, OHSC and RAHSC require a slight modification. The fixated leaf corresponds to the fixed section of the SMA, its relative position with respect to the rotating leaf defines the CHSC, OHSC and RAHSC configurations.

For the integration of the tape spring (Section E.2.1), the primary design constraint is the minimum allowable bending radius. Due to this limitation, under-hinge configurations were excluded from consideration. Similarly, for the SMA actuation method, under-hinge configurations are not feasible, as the required bending radius cannot be achieved within the volume constraints outlined in Section 4.2. Additionally, as detailed in Appendix B, there is a difference in required deployment torque between the stowed and unfolded states of the RABSII antenna, if similar deployment times are adhered to. To ensure deployment occurs before the unfolding of the RABSII antenna, it is essential to maximize thermal flux exposure to the SMA. Consequently, SMA placement must prioritize positions that allow for optimal thermal flux absorption.

For the integration of the tape spring (Section E.2.1), the main design constraint is the minimum allowable bending radius. Due to this constraint, under-hinge configurations were excluded from consideration. Similarly for the SMA actuation method, under-hinge configurations are excluded as the required bending radius within the volume constraints (Section 4.2) is infeasible. Additionally, as detailed in Appendix A, there is a significant difference in I_{RABSII} between the stowed and unfolded state of the

RABSII antenna. To ensure deployment before unfolding of the RABSII antenna, it is essential to maximize the thermal flux exposure to the SMA. Consequently, the placement of the SMA must prioritize positions that allow for maximum thermal flux absorption.

These constraints significantly limit the number of feasible SMA configurations. For the CSHC, no viable configurations exist, as the SMA would always be partially positioned beneath the hinge leaf. For the OHSC and RAHSC, only one SMA configuration is applicable, as depicted in Figure 5.12.

The primary difference between the OHSC and RAHSC configurations shown in Figure 5.12 is the placement of the fixated section of the SMA. Onboard Delfi-Twin, the RABSII antenna and its deployment system are stowed beneath the solar panels. The RAHSC configuration allows exposure of the SMA to thermal flux before solar panel deployment, enabling the deployment system to actuate prior to the unfolding of the RABSII antenna elements. Additionally, the shadowing effect caused by the RABSII antenna elements is less significant in the RAHSC configuration than in the OHSC, especially considering that thermal flux variation between external panels is minimal [87].

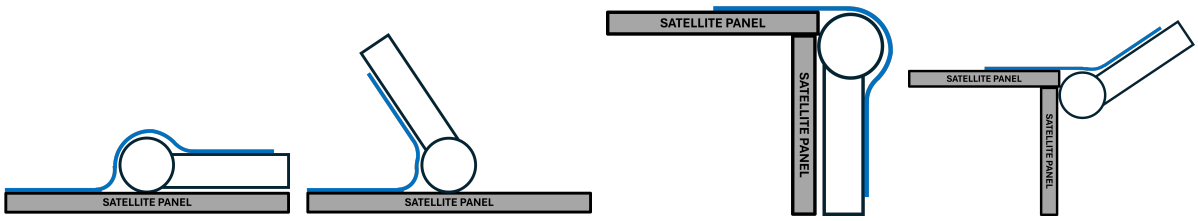

(a) OHSC, SMA configuration, stowed

(b) OHSC, SMA configuration, deployed

(c) RAHSC, SMA configuration, stowed

(d) RAHSC, SMA configuration, deployed

Figure 5.12: Stowed and deployed state of OHSC and RAHSC with corresponding SMA configurations.

Final Design

The design of Concept 5 consists of a hinge mechanism with integrated modularity, a burn wire mechanism and an SMA-based actuation method. The SMA-based actuation method consists of a 0.25 mm thick sheet of $Ti_{49.5}Ni_{50.5}$, directly attached to the hinge leaf. The complete mechanical design of Concept 5, including both the stowed and deployed configurations, is shown in Figure 5.13.

The modular design of Concept 5 is shown in Figure 5.14, with the hinge brackets detailed in Figure 5.15. Each hinge bracket integrates MIALC through a physical stop block that prevents angular overshooting. The middle hinge block has been designed to minimize the use of fasteners while maximizing the width of the hinge leaf. This width is critical, as it directly influences the SMA's surface area and the resulting deployment torque.

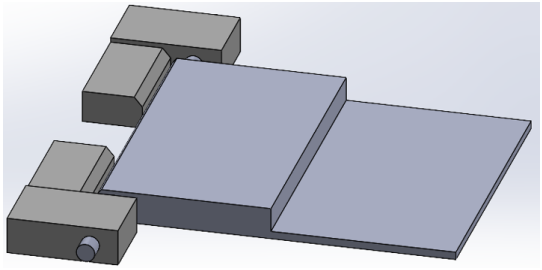

(a) Isometric view of Concept 5's stowed configuration

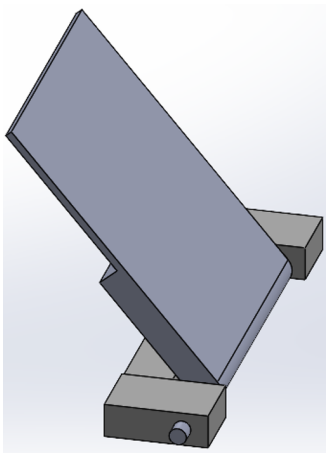

(b) Isometric view of Concept 5's deployed configuration

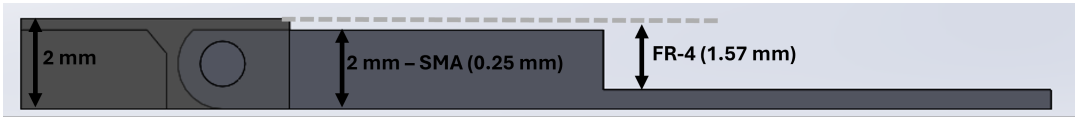

(c) Side view of Concept 5's stowed configuration

Figure 5.13: Concept 5's stowed and deployed configurations (Single Leaf).

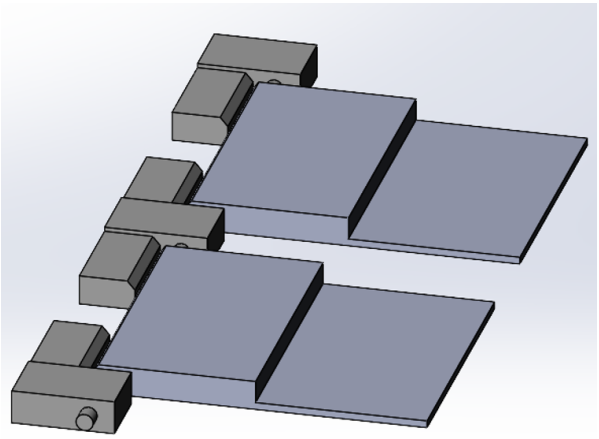

Figure 5.14: Concept 5, modular design.

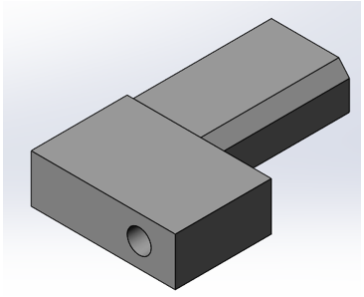

(a) Concept 5, Left-Placed Hinge Bracket

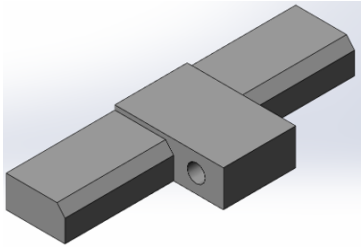

(b) Concept 5, Middle-Placed Hinge Bracket

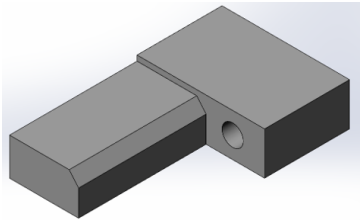

(c) Concept 5, Right-Placed Hinge Bracket

Figure 5.15: Concept 5, all three utilized hinge brackets.

5.3.3. Design Analysis

This section presents a detailed design analysis of both revised concepts. Each design is evaluated using the assessment method defined in Section 5.1.2, with a focus on reliability and compatibility within the design framework of this research.

Concept 4

The design of Concept 4 is a revision Concept Tape Spring, where various design modifications were made based on the design analysis and trade-off results (see Section 5.2.1). Uncertainties and the inability to achieve a reliable deployment performance due to the MIALC implementation and actuation method were reassessed. This resulted in a different actuation method, a torsion spring instead of a tape spring and a MIALC implementation of the hinge leaf instead of the hinge knuckle. Susceptibility to angular overshooting and complex integration within the Delfi-Twin were major concerns for Concept Tape Spring, but these were both mitigated in Concept 4.

The hinge mechanism was modified to incorporate a physical stop block, functioning as the MIALC. Design analysis indicates that manufacturing tolerances have minimal impact on the deployment angle. For example, a 0.1 mm manufacturing margin results in a deviation of only $\pm 2^{\circ}$.

The torsion spring-based actuation method consists of two torsion springs placed in parallel. Integration of Concept 4 into the Delfi-Twin requires only minor milling, as the smallest available COTS torsion spring has an outer diameter exceeding the allocated thickness. The torque generated by the torsion springs is currently deemed insufficient. Its effectiveness in overcoming resistive torque must be further assessed. A simple parallel arrangement of four springs could compensate for this torque deficiency.

The compatibility of Concept 4 with Delfi-Twin, other nanosatellites and the RABSII antenna has slightly improved. Enhanced manufacturability for Delfi-Twin, a scalable design adaptable to other nanosatellites and COTS availability for the actuation method contribute to higher trade-off scores for these criteria. However, a reduction in applicable stowed configurations slightly decreases nanosatellite compatibility.

Concept 5

Concept 5 introduces design changes relative to Concept SMA (see Section 5.2.2). These modifications primarily enhance flexibility in SMA material selection by expanding the allowable temperature range. The broader range improves risk mitigation by addressing concerns such as delayed deformation and phase cycling. In combination with hinge mechanism modifications, these changes also improve the ability of Concept 5 to prevent angular overshooting while providing deformation margins for the SMA.

In Concept SMA, reliability depended heavily on the selected SMA material properties, with environmental conditions directly influencing performance within narrow temperature limits. In Concept 5, the SMA primarily determines the deployment angle, while premature deployment and angular overshooting are mitigated by a HDRM and MIALC. These additions expand the operational temperature range for the SMA, allowing greater design margins and enabling the use of more reliable and adaptable SMA materials. This broader temperature tolerance also improves compatibility with other nanosatellites, thereby enhancing both Delfi-Twin and general nanosatellite compatibility.

The hinge mechanism in Concept 5 has also been modified compared to Concept SMA. The current design supports integration of up to two hinge leaves on the Delfi-Twin (and other PocketQubes). Furthermore, it enables both OHSC and RAHSC configurations, with RAHSC being the preferred option due to its better thermal flux exposure.

Despite these improvements, Concept 5 retains certain limitations inherent to SMA behavior. The deployment torque generated by the SMA remains uncertain. The ALBus mission provides only a numerical value (0.125 Nm) without specifying the corresponding SMA volume [31, 39]. Deployment is still dependent on environmental conditions and delayed deformation may occur. In such cases, the SMA

may begin deforming while constrained by the HDRM, potentially resulting in incomplete deployment, where the SMA gets stuck at an lower angle. Delayed or incomplete deformation can permanently affect the deployment angle and the RABSII antenna performance. Fortunately, the selected SMA has an A_s value that prevents thermal cycling, which also precludes 'resetting' of the shape memory effect (SME).

5.4. Concept Choice

This chapter presented multiple design concepts for the deployment system and evaluated their expected performance using the assessment method described in Section 5.1.2. The initial concepts (Concept Tape Spring, Concept SMA and Concept Torsion Spring) were estimated to perform poorly, particularly in the criteria of *Reliability* and *Delfi-Twin Compatibility*. As a result, Concept Tape Spring and Concept SMA were selected for further development, leading to the creation of Concept 4 and Concept 5.

Table 5.4 presents the updated Trade-Off Matrix, including the scores of Concept 4 and Concept 5. A significant improvement in performance is evident, with normalized scores of 0.7875 and 0.7, respectively.

Concepts / ***Criterion***		***Concept Tape Spring***		***Concept SMA***		***Concept Torsion Spring***		***Concept 4***		***Concept 5***	
	Weight	**Score**	**Sc x W**	**Score**	**Sc x W**	**Score**	**Sc x W**	**Score**	**Sc x W**	**Score**	**Sc x W**
Reliability	6	2	12	2	12	2	12	4	24	3	18
Delfi-Twin Compatibility	5	1	5	3	15	1	5	4	20	4	20
RABSII Antenna Compatibility	3	2	6	2	6	3	9	3	9	4	12
Nanosatellite Compatibility	2	5	10	2	4	2	4	4	10	3	6
Weighted Score	80	33		37		30		63		56	
Normalized Score	1	0.4125		0.4625		0.375		0.7875		0.7	

Table 5.4: Trade-Off Matrix of all designed Concepts

In conclusion, the design modifications implemented in Concepts 4 and 5 led to a significant improvement in overall performance (Table 5.4). Ultimately, Concept 4 was selected as the final deployment system design. While Concept 5 achieved comparable performance, its actuation method introduced considerable uncertainties, making Concept 4 the preferred choice.

6

Design Analysis

Concept 4, introduced in Section 5.3.1, has been developed to be in compliance with the design requirements outlined in Section 4.2. As a preliminary concept, its geometry, parameters and design choices have not yet been optimized. In this chapter, the design of Concept 4 will be refined through a comprehensive risk assessment process. This involves the evaluation of potential failure modes and their associated risks using a Failure Mode and Effects Analysis (FMEA). Based on the outcomes of this analysis, the design is subjected to an iterative design process, addressing the identified failure modes and incorporating appropriate mitigation strategies.

6.1. Concept 4's Failure Mode and Effects Analysis

Failure Mode and Effects Analysis (FMEA) is a systematic approach used to identify, assess and mitigate potential failure modes within a system. Table 6.2 presents the FMEA for Concept 4, where various failure modes associated with its components are analyzed. Based on this analysis, an iterative design process is implemented, where systematically failure modes are addressed at each iteration step. The process consists of four distinct iterations, each dedicated to specific risk factors and design improvements, which are elaborated upon in the following sections. Table 6.1 provides definitions of the severity levels applied in Table 6.2.

The last column in Table 6.2, 'Iteration,' refers to the following subsections:

1. Manufacturing and Deployment, Section 6.2.1
2. Stress Simulations and Material Selection, Section 6.2.2
3. Cold Welding and Actuation Method Failure, Section 6.2.3
4. HDRM Risks, Section 6.2.4

Severity Level	Degree of Severity	Rationale
0	Negligible	Small or no impact pre-launch
1	Low	Results in a decrease in deployment system performance
2	Moderate	Leads to mission failure of the RABSII antenna
3	Critical	Leads to mission failure of the host satellite

Table 6.1: Definition of Severity Levels in the FMEA.

Component	Failure Mode	Potential Causes of Failure	Potential Effects of Failure	Potential Effects of Failure on System Level	Severity in Concept 4	Mitigation Steps Taken for Final design	It. Step
Hinge Mechanism	Deadlocking	Manufacturing defects	- Incompatible components - Increased friction between moving parts	Increased restistive torque, decreased deployment performance	0	Sufficient margins, adherence to DIN2786-F Standard (Structure) and H8/h9 (hinge rod and tapped holes)	1
		Thermal expansion	- Increased friction between moving parts	Increased restistive torque, decreased deployment performance	1	Sufficient margins based a thermal simulation	2
		Cold welding	- Increased friction between moving parts	Increased restistive torque, decreased deployment performance	2	Hard-Anodizing MoS_2 Coating Material study	3
	Component fracture and/or failure	Acceleration loads during launch and bending stresses in-orbit	- Rod fracture	Formation of space debris, detachment of the RABSII antenna element	3	Stress simulations Material study	2
			-Fastener Failure	Formation of space debris, detachment of the hinge mechanism	2	Stress simulations Redundant fasteners	2
			- Hinge leaf failure	Formation of space debris, detachment of the RABSII antenna element	3	Stress simulations	2
			- Excessive deformations	Increased restistive torque, decreased deployment performance	2	Stress simulations Material study	2
HDRM (Burn Wire Mechanism)	Low pre-load or pre-mature deployment	Improper assembly	- Damages to the deployment system due to vibrations during launch	Damges to other external appendages and host-satellite	2	Improve Assembly Process	4
	Delayed or no Deployment	Retention wire stuck	- Complications in, or lack of deployment	Antenna elements unfolding, causing interference with other external appendages. Resistive torque significantly larger in an unexpected movement pattern (closed-to-open)	3	Improve Assembly Process Extensive testing Retention wire with high outgassing	4
		Thermal knife failure	- Complications in, or lack of deployment	Antenna elements unfolding, causing interference with other external appendages. Resistive torque significantly larger in an unexpected movement pattern (closed-to-open)	3	Improve Assembly Process Extensive testing Retention wire with high outgassing	4
Actuation Method (Torsion Spring)	High resistive torque	Increased friction between moving components	- Insufficient deployment torque	Decreased deployment performance	2	Increased multitude of torsion springs	1
		Large variations in host-satellites pitch and yaw angle	- Insufficient deployment torque	Decreased deployment performance	2	Increasing actuation torque Assessing performance	1
			- Excess torque by actuator	Increased stresses in the hinge mechanism Increased angular accelerations	2	Addition of Dampeners Assessing performance	3
	Deadlocking	Cold welding	- Increased friction between moving parts	Increased restistive torque, decreased deployment performance	1	Assessment on occurrence	3
	Plastic Deformation	Extended duration in stowed configuration	- Decreased deployment torque	Decreased deployment performance	2	Increasing actuation torque Assessing performance Redundancy	3
Appendage (RABSII Antenna)	Detachment	Insufficient fastening	-Detachment of the RABSII antenna	Formation of space debris, RABSII antenna mission failure	3	Peel strength calculation Increasing area of adhesive bond Qualitative adhesive selection	4

Table 6.2: FMEA of Concept 4, combined with the mitigation steps taken.

6.2. Design Iteration Process

6.2.1. Iteration: Manufacturing and Deployment

To define the rough geometry and further specify the design, several constraints must be established. First, the available manufacturing tolerances need to be determined. These are relevant not only for the overall mechanical structure but also for the required fit between the hinge rod and hinge leaves. For the mechanical structure, commercially available and commonly used CNC machining services by the Delfi Program are considered. These include JLCNC and ProtoLabs; both providers offer tolerances as low as 0.05–0.1 mm for the expected dimensions of Concept 4's components, which comply with the **ISO 2768 Fine** standard. For the fit between the hinge rod and the hinge leaves, a loose fit is selected to account for potential dimensional changes due to thermal loads. An H8/h9 tolerance fit is applied, allowing for a clearance range of 0 to 50 µm.

The required actuation torque and the overall deployment performance are both dependent on the resistive torque of the deployment system. According to the ECSS standard [85], the resistive torque defines the minimum torque that the actuation method must generate to ensure successful deployment. It is determined using the following equation:

$$T_{min} = 2 \cdot (1.1 \cdot I + 1.2 \cdot S + 1.5 \cdot H_m + 3 \cdot F_r + 3 \cdot Hy + 3 \cdot H_a + 3 \cdot H_d) + 1.25 T_D + T_L \tag{6.1}$$

where:

- I – Resistive inertial torque applied to the deployment system due to accelerations in the inertial frame of reference.
- S – Resistive torque due to spring load.
- H_m – Resistive torque due to magnetic effects.
- F_r – Resistive torque due to friction.
- H_y – Resistive torque due to hysteresis.
- H_a – Resistive torque due to other influences, such as parasitic torque from wire harnesses and/or drag experienced by the deployable appendage.
- H_d – Resistive torque due to adhesion.
- T_d – Inertial resistance caused by the worst-case acceleration function.
- T_l – Deliverable output torque.

Assuming a deployment system onboard the Delfi-Twin, both S and H_m are considered zero. T_l is set to zero, as no definitive value is provided other than the requirement that deployment must occur. H_y is also assumed to be zero due to the complexity of simulating and determining this value. F_r primarily arises from interactions between the hinge rod and hinge leaves, both of which are subject to a different material selection. In the current iteration, both components are assumed to be manufactured from Al7075-T6. The static coefficient of friction (μ_s) between Al7075-T6 surfaces is 0.32 [88] and this value is used in the present numerical estimations.

Table 6.3 provides a summary of the worst-case numerical values of the resistive torque, where both the FOS and uncertainty factors are incorporated. Appendix A provides a detailed breakdown on the assumptions, calculations and numerical values of the resistive torque.

T_{min} is equal to 10.223 Nmm. The selected actuation method (Lesjöfors 8318, Torsion Spring) supplies a torque dependent on the deployment angle:

$$T_{actuation} = n_{springs} \cdot (190 - \alpha_{dep}) \cdot k_{spring} \tag{6.2}$$

where $n_{springs}$ is the amount of parallel placed torsion springs [-], α_{dep} is the deployment angle [°] and k_{spring} is the spring constant of the selected torsion spring (0.045 [Nmm/°].

Resistive Force/ Torque Contributor	**Symbol**	**Value [Nmm] Folded**	**Value [Nmm] Unfolded**	**Uncertainty Factor Theoretical**	**Factor of Safety**	**Value Factored [Nmm] Folded**	**Value Factored [Nmm] Unfolded**
Inertia (Satellite Level)	I	0.00322	0.635	1.1	2	0.00708	1.397
Friction	F_r	0.314	0.314	3	2	1.884	1.884
Harness	H_a	1.243	1.243	3	2	7.458	7.458
Drag	H_a	0.000142	0.000142	3	2	0.000852	0.000852
Inertia (Deployment System)	T_d	0.959	0.959	1	1.25	1.198	1.198
Total		**2.512**	**3.117**			**10.547**	**11.937**

Table 6.3: Resistive Torque applied to preliminary design of the Deployment System.

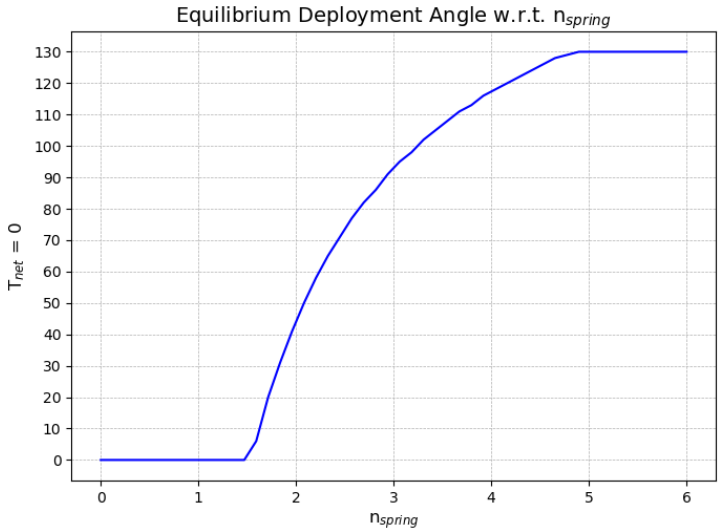

Figure 6.1: Equilibrium deployment angle due to the resistive torque as a function of the number of springs used.

The ECSS standard defines the following Motorization Factor applicable to the actuation method, with complementary non-ECSS guidelines indicated in **bold** [85]:

- To derive the factored worst-case resistive torques or forces, **each contributors**, considering **all mission phases** worst-case conditions , shall be multiplied by the **applicable** minimum uncertainty factor specified in Table 6.3.
  - **Increased factors are typically applied to take into account effects that cannot be measured by test.**
- A spring actuator shall be redundant unless other specified by the customer
- **The actuation torque supplied by the spring shall be multiplied with in uncertainty factor of 0.8.**

Conclusively, Figure 6.1 depicts the resulting deployment angle as a function of n_{spring}. To achieve an equilibrium deployment angle greater than 90° (requirement MIS-MH-014), a minimum of three springs is required. For a deployment angle of 130° (requirement MIS-SH-015), at least five springs are necessary.

Concept 4 has an approximate width of 35 mm; reducing this to 25 mm is not feasible. The design includes components with fixed widths, such as the selected torsion springs (10.4 mm) and the fasteners for the hinge rod (1 mm nut and 1 mm clearance). Additional space is required for margins between the hinges knuckles and the actuation method (approximately 4 mm), as well as overlap for one of the torsion spring pokes (twice the minimum of 2 mm). These factors contribute to a total width

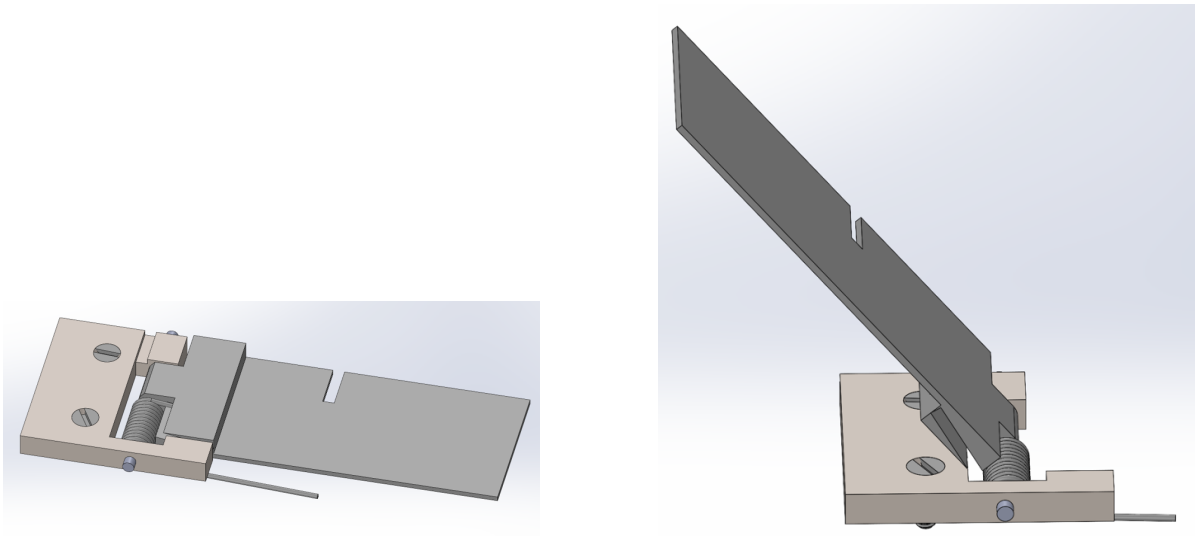

(a) Isometric view of preliminary dimensioned final design, stowed

(b) Isometric view of preliminary dimensioned final design, deployed

Figure 6.2: Isometric views of preliminary dimensioned final design.

of 20.4 mm. As a result, the hinge knuckles would be limited to a total width of 4.6 mm, meaning that each individual knuckle would be approximately 1.53 mm wide. This is impractical, particularly when considering manufacturing tolerances that have not yet been accounted for.
A three-spring configuration with independent hinges, each housing one spring, is shown in Figure 6.2. Each hinge system is limited to a width of 16 mm. Preliminary estimates indicate that the target width is achievable within 15.2 mm, with hinge knuckle widths of 3.5 mm (FHL) and 4.0 mm (RHL).

6.2.2. Iteration: Stress Simulations and Material Choice

This subsection presents various analyses of acceleration loads, thermal loads and in-orbit loads acting on the system. The von Mises stresses under the maximum expected loads serve as the basis for material selection. Subsequently, deformations resulting from these stresses and thermal loads are evaluated to determine whether sufficient safety margins exist, and if not, design modifications are required.

Loads, Fixtures and Simplifications

For the simulations performed, the following simplifications have been applied:

- Only quasi-static loads are considered for the failure mode ”Component Fracture/Failure.”
- Deformations in the structural FR-4 of the host satellite are neglected. The FR-4 plate is assumed to be rigid.
- Acceleration design loads for ”light” payloads are extracted from SpaceX Falcon User’s Guide [89].
- Thermal expansion of the actuation method is assumed to be negligible.
- Induced stresses due to acceleration and in-orbit loads are considered independent of material choice.
- The RABSII antenna element is simplified to resultant forces where applicable.

Furthermore, all fasteners comply with the ECSS standard [90], which specifies a minimum thread engagement of 1.5d for aluminum tapped holes and 0.8d for high-strength steel or titanium tapped holes. Accordingly, M1.2 bolts are selected, as this represents the maximum allowable COTS thread size that

fits within the deployment system's thickness of 2 mm.

Table 6.4 presents the applied loads and corresponding simulations for each failure mode identified in the FMEA (Table 6.2).

Failure Mode	Component	Worst-Case	Value	Source	Type of Simulation
Component Fracture/Failure	Fastener	During Launch	Axial +- 8.5g Lateral +- 2g	[89]	Static (VMS, Deformation)
Component Fracture/Failure	Rod	During Launch	Axial +- 8.5g Lateral +- 2g	[89]	Static (VMS, Deformation)
Component Fracture/Failure	Hinge Leaves	During Launch	Axial +- 8.5g Lateral +- 2g	[89]	Static (VMS, Deformation)
Component Fracture/Failure	RHL	In-Orbit, Decelerations Load	19.04 rad/s	Self-Derived	Manual
Deadlocking	Hinge Mechanism	In-Orbit	-20°C to +80°C	Delfi-Twin Mission	Static (Thermal)

Table 6.4: Expected worst-case quasi-static acceleration and thermal loads for the deployment system.

Simulation Set-Up

Simulations in this study were performed using SolidWorks Simulation. The applied constraints and fixtures are shown in Figure 6.3. M1.2 countersunk screws were used as the connectors, with a pre-load of 0.056 Nm applied. This torque value is based on standard recommendations for the selected fastener size. The numerical values for the applied loads are provided in Table 6.4.

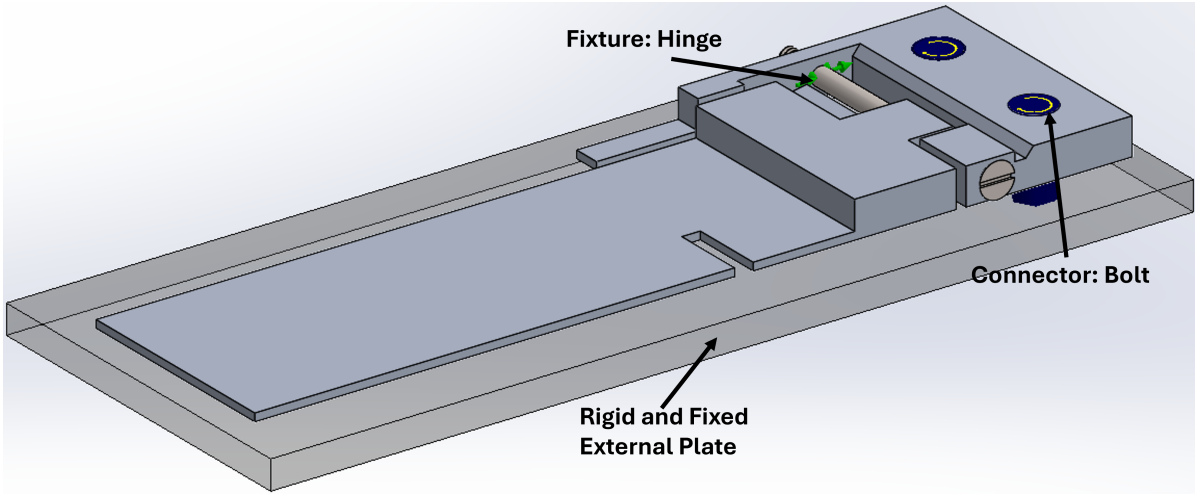

Figure 6.3: General Constraints (Green) and Connectors (Dark Blue) applied for Acceleration Load Simulations

Acceleration Load Stress Simulations

The maximum axial and lateral acceleration loads occur during launch [91]. Their magnitudes, derived from the Falcon User's Guide [89], are listed in Table 6.4. For the simulations, the RABSII antenna is replaced by a resultant force calculated as the product of acceleration and its maximum mass (20 grams). The maximum acceleration load is considered along all three axes, as the orientation of the host satellite is unknown. Although a three-hinge system is implemented, the complete resultant force of the RABSII antenna is applied to each hinge independently to ensure redundancy, as detailed in Section 6.2.3.

Figure 6.4a presents the resulting Von Mises Stresses (VMS), demonstrating that the maximum stresses occur at the fasteners due to pre-load (0.05 Nm), reaching a value of 188 MPa. Figure 6.4b shows a maximum stress of 54 MPa in the deployment system, excluding the FHL.

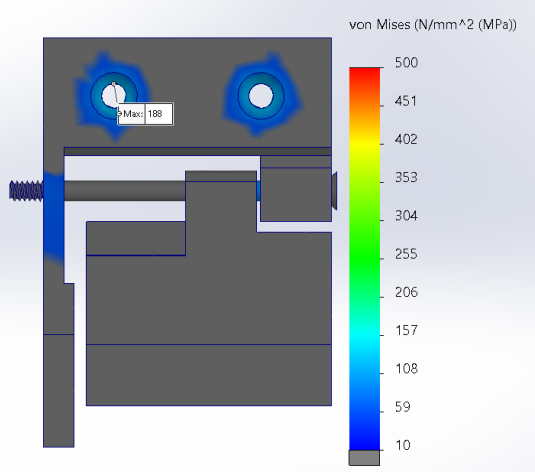

(a) Top View of the von Mises Stresses in the final design with 2 fasteners

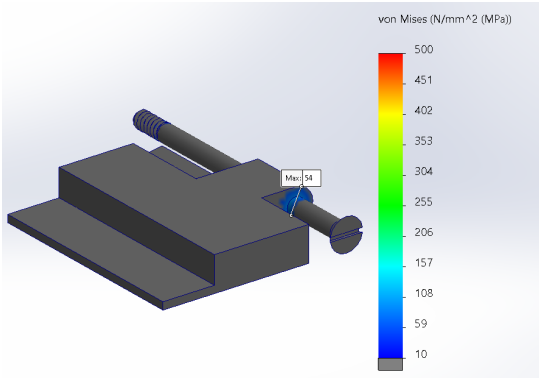

(b) Isometric View of the von Mises Stresses, excluding the FHL

Figure 6.4: Von Mises stresses in the deployment system due to acceleration loads as specified in [89]

Bending Stresses in-orbit

Beside the quasi-static loads occurring during launch, a significant load case occurs in-orbit. Deployment of the RABSII antenna is stopped at a deployment angle of 130° by the physical stop block; this results in significant deceleration. A conservative approach where the resistive torque and uncertainty factor are neglected, resulted in a linear dependent torque between 25.65 (α_{dep} = 0°) and 8.1 Nmm (α_{dep} = 130°). These values where used in the following equation:

$$\omega = \sqrt{\frac{2 \cdot T_{avg} \cdot \alpha_{dep}}{I_{fold}}} \tag{6.3}$$

where T_{avg} is the average resultant torque of a 3 spring actuation method, α_{dep} is the deployment angle of 130 degrees and I_{fold} is the inertia of the folded RABSII antenna. This results in an impact velocity of 19.04 rad/s.

In addition to the quasi-static loads experienced during the launch phase, a significant load case arises during in-orbit operations: deployment of the RABSII antenna is halted at a deployment angle of 130° by the physical stopblock. This results in significant deceleration. A conservative approach, where the resistive torque and uncertainty factor are neglected, resulted in a linear dependent torque between 25.65 (α_{dep} = 0°) and 8.1 Nmm (α_{dep} = 130°). These values where used in the following equation:

$$\omega = \sqrt{\frac{2 \cdot T_{avg} \cdot \alpha_{dep}}{I_{fold}}} \tag{6.4}$$

where T_{avg} is the average resultant torque of a 3 spring actuation method, α_{dep} is the deployment angle of 130 degrees and I_{fold} is the inertia of the folded RABSII antenna. This results in an impact velocity of 19.04 rad/s.

Figure 6.5 depicts the VMS in the deployment system under maximum deceleration, assuming a shock duration of 20 ms in accordance with the ECSS Standard [92]. Although the overall stresses within the deployment system appear to be low, the pre-load in the fasteners is reduced by approximately 120 MPa. Furthermore, an almost linear relationship is observed between the peak stresses in the FHL, RHL and hinge rod and the maximum deceleration loads. As a result, although the shock duration is limited to 20 ms and no peak impulse factor was included, the simulation results demonstrate susceptibility to variations in deceleration. This sensitivity must be taken into account in future analyses.

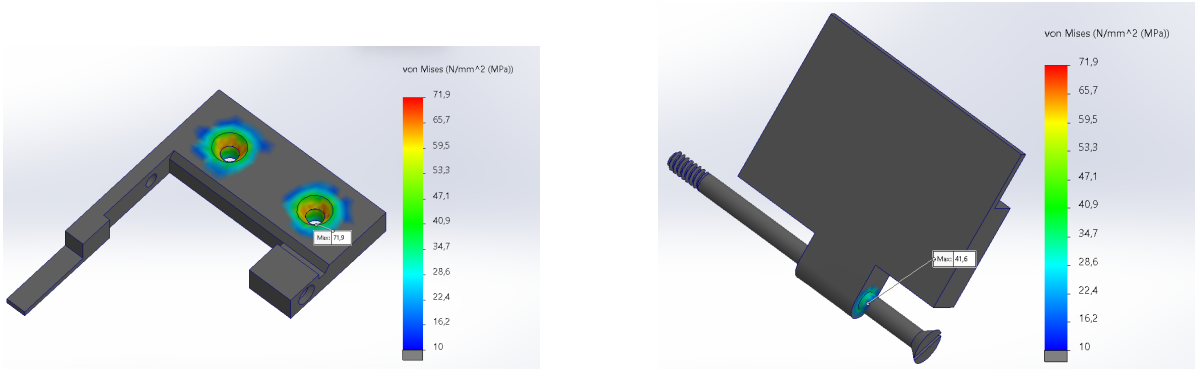

(a) von Mises Stress of the FHL

(b) von Mises Stress of the RHL and Hinge Rod

Figure 6.5: von Mises stresses of the deployment system due to in-orbit parameters.

Material Choice

The material selection for the deployment system is primarily driven by the stresses experienced under worst-case load conditions. This study considers only quasi-static loads, as dynamic loads fall outside its scope. Figure 6.4 and Figure 6.5 show the maximum stresses in the hinge leaves and hinge rod, measured at 188 MPa and 41.6 MPa, respectively. Table 6.5 presents the required yield and ultimate tensile strengths for each component, incorporating a FOSY of 1.25 and a FOSU of 2.

Component	Max. VMS [MPA]	Load Case	Max. VMS x FOSY [MPA]	Max. VMS x FOSU [MPA]
RHL	54	During Launch	67.5	108
FHL	188	During Launch	235	376
Rod	41.6	In-Orbit	52	104

Table 6.5: Von Mises stress of the FHL, RHL and hinge rod under quasi-static acceleration or thermal loads

Material	AL7075 T6	Ti6Al4V	Alloy Steels (4130, 4140 and 4340)	Stainless Steel (15-5, 17-4, 416, 440C)	Tool Steel (A2, D2, O1)
Density [g/cc]	2.8	4.4	7.8	7.8	7.7-7.9
Yield Strength [MPa]	503	883	415-460	445-1000	1970-2075
Ultimate Tensile Strength [MPa]	572	951	560-745	740-1114	2190-2355
Magnetism	Non-Magnetic	Weak	High	Moderate-High	Moderate
Thermal Expansion Coefficient $[\mu m \cdot (m \cdot K)^{-1}]$	21.6	8.6	12.2-12.3	10.1-11.0	10.8-12
Corrosion Resistance	Moderate	Excellent	Good-Very Good	Excellent	Poor-Moderate
Cost	Low	Moderate	Low	Low-Moderate	Low

Table 6.6: Material properties of available and applicable metals at ProtoLabs and/or JLCNC.

Table 6.6 lists the material properties of potential candidates, sourced from ProtoLabs and/or JLCNC. Currently, Al7075-T6 is used for the entire mechanism due to its extensive heritage and its sufficient yield and ultimate tensile strengths. Future iterations may involve slight deviations and will include a more detailed analysis of material selection for individual components.

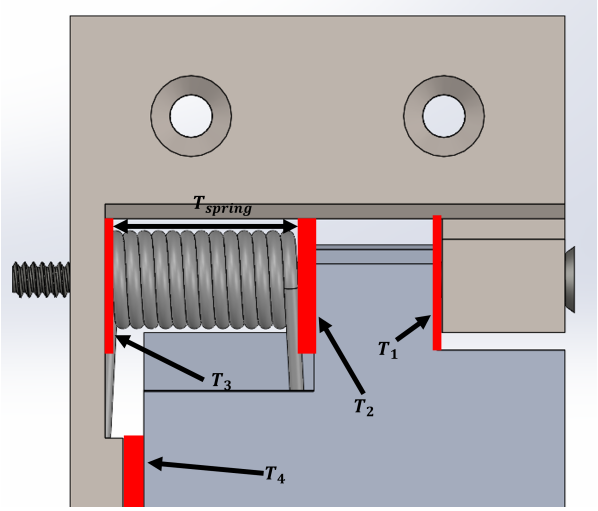

Figure 6.6: Critical margins required for potential thermal deformation of the final design

Thermal and Acceleration Deformations

The current iteration of the deployment system (Figure 6.2) allows for minimal design margins due to strict volume constraints. Consequently, its deployment performance could be significantly affected by deformations resulting from acceleration and thermal loads. Potential issues include increased stresses, elevated friction and the risk of deadlocking. Therefore, deformations due to both thermal and acceleration induced loads, combined with manufacturing tolerances (DIN 2786-F), are assessed. Hot and cold case simulations are conducted using Al7075-T6 as the selected material, in order to evaluate thermal deformation and stress behavior under extreme temperature conditions.

Figure 6.6 highlights the critical edges where deformations could potentially impair deployment. The simulations (hot and cold case) used 20°C as the zero-strain reference temperature (room temperature) and thermal deformations, resulting from heating the deployment system to 80°C (MIS-MH-012), were assessed. The results are presented in Figure 6.7.

It is apparent that the deformations resulting from thermal loads are significantly greater than those induced by maximum acceleration loads, exceeding them by approximately two orders of magnitude. From this, it can be concluded that acceleration-induced deformations are negligible. Table 6.7 presents the maximum deformations along the critical edges. The required margins for these critical edges can be determined using the following formulas:

$$T_1 > T_{1-FHL} + T_{1-RHL} + 2 \cdot DIN2786 - F \tag{6.5}$$

$$T_2 > T_{2-RHL} + DIN2786 - F \tag{6.6}$$

$$T_3 > T_{3-FHL} + DIN2786 - F \tag{6.7}$$

$$T_4 > T_{4-FHL} + T_{4-RHL} + 2 \cdot DIN2786 - F \tag{6.8}$$

$$T_{spring} > T_2 + T_3 + W_{spring} \tag{6.9}$$

where DIN 2786-F is 0.05 mm and W_{spring} is 5.2 mm.
The determined margins required to prevent deadlocking, along with the actual applied margins, are presented in Table 6.8. Thermal deformations in the hinge rod (R_{rod}) fall within the allowance of the H8/h9 loose fit.

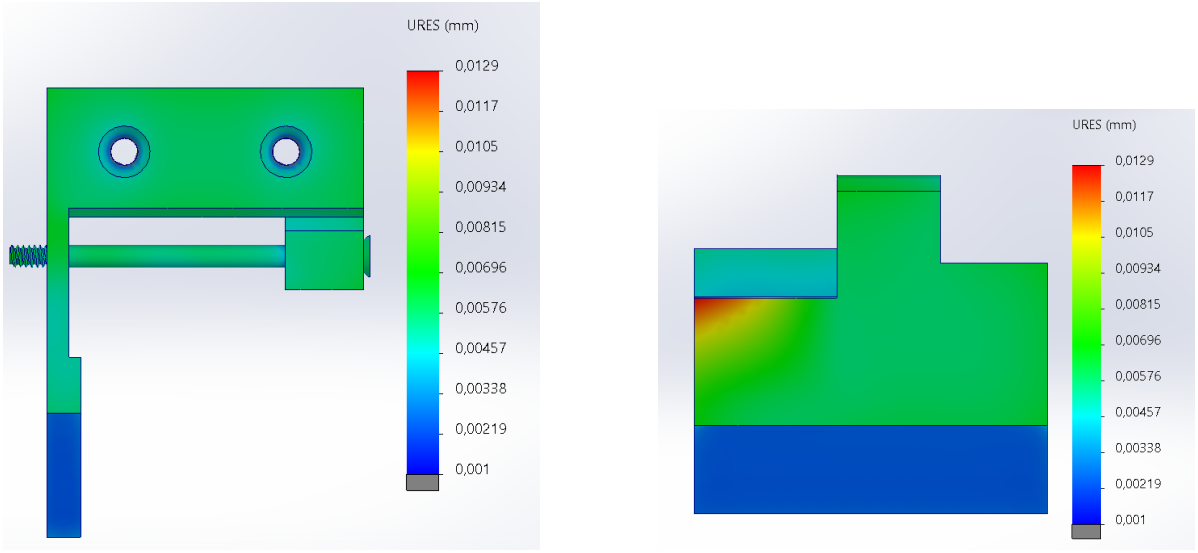

(a) Thermal expansion of the FHL and hinge rod

(b) Thermal expansion of the RHL

Figure 6.7: Thermal expansion of the deployment system due to the hot case of 80°, from a zero-strain temperature at 20°.

Critical Points	Value
T_{1-FHL}	0.0207
T_{1-RHL}	0.0215
T_{2-RHL}	0.0226
T_{3-FHL}	0.0218
T_{4-RHL}	0.023
T_{4-FHL}	0.0236
R_{rod}	0.0226

Table 6.7: Maximum thermal deformation at various critical edges.

6.2.3. Iteration: Cold Welding and Actuation Method Performance

Cold welding is a solid-state welding process in which materials are joined by applying force without the use of heat. Metals in a vacuum environment are particularly susceptible to this phenomenon, with applied forces as low as 0.3 N potentially causing adhesion [93]. In other words, cold welding can unintentionally function as a HDRM, where breaking the newly formed bond may require significant forces. A notable example is the Galileo spacecraft, where antenna deployment failure occurred due to a cold welding incident [94].

In Concept 4, both the hinge mechanism and actuation method primarily consist of metallic components. The hinge mechanism is made of Al7075-T6, while the actuation method uses stainless steel ISO 6931-1. To prevent cold welding, potential points of occurrence must first be assessed. Cold welding between the torsion spring coils is highly unlikely due to the low mass of the spring. With a weight of less than 0.3 grams, achieving an impact force of 0.3 N would require accelerations of 3000 m/s^2, which is outside the expected domain of acceleration.

Cold welding between the hinge leaves presents a credible risk. Due to the added mass of the RABSII antenna elements, the threshold force for cold welding could be reached under accelerations of 1.5G, which are common during launch. Consequently, mitigation measures are necessary. The critical contact points correspond to those identified for thermal expansion and are shown in Figure 6.6.

Mitigation strategies include using dissimilar materials or applying surface coatings. However, material substitution alone is not always effective. In some cases, adhesion forces may increase when dissimilar

Critical Points	Req. Margins	Applied Margins
T_1	0.1422	0.20
T_2	0.0726	N/A
T_3	0.0718	N/A
T_4	0.1666	0.54
T_{spring}	5.244	5.4

Table 6.8: Applied margins due to thermal deformations.

metals are used [94]. This typically necessitates the use of coatings. To mitigate cold welding between the hinge leaves and hinge rod, a different material is selected for the hinge rod, combined with surface treatments and soft coatings. Soft coatings composed of solid lubricants, such as MoS_2, are preferred over hard coatings, due to their ability to self-repair upon impact, providing enhanced protection against cold welding [93]. Coating should be applied to both contact surfaces, along with surface treatments such as hard anodizing [94]. Accordingly, hard anodizing is proposed for the Al7075-T6 components (RHL and FHL) and a material substitution is proposed for the hinge rod. Given the susceptibility of the hinge rod to thermal buildup, a material with a lower thermal expansion rate is preferred. Hinge rods made from titanium or stainless steel (M1 bolts) are available (CNC Machining), are both suitable based on their yield and ultimate tensile strengths.

6.2.4. Iteration: HDRM and Antenna Fastener Risks

This section present the accompanied risks with the implementation and integration of the HDRM and adhesive fastening of the RABSII Antenna.

HDRM Risks

For integration of the burn wire mechanism, a simple yet effective approach has been selected. The PCB of the RABSII antenna incorporates a hole through which the retention wire is threaded. A small cutout in the RHL ensures flush placement of the wire, minimizing the risk of it getting stuck and reducing the required length of the retention wire.

The burn wire mechanism has well-established heritage within the DSSP, with numerous safety measures already implemented on previously launched satellites. Material selection for the retention wire is primarily driven by outgassing properties. In the vacuum environment of space, the retention wire evaporates due to exposure to thermal and environmental conditions, effectively reducing the risk of deployment failure caused by the HDRM. As a result, critical failure modes, such as a stuck retention wire or thermal knife malfunction resulting in no deployment, are considered highly unlikely.

The primary risk associated with the HDRM is delayed deployment. The RABSII antenna elements are composed of SMA wire, which unfolds in response to thermal flux in orbit. If deployment of the system is delayed, the antenna elements may unfold prematurely. This could potentially result in interference with or damage to other external appendages of the host satellite. Additionally, due to increased inertia of the unfolded antenna, the resistive torque acting on the system also increases. Ensuring sufficient deployment torque under all configurations of the antenna elements is therefore critical.

Improper assembly introduces further risks, such as insufficient pre-load or premature deployment. These issues can induce unwanted vibrations and impose unnecessary mechanical stress on the deployment system components, compromising performance and reliability.

Mitigation strategies to prevent low pre-load, premature deployment and delayed deployment include meticulous assembly and extensive testing under mission-like conditions. The addition of redundancy in the thermal knives should also be considered. However, as the deployment system shares the burn wire mechanism of the solar panels, this decision ultimately rests with the Delfi-Twin stakeholders.

RABSII Antenna Adhesive Fastening

The current design of a RABSII antenna element includes an FR-4 plate with a thickness of 1.57 mm, an SMA wire with a ⌀0.3 mm and a mini-coax cable (serving as the communication and electrical interface). The FR-4 plate acts as the bonding interface between the deployment system and the RABSII antenna. A conventional bolt fastener requires a minimum thread engagement of 1.5d in an aluminum tapped hole, along with a separate nut. Combined with the FR-4 plate, this results in a total thickness of at least 4.07 mm. A threaded insert eliminates the need for a nut and offers a more compact fastening method. However, similar to a conventional bolt, the bolt head exceeds the 2 mm envelope, assuming that the RHL has a thickness of 0.43 mm at the bonded area. This results in a total thickness of approximately 3 mm. Since the FR-4 plate nearly occupies the allocated 2 mm, both bolted connections and threaded inserts violate the volume constraints specified in BDG-MH-020 and are therefore infeasible. As a result, an alternative fastening method is required.

Adhesive bonding provides a viable solution under strict thickness constraints. A simple single lap joint forms the bond between the RABSII antenna and the RHL. Key adhesive properties include peel and shear strength. According to Table 6.4, the worst-case acceleration loads occur during launch and in-orbit. During launch, shear forces dominate due to restricted movement, whereas in orbit, peel forces become more critical. Both load cases must influence adhesive selection and require careful consideration to ensure reliable performance.

For the required shear strength during launch, the following equations is applied:

$$\sigma_{shear} = \frac{m \cdot 8.5G}{A_{bond}} \tag{6.10}$$

The peel strength (p_s) is critical during in-orbit deployment, particularly at the moment of impact when the deployment system decelerates. The deceleration load differs between the folded and unfolded configurations of the antenna element. The highest deceleration occurs when the antenna is fully folded. Assuming a deceleration from 19.04 rad/s to 0 rad/s within 20 ms, the strain on the adhesive bond can be determined as follows:

$$p_s = \frac{F_{peel}}{L_{bond}} \tag{6.11}$$

with

$$F_{peel} = \frac{3 \cdot T}{2 \cdot L_{bond}} \tag{6.12}$$

which results in:

$$p_s = \frac{3 \cdot I \cdot \alpha}{2 \cdot L_{bond}^2} \tag{6.13}$$

Adhesive Type	Shear Strength [MPa]	Peel Strength [N/mm]	L_{bond} [mm]
Cyanoacrylate	7 to 14	0.2 to 3.5	38.84 to 9.28
Anaerobic Acrylic	7 to 14	0.2 to 2.0	38.84 to 12.28
Polyurethane	7 to 17	2.0 to 9.0	12.28 to 5.78
Modified phenolic	14 to 28	3.5 to 7.0	9.28 to 6.56
Epoxy	10 to 28	0.4 to 2.0	27.46 to 12.28
Bismaleimide	14 to 28	0.2 to 3.5	38.84 to 9.28
Polyimide	14 to 28	0.2 to 1.0	38.84 to 17.36
Modified epoxy	20 to 40	4.5 to 14	8.19 to 4.64

Table 6.9: Typical shear strength and peel strength characteristics [95], with their corresponding required range for L_{bond}.

Table 6.9 presents typical shear and peel strength characteristics, along with the minimum required bond length (L_{bond}). Assuming a factor of safety (FOS) of 1.2, L_{bond} can be less than 32.952 mm. The use of an epoxy adhesive is recommended, as epoxies are widely used for bonding metal and composite materials. However, final adhesive selection remains complex, as many relevant factors are not yet

fully defined [95]. Figure 6.8 provides an overview of key factors influencing the final adhesive choice from the ECSS Handbook [95].

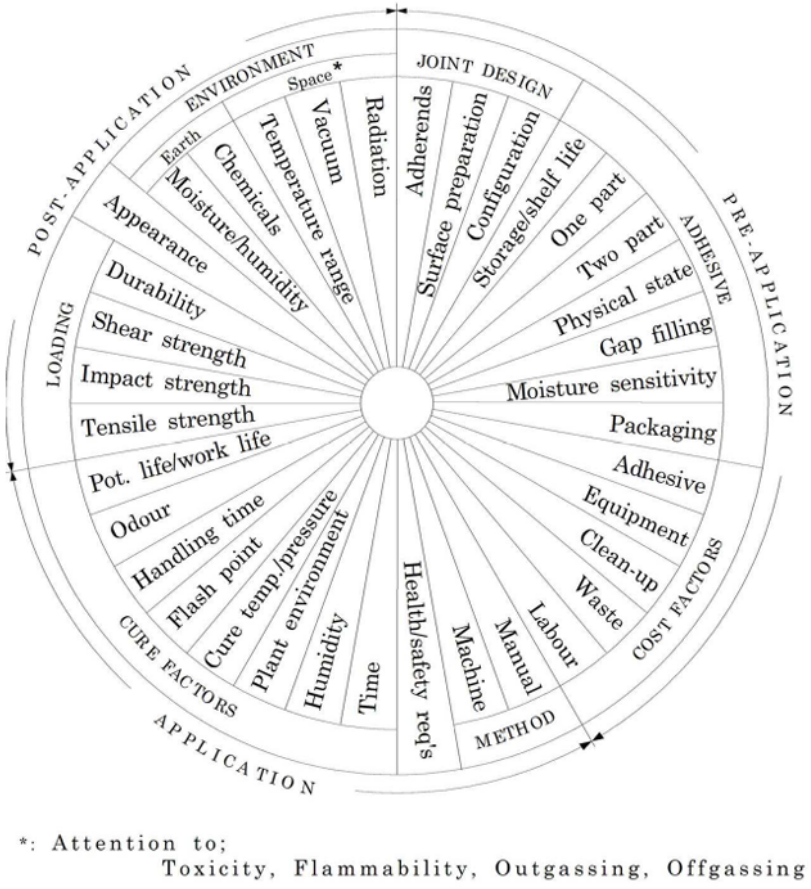

Figure 6.8: Adhesive selection factors, as defined by the ECSS Standard [95]

7

Design Overview and Reflection

Based on the results of the concept study and design analysis, the final design of the deployment system is presented in this chapter. This includes the complete design with finalized parameters, along with the associated budgets for volume, power and mass. Subsequently, the system's performance is assessed through a series of validation simulations. This is followed by a risk analysis, in which the most significant risks are identified and mapped. Finally, the compliance of the deployment system with the requirements and key performance parameters outlined in Section 4.2 are evaluated.

7.1. Design Overview

The final design of the deployment system for a RABSII antenna element consists of three identical hinge mechanisms, each housing a torsion spring as the actuation method. A burn wire mechanism has been integrated to mitigate the risk of premature deployment. This section presents the components of each hinge mechanism and the rationale behind key design choices. Next, renders of the final design are provided which includes its effective area and volume. Finally, the mass budget is detailed based on CAD model (Solidworks 2024) estimates and the cost budget is presented using supplier-provided quotes.

7.1.1. Mechanism

Figure 7.1 presents the hinge mechanism used for the deployment system of the RABSII antenna. Each hinge mechanism consists of six distinct components, excluding the HDRM. These include the FHL, RHL, actuation method, two types of fasteners and the hinge rod. While the actuation method and fasteners are COTS components, the FHL, RHL and hinge rod are custom-made. The following sections present each component individually, along with the rationale behind their design choices.

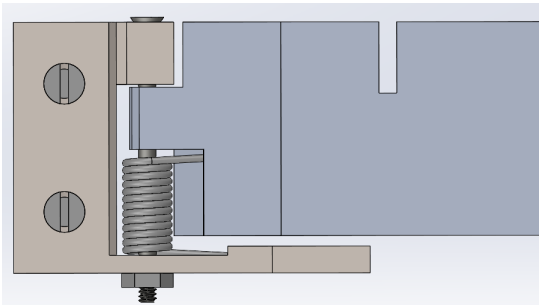

(a) Top View of the Hinge mechanism's Stowed Configuration

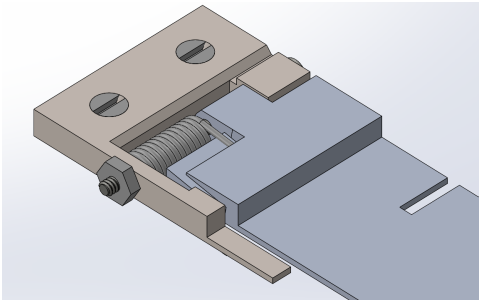

(b) Isometric View of the Hinge mechanism's Stowed Configuration

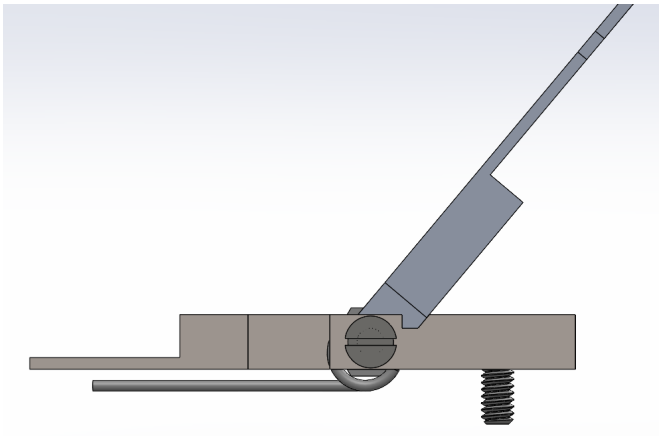

(c) Side View of the Hinge mechanism's Deployed Configuration

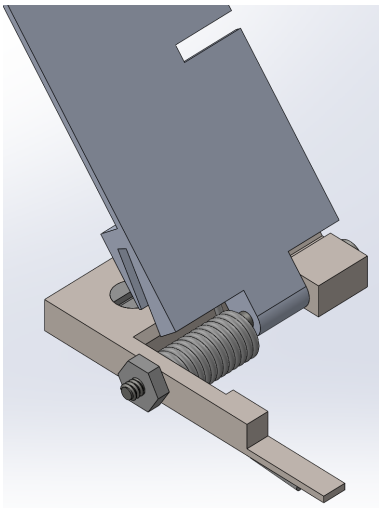

(d) Isometric View of the Hinge mechanism's Deployed Configuration

Figure 7.1: Hinge mechanism's stowed and deployed configurations.

Fixated Hinge Leaf

The FHL is mounted on the external side of the host satellite, where it consists of a physical stop block to prevent angular overshooting. It also serves as the fixed interface between the host satellite and the RHL. The FHL has a width of 14.1 mm and a length of 20 mm. Figure 7.2 presents various views of the final FHL design. Detailed drawings of the FHL can be found in Appendix D.

Important design choices of the FHL include:

- The unusual geometry of the FHL, which features an additional 'poke' parallel to its main hinge knuckle, is imposed by the actuation method. One of the torsion spring legs is positioned beneath this 'poke'.
- The width of the FHL is smaller than the maximum allocated width of 16 mm for the hinge mechanism. On one side, ECSS standards mandate that a bolt length of at least two pitches must protrude beyond the threaded part [90]. On the other side, to avoid a 0.05 mm border, as the countersunk fasteners have an outer radius of 1.90 mm, the hinge rod is slightly extruded, increasing the border to 0.25 mm.
- The FHL is made of Al7075-T6, hard-anodized, with an additional MoS_2 coating. Hard anodizing and the MoS_2 coating reduce the risk of cold welding between the FHL and other metallic components [94].
- The FHL is secured to the host-satellite using three M1.2 bolts. Simulations in Section 6.2.2 indicate that two bolts would suffice.

- The placement of the FHL fasteners is carefully designed to comply with ECSS standards [90]. The standard mandates that the minimum distance from the center of a bolt hole to the edge must be at least 1.5 times the nominal diameter of the bolt.

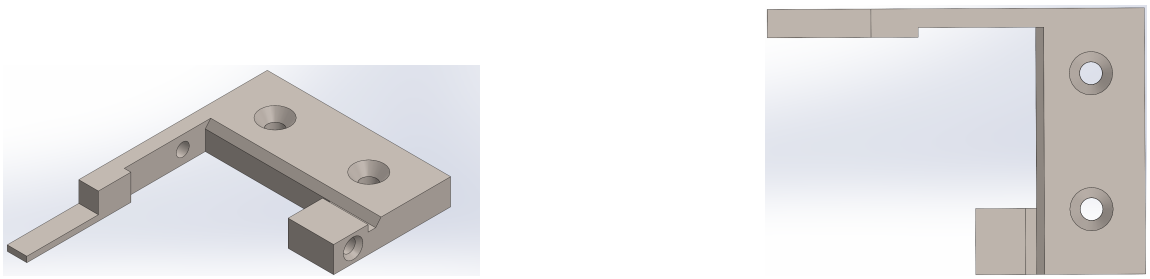

(a) Isometric view of the FHL **(b)** Top view of the FHL

Figure 7.2: Various perspectives of the FHL model.

Rotational Hinge Leaf

The RHL is fixed to the RABSII antenna, rotates around the hinge rod, enables integration with both the HDRM and the actuation method and serves as the interface between the FHL and the RABSII antenna. The RHL has a width of 12 mm. While its length depends on the applied epoxy adhesive, it will vary between 14.8 and 33 mm. Figure 7.3 presents various views of the final RHL design. Detailed drawings of the RHL can be found in Appendix D.

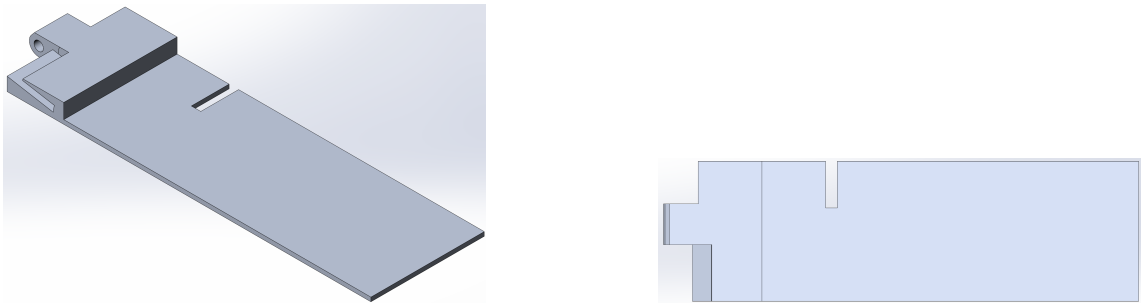

(a) Isometric View of the RHL **(b)** Top View of the RHL

Figure 7.3: Various perspectives of the RHL model.

Important design choices of the RHL include:

- The RHL consists of an extended thinner plate, significantly longer than any other parts. This is where the RABSII antenna is bonded with an epoxy adhesive, where its length varies between 14.8 and 33 mm (Table 6.9 and a FOS of 1.2 [95]).
- The geometry of the RHL includes various cutouts to enable integration with the actuation method. One cutout is angled at 10° and allows the torsion spring leg to be secured without additional fasteners.
- The RHL consists a cutout for integration with the HDRM. Since the retention wire of the HDRM is looped through the RABSII antenna's PCB, this cutout allows for flush placement. This ensures compliance with volume constraints while also preventing the risk of delayed deployment.
- The RHL is made of Al7075-T6, hard-anodized, with an additional MoS_2 coating. Hard anodizing and the MoS_2 coating reduce the risk of cold welding between the RHL and other metallic components.

Hinge Rod

The hinge rod passes through the FHL, RHL and actuation method. Figure 7.4 presents its final design. Detailed drawings of the hinge rod can be found in Appendix D.

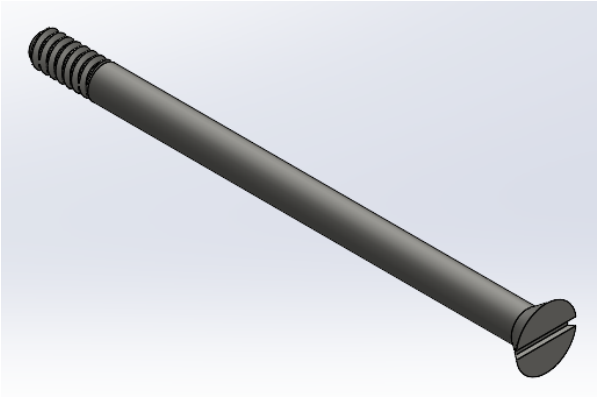

Figure 7.4: Isometric view of the Hinge rod.

Important design choices of the hinge rod include:

- The total length of the hinge rod is 16 mm, allowing three hinges to be placed parallel to each other along the lateral axis of a PocketQube (50 mm).
- The hinge rod has an M1 threaded end with a length of 2 mm. The ECSS standard requires that the thread must protrude by a minimum of two pitches, which has a length of 0.5 mm [90]. Additionally, since the nut has a thickness of 0.8 mm, the threaded end must be at least 1.3 mm long.
- The hinge rod is modeled after a countersunk M1 bolt, reducing its required extrusion relative to the external face of the FHL.
- The hinge rod is made of Ti6Al4V, distinct from the hinge leaves and is coated with MoS_2. The material selection reduces the risk of cold welding between the hinge rod and the hinge leaves. The additional coating further mitigates the risk of cold welding. Especially as soft lubricant coating allow for minor 'self-repair' during small and recurring vibrations [94], which represents the expected load case for the hinge rod.

Actuation Method

The actuation method for the final design is the Lesjöfors 8318, a torsion spring with an outer diameter of 2.8 mm and a maximum rotation angle of 227°. In the stowed configuration, the torsion spring is pre-loaded to 190°, which corresponds to 83.7% of its maximum rotation angle.

Table 5.2 presents the relevant parameters of the actuation method. Section 5.3.1 provides a detailed discussion of the torsion spring selection.

Other Components

In addition to the custom-made components and the actuation method, the deployment system includes three M1.2 bolts and an M1 nut.

The selection of M1.2 bolts is driven by the ECSS standard, which requires a minimum thread engagement in aluminum of 1.5 times the nominal diameter [90]. Given that the thickness of the FHL is 2 mm, the maximum metric bolt that could theoretically be used is M1.3. However, as M1.3 bolts are not COTS, an M1.2 bolt is selected.

For the M1 nut, the material selection is also driven by the ECSS standard, which states that the nut material must be more ductile than the bolt material [90]. This requirement ensures that during tightening, the nut threads can deflect appropriately and properly seat onto the bolt threads. The hinge rod is made of Ti6Al4V, which has an elongation at break of 14%. To satisfy this requirement, the M1 nut is made of stainless steel A1, which has an elongation at break of 60%. Lastly, since a standardized M1 nut is a hexagon with a minimum height of 2.5 mm, it must either be sanded down or replaced with a custom-made smaller nut to comply with BDG-MH-019.

7.1.2. Complete Deployment System

The final deployment system for each antenna element consists of three parallel hinge mechanisms, each with its own actuation method. The system has an envelope of 50x20x2 mm^3, where the length (20 mm) varies depending on the RABSII antenna. Figure 7.5 illustrates both the stowed and deployed states of the deployment system, including a transparent mock PCB to indicate the placement of the RABSII antenna.

Important design choices for the deployment system include:

- The three hinge mechanisms per antenna element differ slightly depending on its role; One hinge mechanism is not fixed to the RABSII antenna and serves solely as an actuator, whereas the other two hinge mechanisms are fixed to the RABSII antenna, with Section 6.2.2 indicating that one of them functions as a redundant component.
- A 1 mm border has been added along the absolute width of the hinge mechanisms. This results in a spacing of approximately 2.6 mm between the FHLs and 1 mm between the hinge rods of each hinge mechanism.
- Since the outer diameter of the actuation method exceeds 2 mm, milling in the external plate is required to ensure that the deployment system does not protrude beyond 2 mm.

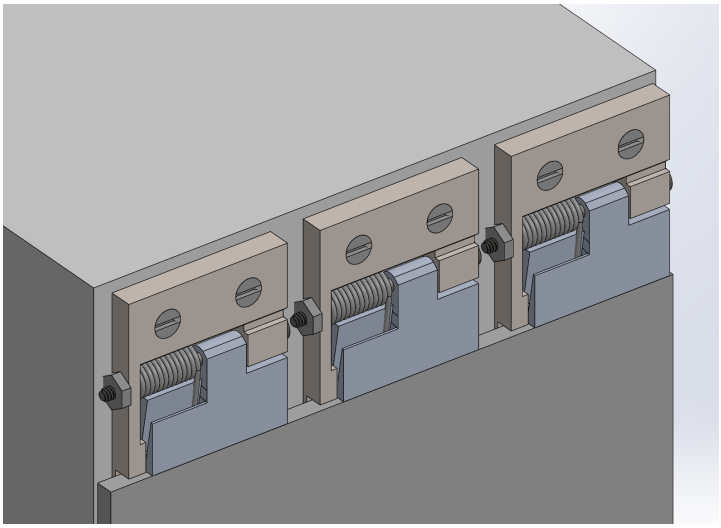

(a) Isometric View of the deployment system's stowed configuration

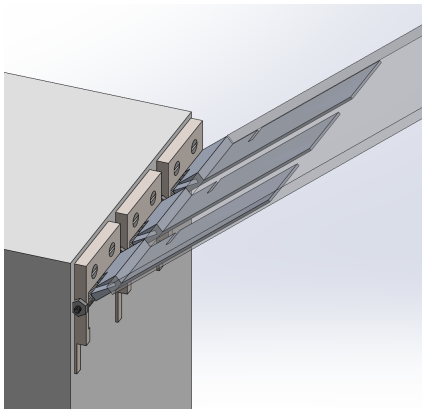

(b) Isometric view of the deployment system's deployed configuration

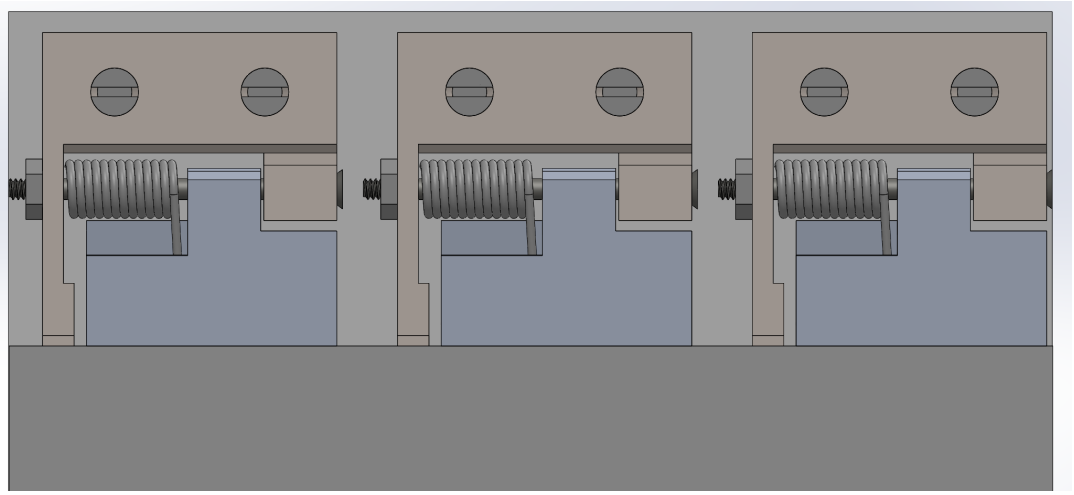

(c) Top View of the Deployment System's Stowed Configuration

Figure 7.5: Deployment system in stowed and deployed configurations.

7.2. Performance

The performance of the deployment system is assessed based on three general criteria. These are the deployment performance, structural integrity and compliance with mass and volume budgets. Deployment performance refers to the system's ability to successfully initiate and complete deployment, including achieving the required deployment angle. Structural integrity involves the system's capacity to withstand loads and mitigate failure risks. Finally, adherence to mass and volume budgets ensures compatibility with the overall satellite mass, power and volume constraints.

7.2.1. Deployment Performance

The deployment performance of the deployment system is evaluated based on the motorization factors defined in the ECSS standard [85] (also defined in Section 6.2.1). Uncertainty factors applicable to a theoretical approach are included and a conservative methodology is applied throughout the analysis. While certain components of the resistive torque vary with the deployment angle (e.g., reduction in F_r and a non-resistive nature of I beyond a deployment angle of 90°), only the absolute maximum values of each component are considered in the initial analysis. Appendix A provides the necessary calculation and assumptions.

Figure 7.6 shows the actuation torque for both 2-spring and 3-spring configurations, as well as the maximum resistive torque for the folded and unfolded states of the RABSII antenna. The final deployment angle achieved with the 2-spring configuration is equal to 43.47°, while the 3-spring configuration achieves a value of 92.47°.

Figure 7.6 shows that the actuation torque at low deployment angles exceed the resistive torque. However, at a larger deployment angle, there is insufficient actuation torque. As discussed in Section 6.2.1, optimal conditions suggest implementing a 5-spring configuration to ensure sufficient actuation torque throughout the entire deployment. However, this recommendation is based on overly conservative assumptions (see Appendix A). Both F_r and the wire harness contribution to H_a have been conservatively estimated. Similarly, for H_a due to aerodynamic drag, the stowed configuration of the RABSII antenna was assumed to have a relatively large surface area, leading to an overestimation of the resistive torque. A more accurate approach would significantly reduce the resistive torque, potentially allowing for a successful deployment with two torsion springs instead of five.

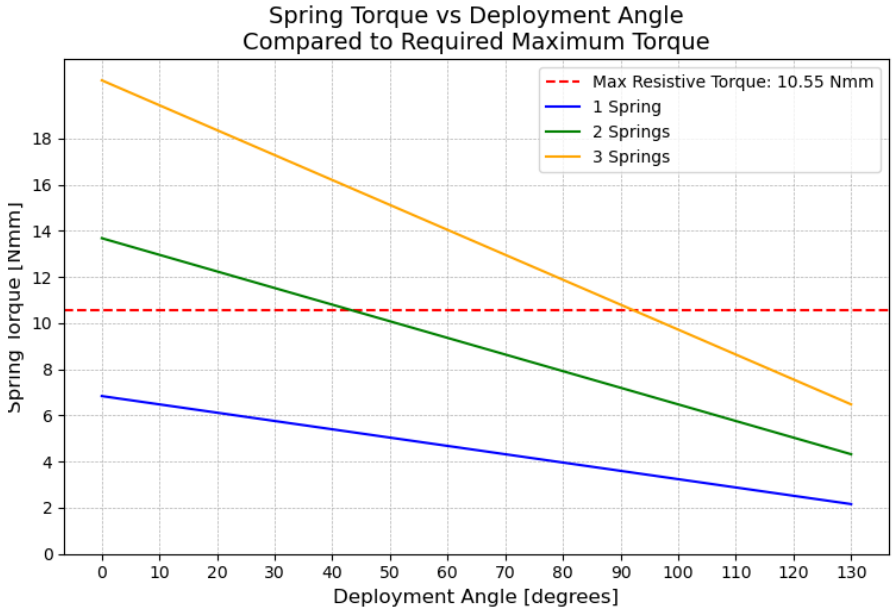

Figure 7.6: Actuation torque supplied by a 2 and 3 spring configuration compared to the resistive torque.

7.2.2. Structural Integrity

The structural integrity of the deployment system is assessed through various simulations. These include evaluations of VMS under launch and bending loads, as well as deformation analysis under thermal loads. Table 6.4 summarizes the worst-case scenarios for each type of load. While initial simulations were conducted in Section 6.2.2, the analyses presented in this section are performed using the final design configuration.

Figure 7.7 illustrates the VMS under launch loads, while Figure 7.8 presents the VMS under maximum impact loads in-orbit. It is notable that the VMS under impact loads is significantly higher, especially in the area around the rod. All expected VMS values remain well below the yield and ultimate tensile strength of the respective materials, even when FOSU and FOSY are applied.

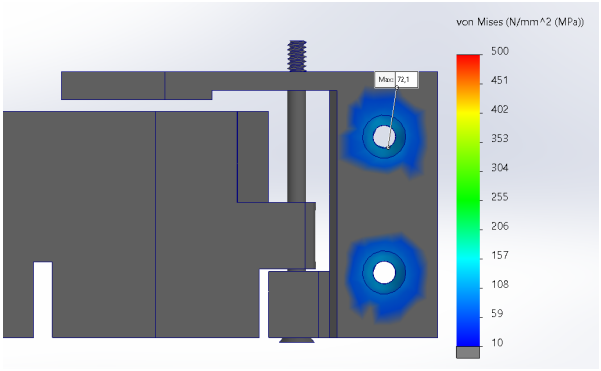

Figure 7.7: Von Mises Stresses of the Final Design of the Deployment System due the Quasi-Static Acceleration Loads during Launch

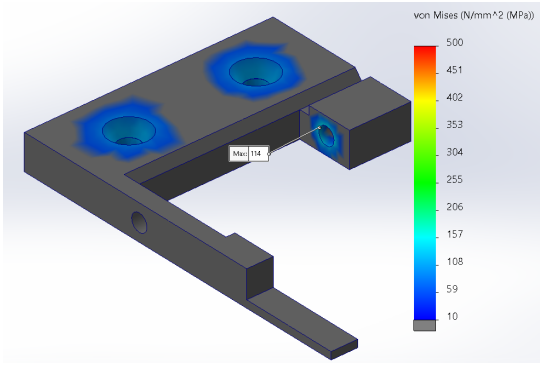

(a) Von Mises Stresses of the FHL due to the in-orbit acceleraton loads

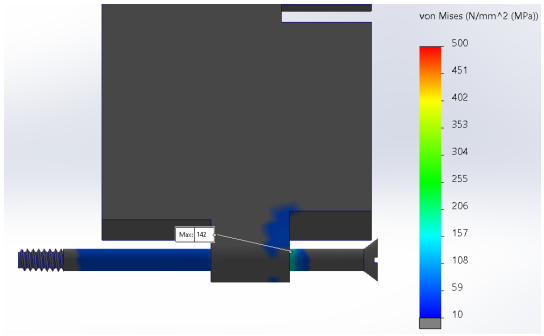

(b) Von Mises Stresses of the RHL and Hinge Rod due to the in-orbit acceleraton loads

Figure 7.8: Von Mises Stresses of the Final Design of the Deployment System due the Quasi-Static Impact Acceleration loads during Deployment

Figure 7.9 shows the deformations for both the hot and cold-case. The zero-strain temperature is 20°C, with the hot-case at 80°C and the cold-case at -20°C. Similar critical areas as identified in Figure 6.6 are considered, and Table 7.1 reassesses them to ensure that the environmental conditions do not result in deadlocking.

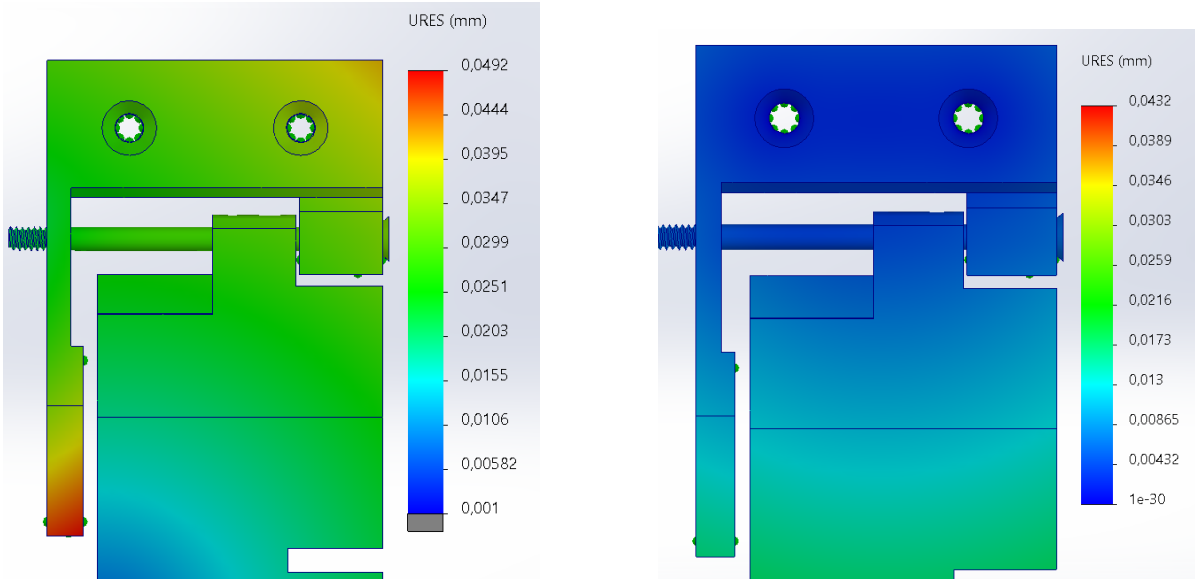

(a) Isometric View of the Deployment System's Stowed Configuration

(b) Isometric View of the Deployment System's Deployment Configuration

Figure 7.9: Thermal expansion of the final design of the deployment system under a hot case of 80°C and a cold case of -20°C.

Critical Points	Critical Edges	Deformation [mm] Hot Case	Deformation [mm] Cold Case	Margin req. [mm]	Margin applied [mm]
T_1	T_{1-RHL}	0.03209	0.006253	0.16415	0.2
	T_{1-FHL}	0.03206	0.006907		
T_{spring}	T_{2-RHL}	0.03030	0.006357	5.2610	5.4
	T_{3-FHL}	0.03080	0.008364		
T_4	T_{4-RHL}	0.03713	0.04302	0.18684	0.54
	T_{4-FHL}	0.04971	0.007862		
R_{rod}	R_{rod}	0.03307	0.003704	0.03307	

Table 7.1: Maximum Thermal Deformation at critical edges and applied margins.

7.2.3. Mass, Volume and Power Budgets

The RABSII antenna consists of two elements, each antenna requires an independent deployment system. Each deployment system consists of three hinge mechanisms. Table 7.2 presents the estimated mass of the six hinges, with a total mass of 9.956 g and an individual hinge mass of 1.659 g. Similarly, Table 7.3 presents the estimated cost of the six hinges, with a total cost ranging from 331.08 to 613.08 euros and a per-hinge cost between 55.18 and 102.18 euros.

This mass estimate excludes the HDRM and additional fasteners required to connect the RABSII antenna to the RHL. The latter is expected to increase the total system mass by no more than 0.5 g. Also, the deployment system is likely to utilize the HDRM of the solar panels. This means its additional mass contribution is limited to the retention wire and thermal knife, which are expected to add less than 0.5 g.

The power budget of the antenna system is considered negligible. The requirement for limited power consumption is derived from the overall Delfi-Twin mission constraints for the antenna deployment system. As the HDRM is expected to operate in conjunction with the burn wire mechanism of the solar panel, its power consumption is accounted for within the existing budget of that mechanism, thereby imposing no additional power demand.
For custom-made components, quotes were obtained from both JLCNC and Protolabs. However, no direct quote could be provided for the hinge rod, as it requires manual revision by the supplier. Nevertheless, based on the estimated cost of the FHL and RHL, the cost of the hinge rod is not expected to

significantly exceed 20 euros. The total deployment system cost is estimated to range between 331.08 and 613.08 euros, with a per hinge mechanism cost between 55.18 and 102.18 euros. This cost estimate excludes labor hours, shipping, handling and additional spare parts. The HDRM is also excluded, as the deployment system is expected to integrate with the solar panel HDRM, making its additional cost negligible.

Part	**Material**	**Qty. [-]**	**Mass per Part [g]**	**Mass at Qty. [g]**
FHL	Al7075-T6	6	0.550	3.30
RHL	Al7075-T6	6	0.850	5.10
Hinge Rod	Ti6Al4V	6	0.056	0.336
Torsion Spring	Stainless Steel	6	0.108	0.648
M1 Nut	Stainless Steel A1	6	0.030	0.18
M1.2 Bolt	Stainless Steel A1	12	0.034	0.408
			Total Mass	**9.956**

Table 7.2: Mass budget for complete deployment system onboard the host-satellite.

Part	**Supplier**	**Name**	**Qty. [-]**	**Cost per part [€]**	**Cost at Qty. [€]**	**Cost [€]**
FHL	JLCNC ProtoLabs	N/A	6	24.66 107.74	13.82 38.37	82.89 230.22
RHL	JLCNC ProtoLabs	N/A	6	21.16 101.16	12.37 34.81	74.19 208.86
Hinge Rod	Estimate**	N/A	6	20**	20**	120
Torsion Spring	Lesjöfors	8318	6	6.37	6.37	38.22
M1 Nut	King Micro-Schroeven	Hex Nut M1 RVS DIN 934	6	0.22	0.22	1.32
M1.2 Bolt	McMaster-Carr	18-8 Stainless Steel Slotted Flat Head Screws	12	0.80	0.80	14.46
				Total Cost (JLCNC) **Total Cost (ProtoLabs)**		**331.08** **613.08**

Table 7.3: Cost budget for complete deployment system (6 hinges) onboard the host-satellite
**Quote could not be provided, estimate is based on complexity of the design and its volume.

7.3. Proof of Concept

To validate the working principle of the proposed deployment mechanism, a proof of concept is developed in the form of a five-times scale model. This model is fabricated using 3D printing technologies and incorporates a torsion spring. An iterative refinement process is applied to improve dimensional accuracy and ensure a proper fit between components.

The initial design parameters adhere to ISO 2768 tolerances. The practical limitations of 3D printing, particularly the relatively large nozzle size (0.4 mm), necessitated several small iterations to achieve a proper fit. This was especially relevant for the interface between the hinge rod and the (normally) tapped holes. Additionally, T_{spring} (Figure 6.6) was selected based on the available torsion spring used in the prototype, which required a scaling factor of approximately two rather than five. Finally, to avoid incorporating a large adhesive bond area that would not contribute meaningful insight at this stage, the length of the flat plate was reduced from the nominal 20 cm to a minimal 2 cm.

Figure 7.10 shows the final assembly of the proof of concept. This scaled model effectively demonstrates the functionality of the proposed deployment mechanism, where the importance of tight margins is also reaffirmed.

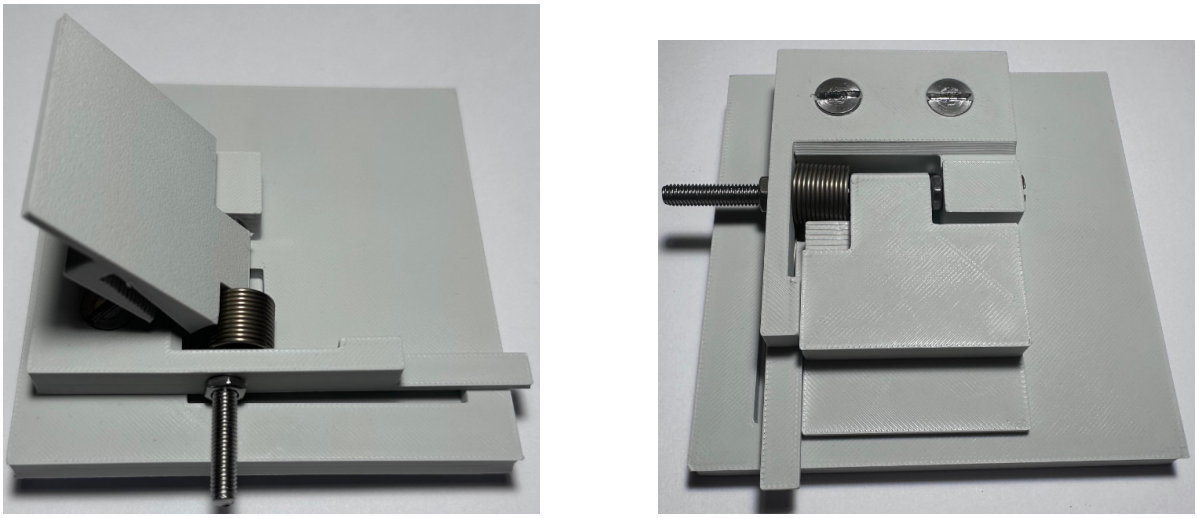

(a) Proof of Concept in its deployed configuration.

(b) Proof of Concept in its stowed configuration.

Figure 7.10: Scale model (Proof of Concept) of the final design of the deployment system.

7.4. Risk Analysis

Identifying the technical risks associated with the deployment system enhances understanding and enables the implementation of mitigation strategies. Following the iterative process described in Section 6.1, which resulted in the current design, several risks have been identified and a corresponding risk map has been developed.

7.4.1. Risks

Table 6.2 presents various failure modes of Concept 4 and the mitigation steps incorporated into the final design. Based on the FMEA, the following risks have been identified:

- **RISK-01**: Detachment of the RABSII antenna element from the deployment system, causing loss of functionality and space debris generation.
- **RISK-02**: Structural failure of a hinge mechanism, resulting in detachment from the RABSII antenna.
- **RISK-03**: Structural failure of a hinge mechanism, resulting in detachment from the host-satellite.

- **RISK-04**: Structural failure of a 'pusher' hinge mechanism, resulting in detachment from the host-satellite and space debris generation.
- **RISK-05**: Failure to initiate deployment of the RABSII antenna element, due to faulty HDRM or cold welding.
- **RISK-06**: Delayed deployment, causing initiation of deployment in the unfolded state of the RABSII antenna.
- **RISK-07**: Minor angular overshoot (<10°) of the maximum deployment angle (130°), caused by small deformation of the hinge leaves or slack in the fasteners.
- **RISK-08**: Excessive angular overshoot (>10° of the maximum deployment angle (130°), caused by large deformation of the hinge leaves.
- **RISK-09**: Fluctuations of the deployment angle in the unfolded state of the RABSII antenna element between 90 and 130°.
- **RISK-10**: Fluctuations of the deployment angle in the unfolded state of the RABSII antenna element between 0 and 130°.

7.4.2. Risk Map

Severity	Rare	Unlikely	Possible	Likely	Almost Certain
Catastrophic		RISK-01			
Major		RISK-04 RISK-05 RISK-08 RISK-10			
Moderate		RISK-02 RISK-03	RISK-06		
Minor					RISK-09
Insignificant				RISK-07	

Likelihood

Figure 7.11: Risk map of the deployment system.

7.5. Compliance

This section presents the final phase of the design overview. Table 7.4 verifies compliance with the requirements defined in Section 4.2.

Requirement	Compliance
GEN-MH-001	Fully compliant – Deployment system is compatible with the Delfi-Twin.
GEN-MH-002	Fully compliant – Deployment system is compatible with the current design of the RABSII Antenna.
GEN-MH-003	Fully compliant – Enables deployment of the folded RABSII Antenna.
GEN-SH-004	Fully compliant – Enables deployment of the unfolded RABSII Antenna.
GEN-CH-005	Not compliant – Deployment system only accommodates an OHSC (Open Hinge Stowed Configuration).
GEN-MH-006	Fully compliant – Uses a burn wire mechanism as its HDRM.
GEN-CH-007	Fully compliant – Influence of communicational/electrical interface has been assessed (resistive torque).
GEN-CH-008	Fully compliant – Influence of communicational/electrical interface has been assessed (resistive torque).
GEN-MH-009	Fully compliant – Stresses and deformations remain below safe structural limits.
GEN-MH-010	Fully compliant – FOS and uncertainty factors derived from the ECSS Standard. Qualitative reasoning established based on ECSS standard [85, 90, 92, 95].
MIS-MH-011	Not assessed.
MIS-MH-012	Not assessed.
MIS-MH-013	Fully compliant – Both hot and cold thermal cases have been assessed.
MIS-MH-014	Fully compliant – Three-spring configuration enables a deployment angle of 92.47°, based on worst-case and conservative estimates of the resistive torque.
MIS-SH-015	Not assessed – Similar approach as used on Delfi-PQ can be applied.
BDG-MH-016	Fully compliant – Deployment system weighs 9.956 grams, excluding the burn wire mechanism.
BDG-MH-017	Fully compliant – Burn wire mechanism is expected to draw 1.26 watt for 6.2 seconds to power the HDRM [60].
BDG-SH-019	Fully compliant – Manufacturing cost is 331.08 euros.
BDG-MH-020	Fully compliant – Mechanical structure fits within required dimensions, occupying an area of **47.5x16 mm**^{2} at an maximum height of 2 mm.
BDG-SH-021	Partially compliant – Actuation method has an outer diameter of 2.8 mm, which exceeds the 2 mm limit. However, the design integrates it within the external bus structure, so it does not cause any extrusion beyond the allowed envelope.
SFT-MH-022	Fully compliant – No deliberate detachment of components occurs during the mission.
SFT-MH-023	Fully compliant – Deployment system contains no pyrotechnics.
SFT-MH-024	Fully compliant.
SFT-MH-025	Fully compliant – Deployment system does not contain any magnets.
SFT-MH-026	Fully compliant.
MAT-MH-027	Fully compliant – All potential metallic structural components are (hard-)anodized.
MAT-MH-028	Fully compliant – All potential metallic structural components are made of Aluminum 7075-T6.
MAT-MH-029	Fully compliant – Stresses remain within limits under all quasi-static loads during launch and in-orbit conditions.

Continued on next page

Table 7.4 – continued

Requirement	Compliance
MAT-MH-030	Fully compliant – FOSU of 2 is maintained.
MAT-MH-031	Fully compliant – FOSY of 1.25 is maintained.

Table 7.4: Compliance of the deployment system with requirements.

8

Conclusion

Throughout this research, the mechanical design of a deployment system for the RABSII antenna onboard the Delfi-Twin was developed. The research aimed to address the following research question (**RQ**):

"What is a reliable deployment system design for a 5-meter long dipole antenna onboard a 3P PocketQube that optimizes deployment success while minimizing the risk of mechanical or operational failure?"

Additionally, the following sub-questions were derived:

- ***SQ1****: What is an actuation method, hold-down-and-release-mechanism and deployment mechanism suitable for integration into a 3P PocketQube?*
- ***SQ2****: What are the critical factors that influence the successful deployment of a dipole antenna onboard a 3P PocketQube?*
- ***SQ3****: How effectively can an actuation method achieve the full deployment of an unfolded 5m dipole antenna?*
- ***SQ4****: How can the deployment system be assessed to ensure validation with system requirements and determine its reliability?*

Following an in-depth literature study, a design framework was established to evaluate potential actuation methods, hold-down-and-release mechanisms (HDRMs) and deployment mechanisms suitable for integration into a 3P PocketQube. A design option tree was constructed, consisting of both commercially off-the-shelf (COTS) and state-of-the-art (SOA) options. Each option was assessed for feasibility within the defined research framework, specifically focusing on the Delfi-Twin satellite, a 3P PocketQube. The following design options were suitable for integration into the Delfi-Twin(**SQ1**):

- **Actuation method:** Tape spring, Shape Memory Alloy (SMA) and (torsion) spring.
- **HDRM:** Embedded/none or burn wire mechanism.
- **Deployment mechanism:** Hinge or turntable mechanism.

A concept study followed, supported by a structured assessment method incorporating the critical factors for successful deployment (**SQ2**). The structural integrity of the hinge mechanism and the deployment system's ability to mitigate angular overshooting were incorporated into the criterion *Reliability*. The deployment system's ability to achieve a deployment angle between 90 and 130° was incorporated into the criterion *RABSII Antenna Compatibility*. Adherence to the strict mass, volume and power budget of a 3P PocketQube mission was assessed in the criterion *Delfi-Twin Compatibility*. The last criterion, *Nanosatellite Compatibility*, assessed the potential scalability of the deployment system and the accompanied performance increase.

The final design of the deployment system is depicted in Figure 8.1, which is deemed a reliable system for a 5-meter long dipole antenna (**Research Question**). This design follows a modular architecture where each module consists of a hinge mechanism that houses a COTS torsion spring. On a PocketQube, a total of three modules can be parallel-placed along the short edge of 5 cm. The hinge mechanism consists of two hard-anodized Al7075-T6 hinge leaves and an anodized Ti6-Al4-V hinge rod. To mitigate potential cold welding, which can occur between metallic components in a cold and vacuum environment, an additional soft coating of MoS_2 is applied between the hinge leaves and the hinge rod. This is recommended due to its self-repairing properties.

The actuation method utilizes a torsion spring with an outer diameter of 2.8 mm. Since the Delfi-Twin volume requirements specify that no component should extrude beyond 2 mm from the external panel, an area of 37.12 mm^2 is milled to a depth of 1 mm to ensure compliance. Each module supports integration with the burn wire mechanism, facilitated by a simple cutout in the hinge leaf. Additionally, the rotating hinge leaf incorporates an extended bonding area to attach the RABSII antenna using an epoxy adhesive. Based on the peel strength characteristics of epoxy-based adhesives (ECSS), this bonding area measures 32.5x12 mm^2 per module.

The deployment system's performance was evaluated based on the achievable deployment angle, structural integrity, compliance with the pre-determined design requirements and a risk assessment (**SQ4**). The deployment system was subjected to a resistive torque of 10.547 Nmm for a folded RABSII antenna and 11.937 Nmm for an unfolded RABSII antenna. These values were determined in accordance with the ECSS standard, where theoretical uncertainty and safety factors were applied. The final achievable deployment angles from a stowed configuration were 92.57° and 79.42° for the folded and unfolded RABSII antenna, respectively (**SQ3**).

The dominant contributor to the resistive torque was the parasitic torque introduced by the wire harness. A conservative value from literature was used for this estimate [96]. Under these assumptions, a deployment angle of 130° requires five torsion springs to be achieved. However, a measured approach, expected in later development stages, may reveal a significantly lower resistive torque. Potentially a two-spring configuration could be sufficient to achieve a deployment angle of 130°.

The structural integrity of the deployment system was evaluated under quasi-static loads expected during launch and in-orbit conditions (**SQ4**). During launch, acceleration loads of 8.5G were considered. In orbit, a bending impact scenario was assessed, where the absolute actuation torque was applied without a resistive torque. This resulted in an angular velocity of 19.04 rad/s at impact, with an ECSS-advised impact duration of 20 ms. The resulting von Mises stresses due to these acceleration loads remained well within the yield and ultimate tensile strength limits of the selected materials.

The overall compliance with the non-negotiable design requirements was verified, except for **MIS-MH-011** and **MIS-MH-012**. These requirements refer to performance over an extended duration, which was not assessed within the scope of this research. A final risk assessment of the design was conducted, and the resulting risk map confirmed that no risks were identified at an unacceptable level.

The estimated mass per module is 1.66 grams, with a cost ranging from €55.18 to €102.18, depending on the selected CNC service. The occupied area on the external panel is approximately 47.5x16 mm^2, where a length of 32.5 mm overlaps the RABSII antenna element. The complete deployment system per satellite consists of six modules, resulting in a total mass of 9.956 grams and a total cost between €331.08 and €613.08. These modules are arranged in parallel along the entire short edge of the external panel, with a 1 mm gap between each module.

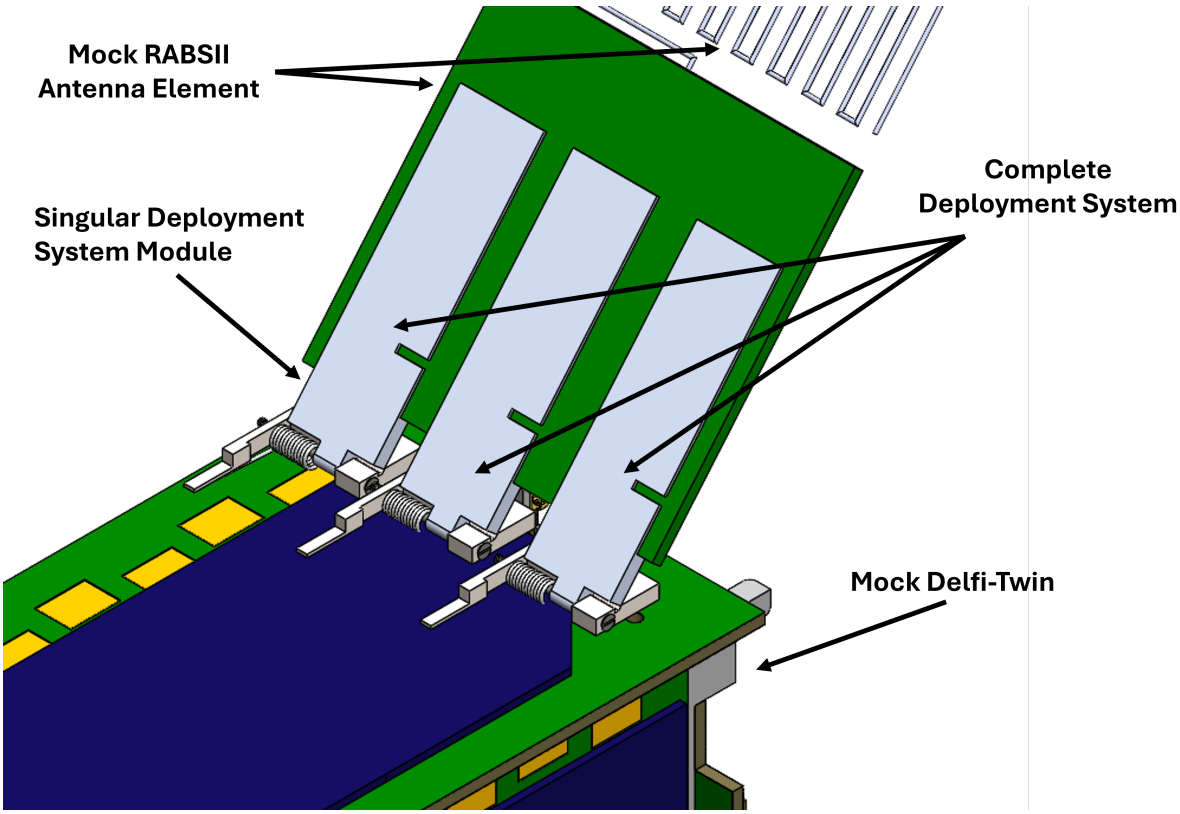

Figure 8.1: Deployment System per RABSII Antenna Element onboard the Delfi-Twin

9

Future Work

Based on the scope of this research, recommendations are proposed that could improve on or build upon this work:

- **Determining Resistive Torque**
  The deployment performance is determined by the achieved deployment angle when the deployment system is subjected to a resistive torque. Currently, a theoretical approach has been applied to determine the resistive torque, where a conservative approach of each torque and force contributor is taken. This, accompanied with high uncertainty factors provided by the ECSS Standard [85], might provide an unrealistic view on the actual magnitude of the resistive torque. A measured approach, where also the influence of hysteresis is accounted for, allows for a more realistic assessment of the actual deployment performance. A better understanding of the true resistive torque could decrease the required actuation torque, enabling a smaller, lighter and more compact design.

- **Supportive Analysis**
  The design analysis in this work focuses on quasi-static acceleration and thermal loads, while dynamic effects such as vibrations are not considered. Vibrational loads, either during launch or induced through the deployment of the RABSII antenna in orbit, can degrade surface coatings, increase the risk of cold welding and contribute to fatigue. A vibration analysis that includes random vibrations and resonance behavior helps identify critical design vulnerabilities. These insights could further validate the material choices and mechanical interfaces to improve structural integrity throughout the mission.

- **Integration of the RABSII Antenna**
  The RABSII antenna evolved into a dipole configuration with element lengths of either 1.5 or 2.5 m, depending on its operational frequency. This change significantly affects the deployment system. Longer elements introduce increased bending under inertial loads, which can alter the stress distribution and increase vibrational response. The current analysis does not capture this interaction in full detail. A reassessment is required using the final configuration, including the antenna's mechanical properties and dynamic coupling with the deployment system. This reassessment should involve rotational motion of the satellite and the resulting deformation and reaction forces. A modal analysis is also recommended to determine natural frequencies and mode shapes of the integrated system, ensuring robustness against vibrational resonance during launch and in-orbit operations.

- **Proto-Flight Model Build and Design Additions**
  Following the completion of the supportive analysis, a proto-flight model should be built to validate the final design. The current scaled-up model allows for a simplified assembly, but it does not fully represent the geometric and mechanical constraints of the flight version. The final design involves extremely thin components and tight tolerances, which demands high precision during manufacturing and assembly. Building a proto-flight model enables verification of tolerances, fit

and interface quality under realistic conditions. It also allows for assessment of thermal behavior, structural integrity and the interaction between subsystems.

- **Functional Test Campaign**
  Before a proto-flight test campaign is initiated , functional tests must verify that the deployment system meets its intended performance [92, 97]. These tests should simulate a zero-g environment and evaluate whether the deployment operates reliably within sufficient margins. The test campaign also checks if the assembly process is suitable for repeatable integration while maintaining quality. Visual inspections and dimensional checks come before and after testing to confirm structural integrity and dimensional accuracy.

Bibliography

[1] Cal Poly SLO. “CubeSat Design Specification”. Version 14. In: (July 2020). URL: https://www.cubesat.org/s/CDS-REV14_1-2022-02-09.pdf.

[2] Siegfried Janson. “A Brief History of Nanosatellites”. In: May 2020, pp. 1–30. DOI: 10.1002/9781119042044.ch1.

[3] NASA. *What are SmallSats and CubeSats?* https://www.nasa.gov/what-are-smallsats-and-cubesats. Accessed: 18-5-2024.

[4] Erik Kulu. *Nanosats Database*. Accessed: 2025-04-05. 2024. URL: https://www.nanosats.eu.

[5] S. Radu et al. “The PocketQube Standard”. Version V1. In: (2018). DOI: 10.34894/FOBWZU. URL: https://doi.org/10.34894/FOBWZU.

[6] Jurgen Vanhamel et al. “Concept of Sporadic E Monitoring Using Space-Based Low Power Multiple Beacon-Systems”. In: *Atmosphere* 15.11 (2024), p. 1306.

[7] TU Delft. *The Delft Satellite Delfi-C3 Has Come to Its End*. Accessed: 18-5-2024. URL: https://www.tudelft.nl/en/2023/lr/the-delft-satellite-delfi-c3-has-come-to-its-end.

[8] TU Delft. *Delfi-C3*. Accessed: 18-5-2024. URL: https://www.tudelft.nl/lr/delfi-space/delfi-c3.

[9] eoPortal. *Delfi-C3 (Triple-unit CubeSat Configuration of TU Delft)*. Accessed: 18-5-2024. URL: https://www.eoportal.org/satellite-missions/delfi-c3.

[10] G. F. Brouwer et al. “Assembly, integration and testing of the Delfi-C3 nanosatellite”. In: *59th International Astronautical Congress: IAC 2008, 29 September-3 October 2008, Glasgow, Scotland* (2008). URL: https://repository.tudelft.nl/islandora/object/uuid%3Ac78d8369-34fc-4126-9bd9-9c987a99a4b4.

[11] G. F. Brouwer and J. Bouwmeester. “From the Delfi-C3 nanosatellite towards the Delfi-n3Xt nano-satellite”. In: *23rd Annual AIAA/USU Conference on Small Satellites* (2013). URL: https://digitalcommons.usu.edu/smallsat/2009/all2009/87/.

[12] Isispace. *CubeSat Antenna System for 1U/3U*. Accessed: 18-5-2024. URL: https://www.isispace.nl/product/cubesat-antenna-system-1u-3u/.

[13] eoPortal. *Delfi-n3Xt (Triple-unit CubeSat Configuration of TU Delft)*. Accessed: 18-5-2024. URL: https://www.eoportal.org/satellite-missions/delfi-n3xt.

[14] TU Delft. *Delfi-n3Xt*. Accessed: 18-5-2024. URL: https://www.tudelft.nl/lr/delfi-space/delfi-n3xt.

[15] Jian Guo, Jasper Bouwmeester, and Eberhard Gill. “In-orbit results of Delfi-n3Xt: Lessons learned and move forward”. In: *Acta Astronautica* 121 (2016), pp. 39–50. ISSN: 0094-5765. DOI: https://doi.org/10.1016/j.actaastro.2015.12.003.

[16] S.Y Go, G.F. Brouwer, and E.K.A. Gill. “Mechanical Design and Arrangement of nanosatellite Delfi-n3Xt”. In: (June 2009).

[17] TU Delft. *Delfi-PQ*. Accessed: 18-5-2024. URL: https://www.tudelft.nl/lr/delfi-space/delfi-pq.

[18] Silvana Radu et al. “Delfi-PQ: The first PocketQube of Delft University of Technology”. In: (Oct. 2018).

[19] V. Pallichadath et al. “In-orbit micro-propulsion demonstrator for PICO-satellite applications”. In: *Acta Astronautica* 165 (2019), pp. 414–423. DOI: https://doi.org/10.1016/j.actaastro.2019.09.004.

[20] Stefano Speretta et al. “A Multi Frequency Deployable Antenna System for Delfi-PQ”. In: *Proceedings of the International Symposium on Space Technology and Science, Fukui (Japan), June 15th-21st, 2019*. 2019.

[21] JD Mathews. “Sporadic E: Current views and recent progress”. In: *Journal of atmospheric and solar-terrestrial physics* 60.4 (1998), pp. 413–435. DOI: https://doi.org/10.1016/S1364-6826(97)00043-6.

[22] Christina Arras. “A global survey of sporadic E layers based on GPS Radio occultations by CHAMP, GRACE and FORMOSAT–3/COSMIC”. PhD thesis. Deutsches GeoForschungsZentrum GFZ Potsdam, 2010. DOI: 10.2312/GFZ.b103-10097.

[23] Sining Liu et al. “A survey on CubeSat missions and their antenna designs”. In: *Electronics* 11.13 (2022), p. 2021. DOI: 10.3390/electronics11132021.

[24] Shahin Farahani. “Chapter 5 - RF Propagation, Antennas, and Regulatory Requirements”. In: Newnes, Dec. 2008, pp. 171–206. DOI: 10.1016/B978-0-7506-8393-7.00005-4.

[25] Tony J. Rouphael. “Chapter 1 - Antenna Systems, Transmission Lines, and Matching Networks”. In: *Wireless Receiver Architectures and Design*. Academic Press, 2014, pp. 1–60. DOI: https://doi.org/10.1016/B978-0-12-378640-1.00001-9.

[26] Kshitij Sandeep Sadasivan et al. “Design and analysis of antennas for a nano-satellite”. In: *2017 IEEE Aerospace Conference*. IEEE. 2017, pp. 1–9.

[27] Yuichi Tsuda et al. “University of Tokyo’s CubeSat project: its educational and technological significance”. In: (2001).

[28] Sining Liu et al. “Dual-band folded-end dipole antenna for plastic CubeSats”. In: *IEEE Journal on Miniaturization for Air and Space Systems* 1.3 (2020), pp. 172–178. DOI: 10.1109/JMASS.2020.3022457.

[29] eoPortal. *HIT-Sat (Hokkaido Institute of Technology Satellite)*. Accessed: 25-3-2024. URL: https://www.eoportal.org/satellite-missions/hit-sat.

[30] Tatsuhiro Sato, Ryuichi Mitsuhashi, and Shin Satori. “Attitude estimation of nano-satellite ”HIT-SAT” using received power fluctuation by radiation pattern”. In: (June 2009), pp. 1–4. DOI: 10.1109/APS.2009.5172007.

[31] Allen T Guzik and Othmane Benafan. *Design and development of CubeSat solar array deployment mechanisms using shape memory alloys*. Tech. rep. 2018.

[32] Nobukatsu Okuizumi et al. “Development of deployment structures and mechanisms of spinning large solar power sail”. In: *4th International Symposium on Solar Sailing,(Kyoto Research Park, Kyoto, Japan, 2017)*. 2017.

[33] Stefano Viscuso et al. “Shape memory alloys for space applications”. In: *Shape Memory Alloy Engineering*. 2021, pp. 609–623. DOI: https://doi.org/10.1016/B978-0-12-819264-1.00018-2.

[34] Jaronie Mohd Jani et al. “A review of shape memory alloy research, applications and opportunities”. In: *Materials & Design (1980-2015)* 56 (2014), pp. 1078–1113. DOI: https://doi.org/10.1016/j.matdes.2013.11.084.

[35] N Vasudha and K Uma Rao. “Shape memory alloy properties, modelling aspects and potential applications – a review”. In: *Journal of Physics: Conference Series*. Vol. 1706. 1. IOP Publishing. 2020, p. 012190. DOI: 10.1088/1742-6596/1706/1/012190.

[36] D Hartl and D Lagoudas. *Shape memory alloys: modeling and engineering applications*. 2008.

[37] Mladen Franz and Erhard Hornbogen. “Martensitic transformation of a CuZnAl-shape memory alloy strengthened by hot-rolling”. In: *Materials Science and Engineering: A* 252.2 (1998), pp. 157–165.

[38] Safaa N Saud et al. “Effect of a fourth alloying element on the microstructure and mechanical properties of Cu–Al–Ni shape memory alloys”. In: *Journal of Materials Research* 30.14 (2015), pp. 2258–2269.

[39] Deboshri Sadhukhan et al. “Advanced eLectrical Bus (ALBus) CubeSat: From Build to Flight”. In: *34th Annual Small Satellite Conference*.

[40] KA Seffen and S Pellegrino. “Deployment dynamics of tape springs”. In: *Proceedings of the Royal Society of London. Series A: Mathematical, Physical and Engineering Sciences* 455.1983 (1999), pp. 1003–1048.

[41] Thomas W. Murphey et al. “Deployable Booms and Antennas Using Bi-stable Tape-springs”. In: 2010.

[42] Sungeun Jeon and Thomas Murphey. “Design and analysis of a meter-class CubeSat boom with a motor-less deployment by bi-stable tape springs”. In: *52nd AIAA/ASME/ASCE/AHS/ASC Structures, Structural Dynamics and Materials Conference 19th AIAA/ASME/AHS Adaptive Structures Conference 13t*. 2011, p. 1731. DOI: 10.2514/6.2011-1731.

[43] Thomas Murphey and Sergio Pellegrino. “A novel actuated composite tape-spring for deployable structures”. In: *45th AIAA/ASME/ASCE/AHS/ASC structures, structural dynamics & materials conference*. 2004, p. 1528. DOI: 10.2514/6.2004-1528.

[44] Jakob Ekelow. *Design and manufacturing of thin composite tape springs*. 2014.

[45] Huina Mao and Gunnar Tibert. “Experiments and analytical modeling for designing tape spring composites”. In: (2017).

[46] Zakariya Loulou and Tomohiro Yokozeki. “Evolution prediction of bistable tape springs’ deployed shape while undergoing stowage at high temperature”. In: *Transactions of the Japan Society for Aeronautical and Space Sciences, Aerospace Technology Japan* 18.6 (2020), pp. 404–411. DOI: 10.2322/tastj.18.404.

[47] SJI Walker and GS Aglietti. “A study of tape spring fold curvature for space deployable structures”. In: *Proceedings of the Institution of Mechanical Engineers, Part G: Journal of Aerospace Engineering* 221.3 (2007), pp. 313–325.

[48] Megha Thaker et al. “Tape spring for deployable space structures: A review”. In: *Advances in Space Research* 73.10 (). DOI: https://doi.org/10.1016/j.asr.2024.02.027.

[49] C Boesch et al. “Ultra light self-motorized mechanism for deployment of light weight spacecraft appendages”. In: *Proceedings of 39th Aerospace Mechanisms Symposium*. 2008, pp. 7–9.

[50] Richard E. Hodges et al. “A Deployable High-Gain Antenna Bound for Mars: Developing a new folded-panel reflectarray for the first CubeSat mission to Mars”. In: *IEEE Antennas and Propagation Magazine* 59.2 (2017), pp. 39–49. DOI: 10.1109/MAP.2017.2655561.

[51] Richard E Hodges et al. “The Mars Cube One deployable high gain antenna”. In: *2016 IEEE International Symposium on Antennas and Propagation (APSURSI)*. IEEE. 2016, pp. 1533–1534.

[52] Jonathan Sauder et al. “Lessons learned from a deployment mechanism for a Ka-band deployable antenna for CubeSats”. In: *44th Aerosp. Mech. Symp*. Vol. 361. 2018.

[53] Jonathan Sauder et al. “Ultra-Compact Ka-Band Parabolic Deployable Antenna for RADAR and Interplanetary CubeSats”. In: *Small Satellite Conference* ().

[54] Eva Peral et al. “RainCube: the first ever radar measurements from a CubeSat in space”. In: *Journal of Applied Remote Sensing* 13.3 (2019), pp. 032504–032504.

[55] SBM Zaki et al. “Design, analysis and testing of monopole antenna deployment mechanism for BIRDS-2 CubeSat applications”. In: *Journal of Physics: Conference Series*. Vol. 1152. 1. IOP Publishing. 2019, p. 012007.

[56] Mark Honeth, Akash Yalagach, and Guglielmo Aglietti. “Wire Driven Mechanisms for Deployable Components for Optical Payloads”. In: (Aug. 2022).

[57] Kanthal. *Kanthal A1 Resistance heating wire and resistance wire Datasheet*. Accessed: 14-11-2024. URL: https://www.kanthal.com/en/products/material-datasheets/wire/resistance-heating-wire-and-resistance-wire/kanthal-a-1/.

[58] Francois Cardarelli. “Materials handbook: a concise desktop reference”. In: (2008).

[59] Tae-Yong Park, Byung-Gon Chae, and Hee-Ung Oh. “Development of 6U CubeSat’s Deployable Solar Panel with Burn Wire Triggering Holding and Release Mechanism”. In: *International Journal of Aerospace Engineering* 2019 (2019), pp. 1–13. DOI: 10.1155/2019/7346436.

[60] Adam Thurn et al. “A nichrome burn wire release mechanism for CubeSats”. In: *The 41st Aerospace Mechanisms Symposium, Jet Propulsion Laboratory*. 2012, pp. 479–488.

[61] Shankar Bhattarai et al. “Development of Pogo Pin-Based Holding and Release Mechanism for Deployable Solar Panel of CubeSat”. In: *International Journal of Aerospace Engineering* 2019 (May 2019). DOI: 10.1155/2019/2580865.

[62] Tae-Yong Park et al. “Experimental Investigation on the Feasibility of Using Spring-Loaded Pogo Pin as a Holding and Release Mechanism for CubeSat’s Deployable Solar Panels”. In: *International Journal of Aerospace Engineering* 2018.1 (2018), p. 4854656. DOI: 10.1155/2018/4854656.

[63] Maria Grulich et al. “Smard-rexus-18: Development and verification of an sma based cubesat solar panel deployment mechanism”. In: *22nd ESA Symposium on European Rocket and Balloon Programmes and Related Research*. Vol. 730. 2015, p. 421.

[64] DCUBED. *DCUBED Nano Release nut nD3RN*. Accessed: 25-5-2024. URL: https://dcubed.space/products/release-nuts/.

[65] EBAD. *TiNi Pin Puller*. Accessed: 25-5-2024. URL: https://www.ebad.com/tini-pin-puller/.

[66] Mark A Gummin, William Donakowski, and Geoffrey Gaines. *Shape memory alloy actuators*. US Patent 7,256,518. Aug. 2007.

[67] LEAT. *SMA-based Frangibolt*. Accessed: 20-5-2024. URL: http://en.le-aerospace.com/index/index/product_details/listid/12/id/45.html.

[68] P.M.C.L. Pacheco and Marcelo Amorim Savi. “Modeling and simulation of a shape memory release device for aerospace applications”. In: *Revista de Engenharia e Ciências Aplicadas* (2000), pp. 1–16.

[69] John D. Busch, William E. Purdy, and David A. Johnson. “Development of a non-explosive release device for aerospace applications”. In: *26th Aerospace Mechanisms Symposium* (May 1992).

[70] EBAD. *TiNi Frangibolt Actuator*. Accessed: 20-5-2024. URL: https://www.ebad.com/tini-frangibolt/.

[71] David B. Carte et al. “Design and Test of a Deployable Radiation Cover for the REgolith X-ray Imaging Spectrometer”. In: *42nd Aerospace Mechanisms Symposium* (May 2014).

[72] Chad Fish et al. “Dice mission design, development, and implementation: Success and challenges”. In: (2012).

[73] EBAD. *TiNi Mini Frangibolt Actuator*. Accessed: 20-5-2024. URL: https://www.ebad.com/tini-mini-frangibolt.

[74] Scott Tibbitts. “High output paraffin actuators: Utilization in aerospace mechanisms”. In: *NASA. Langley Research Center, The 22nd Aerospace Mechanisms Symposium*. 1988.

[75] Sierra Space. *High Output Paraffin (HOP) Actuators and Mechanisms*. Accessed: 25-5-2024. URL: https://www.sierraspace.com/space-technology/spaceflight-hardware/high-output-paraffin-hop-actuators-and-mechanisms/.

[76] Clarence Korendyke et al. “MiniCOR: A miniature coronagraph for interplanetary cubesat”. In: (2015).

[77] Sezgin Ersoy and Tayyab Waqar. “Surface acoustic wave sensing”. In: (2023), pp. 129–141. DOI: https://doi.org/10.1016/B978-0-12-822548-6.00103-5.

[78] Lingfeng Tang et al. “A Novle Deployment Mechanism for a Ka-band Deployable Antenna Driven by Piezoelectric Actuator”. In: *2022 16th Symposium on Piezoelectricity, Acoustic Waves, and Device Applications (SPAWDA)*. 2022, pp. 105–108. DOI: 10.1109/SPAWDA56268.2022.10046041.

[79] A Omari et al. “Development of High Precision Mounting Robot with Fine Motion Mechanism: Design and Control of the Fine Motion Mechanism”. In: *Human Friendly Mechatronics*. Elsevier, 2001, pp. 333–338.

[80] Yong Qing Fu et al. “Smart microgrippers for bioMEMS applications”. In: *Mems for biomedical applications*. Elsevier, 2012, pp. 291–336.

[81] D. Rockberger and H. Abramovich. “Piezoelectric Assisted Smart Satellite Structure (PEASSS) - An Innovative Low Cost Nano-Satellite”. In: Mar. 2014, p. 905714. DOI: 10.1117/12.2045002.

[82] Richard E Hodges et al. “ISARA-integrated solar array and reflectarray CubeSat deployable Ka-band antenna”. In: *2015 IEEE International Symposium on Antennas and Propagation & USNC/URSI National Radio Science Meeting*. 2015, pp. 2141–2142. DOI: 10.1109/APS.2015.7305460.

[83] Richard Hodges et al. “The ISARA mission-flight demonstration of a high gain Ka-band antenna for 100Mbps telecom”. In: (2018).

[84] Evan Hilgemann et al. “Development of a 6-meter crossed dipole antenna deployment mechanism for CubeSat applications”. In: *AIAA SCITECH 2024 Forum*. 2024, p. 1430. DOI: 10.2514/6.2024-1430.

[85] European Cooperation for Space Standardization. *Space engineering – Mechanisms (ECSS-E-ST-33-01C Rev.2)*. Mar. 2019. URL: https://ecss.nl.

[86] European Cooperation for Space Standardization. *Space engineering – Structural factors of safety for spaceflight hardware (ECSS-E-ST-32-10C Rev.2)*. May 2019. URL: https://ecss.nl.

[87] Assal Farrahi and Isabel Perez-Grande. “Simplified analysis of the thermal behavior of a spinning satellite flying over Sun-synchronous orbits”. In: *Applied Thermal Engineering* 125 (2017), pp. 1146–1156. DOI: 10.1016/j.applthermaleng.2017.07.033.

[88] G.D. Lempert and A. Tsour. “Reduction of static friction between surfaces of Ti-6Al-4V and between surfaces of Ti-6Al-4V and Al-7075”. In: *Surface and Coatings Technology* 52.3 (1992), pp. 291–295. DOI: https://doi.org/10.1016/0257-8972(92)90029-A.

[89] SpaceX. *Falcon User’s Guide*. Space Exploration Technologies Corp. Sept. 2021.

[90] European Cooperation for Space Standardization. *Space engineering – Threaded fasteners handbook (ECSS-E-HB-32-23A Rev.1)*. Feb. 2023. URL: https://ecss.nl.

[91] Julie Fagerudd. “Stress simulation of the SEAM CubeSat structure during launch”. MA thesis. KTH Royal Institute of Technology, 2015.

[92] European Cooperation for Space Standardization. *Space engineering – Testing (ECSS-E-ST-10-03C Rev.1)*. May 2022. URL: https://ecss.nl.

[93] Andreas Merstallinger, E. Semerad, and Barrie Dunn. “Influence of coatings and alloying on cold welding due to impact and fretting”. In: *10th European Space Mechanisms and Tribology Symposium*. Vol. 524. Aug. 2003, pp. 41–48.

[94] Roland Holzbauer et al. “Cold welding under space and launch conditions”. In: *47th Aerospace Mechanisms Symposium*. 2024.

[95] European Cooperation for Space Standardization. *Space engineering – Adhesive bonding handbook (ECSS-E-HB-32-21A)*. Mar. 2011. URL: https://ecss.nl.

[96] Colin Peter. “Parasitic Torque Characterization of Wire Harness Across Hinge Line of CubeSat Deployable Solar Arrays”. In: *AIAA Scitech 2020 Forum*. Jan. 2020. DOI: 10.2514/6.2020-1896.

[97] European Cooperation for Space Standardization. *Space engineering – Verification guidelines (ECSS-E-HB-10-02A)*. Dec. 2010. URL: https://ecss.nl.

[98] K. S. Mahapatra. “Low Earth Orbiting (LEO) Satellite and Orbital Decay”. In: *International Journal of Engineering and Advanced Technology* 12.1 (2022), pp. 88–91. DOI: 10.35940/ijeat.a3849.1012122.

[99] NanoRacks LLC. *Interface Definition Document (IDD)*. NanoRacks LLC. 2018.

[100] Rui Lin et al. “Microstructure evolution and properties of 7075 aluminum alloy recycled from scrap aircraft aluminum alloys”. In: *Journal of Materials Research and Technology* 19 (2022), pp. 354–367. DOI: 10.1016/j.jmrt.2022.05.011.

Appendices

A

Deployment Torque

A.1. Orientations & Reference Frames

In this study, several reference frames are utilized and are listed below.

1. Body-Centered Inertial Frame (BCIF)
   Used to determine the deployment torque required by the hinge, expressed as:

$$\sum M_y \tag{A.1}$$

2. Aerodynamic Frame (AF)
   Used to express the drag force (F_d), represented as:

$$F_d = \begin{bmatrix} F_d \\ 0 \\ 0 \end{bmatrix} \tag{A.2}$$

Unless otherwise specified, all forces, torques and angles are expressed in the BCIF.

A.2. General Assumptions and Simplifications

For the determination of the required deployment torque, the following assumptions are applied:

- Pitch and Yaw angles vary between -20 and 20°, resulting a full aperture angle of 40°.
- The Roll angle varies between $0°$ and $360°$.
- The deployment torque acts only along M_y in the BCIF.
- Delfi-Twin mission parameters are used for altitude, area and other relevant properties.
- Angular accelerations are independent of the roll angle.
- The host-satellite is in a 'free-fall' environment.

These assumptions allow for the following simplification:

- Variations in the Pitch and Yaw angle are negligible for resistive forces and torque contributors due to their low magnitude and expected influence.
- Resistive forces and Torque contributors due to gravity are negligible due to the 'free-fall' environment.

A.3. Resistive Torque

The deployment torque must be sufficient to overcome all resistive forces and enable successful deployment. According to the ECSS standard, the minimum torque supplied by the actuation method must exceed the total resistive torque. The resistive torque is calculated using the following equation:

$$T_{min} \geq 2 \cdot \sum (k_i \cdot T_{res,i}) + T_L + 1.25 \cdot T_d \tag{A.3}$$

where k is the uncertainty factor and T_{res} the resistive torque. Relevant resistive force and torque contributors for a space appendage are listed in Table A.1, along with their corresponding uncertainty factors based on whether the numerical values are determined theoretically or through measurement. Applying these uncertainty factors, the resistive torque equation becomes:

$$T_{min} = 2 \cdot (1.1 \cdot I + 1.2 \cdot S + 1.5 \cdot H_m + 3 \cdot F_r + 3 \cdot Hy + 3 \cdot H_a + 3 \cdot H_d) + 1.25 T_D + T_L \tag{A.4}$$

Within the scope of this research only I, F_r, H_d (Drag and Wire Harness) and T_d are considered non-zero. The following subsections provide the necessary calculations to determine the minimum deployment torque based on the known resistive torque components.

Resistive Force/ Torque Contributor	**Symbol**	**Uncertainty Factor Theoretical**	**Uncertainty Factor Measured**	**Factor of Safety**
Inertia (Satellite Level)	I	1.1	1.1	2
Spring	S	1.2	1.1	2
Magnetic Effects	H_m	1.2	1.1	2
Friction	F_r	3	1.5	2
Hysteris	H_y	3	1.5	2
Harness	H_a	3	1.5	2
Drag	H_a	3	1.5	2
Adhesion	H_d	3	3	
Inertia (Deployment System)	T_d	1	1	1.25
Deliverable Output Torque of the Mechanism	T_L	1	1	1

Table A.1: Uncertainty and safety factor for torque contributors and resistive forces in the resistive torque calculation.

A.3.1. Inertial Torque (Acceleration in Inertial Frame of Reference), I

The inertial forces impose a distributed load on the RABSII antenna, resulting in deformation and pretension within the antenna element. Along the length of the antenna rod, these inertial forces vary and depend on the angular acceleration. The tangential and radial components of the angular acceleration are given by:

$$a_{tan} = r \cdot \alpha_{sat} \tag{A.5}$$

$$a_{rad} = r \cdot \omega^2 \tag{A.6}$$

where α_{sat} is the angular acceleration [rad/s^2], ω is the angular velocity [rad/s] and r is the distance from the roll axis [m]. a_{tan} and a_{rad} represent the tangential and radial components of acceleration, respectively.

The distributed load along the x-axis due to a_{rad} is:

$$q_I(x) = \frac{m_{RABSII}}{L} \cdot x \cdot \omega^2 \tag{A.7}$$

where m_{RABSII} is the mass of the antenna element, L is its length, and x is the position along the length of the rod. The resulting torque I from this distributed load is calculated using the equation below.

$$I = r_{max} \cdot \frac{2}{3} \cdot \frac{1}{2} q_I(L_{max}) \tag{A.8}$$

This results in a restrictive torque of 0.00322 Nmm and 0.635 Nmm during folded and unfolded state of the antenna element, respectively.

A.3.2. Friction, F_r

Frictional loads in the deployment system primarily occur between the hinge rod and the RHL. The coefficient of static friction between Ti6Al4V and Al7075-T6 surfaces is 0.32 in a non-lubricated state, which may be reduced to 0.18 following (hard-)anodizing of the components [88]. To conservatively estimate the resistive torque due to friction, both the static (μ_s) and dynamic (μ_d) friction coefficients are assumed to be 0.32. Additionally, the normal force (F_n) is calculated under a 1G environment rather than a free-fall (zero-g) condition, for a more conservative approach.

$$F_r = \mu \cdot F_n \cdot r_{rod} \tag{A.9}$$

This results in a resistive torque F_r of 0.314 Nmm, which remains constant and is independent of the deployment angle or the configuration of the RABSII antenna.

A.3.3. Inertial Torque (Deployment System Accelerations), T_d

T_d represents the inertial resistance torque determined by the worst-case accelerations. Assuming a deployment time of 1.0 second for the stowed RABSII antenna, similar to the ALBus [31], the following equations of motion apply:

$$\alpha = \frac{T}{I} \tag{A.10}$$

$$\omega = \omega_0 + \alpha t \tag{A.11}$$

$$\theta = \omega t + \frac{1}{2}\alpha t^2 = \frac{1}{2}\frac{T}{I}t^2 \tag{A.12}$$

These equations yield an inertial torque of 0.959 Nmm for the folded RABSII antenna and 189 Nmm for the unfolded configuration. However, as inertial torque depends on the required angular acceleration, a torque of 0.9585 Nmm corresponds to a deployment time of 14.1 seconds for the unfolded RABSII antenna.

A.3.4. Drag and Wire Harness Resistance, H_a

H_a accounts for additional influences contributing to the resistive torque. For this research, these are considered to be aerodynamic drag and parasitic torque from the wire harness.

The wire harness introduces a resistive torque and a slight damping effect during deployment. A harness which consists of two 26 AWG wires (each with a diameter of 0.4038 mm) imposes a torque of 1.243 Nmm at a deployment angle of 135° [96]. The coaxial cable used in the RABSII antenna is expected to produce significantly lower resistive torque, as it consists of a 38 AWG wire (diameter 0.1016 mm). However, for the current design phase, the 1.243 Nmm value is conservatively used to represent the contribution of the wire harness to H_a.
F_D (Drag Force), can be determined using the following relation [98]:

$$F_d = \frac{1}{2} C_d \frac{A_{satellite}}{M_{satellite}} \rho(h) v_s^2 \tag{A.13}$$

where the atmospheric density is given by:

$$\rho(h) = \rho_0 e^{\frac{(-h)}{H}} \tag{A.14}$$

and the satellite velocity is defined as:

$$v_s^2 = \frac{GM_{Earth}}{h + R_{Earth}} \tag{A.15}$$

The RABSII Antenna's influence on the drag can be determined as follows:

$$2 \cdot F_{D-RABSII} = F_{D-Deployed} - F_{D-Stowed} \tag{A.16}$$

resulting in:

$$2 \cdot F_{D-RABSII} = \frac{1}{2} C_d \frac{2 \cdot A_{RABSII} \cdot sin(\alpha) + A_{satellite}}{2 \cdot M_{RABSII} + M_{satellite}} \rho(h) v_s^2 - \frac{1}{2} C_d \frac{A_{satellite}}{2 \cdot M_{RABSII} + M_{satellite}} \rho(h) v_s^2 \tag{A.17}$$

which simplifies to:

$$F_{D-RABSII} = \frac{1}{4} C_d \rho(h) v_s^2 \left(\frac{2 \cdot A_{RABSII} \cdot sin(\alpha)}{2 \cdot M_{RABSII} + M_{satellite}}\right) \tag{A.18}$$

Since the Pitch and Yaw angle are assumed to be zero, Equation A.19 holds.

$$F_d = \begin{bmatrix} F_d \\ 0 \\ 0 \end{bmatrix}_{\text{AF}} = \begin{bmatrix} F_d \\ 0 \\ 0 \end{bmatrix}_{\text{BCIF}} \tag{A.19}$$

Lastly, F_d is dependent on the deployment angle (α) and unfolded state of the RABSII Antenna. The roll angle does not influence its magnitude. Figure A.1 depicts F_d in both stowed and deployed configuration of the RABSII Antenna. The maximum value of H_a due to drag in both the folded and unfolded state is equal to 0.00142 Nmm.

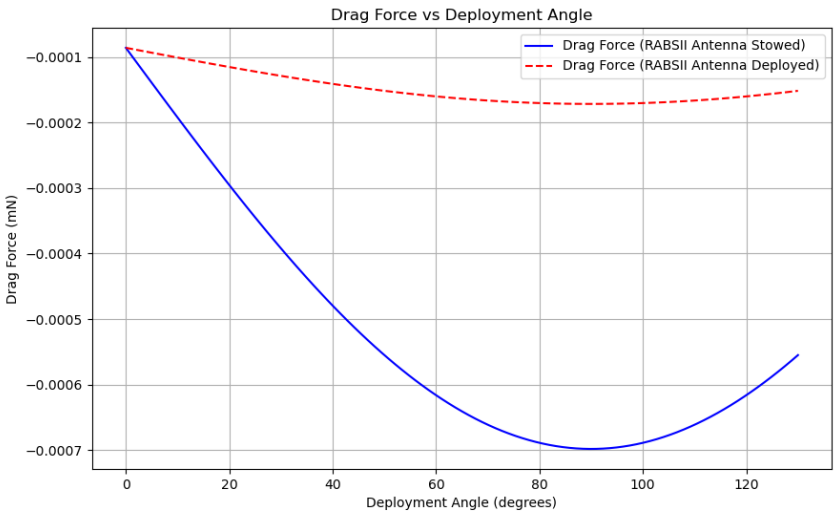

Figure A.1: Drag Force of each antenna element w.r.t. the deployment angle.

B

Requirement Traceability Matrix

The following page presents the Requirement Traceability Matrix, a structured method to ensure that all design requirements are systematically addressed throughout the design development process.

KPPs/Requirements / KPPs/Criterion	KPP1	KPP2	KPP3	KPP4	KPP5	KPP6	KPP7	GEN-MH-001	GEN-MH-002	GEN-SH-003	GEN-SH-004	GEN-CH-005	GEN-MH-006	GEN-CH-007	GEN-CH-008	GEN-MH-009	GEN-MH-010	MIS-MH-011	MIS-MH-012	MIS-MH-013	MIS-MH-014	MIS-SH-015	BDG-MH-016	BDG-MH-017	BDG-MH-018	BDG-SH-019	BDG-MH-020	BDG-SH-021	SFT-MH-022	SFT-MH-023	SFT-MH-024	SFT-MH-025	SFT-MH-026	MAT-MH-027	MAT-MH-028	MAT-MH-029	MAT-MH-030	MAT-MH-031
KPP1	X							X	X		X								X																		
KPP2		X						X	X	X	X					X			X																		
KPP3			X									X			X	X		X	X								X	X	X	X	X	X	X	X	X	X	X
KPP4				X				X	X			X			X	X							X		X	X	X	X		X	X						
KPP5					X			X	X	X	X																											
KPP6						X		X	X				X	X																								
KPP7							X	X															X	X	X	X	X	X										
Reliability	X		X						X			X			X	X	X																			X	X	X
Delfi-Twin Compatibiltiy			X	X			X	X				X			X	X		X	X		X	X	X	X	X	X	X	X	X	X	X	X	X	X	X	X	X
RABSII Antenna Compatibility	X	X			X	X			X	X	X	X	X	X	X		X			X																		
Nanosatellite Compatibility			X	X	X							X	X			X	X				X						X	X	X	X	X	X	X	X	X	X	X

C

COTS TORSION SPRINGS

Table C.1 presents COTS torsion springs from Dutch-based distributors. The listed variants have a D_o of less than 3.57 mm and a maximum rotation angle exceeding 130°, along with their relevant parameters.

Manufacturer	Article No.	D_o [mm]	Max. Rotation [°]	Conf.	Torque [Nm]	$D_{rod-max}$ [mm]	D_{wire} [mm]	Length [mm]	N_t [-]	Left-Coiled
Amatec	T012-270-062	2,59	270	D	0,00531	1,57	0,3	3,53	8,75	T012-270-062L
Amatec	T012-180-067	2,77	180	A	0,00531	1,7	0,3	2,18	5	T012-180-067L
Lesjofors	8317 of 8427	2,8	165	D	0.01	1,5	0,4	4	8,75	8427
Lesjofors	8318 of 8428	2,8	227	A	0.01	1,5	0,4	5,2	12	8428
Tevema	TS100170	2,8	140	D	0.016	1,5	0,4	4	8,75	TS100170
Tevema	TS100180	2,8	192	A	0.00930	1,5	0,4	5,2	12	TS100180L
Amatec	T014-270-063	3,15	270	D	0.00791	1,6	0,36	4,01	8,75	T014-270-063L
Amatec	T015-270-078	3,15	270	D	0.01051	1,98	0,38	4,39	8,75	T015-270-078L
Amatec	T015-180-078	3,3	180	A	0.01051	1,98	0,38	2,72	5	T015-180-078L
Amatec	T014-180-078	3,38	180	ND	0.00791	1,98	0,36	2,67	5	T014-180-07L
Alcomex	TOR180R	3,5	186	A	0.01670	2	0,5	6	12	TOR180L
Lesjofors	7008	3,5	221	A	0.019	2	0,5	6,5	12	7223
Lesjofors	8325	3,8	174	C	0.01	2,5	0,4	2,8	6,5	8435

Table C.1: COTS torsion springs from Dutch-based distributors.

D

Drawings

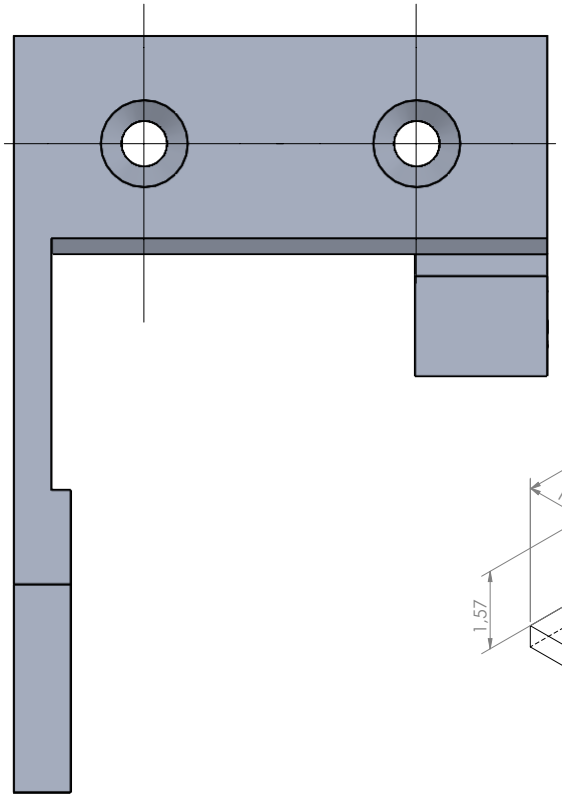

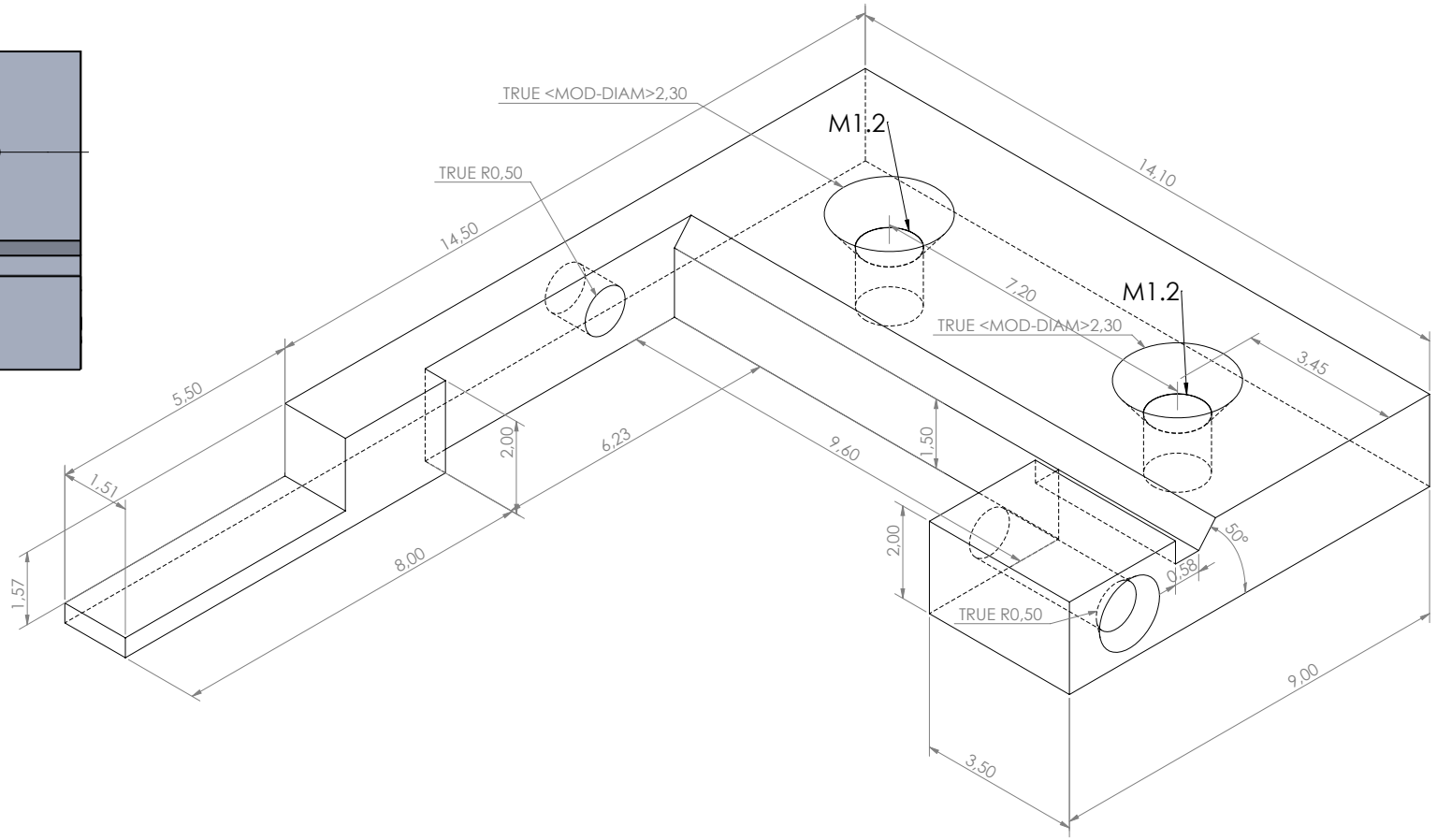

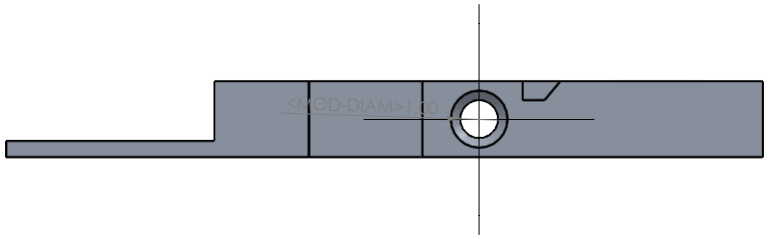

UNLESS OTHERWISE SPECIFIED: DIMENSIONS ARE IN MILLIMETERS SURFACE FINISH: Hard-Anodizing TOLERANCES: H8/h9 LINEAR: ISO-2768-Fine ANGULAR: ISO-2768-FINE	FINISH: Hard-Anodizing		DEBURR AND BREAK SHARP EDGES		DO NOT SCALE DRAWING	REVISION
	NAME	SIGNATURE	DATE		TITLE: Fixated Hinge Leaf Drawing	
DRAWN						
CHK'D						
APPV'D						
MFG						
Q.A						
				MATERIAL: Aluminum 7075-T6	DWG NO. Fixated Hinge Leaf	A2
				WEIGHT:0.550 g	SCALE:5:1	SHEET 1 OF 1

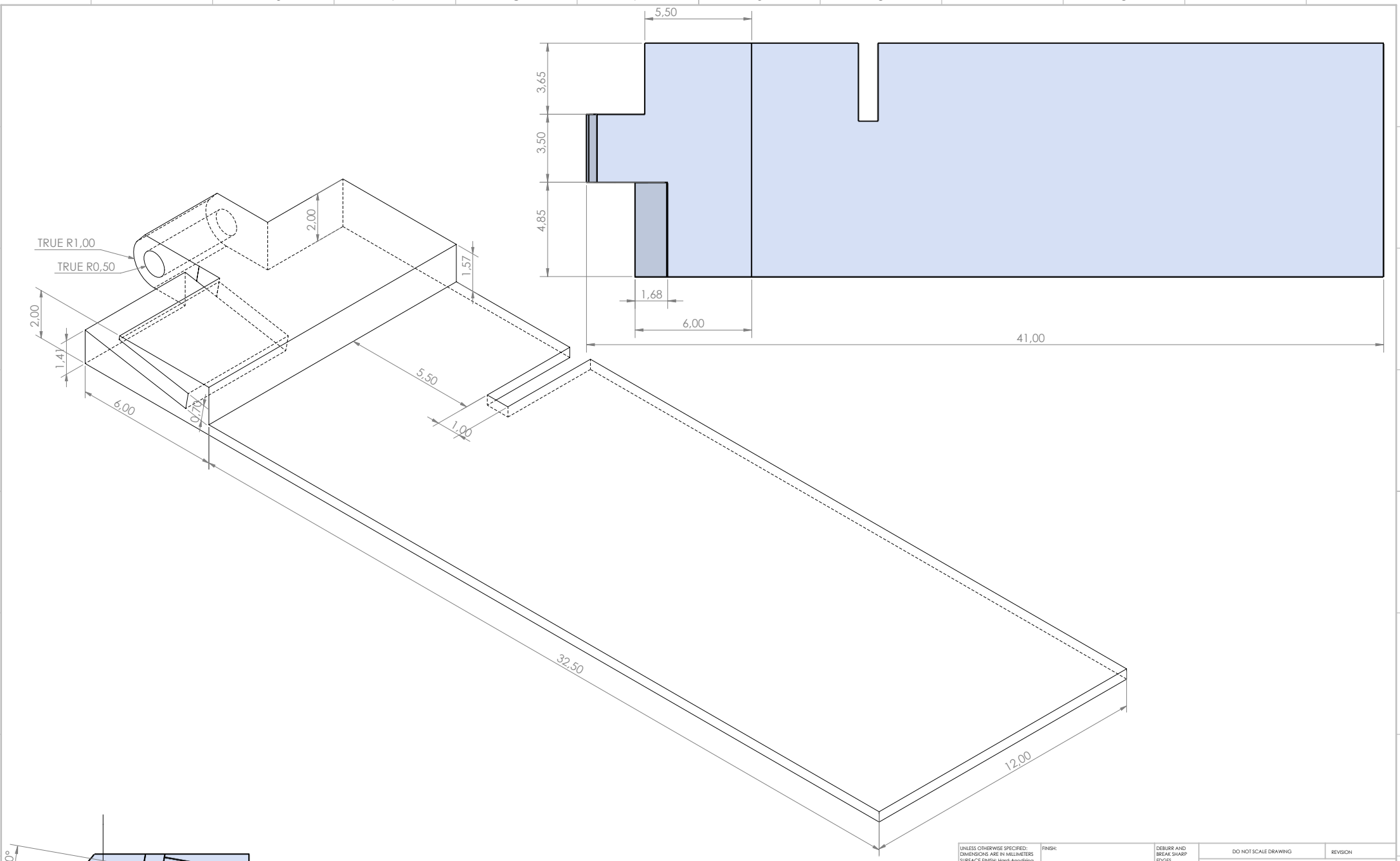

UNLESS OTHERWISE SPECIFIED: DIMENSIONS ARE IN MILLIMETERS SURFACE FINISH: Hard-Anodizing TOLERANCES: H8/h9 LINEAR: ISO2768-Fine ANGULAR: ISO2768-Fine	FINISH: Hard-Anodizing	DEBURR AND BREAK SHARP EDGES	DO NOT SCALE DRAWING	REVISION		
	NAME	SIGNATURE	DATE	TITLE: Rotating Hinge Leaf Drawing		
DRAWN						
CHK'D						
APPV'D						
MFG						
Q.A				MATERIAL: Aluminum 7075-T6	DWG NO. Rotating Hinge Leaf	A2
				WEIGHT: 0.850 g	SCALE:5:1	SHEET 1 OF 1

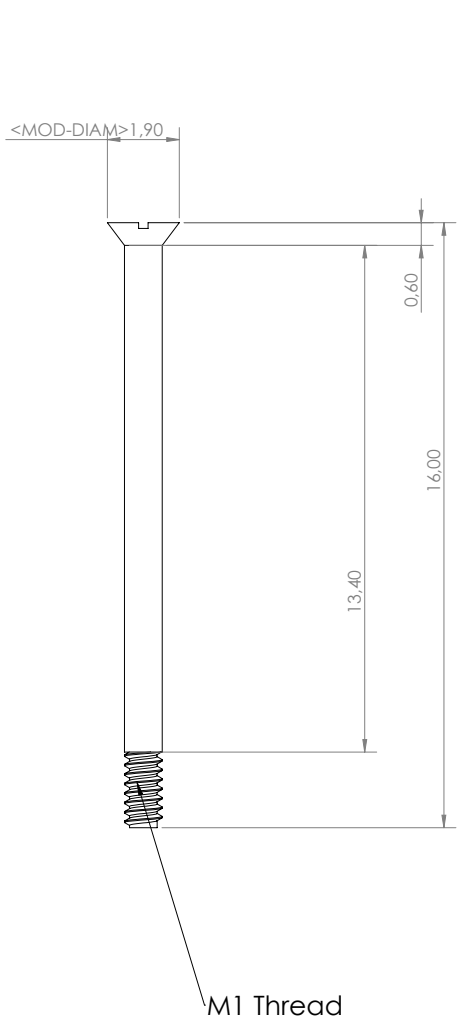

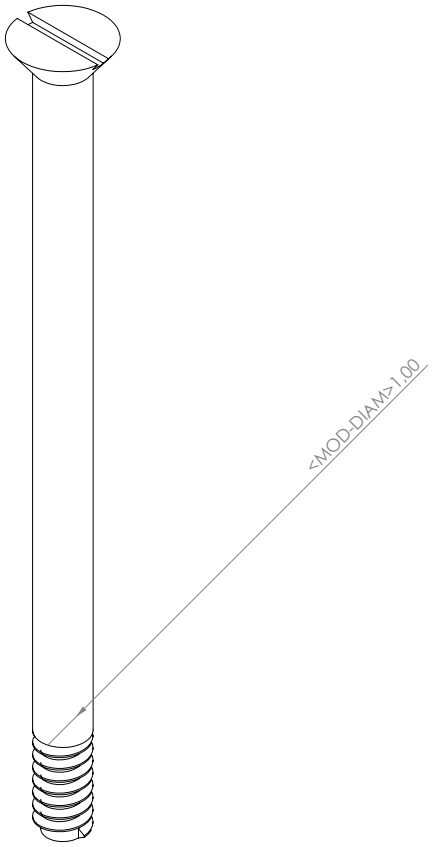

UNLESS OTHERWISE SPECIFIED: DIMENSIONS ARE IN MILLIMETERS SURFACE FINISH: Anodizing TOLERANCES: H8/h9 LINEAR: ISO2768-Fine ANGULAR: ISO2768-Fine		FINISH: Anodizing		DEBURR AND BREAK SHARP EDGES		DO NOT SCALE DRAWING	REVISION
	NAME	SIGNATURE	DATE			TITLE: Hinge Rod Drawing	
DRAWN							
CHK'D							
APPV'D							
MFG							
Q.A				MATERIAL: Titanium Ti-6Al-4V		DWG NO. Hinge Rod	A2
				WEIGHT: 0.056 g		SCALE:10:1	SHEET 1 OF 1

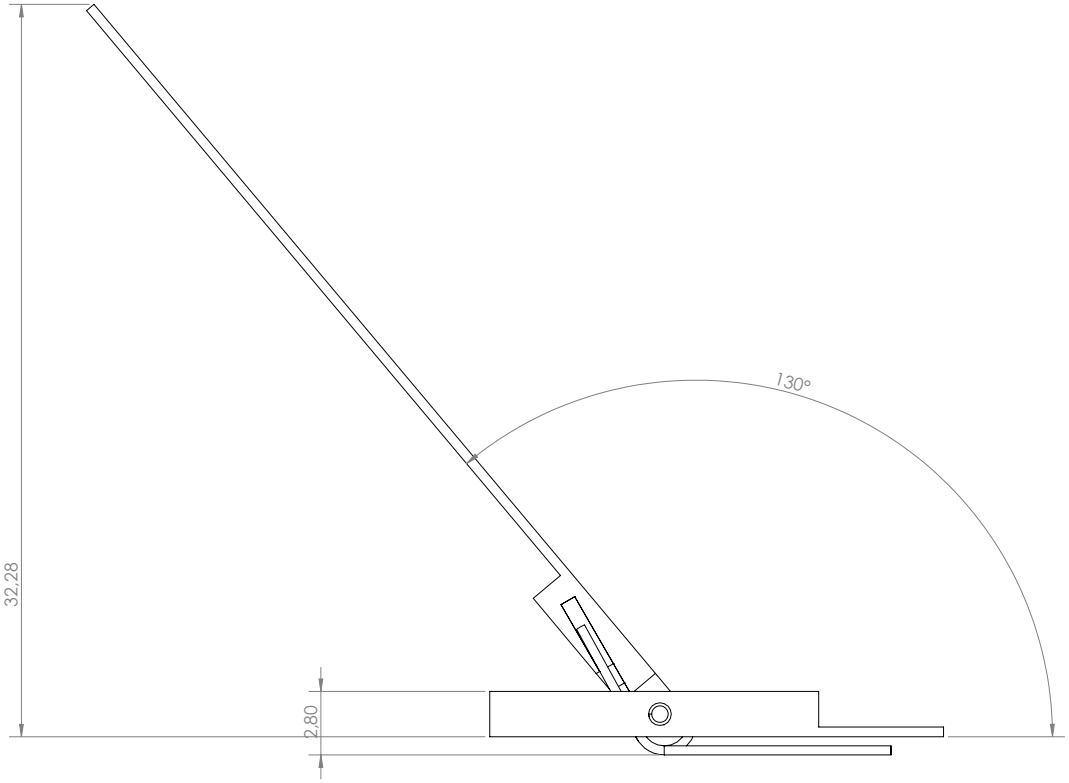

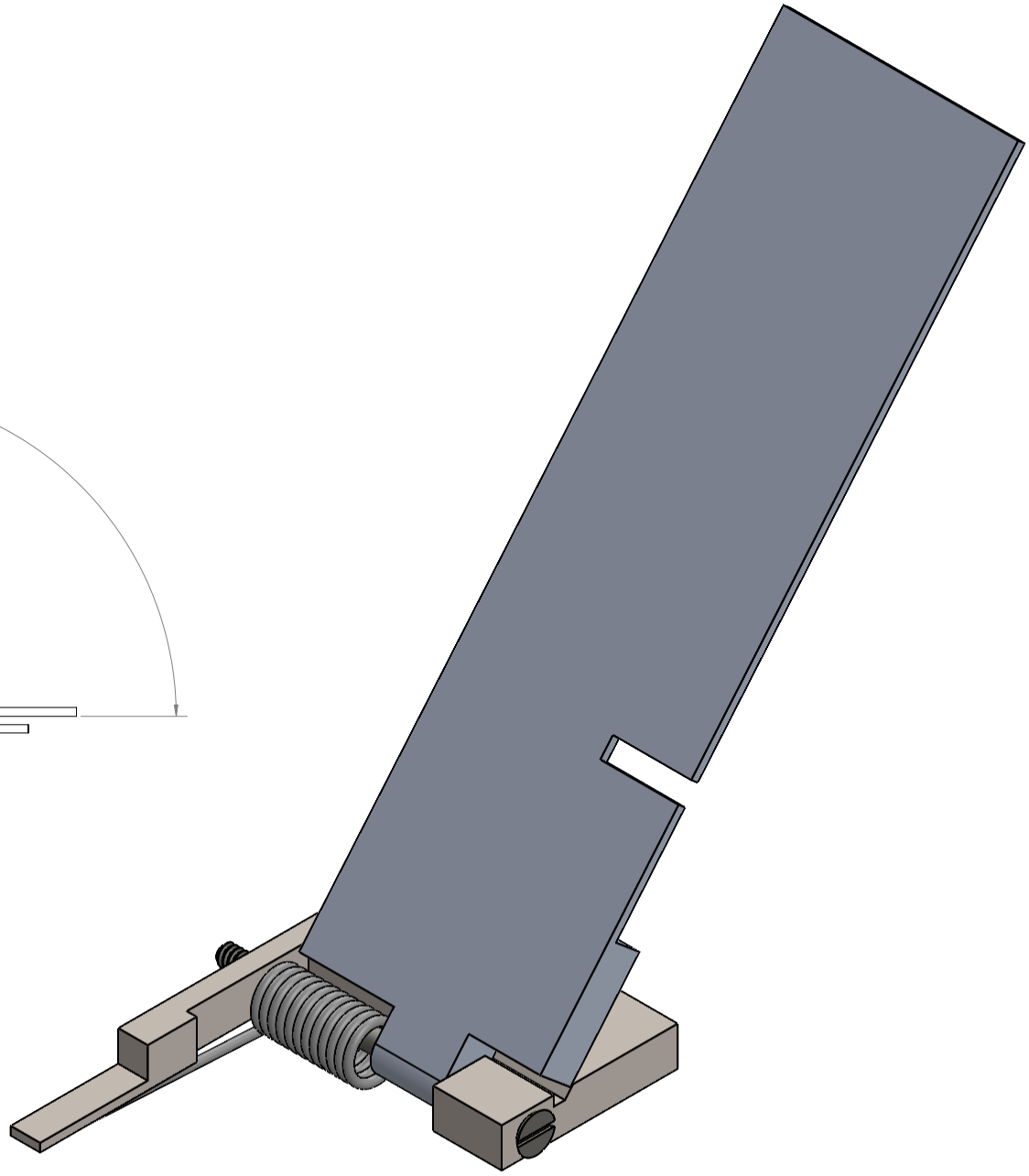

UNLESS OTHERWISE SPECIFIED: DIMENSIONS ARE IN MILLIMETERS SURFACE FINISH: TOLERANCES: H8/h9 LINEAR: ISO2768-Fine ANGULAR: ISO2768-Fine		FINISH: (Hard-)Anodizing, see individual component drawings		DEBURR AND BREAK SHARP EDGES		DO NOT SCALE DRAWING	REVISION
	NAME	SIGNATURE	DATE			TITLE:	
DRAWN						Deployed Configuration of the Deployment System	
CHK'D							
APPV'D							
MFG							
Q.A				MATERIAL: see individual component drawings		DWG NO. Deployment System	A2
				WEIGHT: 1.660 g		SCALE:2:1	SHEET 1 OF 1

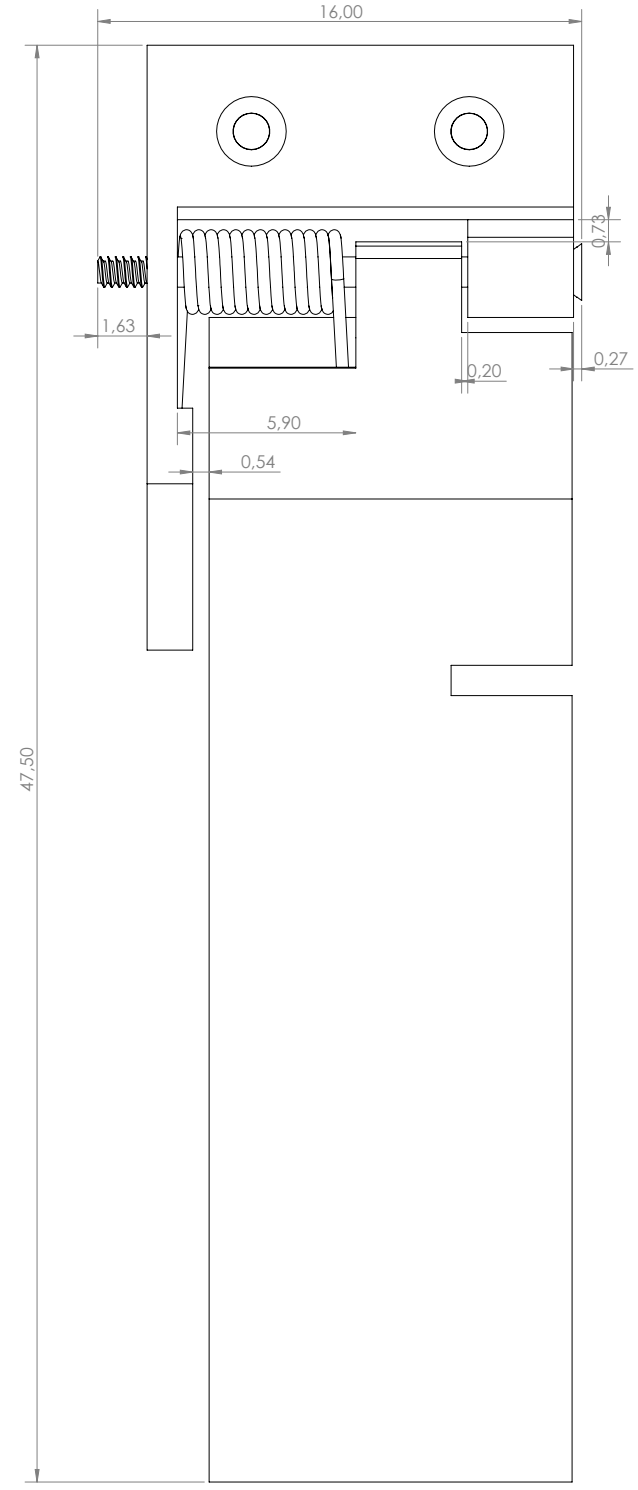

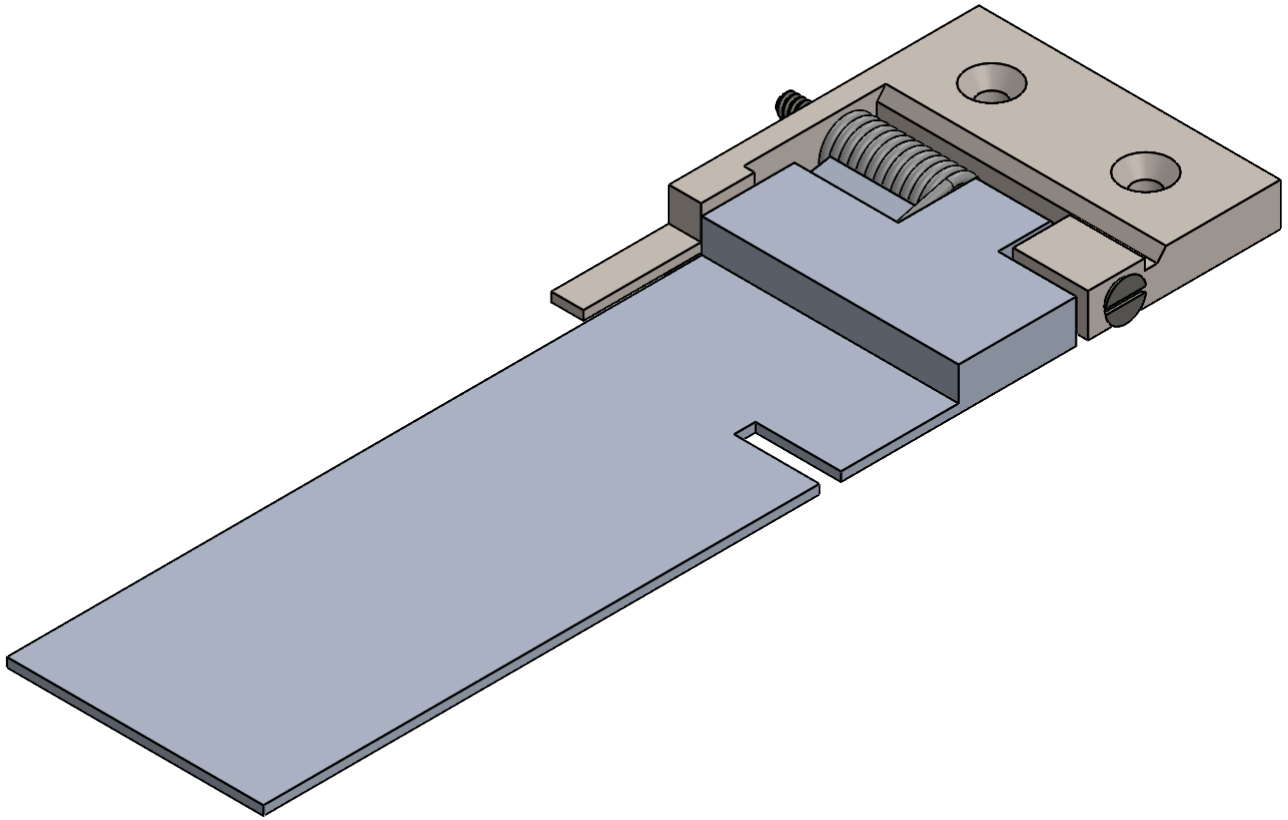

UNLESS OTHERWISE SPECIFIED: DIMENSIONS ARE IN MILLIMETERS SURFACE FINISH: TOLERANCES: H8/h9 LINEAR: ISO2786-Fine ANGULAR: ISO2786-Fine		FINISH: (Hard-)Anodizing, See individual drawings!		DEBURR AND BREAK SHARP EDGES		DO NOT SCALE DRAWING	REVISION
	NAME	SIGNATURE	DATE			TITLE: Stowed Configuration of the Deployment System	
DRAWN							
CHK'D							
APPV'D							
MFG							
Q.A				MATERIAL: See Individual drawings		DWG NO. Deployment System Singular	A2
				WEIGHT: 1.660 g		SCALE:2:1	SHEET 1 OF 1

E

Preliminary Concept Study

In this appendix, a detailed concept study of Concept Tape Spring, Concept SMA and Concept Torsion Spring is presented. The rationale behind the generation of each concept is outlined, followed by an overview of their designs and corresponding design choices. Finally, their designs are assessed based on the pre-determined criterion (see Section 5.1.2).

E.1. Concept Generation

The concept generation process is based on the design option tree shown in Figure 4.2. As the system is divided into various functions and subsystems, each with multiple design options, theoretically many concepts can be generated. However, for this process only feasible design options have been considered. Among the subsystems and functions in Figure 4.2, the actuation method offers the highest number of feasible design options. Based on this observation, three distinct concepts have been generated, each utilizing a unique actuation method.

Concept Tape Spring (Section E.2) combines the inherent behavior of a bi-stable tape spring with a hinge mechanism. The hinge, which enables parallel rotational kinematics, will have embedded angular limit control. A burn wire mechanism will serve as the HDRM. The combination of these elements is expected to ensure efficient and reliable deployment.

Concept SMA (Section E.3) is based on the deployment system onboard the ALBus satellite [31, 39]. Similar to that system, the SMA-based actuation method in this concept has embedded angular limit control and functions as its own HDRM. Additionally, the concept includes a hinge mechanism that enables parallel rotational kinematics. The integration of the HDRM and angular limit control within the SMA-based actuation method simplifies the overall system by reducing the number of required components.

Concept (Torsion) Spring (Section E.4) integrates a potentially feasible deployment mechanism: a turntable with perpendicular rotational kinematics. Due to the simplicity of spring-based actuation, this method can be combined with a more complex deployment mechanism compared to SMA- or tape spring-based alternatives. To avoid unnecessary complexity, straightforward approaches have been selected for the HDRM and angular limit control. A burn wire mechanism will act as the HDRM and angular limit control will be integrated within the actuator to prevent overshooting the deployment angle. This approach balances the simplicity of the actuation method with the complexity of the deployment mechanism, ensuring that its potentially-feasible characterization is not overlooked.

While all feasible design options have been used at least once across the three generated concepts, certain (potentially feasible) options were excluded. These include the bus-mounted stop block for mitigating angular overshooting and the pin-pusher/pin-puller HDRMs. The bus-mounted stop block was excluded because it complicates the integration of the deployment system across different satellite

platforms. Similarly, pin-pusher and pin-puller HDRMs were excluded, because simpler alternatives are available and their integration with specifically the Delfi-Twin mission is challenging due to their dimensions.

E.2. Concept 1

From the design option tree in Figure 4.2, the design of Concept 1 will consist of a hinge mechanism with a tape spring as the actuation method. Within the hinge mechanism, the tape spring, burn wire and angular limit control are integrated. As multiple approaches could be taken to realize this design, all design choices for the integration of each element are considered separately. The considered approaches will be elaborated upon and unfeasible approaches will be discarded. The complete design of Concept 1, where all previously made design choices are combined into one concept, will be depicted in Section E.2.2.

E.2.1. Design Choices

Mechanism Integrated Angular Limit Control

Mechanism-integrated angular limit control is essential to ensure that overshooting of the deployment angle does not occur. After evaluating various methods, the final approach chosen was to implement modifications to the hinge knuckles. Although modifying the hinge leaves was considered as an alternative, for example, locally increasing the height of the hinge leaf to act as a physical stop, these approaches were ultimately deemed unfeasible and impractical. Since switch-ability between stowed configurations is preferred, modifying the hinge leaves would prevent this flexibility. Due to the nature of the considered configurations, any leaf modification to limit the deployment angle would inhibit the ability of the same hinge mechanism to accommodate other configurations. However, this limitation is not present when the hinge knuckle is modified.

The chosen method of modifying the hinge knuckles relies on the principle that a 180° rotation on a flat surface requires the rotating knuckle to have a circular cross-section. By altering the knuckle geometry so that the suspended angle is 130°, the knuckle will collide with the flat surface it rests on, restricting further rotation. This passive mechanical constraint eliminates the need for additional components or complex mechanisms to enforce the angular limit, thereby simplifying the design while achieving precise, measurable control of the deployment angle. Furthermore, only the knuckle associated with the rotating hinge leaf requires modification. The open and closed hinge stowed configurations will each have their own dedicated hinge leaf, as shown in Figure E.1. The hinge knuckle will be custom-made for their respective rotational paths (open-to-closed or closed-to-open). Together, these hinge leaves will form the complete hinge mechanism, ensuring compatibility and switch-ability for use in various configurations.

Figure E.1d shows a side view of the hinge leaf designed specifically for the OHSC, including its preliminary dimensions. The stowed and deployed states of this configuration are shown in Figure E.1a. Similarly, Figure E.1c shows the side view of the hinge leaf customized for the CSHC, along with its associated dimensions, while Figure E.1b depicts the deployed state for this configuration. Together, these two hinge leaves, when combined with a pin, form the complete hinge system. It is important to note that the dimensions shown in the figures are preliminary and subject to further validation. Additional mass optimizations and analyses will be conducted to refine these dimensions, optimize the hinge's performance and ensure full compliance with the system requirements.

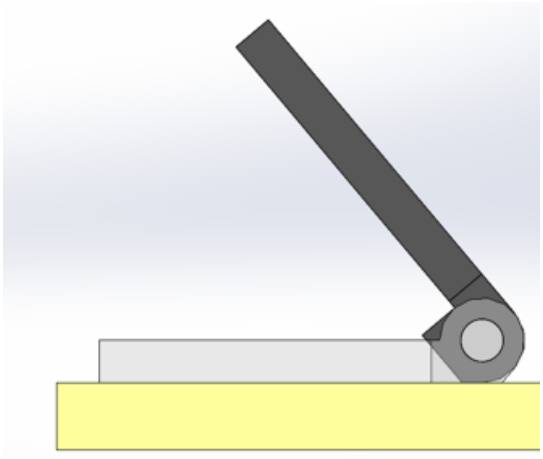

(a) Concept 1 OHSC in its Deployed state

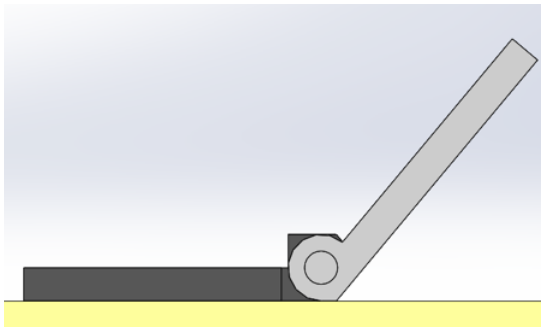

(b) Concept 1 CHSC in its Deployed state

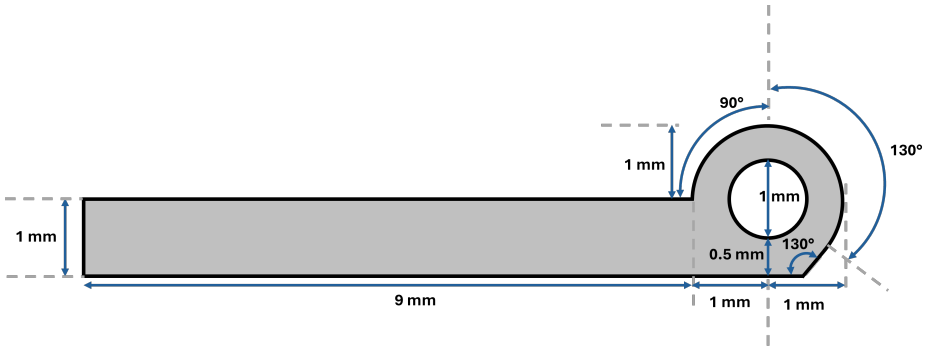

(c) Modified Hinge Leaf with embedded Angular Limit Control designed for CHSC

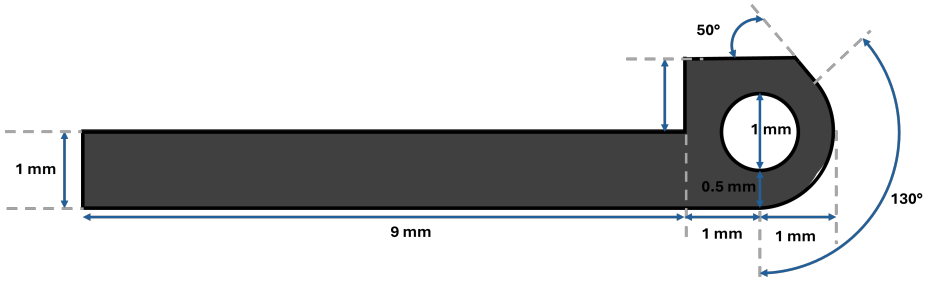

(d) Modified Hinge Leaf with embedded Angular Limit Control designed for OHSC

Figure E.1: Deployed state of concept 1 CHSC and OHSC, with both modified hinge leaves. Preliminary dimensions are also provided to realize the angular limit control.

Tape Spring Integration

The integration of the tape spring must ensure actuation for deployment while potentially conducting current to and from the RABSII antenna for power and communication purposes. Given the many applicable methods for tape spring integration, multiple configurations were considered for each stowed configuration (Figure 5.1).

For the CSHC, the tape spring must enable a closed-to-open movement pattern. Figure E.2 shows the eight configurations considered for integrating the tape spring within the hinge. The first distinction involves categorizing these configurations as either over-hinge or under-hinge. Configurations 5, 7 and 8 are under-hinge configurations and are excluded from further consideration. This is because one of the primary limitations of COTS tape springs is their minimum bending radius. The minimum bending radius is a critical property of tape springs that defines the smallest allowable radius of curvature before plastic deformation occurs. Plastic deformation would limit the deployment angle, potentially causing the deployment to fall significantly short of the intended angle or preventing deployment altogether

in extreme cases. This issue was observed in the Delfi-C^3 mission, where warping of the antennas occurred due to excessive bending [9]. The minimum bending radius can be analytically determined using the following formula [49]:

$$r = \sqrt{\frac{D_{11}^*}{D_{22}^*}} \cdot R \; with [D^*] = [D] - [B][A]^{-1}[B] \tag{E.1}$$

Where [A],[B] and [D] are the non-zero quadrants of the laminate compliance matrix. $[D_{11}^*]$ and $[D_{22}^*]$ are the diagonal terms of the matrix $[D^*]$. R is the curvature of the tape spring and r is the resulting bending radius. However, COTS tape springs (e.g., tape measures) typically do not provide detailed material or structural parameters required for these calculations. To minimize the thickness of the hinge system and maximize the allowable bending radius, under-hinge configurations were excluded from consideration. Additionally, Configuration 6 was excluded as it involves unnecessary bending, which would complicate the system without added benefit.

The remaining configurations (1,2,3 and 4) are suitable methods for integrating the tape spring. Figure E.3 provides the side views of these configurations in the deployed state for better visualization. The final decision on which configuration to implement, will depend on specific factors that will be elaborated upon in subsequent sections.

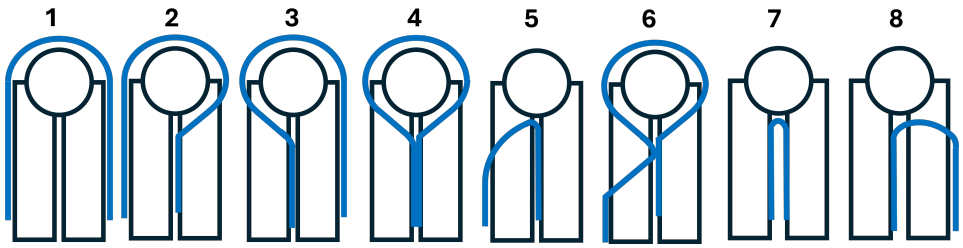

Figure E.2: Eight possible tape spring integration method for the CHSC.

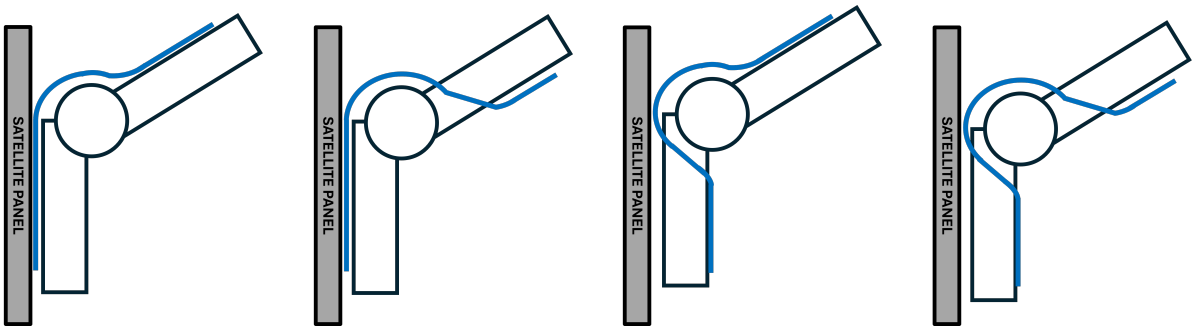

(a) Integration of the Tape Spring Configuration 1, in deployed state

(b) Integration of the Tape Spring Configuration 2, in deployed state

(c) Integration of the Tape Spring Configuration 3, in deployed state

(d) Integration of the Tape Spring Configuration 4, in deployed state

Figure E.3: Deployed state of CHSC with relevant tape spring configurations.

For the OHSC, an open-to-closed movement pattern must be achieved. However, the number of applicable methods for this configuration is limited. As with the CHSC, under-hinge methods are excluded due to the minimum bending radius limitations of tape springs, which could result in plastic deformation and hinder successful deployment. Beyond under-hinge methods, only two additional viable approaches are applicable. The side views of these methods, showing both the stowed and deployed configurations, are shown in Figure E.4. For clarity, the satellite panel is also depicted, as the tape spring will be fixed to it.

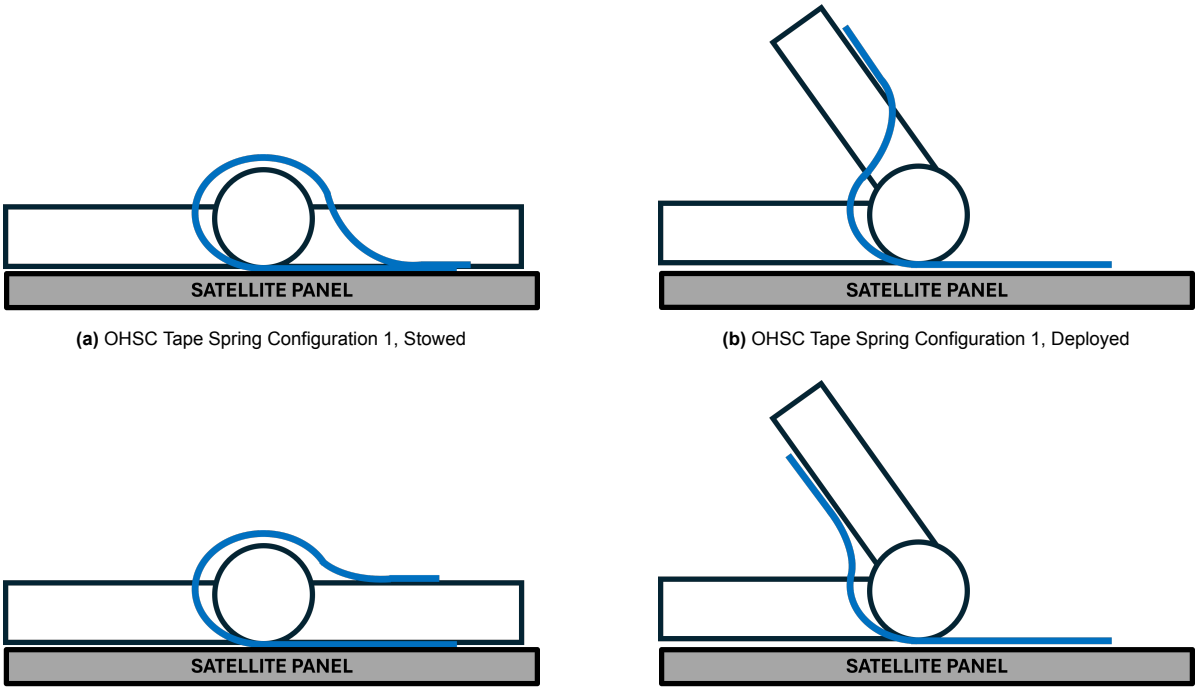

(a) OHSC Tape Spring Configuration 1, Stowed

(b) OHSC Tape Spring Configuration 1, Deployed

(c) OHSC Tape Spring Configuration 2, Stowed

(d) OHSC Tape Spring Configuration 2, Deployed

Figure E.4: Stowed and deployed state of OHSC with relevant tape spring configurations.

For the RAHSC, an open-to-closed movement pattern must be implemented. Although achieving a 130° deployment angle may not be possible in this configuration, the allowable minimum bending radius for the tape spring can be higher, offering greater flexibility in the design. The side views of the applicable methods are shown in Figure E.5, showing both the stowed and deployed configurations. For clarity, the satellite panel is also included in the depiction, as the tape spring will be fixed to it.

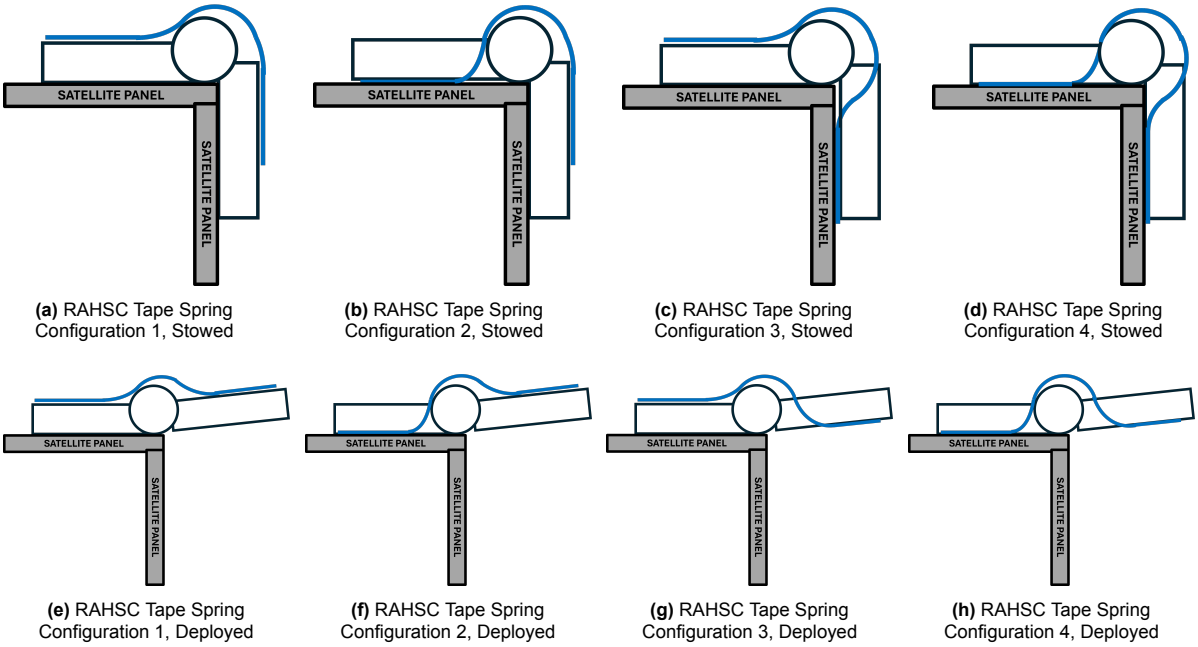

(a) RAHSC Tape Spring Configuration 1, Stowed

(b) RAHSC Tape Spring Configuration 2, Stowed

(c) RAHSC Tape Spring Configuration 3, Stowed

(d) RAHSC Tape Spring Configuration 4, Stowed

(e) RAHSC Tape Spring Configuration 1, Deployed

(f) RAHSC Tape Spring Configuration 2, Deployed

(g) RAHSC Tape Spring Configuration 3, Deployed

(h) RAHSC Tape Spring Configuration 4, Deployed

Figure E.5: Stowed and deployed state of RAHSC with relevant tape spring configurations.

Burn Wire Integration

For the integration of the burn wire mechanism, the only feasible location for the restraining material is on the rotational hinge leaf. Placing the burn wire on the RABSII antenna is not permissible and positioning it on other components would fail to restrict rotation effectively. To provide a dedicated location for the restraining material, grooves have been added into the leaf design. These grooves enable placement of the restraining material. Additionally, to mitigate the risk of the restraining material sliding out of the grooves, a small hole has been added. This hole allows the burn wire to be guided securely, while a groove on the back ensures that the hinge can lay flat during the stowed configurations. Figure E.6 shows the top and bottom views of one of the hinge leaves, highlighting the retention wire grooves and the guiding hole.

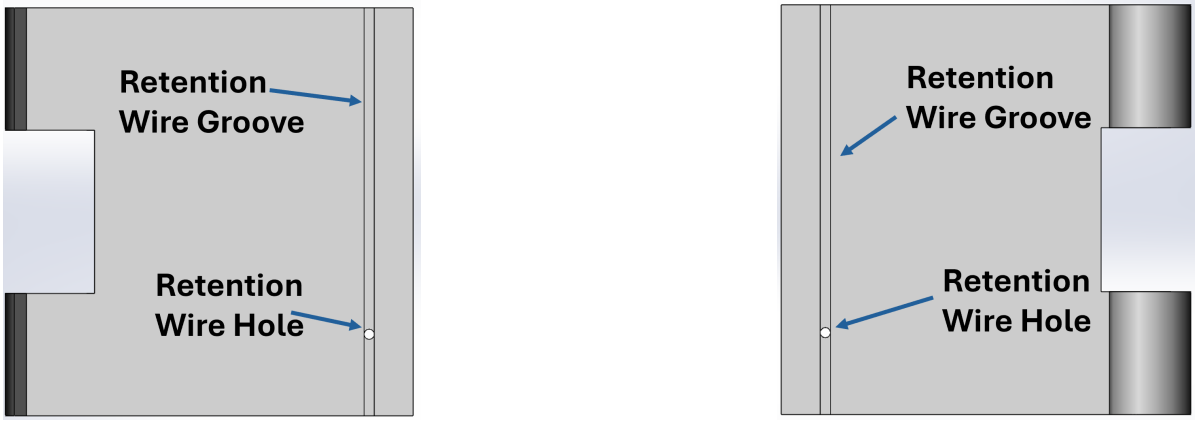

(a) Bottom-view of hinge leaf with a retention wire groove and hole

(b) Top-view of hinge leaf with a retention wire groove and hole

Figure E.6: Top and bottom view of a hinge leaf where burn wire integration is made possible.

E.2.2. Final Design

The final design of Concept 1 consists of two hinge leaves, incorporating various modifications to enable the integration of the tape spring actuation, burn wire HDRM, angular limit control and FR-4 plate. Top and isometric views of each hinge leaf are shown in Figure E.7 and the side view illustrating the relationships between components is provided in Figure E.9. Additionally, the deployed and stowed states for the CHSC, OHSC and RAHSC with the final hinge mechanism design are depicted in Figure E.8.

For clarity, Figure E.9 shows the relationships between variable parameters of both hinge leaves and their respective influences. H_t is the allowable thickness of the system. H_{FR4} is the thickness of FR-4 plate, which is 1.57 mm. $L_{FR4-Req}$ is the minimum overlap length required for the FR-4 plate to ensure a rigid bond, determined based on simulations (to be provided in a later chapter). H_{Leaf} is $\frac{1}{2}H_t$. $D_{retention}$ is the diameter of the retention wire required for the burn wire HDRM.

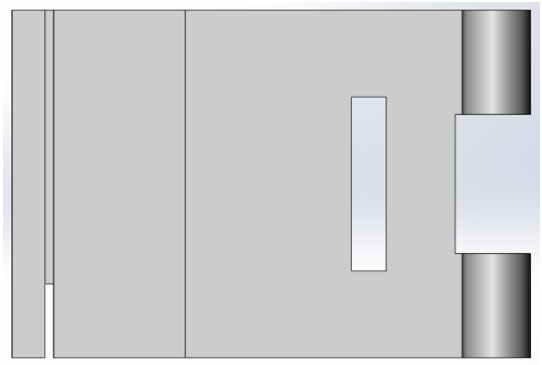

(a) Top-View of Hinge leave enabling CHSC

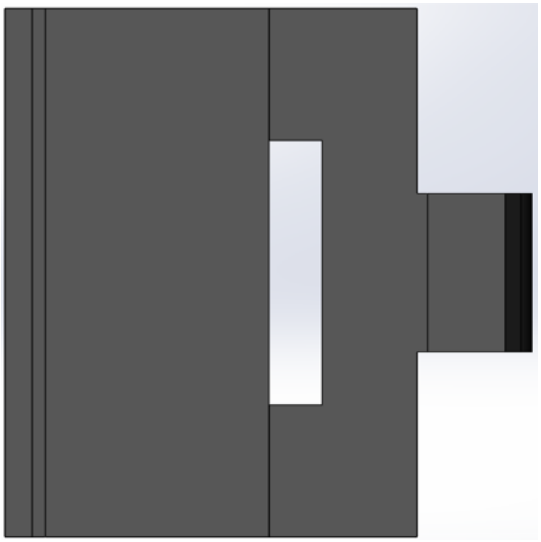

(b) Top-View of Hinge leave enabling OHSC

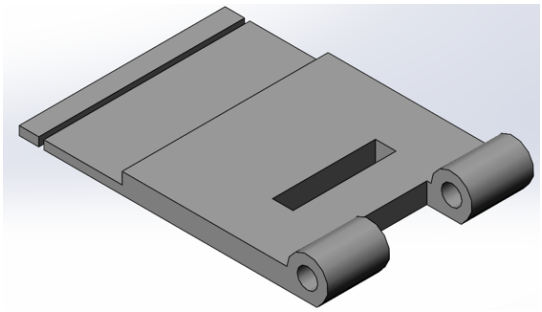

(c) Isometric View of Hinge leave enabling CHSC

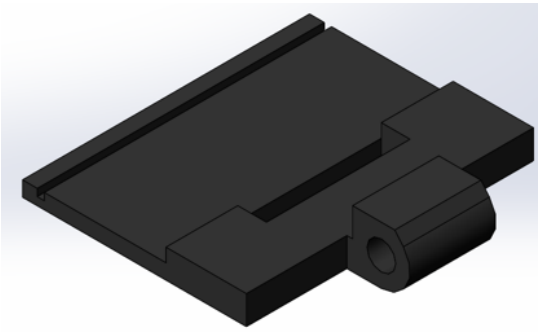

(d) Isometric View of Hinge leave enabling OHSC

Figure E.7: Stowed and deployed state of OHSC with relevant tape spring configurations.

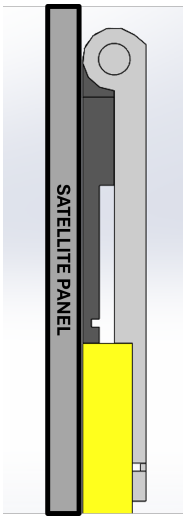

(a) Concept 1, Final Design in CHSC, Stowed

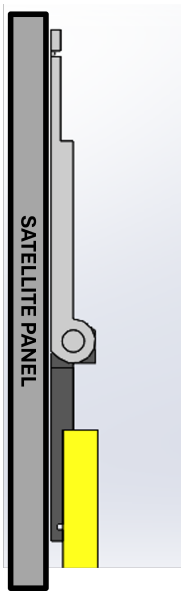

(b) Concept 1, Final Design in OHSC, Stowed

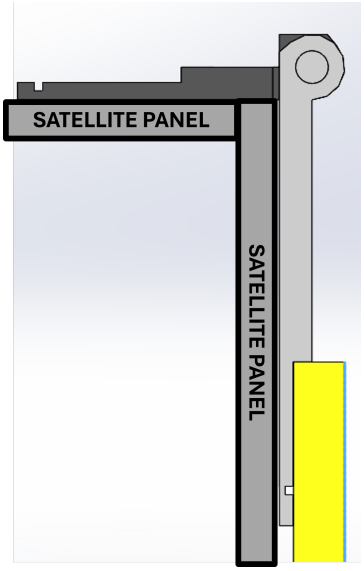

(c) Concept 1, Final Design in RAHSC, Stowed

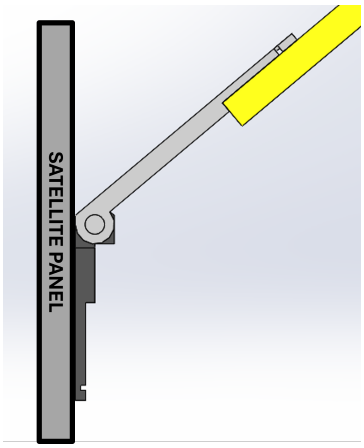

(d) Concept 1, Final Design in CHSC, Deployed

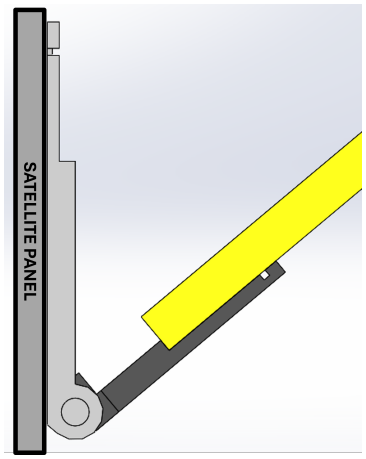

(e) Concept 1, Final Design in OHSC, Deployed

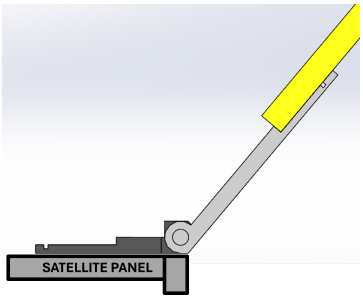

(f) Concept 1, Final Design in RAHSC, Deployed

Figure E.8: Concept 1, deployed and stowed state of CHSC, OHSC and RAHSC.

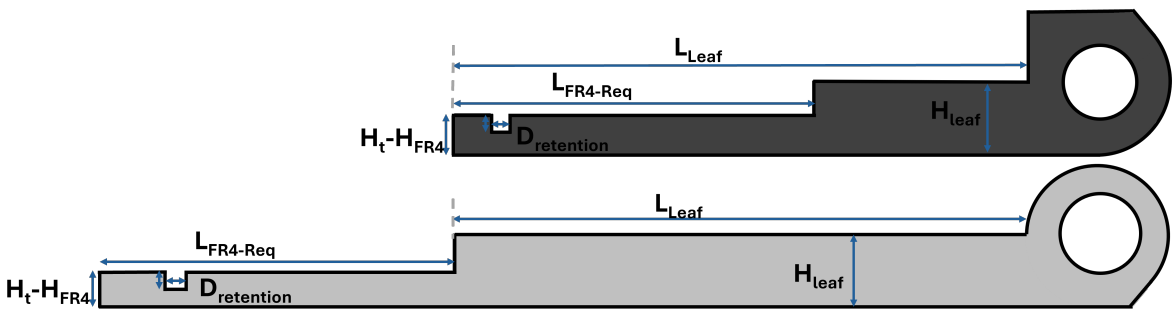

Figure E.9: Variable Parameters of Concept 1's hinge leaves.

E.3. Concept 2

From the design option tree in Figure 4.2, the design of Concept 2 will consist of a hinge mechanism which uses an SMA as the actuation method, angular limit control and HDRM. Various considerations have been made before in Section E.3.2 the complete design could be presented. All considered approaches for the design will be elaborated on in Section E.3.1 and rationale will be provided.

E.3.1. Concept 2 Design Choices

For the Concept study of Concept 2, as the SMA of the RABSII antenna elements will be Nitinol with an activation temperature (M_s) of 40°, the following assumptions are made:

- The thermal flux provided in orbit is sufficient for activation of any SMA with an activation temperature below 40°C.
- Thermal flux in orbit will be (relatively) constant through the operational mission timeline due to the sun-synchronous orbit.

Furthermore, for the ALbus, SMA plates (0.2 mm thick, $Ni_{50.7}Ti_{49.3}$) are used, each generating a torque of 0.190 Nm [39, 31]. Similar thickness and torque will be assumed, experimental validation will be required in later stages to validate this torque.

SMA Material Choice

The SMA acts both as the actuation method and the HDRM, while also mitigating angular overshooting. The phase transformation of the SMA must not occur prematurely and should be restricted to in-orbit conditions. This requires a temperature range for the phase transition. The lower bound of this range is determined by the maximum ambient temperature during pre-launch and launch phases, while the upper bound corresponds to the highest temperature expected in orbit.

During launch, ambient temperature conditions are anticipated to range between 18.3°C and 29.4°C [89, 99]. In a sun-synchronous orbit at an altitude of 550 km, the temperature range is expected to vary from -40°C to +80°C. To prevent premature phase transformation, the activation temperature (M_s) and A_s of the SMA must be within 29.4°C to 80°C. This ensures that the phase transition occurs exclusively in orbit, avoiding any undesired activation during launch phases.
Table 3.1 compares various SMA compositions along with their respective M_s and A_s. Potential candidates include $Ti_{49}Ni_{41}Cu_{10}$, $Ti_{50}Ni_{40}Cu_{10}$ and $Ti_{50}Ni_{50}$.

The SMA selected for the RABSII antenna elements has an activation temperature of 40°C. Due to the significant difference in deployment force between the folded and unfolded states of the RABSII antenna (see Appendix A), an activation temperature below 40°C is preferred. Among the listed compositions, only $Ti_{49}Ni_{41}Cu_{10}$ meets this criterion, with an M_s of 30°C and an A_s of 35°C.

Hinge Mechanism

The hinge mechanism designed for this concept differs from the one utilized in Concept 1 (Concept Tape Spring, Section E.2). Unlike Concept 1, this concept does not require an integrated angular limit control mechanism, which facilitates a simplification of the hinge leaves. The mechanism will consist of three components, a hinge bracket, a rod and a hinge leaf. The mechanism is shown in Figure E.11.

This design offers several advantages. Simplifying the fixated hinge leaf to a bracket will reduce the mass, but will also allow for the implementation of a modular system. As described in Appendix A, the maximum deployment moment ($M_{deployment}$) required in the unfolded state of the RABSII antenna element is calculated to be 1.0325 Nm. This design allows for a configuration where multiple hinge mechanisms are placed on a single rod, increasing the total moment generated by the deployment system (Figure E.10). Furthermore, various stowed configurations (CHSC, OHSC and RAHSC) can still be performed. Lastly, the thickness of the hinge leaves can be designed to match the maximum allowable thickness, improving the structural integrity of the system.

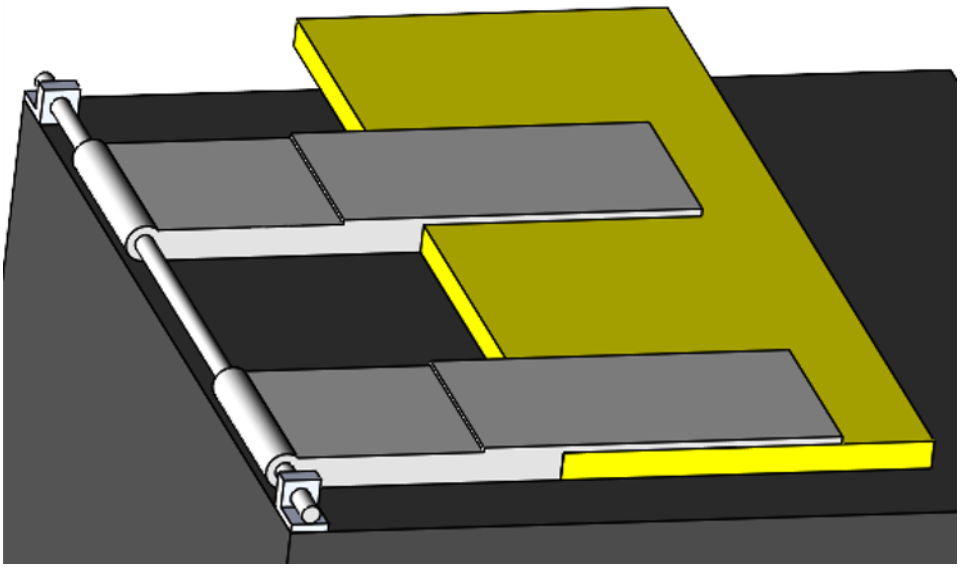

Figure E.10: Example of modular design of Concept 2's hinge mechanism.

SMA Integration

The integration of the SMA must ensure quick and reliable actuation for deployment, while also potentially conducting current to and from the RABSII antenna for power and communication purposes. Similar rationale as stated in Section 5.3.2 can be applied for Concept SMA.

E.3.2. Final Design

The final design of Concept 2 consists of a hinge mechanism composed of a hinge leaf and a hinge bracket. The hinge leaf has been modified to enable the integration of a SMA actuation method and FR-4 plate. The use of a hinge bracket rather than multiple hinge leaves, allows for a modular configuration where additional hinge leaves can be positioned along the rod if needed. Figures E.11 shows different views of the mechanism in both its stowed and deployed configuration, as well as the relationships between important variable parameters of the hinge bracket and hinge leaf.

For clarity, Figure E.12 shows the variable parameter relationships of the hinge leaf of Concept 2. H_t represents the allowable thickness of the system. H_{FR4} denotes the thickness of FR-4, which is 1.57 mm. $L_{FR4-Req}$ is the minimum overlap length required for the FR-4 plate to ensure a rigid bond (which will be validated through simulations and provided in a later chapter). H_{SMA} is the thickness of the SMA sheet used; in the figure it is currently 0.25 mm thick.

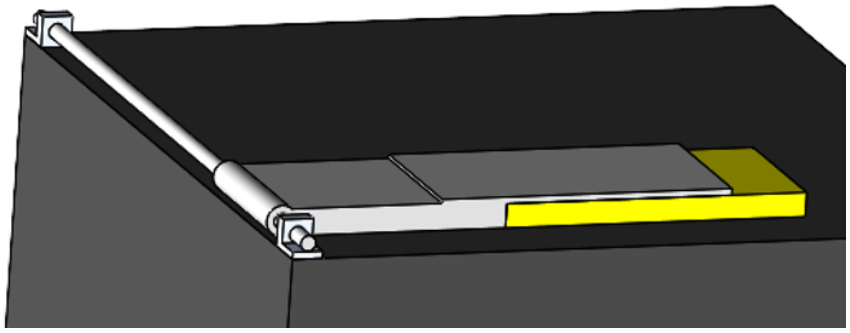

(a) Concept 2, Isometric view of the final design, Stowed

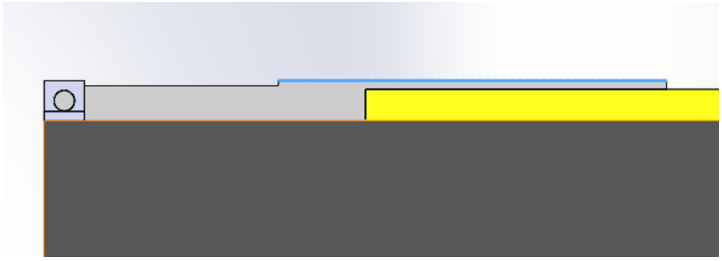

(b) Concept 2, Side view of the final design, Stowed

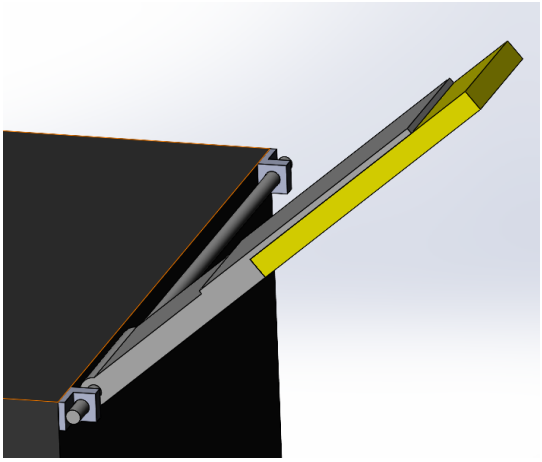

(c) Concept 2, Isometric view of the final design, Deployed

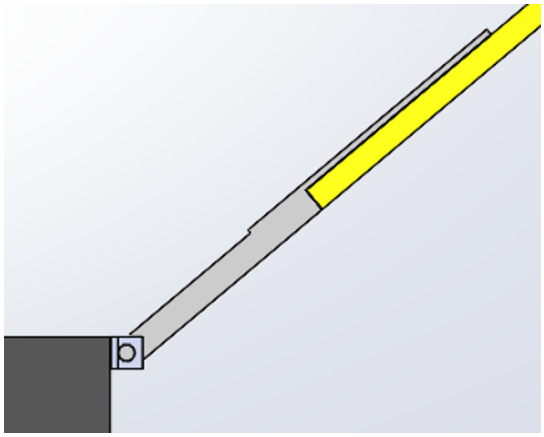

(d) Concept 2, Side view of the final design, Deployed

Figure E.11: Concept 2, multiple views of the deployed and stowed configuration.

Figure E.12: Variable parameters of Concept 2's hinge leaf.

E.4. Concept 3

From the design option tree in Figure 4.2, the design of Concept 3 will feature a turntable mechanism actuated by a torsion spring. The turntable deployment mechanism will enable perpendicular rotational kinematics, with the angular limit control embedded within the actuator. Additionally, a burn wire mechanism will be implemented as the HDRM.

E.4.1. Design Choices

Deployment Mechanism and Kinematics

The turntable mechanism, also referred to as a revolving or swivel hinge, consists of three main components. Similar to the simple hinge depicted in Figure 5.2, these components include the turntable's leaf, knuckle and pin. However, unlike a simple hinge, the external faces of the turntable remain aligned and face each other throughout the movement.

In this concept, a distinction is made between the turntable leaves. The Fixated Turntable Leaf (FTL) will refer to the turntable leaf fixated on the satellite panel and does not rotate. The Rotating Turntable Leaf (RTL) will refer to the turntable leaf which rotates relative to its stowed configuration and is (partially) placed on the FTL.

Initially, the design focused on modifying only the FTL to achieve the desired deployment angle of 50◦ (calculated as 180° - 130° for a mirrored orientation). However, this approach was deemed unfeasible due to geometric constraints. Given the target deployment angle and the maximum allowable stowed thickness of 2 mm, the distance between the highest point of the FTL and the rotation axis of the RTL needed to be 1.678 mm. Within this space, it was impossible to allow for both the pin and the structural components of the RTL.

To overcome these limitations, the chosen approach utilized the geometry of both the FTL and RTL to achieve the desired deployment angle. This solution eliminated the need for the tight margins inherent in the initial approach. By distributing the functional geometry across both components, the distance between the highest point of the FTL and the rotation axis of the RTL was increased to 4.289 mm. The designs of the FTL and RTL, along with their respective preliminary parameters, are shown in Figure E.13 and Figure E.14, respectively.

The parameters of the FTL design are shown in Figures E.13a and E.13b, with the radius r_{FTL} calculated as follows:

$$r_{FTL} = \frac{1}{2} \cdot \frac{2mm}{tan(25°)} \tag{E.2}$$

The design of the RTL is more complex. As shown in the side view in Figure E.14c, a 1 mm thick strip is folded at an angle of 25°. This fold allows the RTL to achieve a 25° angle relative to the FTL when deployed. However, to prevent the RTL from colliding with the flat surface (on which the FTL rests during rotation), the position of the turntable knuckle had to be offset. This offset is depicted in Figure E.14b. The outer radius of the knuckle, measured from its center, was designed to be r_{FTL}, while the inner radius was defined as r_{pin}. Assuming $r_{pin} = 1$ mm, the difference $r_{FTL} - r_{pin}$ was calculated to be 1.145 mm. Fortunately, the opposite side of the turntable did not require similar constraints, allowing for the integration of the FR-4 plate and burn wire mechanism in the final design.

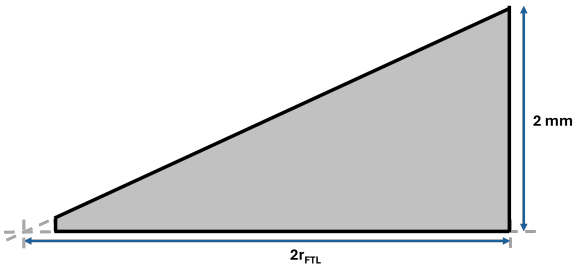

(a) Side-View of the FTL with added parameters

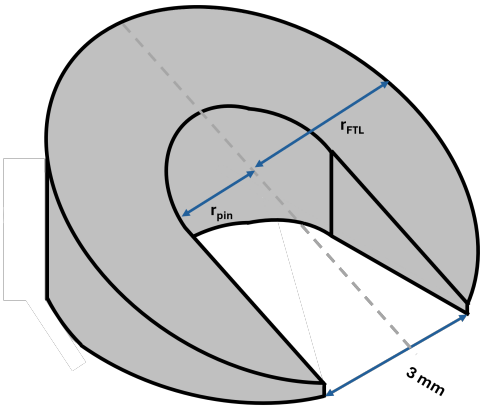

(b) Isometric view of the FTL with added parameters

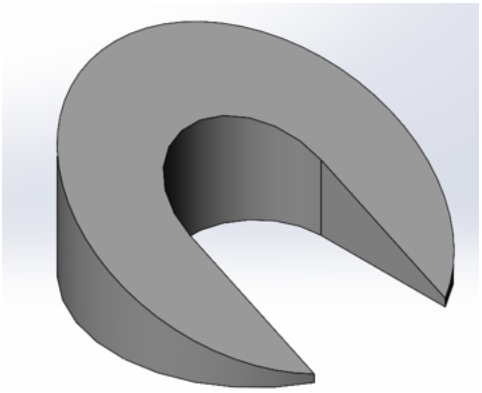

(c) Isometric view of the FTL

Figure E.13: Side and isometric view of the FTL with its corresponding parameters.

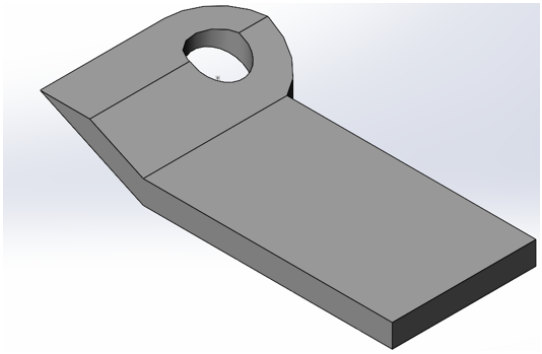

(a) Isometric view of the RTL

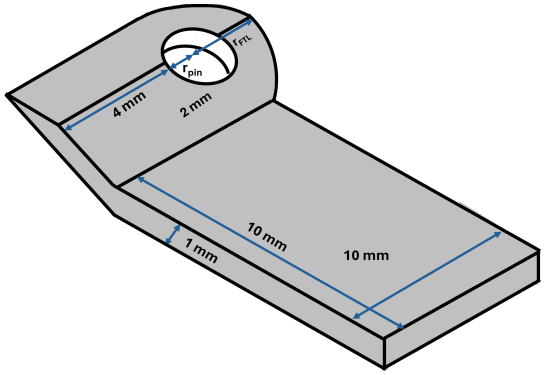

(b) Isometric view of the RTL with added parameters

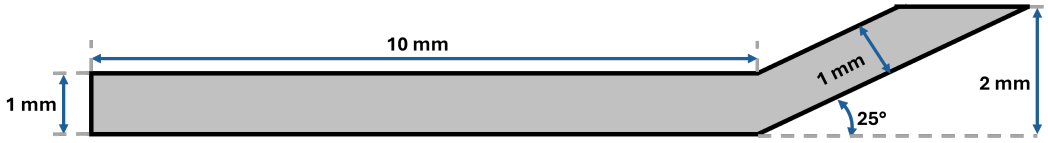

(c) Side-view of the RTL with added parameters

Figure E.14: Side and isometric View of the RTL with its corresponding parameters.

Torsion Spring Integration

The torsion spring will be positioned within the turntable knuckles, serving as both the actuation method and the turntable pin. To simplify the deployment mechanism, the torsion spring will be angled to align with the same 25° angle as the RTL. This alignment simplifies the integration process. The outer radius of the torsion spring must remain below r_{FTL}, while its added height at the 25° angle must adhere to the overall volume budget of the system. For demonstration purposes, an outer radius of 1.3 mm is assumed, corresponding to an allowable height of approximately 2 mm.

On the RTL, grooves and a hole have been added to allow for the integration of the torsion spring. The torsion spring's top poke will be placed within the hole to rotate the RTL. This integration method minimizes the risk of the torsion spring disconnecting from the RTL during operation. On the FTL, the torsion spring will be fixated. A groove has been added at the bottom of the FTL to ensure the external plate supporting the FTL prevents the torsion spring from slipping out or becoming loose. The modifications to the FTL and RTL for torsion spring integration are shown in Figure E.15a.

To secure the torsion spring's pokes, the FTL and RTL have both been modified. The bottom poke will be fixed between the FTL and the plate it rests on, while the top poke will connect to the RTL. The top poke requires an 90° bend to ensure that its connection with the RTL will not be compromised by vibrations and shocks. These modifications, along with the integration details, are depicted in Figure E.15.

Burn wire Integration

The integration of the burn wire mechanism will be on the RTL. Placement on other components, such as the FTL, the pin, or the antenna, was deemed either infeasible, unnecessarily complex, or not permissible. The chosen method for burn wire integration involves a simple hole within the FTL, with an additional groove added underneath to ensure that the thickness of the retention wire does not impose an angle on the RTL. Similar to the turntable knuckle of the FTL, the retention wire hole features an offset. This offset minimizes the risk of the retention wire getting stuck underneath the RTL. The integration of the burn wire mechanism is shown in Figure E.15b.

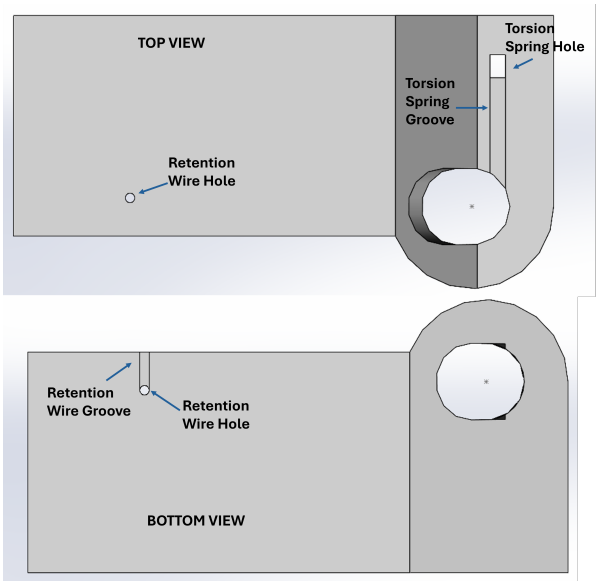

(a) Top and Bottom View of the RTL with the modifications for the torsion spring actuation method

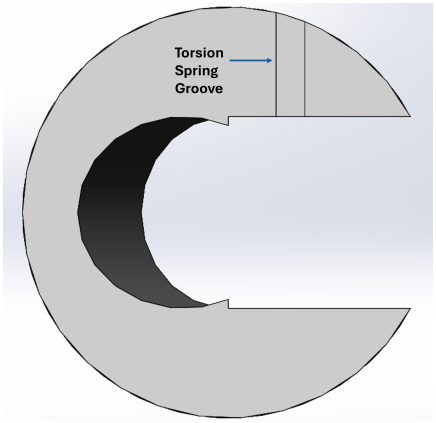

(b) Top View of the FTL with the modification for the torsion spring actuation method

Figure E.15: Various views of the RTL and FTL with added modifications for the burn wire HDRM and the torsion spring actuation method.

E.4.2. Final Design

The final design of Concept 3 will consist of two turntable leaves, which together achieve the required deployment angle of 130°. Various modifications have been made to both leaves to ensure the integration of the torsion spring actuation, burn wire HDRM and the FR-4 plate. Multiple views of the final design are illustrated in Figure E.16.

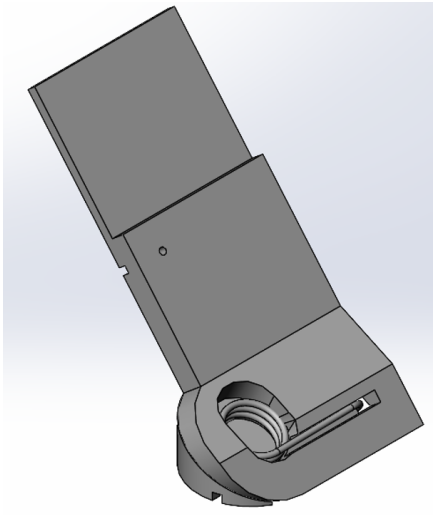

(a) Concept 3, Isometric view of the final design, Deployed

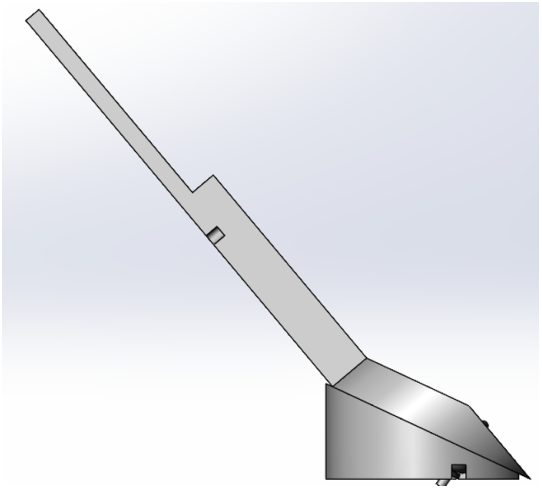

(b) Concept 3, Side view of the final design, Deployed

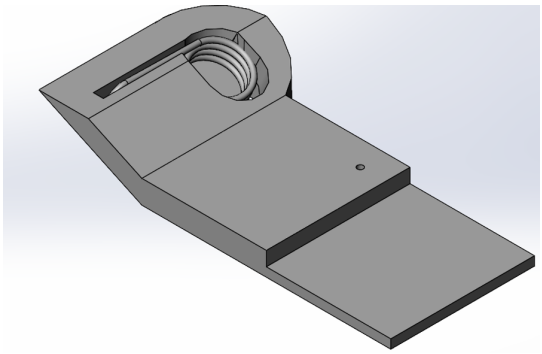

(c) Concept 3, Isometric view of the final design, Stowed

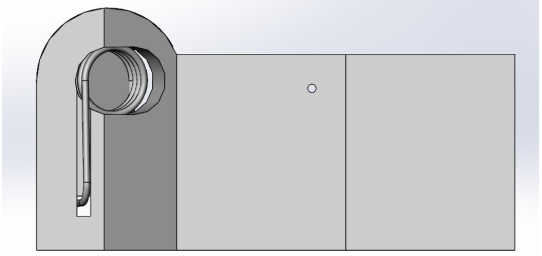

(d) Concept 3, Top view of the final design, Stowed

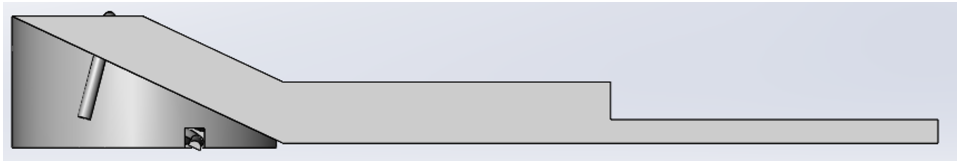

(e) Concept 3, Side view of the final design, Stowed

Figure E.16: Concept 3, multiple views of the deployed and stowed configuration.

For clarity, Figure E.17 shows the variable parameter relationships between both turntable leaves based on the requirements. H_t represents the allowable thickness of the system. H_{FR4} denotes the thickness of FR-4, which is 1.57 mm. $L_{FR4-Req}$ is the minimum overlap length required for the FR-4 plate to ensure a rigid bond which will be validated through simulations (provided in a later chapter). H_{Leaf} is defined as $\frac{1}{2}H_t$. $D_{retention}$ refers to the diameter of the retention wire required for the burn wire HDRM. L_{FTL} is given by $\frac{H_t}{\tan(25°)}$.

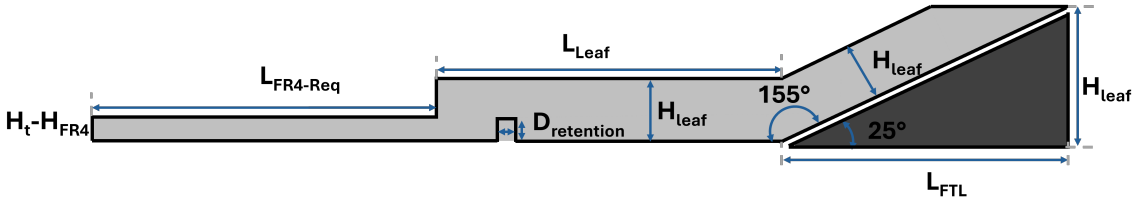

Figure E.17: Variable parameters of Concept 3's turntable leaves.

E.5. Trade-Off of Preliminary Concepts

Note: The values used for the load cases are based on incorrect calculations. However, the resulting variations in the conclusions are minimal and do not significantly affect the overall outcome.

E.5.1. Concept 1

Reliability

To ensure a reliable deployment angle and prevent overshooting, the hinge knuckles were modified. This modification is illustrated in Figure E.9, where each hinge leaf features distinct hinge knuckles, enabling three stowed configurations. However, the intricate geometry of the hinge leaves introduces a low reliability, as it is vulnerable to various assembly or minor design errors.

Analysis of the CAD model revealed that a slack of just 0.1 mm could result in an increase in the deployment angle from 130° to 150°. Potential design errors include unaccounted manufacturing tolerances, which is expected to be on the order of 0.05 mm, unaccounted deformations, or uneven surfaces on which the deployment system rests. Assembly errors, such as over- or under-tightening the connections to the host satellite, further increase reliability issues. These errors, either individually or in combination, could significantly decrease deployment performance. Even a simple overshoot could render the RABSII antenna unusable.

In addition to hinge knuckle modifications, the burn-wire mechanism poses challenges, particularly for Concept 1. Improper tightening of the retention wire, whether over- or under-tightened, can result in vibrations that deform the deployment system or its connected components. Such deformations can lead to similarly poor deployment performance outcomes.

Load Case Simulation and Results

Figure E.18 depicts the simulation constraints and results for the load case defined in Appendix A. The simulation includes both hinge leaves, with Von-Mises stresses and deformations analyzed for each. The peak stresses in both hinge leaves are determined to be no greater than 9.511 MPa (see Figure E.18e) and the maximum deformation is less than $8{\cdot}10^{-3}$ mm (1.86%, Figure E.18c). These peak stresses are concentrated around the corners of the design, which could be mitigated by rounding these corners. The observed deformations, given an aluminum hinge leaf, remain below the material's plastic strain limit of 6% [100]. A potential change in materials could further reduce deformation.

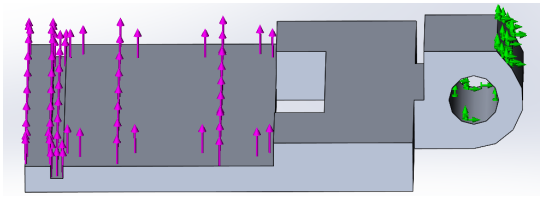

(a) Concept 1 Hinge Leaf enabling OHSC, Applied Constraints (Green Arrows) and Applied Forces (Purple Arrows)

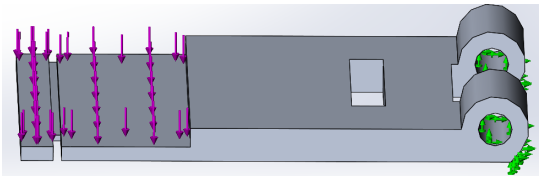

(b) Concept 1 Hinge Leaf enabling CHSC, Applied Constraints (Green Arrows) and Applied Forces (Purple Arrows)

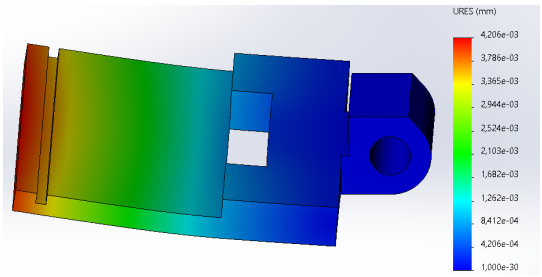

(c) Concept 1 Hinge Leaf enabling OHSC, Deformation occurring due to Load Case 1, [Min:≈0 mm;Max: $4.206 \text{x} 10^{-3}$ mm]

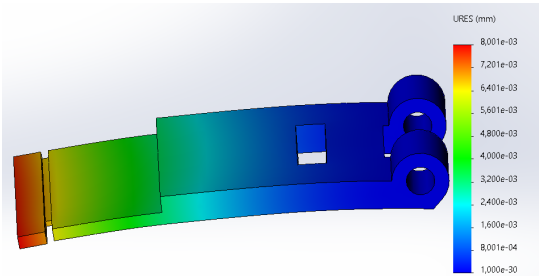

(d) Concept 1 Hinge Leaf enabling CHSC, Deformation occurring due to Load Case 1, [Min:≈0 mm;Max: $8.001 \text{x} 10^{-3}$ mm]

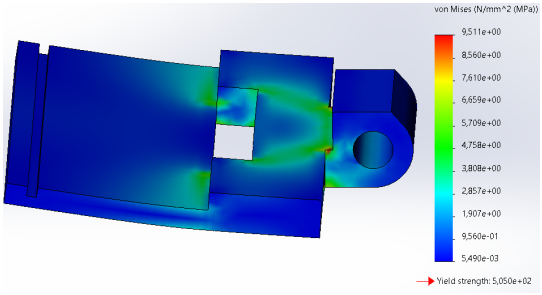

(e) Concept 1 Hinge Leaf enabling OHSC, Von-Mises Stress occurring due to Load Case 1, [Min: $5.490 \text{x} 10^{-3}$ MPa; Max: 9.511 MPa]

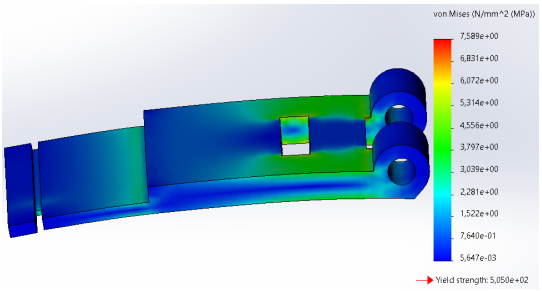

(f) Concept 1 Hinge Leaf enabling CHSC, Von-Mises Stress occurring due to Load Case 1, [Min: $5.647 \text{x} 10^{-3}$ MPa; Max: 7.589 MPa]

Figure E.18: Concept 1 Loadcase 1, initial parameters and results of the simulation.

Compatibility (Delfi-Twin, RABSII Antenna and Nanosatellites)

Limitations in the compatibility with the Delfi-Twin, RABSII antenna and other nanosatellites are mainly due to volume constraints imposed on the deployment system.

The volume constraints specified by the Delfi-Twin mission (17.8x5x0.2 cm^3) or other nanosatellite missions (e.g. 3P PocketQube 17.8x5x0.6 cm^3) restrict the thickness of the hinge knuckles. Adhering to the Delfi-Twin's constraints render the intricate hinge knuckle geometry complicated to manufacture. Furthermore, the design is highly susceptible to minor assembly or design errors, which could prevent the RABSII antenna from functioning correctly. In contrast, nanosatellites with less stringent volume constraints can enable the intricate geometry, reducing susceptibility to errors and thereby improving reliability in these cases.

Volume constraints also present challenges for integrating a tape-spring based actuation method, even disabling certain stowed configurations. Section E.2.1 provides various integration methods for tape springs, assessing potential stowed configurations and their associated limitations. For example, at a folding angle of 180° and a minimum bending radius of 2 mm, it is impossible to find a COTS tape spring that meets these requirements. The OHSC and CSHC cannot be achieved within the Delfi-Twin's volume constraints. However, a folding angle of 90° makes the RAHSC feasible, at the cost of limiting the deployment angle to 90° and thus reducing the RABSII antenna compatibility. For larger nanosatellites that have a larger allocated volume, the feasibility of integrating the tape springs increases, enabling a wider range of stowed configurations and increasing the compatibility.

Conclusion

Concept 1 offers a variety of stowed configurations and utilizes a well-understood HDRM. However, its disadvantages originate primarily from the stringent volume constraints typical of nanosatellite missions.

For the Delfi-Twin mission, the volume constraints imposed on the deployment system significantly reduce the reliability of Concept 1. The design is prone to angular overshooting due to its susceptibility to minor design or assembly errors. The intricate geometry is complex to manufacture and the integration of the actuation method is infeasible for almost all stowed configurations. Although the deployment system utilizes an HDRM similar to that of the Delfi-Twin's solar panels, only the RAHSC configuration is feasible within the volume constraints, limiting the deployment angle to approximately 90°. As a result, the Delfi-Twin and RABSII antenna compatibility of Concept 1 are both both low.

On the contrary, Concept 1 demonstrates relatively high compatibility with larger nanosatellites. Many of the associated risks are due to the volume constraints imposed by the Delfi-Twin mission and are decreased with an increase in available volume for larger nanosatellite platforms. Additionally, a broader range of stowed configurations become feasible. Finally, the expected cost remains low and the system only requires basic tools for assembly. These factors contribute to an increase in compatibility with other nanosatellites.

E.5.2. Concept 2

Reliability

The reliability of Concept 2 is primarily dependent on the used SMA. In this concept, the SMA serves as the actuation method, the HDRM and prevents overshooting of the deployment angle. The proposed SMA is based on the activation temperature of a Nitinol alloy. However, uncertainties regarding the achievable deployment performance and the quality of the phase transformation reduce the overall reliability of this concept. Especially as many COTS SMAs often only provide their activation temperature instead of detailed specifications. Additionally, further analysis is required to evaluate the SMA's ability to withstand vibrations and external forces, which is critical for ensuring its performance as an HDRM. The reliability of this concept may benefit slightly from the SMA implementations of the ALBus mission, as inspiration was also drawn from their implementation. While the Technology Readiness Level (TRL) of their implementation is high due to its flight heritage, the significant design changes implemented in Concept 2 result in a reduced TRL.

Lastly, one of the challenges identified during the ALBus mission was the low deployment force generated by the SMAs, necessitating the use of a larger SMA plate to achieve the actuation. Concept 2 solves this potential problem by enabling a modular design. However, experimental validation is required to validate the ability to enable deployment.

Load Case and Simulations

Figure E.19 depicts the simulation constraints and results for Load Case 1 applied to the single hinge leaf. The peak stress remains below 9.100 MPa (Figure E.19c) and the deformation is less than 3.710x10^{-2} mm (8.628%). Unfortunately, this exceeds the plastic strain limit of Aluminum (6% [100]). Though, this requires minor design modifications that are achievable. Alternatively, selecting a different material with a higher strain limit could further reduce deformation.

Compatibility (Delfi-Twin, RABSII Antenna and Nanosatellites)

The compatibility of Concept 2 with the Delfi-Twin, RABSII antenna and other nanosatellites is primarily limited by the integration of the Shape Memory Alloy (SMA). The material selection for the SMA is tailored to the environmental parameters of the Delfi-Twin mission and the specific requirements of the RABSII antenna.

Section E.3.1 provides details on the SMA material selection for Concept 2. While this selection is optimized to meet the Delfi-Twin mission requirements, the deployment performance cannot yet be

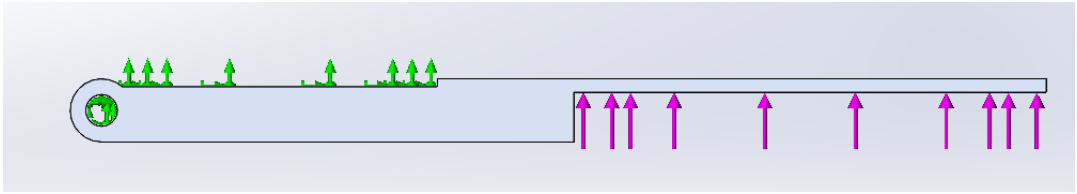

(a) Concept 2 Hinge Leaf, Applied Constraints (Green Arrows) and Applied Forces (Purple Arrows)

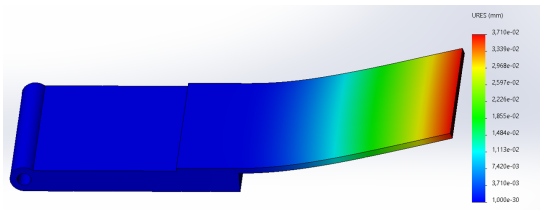

(b) Concept 2, Deformation occurring due to Load Case 1, [Min:≈0 mm;Max: 3.710x10^{-2} mm]

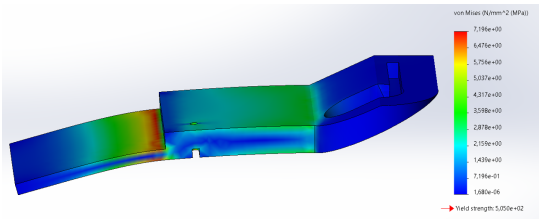

(c) Concept 2, Von-Mises Stress occurring due to Load Case 1, [Min: 2.530x10^{-5} MPa; Max: 9.100 MPa]

Figure E.19: Concept 2 Load Case 1, initial parameters and results of the simulation.

guaranteed. During the ALBus mission, a low deployment torque (0.125 Nm) was observed [31], highlighting the need for modularity in Concept 2's design. However, experimental validation is necessary to confirm both deployment performance and transformation quality.

The integration of Concept 2 with other nanosatellites is further complicated by several factors. The current SMA material choice is optimized for the Delfi-Twin mission, which requires a relatively high activation temperature. This presents challenges for other orbital environments, particularly those not sun-synchronous, where insufficient thermal flux may complicate deployment. Additionally, pre-launch environmental parameters might necessitate an even higher activation temperature, further narrowing the range of suitable SMA materials.

For the RABSII antenna, the SMA allows for the integration of communication and power interfaces, but this increases complexity. Moreover, variations in temperature, combined with uncertainties in the quality of the SMA's phase transformation, may negatively impact the deployment angle. A trade-off, considering the expected thermal profile of the mission orbit, is essential to ensure a complete austenite transformation and reliable performance.

Conclusions

Concept 2 is a modular hinge mechanism that supports two stowed configurations, RAHSC and CSHC. Disadvantageous of this concepts is due to the complex actuation method and the additional roles it must fulfill.

The reliability of Concept 2 is low, mainly due to a limited understanding of the SMA's performance. While the geometry of the mechanism is relatively simple, and the potential failure points can be addressed through minor redesigns or material changes, the SMA introduces significant uncertainties. Currently, the performance of the considered SMA under the Delfi-Twin mission conditions is unknown. Experimental validation is necessary to assess its deployment performance and material properties, as COTS SMA providers do not supply sufficient data.

The limited understanding of the SMA also negatively impacts the Delfi-Twin compatibility of Concept 2. While the activation temperature and A_f of the SMA are theoretically compatible with the Delfi-Twin mission, the narrow margins leave little room for error. Furthermore, Appendix A states that a deployment force of 0.166 is required, which is challenging to achieve using only a singular SMA plate. By comparison, the SMA used in the ALBus mission produced a deployment force of 0.125 N [31]. Although the ALBus SMA used a different material with a lower activation temperature ($\approx 0°$) and only

the SMA thickness was disclosed (0.25 mm), Concept 2's modular design could potentially accommodate multiple SMA plates to achieve the necessary deployment force. Despite this modularity, the lack of understanding of the SMA decreases compatibility with the Delfi-Twin.

For the RABSII antenna compatibility, Concept 2 must ensure a constant deployment angle over time and the ability to accommodate electrical and communication interfaces. The ALBus mission demonstrated the feasibility of integrating electrical interfaces with solar panels through SMA actuation, but highlighted significant challenges. These include isolation and connection issues, which led to the recommendation that such integrations are not recommended. Additionally, although achieving the required deployment angle is theoretically feasible, the thermal profile of the Delfi-Twin mission must be carefully evaluated as it directly influences the deployment angle.

Concept 2 faces similar limitations in nanosatellite compatibility as with Delfi-Twin compatibility, but is complicated by additional considerations. The fixed upper activation temperature bound for the SMA was determined by the RABSII antenna's requirements and limits flexibility. The lower bound imposed by the Delfi-Twin launch deployer might vary between other nanosatellite launch deployers and can further narrow the available temperature range. A different temperature range might force a material change of the SMA and require experimentally validation of the deployment force, performance and quality. Furthermore, the thermal profile of the Delfi-Twin mission, being relatively constant in its sun-synchronous orbit, simplifies the thermal analysis. This also reduces risks associated with deployment angle variations due to SMA heating and cooling. However, nanosatellites operating in more variable orbital environments may experience greater thermal flux variations, which could degrade deployment performance and further reduce reliability and compatibility with the RABSII antenna. As a result of the additional considerations, the nanosatellite compatibility of Concept 2 is also rated as low.

E.5.3. Concept 3

Reliability

Concept 3 was developed to explore the feasibility of a turntable deployment mechanism. This concept incorporates a simple actuation method combined with a burn wire mechanism. The integration of the burn wire mechanism was straightforward, with only the expected challenges associated with a burn wire mechanism. The reliability of Concept 3 is primarily impaired by the deployment mechanism. Within the volume constraints of the Delfi-Twin mission, including additional margins for rotation and lubricants is complex. This reduces the deployment risk and increase risk of failure. More-over, as the torsion spring will act as the turntable pin, it requires a certain level of structural integrity. Achieving this is complex within the Delfi-Twin mission, as the allocated envelope for the actuation method is extremely small. Further details regarding the incompatibility of this approach with the Delfi-Twin mission requirements are provided in the discussion on Delfi-Twin Compatibility.

Load Case and Simulations

Figure E.20 depicts the simulation constraints and results for the load case outlined in Appendix A. The simulation focuses on the Von-Mises stresses and deformation of the RTL. The peak stresses in the RTL are determined to not exceed 7.196 MPa (Figure E.20c) and the maximum deformation is less than 7.274x10^3 mm (1.6%, Figure E.20b. Stress concentrations are primarily observed around the corners of the design. These can effectively be reduced by implementing round finishes to the affected areas. Additionally, the deformations observed in the simulation, assuming the RTL is constructed from aluminum, are well below the material's plastic strain limit. This confirm the structural integrity of the RTL under the simulated conditions. The peak stress is concentrated around the corners of the design and could be mitigated by applying rounded finishes.

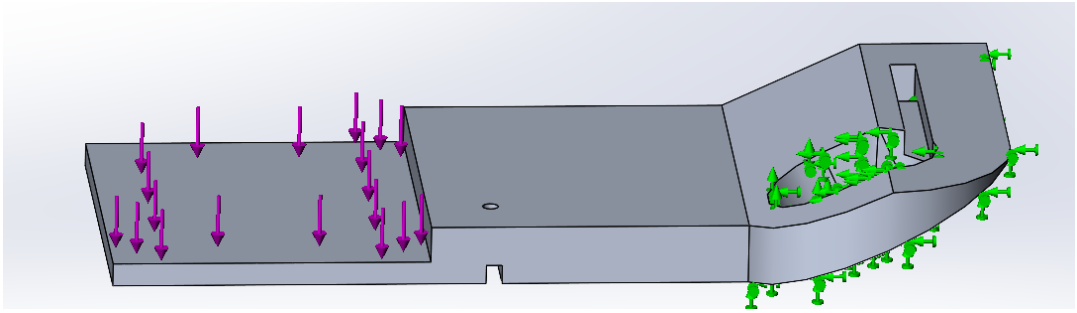

(a) Concept 3, Applied Constraints (Green Arrows) and Applied Forces (Purple Arrows)

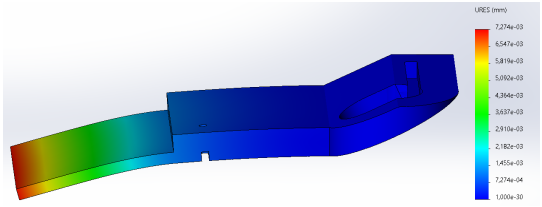

(b) Concept 3, Deformation at Load Case 1, [Min:≈0 mm;Max: 7.274x10^{-3} mm]

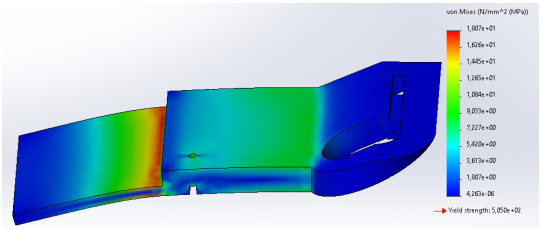

(c) Concept 3, Von-Mises Stress occurring at Load Case 1, [Min: 1.680x10^{-6} MPa; Max: 7.196 MPa]

Figure E.20: Concept 3, rotation turntable leaf Load Case 1, initial parameters and results of the simulation.

Compatibility (Delfi-Twin, RABSII Antenna and Nanosatellites)

Limitations in the compatibility with the Delfi-Twin, RABSII antenna and other nanosatellite are primarily due to the volume constraints and inherent complexity of the deployment mechanism.

Concept 3 utilizes a torsion spring as both the actuation method and turntable pin. The relation determining the maximum external radius of the torsion spring (r_{FTL}) is defined in Equation E.2. Within the Delfi-Twin mission, the r_{FTL} is constrained to 2.144 mm. This tight constraint significantly reduces the feasibility of Concept 3 within the Delfi-Twin mission. Manufacturing a torsion spring that fits within these dimensions while enabling a 180°, is not practical or feasible. However, for larger nanosatellite missions with less stringent volume constraints, particularly those with increased thickness allocations for the deployment system, the feasibility of Concept 3 improves substantially.

Assessing the deployment performance of this concept is challenging given its limited feasibility within the Delfi-Twin mission. Nevertheless, when equipped with a suitable actuation method, Concept 3 is expected to have a good deployment performance and quality. Overshooting is mitigated not only by the actuation mechanism, but also by the concept's geometry. Additionally, the design accommodates the integration of electrical and communication interfaces required for the RABSII antenna.

Conclusions

Concept 3 explores the feasibility of a turntable deployment mechanism utilizing a torsion spring-based actuation method and a burn wire mechanism. While it lacks variability in stowed configurations, Concept 3 shows potential for larger nanosatellites.

Firstly, the reliability of Concept 2 is primarily limited by its deployment performance within the Delfi-Twin mission. The intricate geometry combined with the lack of allocated margins enables significant challenges. These constrains hinder efforts to reduce friction, incorporate lubricants, or accommodate tolerances, all of which are essential for reliable operation. Additionally, the required torsion spring needs to have an extremely thin profile and low rigidity, further reducing reliability. Within the Delfi-Twin mission, these limitations result in low reliability for Concept 3.

Second, the Delfi-Twin compatibility of Concept 3 is a major concern. The design relies on a torsion spring that serves as both the actuation mechanism and the turntable pin. Given the strict volume

constraints of the Delfi-Twin mission, no COTS meets the requirements. Consequently, Concept 3 is deemed infeasible for the Delfi-Twin mission, with extremely low compatibility.

The RABSII Antenna Compatibility of Concept 3 is relatively high compared to its compatibility with Delfi-Twin. The concept enables a deployment angle of 130° with minimal expected fluctuations. Furthermore, the integration of the communication or power interfaces can easily be achieved and integrated within the design.

Lastly, the nanosatellite compatibility of Concept 3 is significantly higher than its Delfi-Twin compatibility. Increasing the allocated dimensions, especially the thickness, significantly increases the feasibility of the design. The radius of the torsion spring, which is directly tied to the thickness, benefits from these increased dimensions, as demonstrated by Equation E.2. Additionally, larger volumes allow for the inclusion of feasible margins and lubricants, reducing friction and improving deployment performance. The only disadvantage is the lack of variety in stowed configurations.